2014

Maria DELLA SALA

GENESIS AND MECHANISMS OF RAINFALL-INDUCED
HYPERCONCENTRATED FLOWS IN GRANULAR SOILS

UNIVERSITÀ DEGLI STUDI DI SALERNO
Via Giovanni Paolo II
84084 Fisciano (SA)
Tel. 089 96 4029 Fax 96 4343
www.unisa.it

UNIVERSITÀ DEGLI STUDI
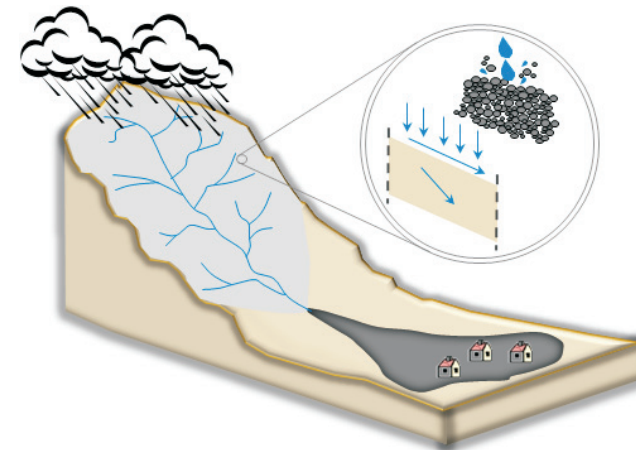DI SALERNO
Dipartimento di
Ingegneria Civile

CORSO DI
DOTTORATO DI RICERCA IN
Ingegneria Civile per
l'Ambiente ed il Territorio

Tesi di Dottorato

GENESIS AND MECHANISMS OF RAINFALL-INDUCED HYPERCONCENTRATED FLOWS IN GRANULAR SOILS

Maria Della Sala

Relatore
prof. ing. Sabatino CUOMO

XII Ciclo Nuova Serie - Coordinatore: prof. ing. Vincenzo BELGIORNO

DOTTORATO DI RICERCA IN INGEGNERIA CIVILE PER L'AMBIENTE ED IL TERRITORIO

XII Ciclo - Nuova Serie (2011-2013)

DIPARTIMENTO DI INGEGNERIA CIVILE, UNIVERSITÀ DEGLI STUDI DI SALERNO

TESI DI DOTTORATO

GENESIS AND MECHANISMS OF RAINFALL-INDUCED HYPERCONCENTRATED FLOWS IN GRANULAR SOILS

(GENESI E MECCANISMI DI FLUSSI IPERCONCENTRATI INDOTTI DA PIOGGIA IN TERRENI GRANULARI)

MARIA DELLA SALA

Relatore
PROF. ING. SABATINO CUOMO

Coordinatore
PROF. ING. VINCENZO BELGIORNO

On the front cover: Hyperconcentrated flow in a mountain basin.

GENESIS AND MECHANISMS OF RAINFALL-INDUCED
HYPERCONCENTRATED FLOWS IN GRANULAR SOILS

Alla mia mamma

INDEX

INDEX OF FIGURES

INDEX OF TABLES

xvi

SOMMARIO

Lungo versanti acclivi, piogge intense possono innescare sia frane superficiali che erosione generando diversi fenomeni tipo flusso che si innescano in aree adiacenti e sovrapposte. Conseguentemente, grandi quantità di acqua e detriti possono raggiungere la sezione di chiusura di bacini montani molto acclivi, facendo registrare spesso conseguenze catastrofiche. Recenti studi evidenziano che frane di primo distacco si trasformano in flussi di detrito o valanghe di detrito, mentre, instabilità di versante generate da fenomeni erosivi, generalmente, si propagano come flussi iperconcentrati. In particolare, la letteratura scientifica evidenzia che questi ultimi si verificano su versanti acclivi costituiti da terreni granulari parzialmente saturi e sono fenomeni di trasporto di massa, costituiti da acqua e detriti la cui concentrazione solida volumetrica varia tra il 20 e il 47%. Generalmente, tali fenomeni sono caratterizzati da un'alta variabilità spaziale e temporale, che caratterizza soprattutto la portata e la concentrazione di sedimenti. Pertanto, improvvisamente e repentinamente, la sezione di chiusura dei bacini può essere interessata da elevati picchi di portate con alte concentrazioni solide causando vittime e danni.

La genesi dei flussi iperconcentrati è legata a tre principali processi: i) infiltrazione delle acque meteoriche; ii) generazione del deflusso superficiale e iii) mobilitazione di particelle solide per effetto dei processi erosivi.

Il principale obiettivo della presente tesi è stato duplice: i) ottenere una migliore comprensione dei meccanismi di genesi alla base dei flussi iperconcentrati ed ii) effettuare valutazioni quantitative delle quantità di acqua e solido che si propagano all'interno di un bacino montano e che raggiungono, infine, la sezione di chiusura.

Per il conseguimento di tali finalità, si è adottato un approccio multi-scalare: i) a scala di pendio sono stati analizzati i meccanismi di generazione del deflusso superficiale mediante un modello agli Elementi Finiti (FEM); ii) su area vasta e a scala di bacino, si sono analizzati l'innesco dei flussi iperconcentrati e la propagazione di acqua e solido con un modello empirico ed un modello fisicamente basato alle

Differenze Finite (FDM), con particolare riguardo ad un'area di studio che è stata ripetutamente interessata da tali fenomeni; iii) a scala di particella, si è analizzato il meccanismo di erosione da impatto delle gocce di pioggia, con un approccio numerico agli Elementi Discreti (DEM).

A scala di pendio sono stati analizzati i processi di infiltrazione delle acque meteoriche e di generazione del deflusso superficiale portando in conto la parziale saturazione dei terreni e l'intensità della pioggia. Ne è risultato che i tempi di generazione del deflusso, i tempi di instabilità e la quantità di acqua che ruscella, dipendono fortemente dalle curve caratteristiche e dalle condizioni iniziali dei terreni, dall'intensità di pioggia e dalla pendenza del versante.

Su area vasta, selezionata un'area campione di rilevante estensione (circa 130 km^2), sono stati condotti studi parametrici relativi all'innesco sia di frane superficiali che di fenomeni erosivi superficiali. Ne è risultato una molteplicità di scenari possibili, in relazione ai valori iniziali di suzione che dipendono dal periodo dell'anno e che, d'altra parte, condizionano fortemente l'evoluzione spazio-temporale del ruscellamento. Tali risultati sono stati confrontati con un evento di particolare rilevanza occorso nel passato, ricavandone un soddisfacente accordo con quanto osservato.

A scala di bacino sono stati scelti due bacini montani (circa 10 km^2) ricadenti nell'area di studio e sono stati condotti studi parametrici al fine di valutare la distribuzione spaziale delle aree erose, la portata di acqua e solido e la concentrazione di solido alla sezione di chiusura. I risultati conseguiti evidenziano la concreta possibilità di simulare eventi meteorici realistici e di poterne prevedere gli effetti in termini di zone erose lungo i versanti e nei canali oltre che di poter computare nel tempo le portate di acqua e solido che raggiungono lo sbocco di un bacino montano.

A scala di particella, è stato approfondito il meccanismo di erosione da impatto delle gocce di pioggia sul terreno attraverso un modello numerico avanzato agli Elementi Discreti (DEM). Tale tipo di analisi ha consentito di verificare la possibilità di un effettivo utilizzo di tale formulazione meccanica per il problema in esame, portando al conseguimento di alcuni risultati preliminari di particolare interesse.

Globalmente, la presente tesi fornisce innovativi contributi specifici a differenti scale di analisi, dall'area vasta (>100km^2) alla scala della singola particella (diametro<1cm), per i processi di genesi di un flusso iperconcentrato.

ABSTRACT

Heavy rainfall on steep hillslopes may cause either shallow landslides or soil superficial erosion and different flow-type phenomena may originate in adjacent/overlapping source areas. Consequently, great amount of water and debris can be conveyed at the outlet of steep mountain basins where huge consequences are often registered.

Recent studies outline that first-time shallow slides may turn into debris flows or debris avalanches; conversely, slope instabilities initiated by erosion phenomena generally propagate as hyperconcentrated flows. In particular, the scientific literature points out that the latter ones are mass transport phenomena, that involve granular unsaturated soils covering steep slopes and are constituted by water and debris with solid concentration (in volume) variable from 20 to 47 %. Generally, these phenomena are characterised by a high spatial and temporal variability, especially in water discharge and sediment concentration. Therefore, suddenly and repeatedly, high peak discharge with high sediment concentration can reach the outlet of the basin and cause victims and damages.

The genesis of the hyperconcentrated flows is related to three main processes: i) rainfall infiltration, ii) runoff generation and iii) solid particle mobilisation due to erosion processes.

The main goal of the PhD research activity is twofold: i) to achieve a better understanding of the genesis mechanisms of hyperconcentrated flows, ii) to perform quantitative evaluations of the amount of water and debris propagating inside a mountain basin and, finally, reaching the outlet of the basin.

A multi-scale approach is used: i) at slope scale, the mechanisms of runoff generation are analysed through a Finite Element Method (FEM) model; ii) over large area and at basin scale, the triggering of hyperconcentrated flows and propagation of water and solid are analysed through an empirical model and a physically-based Finite Difference Method (FDM) model, with special emphasis on a study area repeatedly affected by these phenomena, iii) at particle scale, the rainsplash erosion is preliminary modeled through the numerical Discrete Element Method.

At slope scale, the mechanisms of rainfall infiltration and runoff generation are analysed taking into account the soil unsaturated conditions and rainfall intensity. The analyses show that time to runoff, failure time and the amount of rainfall infiltrating the ground surface and runoff flowing as wash out, strongly depend on soil water characteristic curves, soil initial conditions, rainfall intensity and slope angles.

At large area, a study area (about 130 km^2), repeatedly affected by flow-type phenomena, is selected and parametric analyses are performed concerning either first-time shallow landslides or soil erosion. The results point out that different possible scenarios may occur, depending on soil initial suction, that, in turn, changes during the year and also strongly affects the spatial and temporal occurrence of the runoff generation. These results are compared with a relevant past event occurred in the study area, obtaining a satisfactory agreement with in situ evidences.

At basin scale, two medium-size mountain basins (about 10 km^2) are selected in the previous study area, and parametric analyses are performed in order to evaluate tha spatial distribution of soil erosion, the water and solid discharges and the sediment concentration at the outlet of the basins. The achieved results show the possibility to simulate realistic rainfall events, to forecast the soil erosion along steep slopes and channels and to compute the water and solid discharge over the time that may be conveyed at the outlet of the basin.

At particle scale, the mechanism of rainsplash erosion due to impact of the drops on the ground surface is deepened through a numerical Discrete Element Method (DEM) model. This new type of analysis allowed to verify the applicability of the geomechanical approach to this erosion mechanism, also reaching some interesting preliminary results.

Globally, the PhD thesis provides an update overview of the genesis processes of an hyperconcentrated flow with novel specific contributions at different scales of analysis, from large area (> 100 km^2) to single soil particle (diameter < 1cm).

AKNOWLEDGEMENTS

ABOUT THE AUTHOR

Maria Della Sala graduated in Environmental Engineering at the University of Salerno with 110/110 cum laude. During the PhD course she developed research topics related to the analysis and modeling of the triggering for hyperconcentrated flows with reference to erosion processes induced by heavy rainfall in steep slopes. To deepen these issues, she undertook training activities at the University of Salerno, University of Naples Federico II, University of Cassino and Technical University of Turin. She attended several research meetings and workshops about flow-like phenomena, among which the international LARAM School on landslide risk assessment and mitigation (September 2011) and a on-site stage on landslide risk mitigation in complex geological areas with techniques of Bioengineering (September 2012). On 2011 and 2013, she presented current scientific research works at the Annual Meeting of Italian Geotechnical Researchers. She is co-author of scientific papers published in international journals and in proceedings of international conference.

Maria Della Sala si laurea in Ingegneria per l'Ambiente ed il Territorio presso l'Università di Salerno con voto 110 e lode/110. Durante il Corso di Dottorato si dedica a tematiche di ricerca connesse all'analisi e alla modellazione dell'innesco di flussi iperconcentrati con riferimento ai processi di erosione indotti da piogge intense su versanti acclivi. Per approfondire tali argomenti, svolge attività di formazione presso l'Università di Salerno, Federico II di Napoli, di Cassino e il Politecnico di Torino. Partecipa a diversi incontri di ricerca e workshops riguardanti fenomeni franosi tipo flusso, tra cui la scuola internazionale LARAM sulla valutazione e la mitigazione del rischio da frana (Settembre 2011) e il Campus di Ingegneria Naturalistica sulla Mitigazione del rischio idrogeologico in aree geologicamente complesse con tecniche di Ingegneria Naturalistica (Settembre 2012). Nel 2011 e 2013 ha presentato lavori scientifici all'Incontro Annuale dei Ricercatori di Geotecnica. E' co-autrice di articoli scientifici pubblicati su riviste internazionali e in atti di convegno internazionali.

1   INTRODUCTION

Heavy rainfall on steep hillslopes may cause either shallow landslides or soil superficial erosion and different flow-type phenomena may originate in adjacent/overlapping source areas. Consequently, great amount of water and debris can be conveyed at the outlet of steep mountain basins where huge consequences are often registered.

Recent studies outline that first-time shallow slides may turn into debris flows or debris avalanches; conversely, slope instabilities initiated by erosion phenomena generally propagate as hyperconcentrated flows. These last phenomena are characterised by a high spatial and temporal variability, especially in water discharge and sediment concentration. Thus, high peak discharge with high sediment concentration can reach the outlet of the basin, suddenly and repeatedly, causing victims and damages.

The analysis of the triggering and propagation stages of hyperconcentrated flows inside the mountain basins is an important step in the risk assessment, in order to develop appropriate risk mitigation measures. However, open issues related to the genesis of hyperconcentrated flows still exist in the literature.

The present PhD thesis is aimed to provide a contribution on this topic in order: i) to achieve a better understanding of the genesis and mechanisms of hyperconcentrated flows, ii) to perform quantitative evaluations of the amount of water and debris propagating inside a mountain basin and, finally, reaching the outlet of the basin.

Particularly, Chapter 2 concerns the general features of two types of rainfall-induced slope instabilities: i) hyperconcentrated flows and ii) landslides of flow-types. For these phenomena, a literature review is proposed with reference to the main classifications, triggering mechanisms, spatial and temporal occurrence and approaches available for modeling, also outlining similarities and differences in their main features. Finally, the procedure adopted for the analysis of hyperconcentrated flows is indicated.

Chapter 3 concerns the analysis of rainfall infiltration and runoff generation along steep slopes. In particular, starting from an accurate analysis of the topic and in order to improve the understanding of the governing mechanisms of infiltration and runoff generation, an engineering reference framework is proposed to evaluate the amount of rainfall infiltrating the ground surface and runoff flowing at the ground surface as wash out. A parametric analysis is performed in order to validate the proposed framework and a special attention is devoted to the temporal occurrence of both processes whose combination may cause the occurrence of different types of flow-like phenomena.

Chapter 4 presents a large study area of the Campania region (Amalfi Coast), repeatedly affected by shallow landslides and soil erosion. In particular, the geological setting and the main past events are briefly described.

Chapter 5 concerns the spatially-distributed analysis of flow-like mass movements over the large study area, above described. In particular, the potentialities of two available models are tested to respectively capture the spatial occurrence of first-time shallow landslides and superficial soil erosion. A parametric analysis is performed taking into account the seasonal variation of some input data and the achieved results for each phenomenon are compared.

Chapter 6 deals with the physically-based modeling of soil erosion in two selected basins of the study area. Particularly, the two basins are described and a parametric analysis is performed in order to estimate the amount of water and sediment (discharge and solid concentration) at the outlet of basins for different realistic rainfall scenarios and for distinct soil initial conditions.

Chapter 7 focuses on the modeling of rainsplash erosion through a Discrete Element Method approach. In particular, the method is described and the input data are presented. Then, the results of a wide parametric analysis are discussed.

Finally, in Chapter 8, based on the results obtained for each section, a general discussion is proposed and the conclusions are outlined.

2 RAINFALL-INDUCED SLOPE INSTABILITIES

Heavy rainfall on steep hillslopes may cause either shallow landslides or soil superficial erosion and different slope instabilities may originate in adjacent or overlapping source areas, depending on slope morphology, soil water characteristic curves and shear strength of soils. However, differences in runoff discharges, solid concentration and rheology of the propagating flows may arise. Many worldwide case histories (Hong Kong, Brasil, Canada, Italy) testify the huge consequences caused by slope instabilites in terms of causalities and damages to property. However, the run-out distances and consequences associated to shallow landslides or soil superficial erosion are extremely different and it is important to discriminate among them in order to properly assess and mitigate the risk posed to life and property.

In the following, the main features of hyperconcentrated flows and landslides of flow-type are analysed with reference to: i) classifications proposed in literature, ii) triggering mechanisms, iii) spatial and temporal occurrence of both the phenomena and iv) the current approaches for modeling. Finally, the main aspects of both the phenomena are discussed and the procedure adopted for studying hyperconcentrated flows is presented.

2.1 HYPERCONCENTRATED FLOWS

2.1.1 Classification

The hyperconcentrated flows belong to sediment-water flows that result from the interaction of hydrological processes with slope processes. They are characterised by a very short time-scale and mainly affect mountain areas in a wide range of morphoclimatic environments over the world. However, these phenomena may affect large areas ($>100km^2$) depending on the characteristic of rainfall event. In the

literature, different authors proposed classifications of these phenomena based on distinct characteristics.

Pierson and Costa (1987) gave a classification of sediment-water flows based on thresholds in rheological behavior. This classification is built on a two-dimensional matrix (Figure 2.1) where different phenomena are located in relation to mean flow velocity and volumetric sediment concentration and distinguished by approximated boundaries. They identified two groups of flows: 1) "apparent liquid flow" that include normal streamflows and hyperconcentrated flows and 2) "flow of plastic fluids" that include slurry flows and granular flows. In the scheme, the authors allocate the "hyperconcentrated streamflows" between "normal streamflows" and "debris flows" and defined them as "flowing mixture of water and sediment that possesses measurable yield strength but that still appears to flow like a liquid". According to the authors, these phenomena belong to the category of "streamflows", have sediment concentrations higher than normal streamflows but lower than debris flows but have some rheologic features similar to debris flows. The hyperconcentrated flows are "non-newtonian fluids" with "plastic behaviour" composed by water and fines. The authors specify that the term "streamflow" is used to indicate "the flow of water or a sediment-water mixture that acts like water, a liquid, to the casual observatory", the term "hyperconcentrated flow" is used "when the fluid becomes slighty plastic in the rheologic meaning but still appears to flow like water".
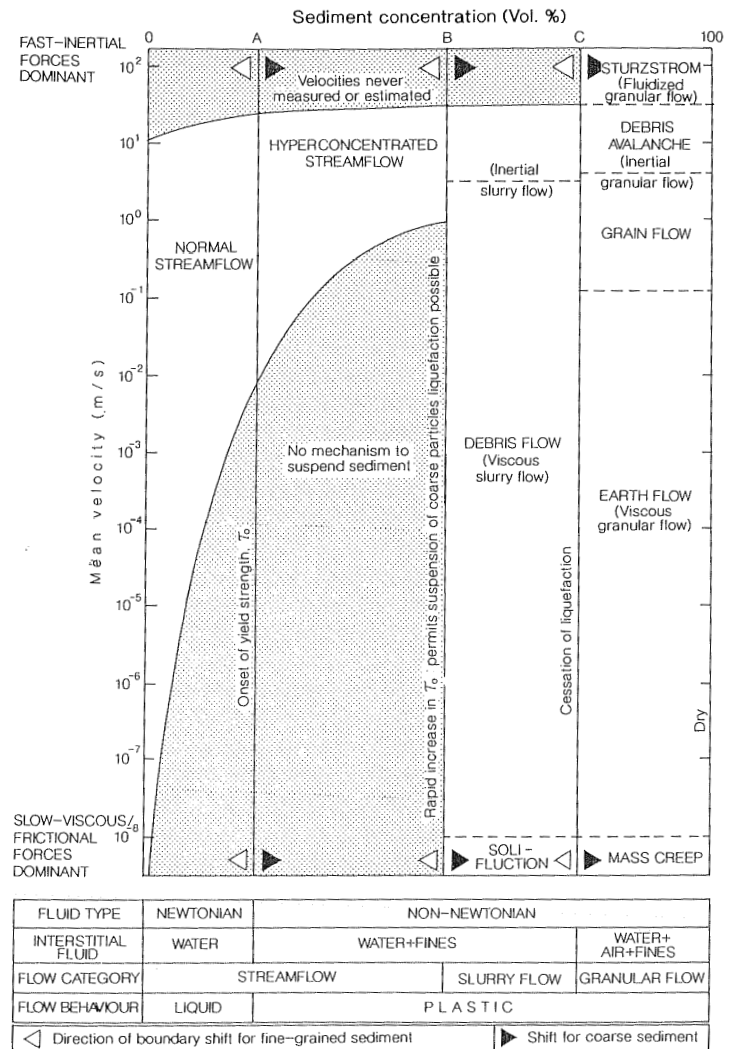
Figure 2.1 The rheological classification of flows (Pierson and Costa, 1987; Selby, 1993).

Slaymaker (1988) incorporates part of the earlier classification of Aulitzky (1980), providing a framework to channelized debris flows, poor in clay and rich in organic material, defined "debris torrent". This term, used in the North-Western of United States and Canada is not shared by other authors (Pierson and Costa, 1987). In particular the author proposed a classification of gravitational and fluvial sediment

transporting processes focusing on the description of debris torrent that identifies as a variety of channelised debris flow which presents the lack of fine-grained fraction, particularly clay, and the large organic debris content. In particular, for debris torrent, the author describes: i) environmental context, ii) triggering mechanisms, iii) rheology of the flow and iv) texture and morphology. In order to describe varieties of debris flow and fluvial debris transport , in his classification, the author considers if the flow is channelised or occur on open slopes, what is the dominant rheology and an index of the texture of entrained material, and allocates debris torrents in a transitional position between channelized coarse debris flows and debris floods (Figure 2.2).
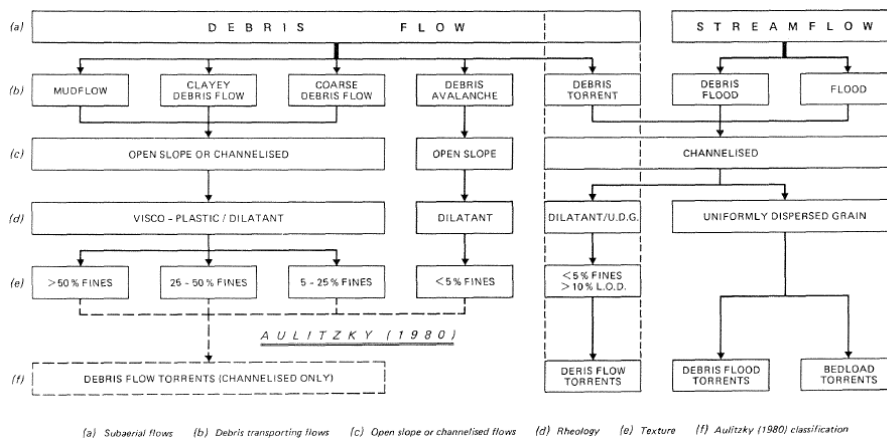
Figure 2.2 The debris flow - stream flow continuum (Slaymaker, 1988).

Costa (1988) deepened the rheologic, geomorphic and sedimentologic features of common flow processes that can occur in the channels of small and steep basins and divided them in three main groups (Table 2.1): 1) water floods, 2) hyperconcentrated flows and 3) debris flows stressing that each class has "some unique and diagnostic effects and products" but "in nature, there exists a continuum of flow conditions and sediment concentration". For each class of phenomena, the author recognized some typical characteristics: i) sediment concentration, ii) bulk density; iii) shear strength; iv) fluid type (Newtonian, non-Newtonian, Viscoplastic); v) major sediment support mechanism; vi) viscosity; vii) fall velocity; viii) sediment concentration profile (uniform, non-uniform) and ix) predominant flow type (turbolent, laminar). With

reference to these features, the author allocated the hyperconcentrated flows between water floods and debris flows. In particular, the transition from water floods to hyperconcentrated flows occurs when sediment concentration, fluid density and viscosity increase and fall velocity of particles decreases. According to the author, the "hyperconcentrated flows are streamflows containing large quantities of sediment (40 to about 70% by weight, 20 to about 47 % by volume), bulk densities in the general range of 1330 – 1800 kg/m^3) and possess a small but measurable shear strength".

Table 2.1 Rheologic classification of water and sediment flows in channels (modified from Costa, 1988).

	Water flood	**Hyperconcentrated flow**	**Debris flow**
Sediment concentration	1-40% by wt. 0.4-20% by vol.	40-70% by wt. 20-47% by vol.	70-90% by wt. 47-77% by vol.
Bulk density (kg/m³)	1010-1330	1330-1800	1800-2300
Shear strength (Pa)	0-10	10-40	>40
Fluid type	Newtonian	Non Newtonian (?)	Viscoplastic (?)
Major sediment-support mechanism	Electrostatic forces, turbulence	Buoyancy, dispersive stress, turbulence	Cohesion, buoyancy, dispersive stress, structural support
Predominant flow type	Turbolent	Turbolent to laminar	Laminar
Sediment concentration profile	Non-uniform	Non-uniform to uniform	Uniform

Starting from a comparison of field characteristics of the main types of natural flows and mass movements on steep slopes, Coussot and Meunier (1996) proposed a "simple global classification" of flows and mass movements involving water and sediments on steep slopes in mountainous areas as a function of only two parameters: solid fraction and material type. In their classification diagram, that is shaped ellipse (Figure 2.3), the limits between the different mass movements are only conceptual and qualitative. With reference to material type, the authors consider the markedly different behavior of fine, cohesive materials and

coarse, cohesionless, granular materials. With reference to solid fraction, many authors have recognised that the sediment concentration globally increases when the flow varies from pure water flow to stream flow with solid transport, then to hyperconcentrated flow, debris flow and landslides or debris avalanches. Furthermore, "the transition from hyperconcentrated flows to debris flows could correspond to a critical solid fraction and material type for which settling is negligible within the material during a given time".
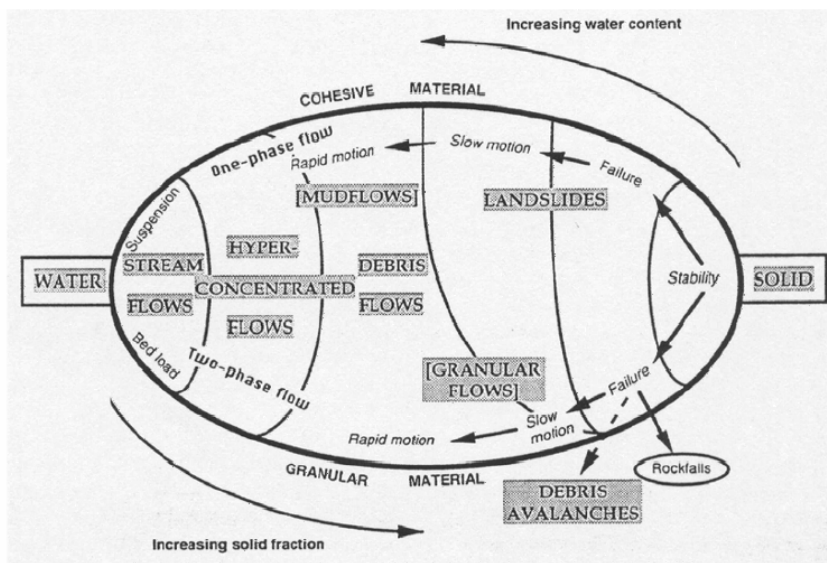
Figure 2.3 Classification of mass movements on steep slopes as a function of solid fraction and material type (Coussot and Meunier, 1996).

2.1.2 Mechanisms for genesis

The transition from water floods (or stream flows) to hyperconcentrated flows is mainly related to the increase in the sediment concentration that, generally, can be linked to detachment and transport of sediment due to soil erosion induced by intense rainfall. The water erosion is a complex process in which sediment particles are removed (or deposited) at various time-space locations by the flow of water (resulting from rainfall) down the hillslope profile. This process involves different stages: 1) detachment (dislodging) of soil particles, 2) transportation

(entrainment and movement of soil particles with the surface flow) and 3) deposition, when the transport capacity of the flow is reduced below that required for the existing suspended load (Kavvas and Govindaraju, 1992).

The main erosive agents of the water erosion in shallow deposits are the raindrops and runoff. Water erosion, therefore, depends on the forces exerted by raindrops and runoff and on the resistance of the soil to detachment. The capacity for runoff transporting sediment is also related to shear stresses applied by runoff to the soil surface and the transportability of the sediment, which is related to the size and the weight of the sediment particles. If the sediment available for transport becomes greater than the transport capacity, deposition results in the accumulation of sediment on the soil surface (Toy et al., 2002). The ability of the erosive agent to generate water erosion is called erosivity, while the ability of the soil to be eroded is called erodibility. The complexity of erosivity and erodibility is shown in Figure 2.4.
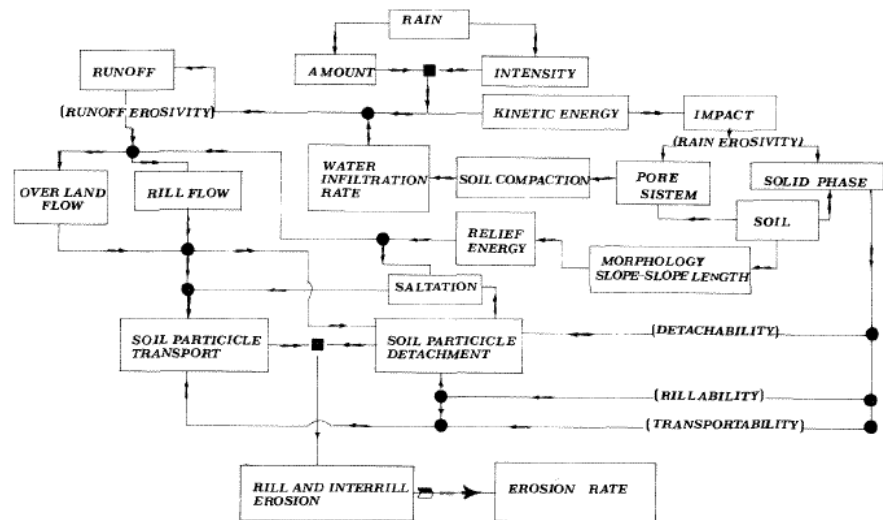
Figure 2.4 Main factors affecting soil loss due to water erosion (Chisci, 1981).

The water erosion varies in time and space. The temporal variability depends on the rainfall intensity that does not remain constant during an event, and depends on the events which follow one another with changeable characteristics (rainfall heights, intensity) and depends on the

soil conditions that vary from event to event. Indeed, the same rainfall event that occurs at two different times, can generate different erosion processes. On the contrary, the spatial variability depends on the morphological characteristics of the area, the lithological characteristics of the soil and the land use. The main variables of the erosion process are shown in Table 2.2.

Table 2.2 Main variables of the erosion process (Bagarello and Ferro, 2006).

Detachment capacity	Maximum amount of sediments that can be detached. It depends on: i) erosivity of the flow; ii) erodibility of the soil
Transport capacity	Maximum amount of sediments that can be transported. It depends on: i) erosivity of the flow; ii) transportability of the sediments
Detachment rate	Amount of sediments that are detached. It depends on: i) detachment capacity; ii) transport capacity
Deposition rate	Amount of sediments that are deposited. It depends on: i) difference between transport capacity and sediment load; ii) height of the sediments in the flow; iii) velocity of deposition of the solid particles

Soil eroded at a given area in time is defined erosion rate. Total sediment outflow from a watershed per unit time is called sediment yield. The transported portion of the eroded sediment (ratio of yield to the total eroded material) is called sediment delivery or sediment delivery ratio (Aksoy and Kavvas, 2005). Sediment delivery decreases with increasing basin size as large basins have more sediment storage sites where eroded sediment is kept. Sediment delivery can be limited by reducing either the detachment rate or the transport capacity depending on which has a lower value (Aksoy and Kavvas, 2005).

If the sediment load in the flow is smaller than the transport capacity of the flow, the sediment particles are detached from their current places. For this reason, the shear stress exerted by flow should be greater than the critical shear stress that is required for the detachment of the sediment particles. Otherwise, when the sediment load of the flow is larger than its transport capacity, the deposition occurs. This is illustrated by Aksoy and Kavvas (2005) in Table 2.3.

Table 2.3 Different cases of transport capacity (Tc) of the flow and sediment load (Qs) in the flow (Aksoy and Kavvas, 2005).

	Case	Deposition	Transport	Erosion
I	Tc<Qs	X	X	
II	Tc=Qs		X	
III	Tc>Qs		X	X

Climate, soil, topography and land use are the main factors affecting water erosion and each factor operates both independently and interactively (Toy et al., 2002).

The most important climatic variable affecting water erosion is the rainfall, that is expressed by rainfall erosivity. Several variables could be used to describe the rainfall erosivity, that include rainfall amount, kinetic energy, momentum and intensity (Foster, 1982, Wischmeier, 1959). Common observations show that the most important rainfall variables that determine storm erosivity are rainfall amount and rainfall intensity. Another important consideration is related to raindrop size because the forces applied to the soil by the raindrop impact are related to the drop size. A very small raindrop impacts the ground surface with a low impact velocity exerting a very low force on the soil and causing very little erosion regardless of rainfall amount and intensity (Toy et al., 2002). The variable that can be used to describe this effect is the kinetic energy of a raindrop that impacts the soil surface, which is related to the drop mass and drop impact velocity. These two parameters, in turn, are very closely related. A very small drop has a very low impact velocity and thus very low impact energy (Toy et al., 2002). A rainfall event is made of up of thousands of waterdrops and its kinetic energy is the sum of the kinetic energies of individual raindrops. Generally, the rainfall erosivity is expressed by an index that takes into account the rainfall kinetic energy (function of mass, diameter and velocity of the raindrops) and the rainfall intensity and duration. For example, Wischmeier and Smith (1958) found by experimental measurements that soil loss due to splash, overland flow and rill erosion is related to a compound index of kinetic energy (E) and the maximum 30-minute rainfall intensity (I_{30}).

With reference to the soil, erodibility defines the resistance of the soil to both detachment and transport. Although the resistance of soil to erosion depends in part on topographic position, slope steepness and the amount of disturbance, such as during tillage, the most important factors are related to the soil properties; in particular erodibility varies with soil

texture, aggregate stability, shear strength, infiltration capacity and organic and chemical content (Toy et al., 2002). The role of soil texture is very important in the erosion process: indeed, large particles are resistant to transport because of greater force required entraining them, while fine particles are resistant to detachment because of their cohesiveness. According to Evans (1980), the soil erodibility depends on the clay content, indicating that soils with clay content between 9 and 30 per cent are more susceptible to erosion and an increase in the moisture content of a soil decreases its shear strength. In the scientific literature, many efforts have been made to obtain an erodibility index based on either the soil properties as determined in the laboratory or the field, or the soil response to rainfall. The most commonly used erodibility index is the K value which represents the soil loss per unit of EI_{30} as measured in the field on a standard bare soil plot, 22 m long and at 5° slope. Estimates of the K value may be made if the grain-size distribution, organic content, structure and permeability of the soil are known (Wischmeier et al., 1971, 1978).

Another important factor affecting water erosion is the topography that refers to the geometry of the land surface. The important geometric variables are slope length and steepness, shape in the profile view and shape in the plan view. For a uniform slope, where steepness does not change along the slope, the erosion is related to the steepness of the slope. As slope steepness increases, the increase in erosion is linear with the increase in steepness (Toy et al., 2002). According to Foster (1982), the slope steepness has a greater effect on erosion by flow than by raindrop impact. Thus, erosion at a point on a slope is function of the distance from surface runoff origin and the steepness at that point (Foster and Meyer, 1977). If the considered point is far down the slope where much runoff has accumulated, the erosion rate will be high. For a given point, erosion will be proportional to the steepness at that location (Toy et al., 2002). For a convex slope, where the steepness increases continuously along the slope, the maximum erosion rate is much greater than maximum erosion on the uniform slope, and sediment delivered from the end of the convex slope is greater than that from the uniform slope. For the concave slope, where the runoff is least where the steepness is greatest, the maximum erosion rate and sediment yield are slightly less than on a uniform slope (Toy et al., 2002).

Finally, the land use mainly refers to the vegetation cover. Vegetation acts as a protective layer between the atmosphere and the soil. In

particular, it is possible to consider two effects: i) the aboveground components, such as leaves and stems, absorb part of the energy of falling raindrops and running water, so that less energy is directed at the ground surface, and ii) the below-ground components, comprising the root system, contribute to the mechanical strength of the soil. The effectiveness of a plant cover in reducing erosion by raindrop impact depends upon the height and continuity of the canopy, and the density of the ground cover . In addition to modifying the drop-size distribution of the rainfall, a plant canopy changes its spatial distribution at the ground surface. Moreover, a plant cover dissipates the energy of running water by imparting roughness to the flow, thereby reducing its velocity. The level of roughness with different shapes of vegetation depends upon the morphology and the density of the plants, as well as their height in relation to the depth of flow (Toy et al., 2002).

During a rainfall event, part of the rainfall falls directly on the ground surface because either there is no vegetation or it passes through gaps in the plant canopy (Morgan, 2005). This component of the rainfall is known as direct throughfall. Another part of the rainfall is intercepted by the canopy, from where it either returns to the atmosphere by evaporation or reaches the ground surface by dripping from the leaves, a component termed leaf drainage, or by running down the plant stems as stemflow (Morgan, 2005). The action of direct throughfall and leaf drainage produces "rainsplash erosion" which causes the detachment of soil particles when a raindrop falls on the ground surface and overcomes the cohesion of the soil. The rain that reaches the ground surface may be stored in small depressions on the surface or it may infiltrate the soil, contributing to soil moisture storage, to lateral movement downslope within the soil as subsurface or interflow or, by percolating deeper, to groundwater. The process of rainfall infiltration and runoff generation depend on the rainfall intensity and soil infiltration capacity which, in turn, is a function of the soil hydraulic properties (hydraulic conductivity, volumetric water content, initial suction). Once water starts to pond on the surface, it is accumulated in depressions on the ground surface and runoff does not begin until the storage capacity of these depressions is satisfied. When the soil and the depressions are unable to take in more water, the excess of rainfall contributes to runoff on the surface, resulting in "erosion by overland flow". Figure 2.5 shows a simplified

and qualitative scheme of temporal occurrence of both erosion processes.
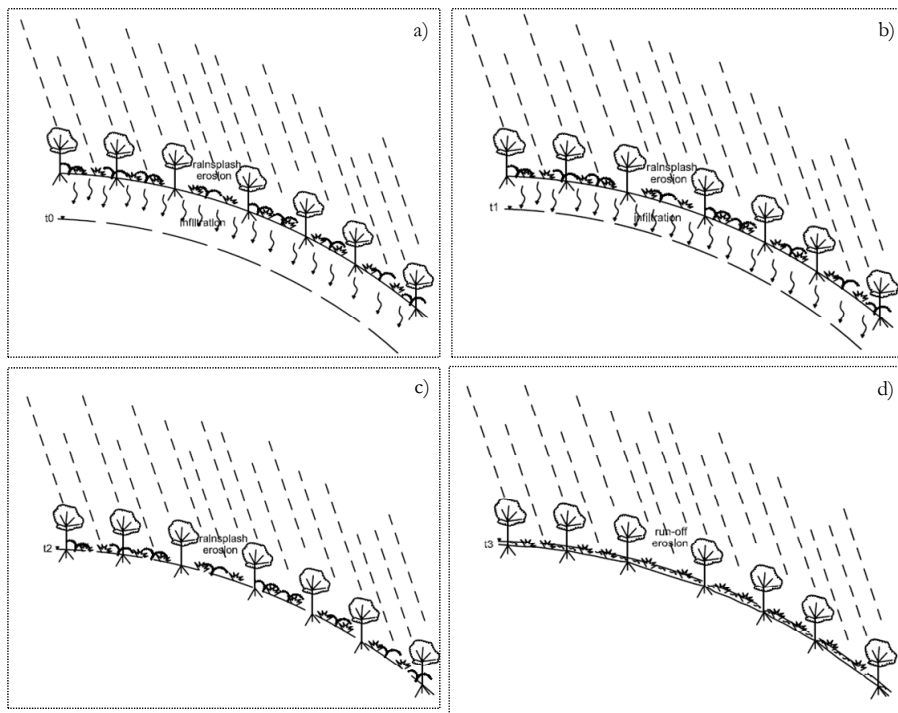
Figure 2.5 A qualitative scheme of temporal occurrence of water erosion: a) t=t_0; b) t_1>t_0; c) t_2>t_1; d) t_3>t_2.

The *rainsplash erosion* is caused by the fall of raindrops on the ground surface (Figure 2.6). The action of raindrops on soil particles is most easily understood by considering the momentum of a single raindrop falling on a sloping surface (Morgan, 2005). The downslope component of this momentum is transferred in full to the soil surface but only a small proportion of the component normal to the surface is transferred, the remainder being reflected (Morgan, 2005). The transfer of momentum to the soil particles has two effects: i) it provides a consolidating force, compacting the soil; and ii) it produces a disruptive force as the water rapidly disperses from and returns to the point of impact in laterally flowing jets. These fast moving water jets impart a velocity to some of the soil particles and launch them into the air, entrained within water droplets that are themselves formed by the break-

up of the raindrop on contact with the ground (Mutchler and Young, 1975). Thus, raindrops are agents of both consolidation and dispersion.

The rainsplash erosion depends on the rainfall characteristics (rainfall intensity and duration, raindrop diameter, kinetic energy, terminal velocity, drop pressure, drop size distribution, number of raindrops), the soil properties (soil texture, soil particles diameter, initial condition, top soil shear strength, hydraulic properties, saturated or unsaturated conditions) and the surface conditions (roughness, vegetation, slope angle, water depth on the surface). In general, the energy of raindrops is expended to do work on soil surface in several ways (Bennett, 1974). It lifts soil particles, it breaks down soil aggregates and it compacts aggregates. Splashed soil particles move into the surface water, and when deposited, act to seal the soil surface. These actions reduce the infiltration capacity of the soil and move soil into the surface water, increasing both the expected runoff and its associated sediment load. The tendency to seal the soil surface increases with the energy of falling rain, and it is an important contribution to increasing rates of erosion (Dohrenwend, 1977). The rainsplash erosion is most important for detaching the soil particles that are subsequently transported by running water.
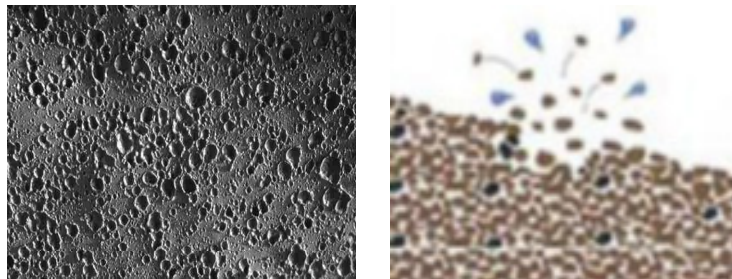
Figure 2.6 Rainsplash erosion.

The *erosion by overland flow* depends, in particular, on the flow velocity and it starts when the flow velocity attains a threshold value (critical flow velocity). Basically, the detachment of an individual soil particle from the soil mass occurs when the forces exerted by the flow exceed the forces keeping the particle at rest (Morgan, 2005). Shields (1936) made a fundamental analysis of the processes involved and the forces at work to determine the critical conditions for initiating particle movement over relatively gentle slopes. Other authors (Govers, 1987; Guy and

Dickinson, 1990; Torri and Borselli, 1991) indicated that the initiation of movement is not solely a phenomenon of flow shear stress but is related to other factors, such as the effects of raindrop impact on the flow, the angle of repose of the particle in relation to ground slope, the strong influence of gravity as the slope steepness increases, the soil cohesion, the changes in the density of the fluid as sediment concentration in the flow increases and abrasion between particles moving in the flow and the underlying soil (Morgan, 2005). Once the critical conditions for particle movement are exceeded, soil particles may be detached from the soil mass at a rate that depends on the shear velocity of the flow and the unit discharge (Govers, 1987). Moreover, based on the findings from laboratory experiments, Meyer and Monke (1965) observed that the rate of detachment depends on the amount of sediment in the flow; in particular, the detachment rate decreases as sediment concentration in the flow increases and, when the maximum sediment concentration is reached, the detachment rate is zero. Once sediment has been entrained within the flow, it will be transported until such time as deposition occurs (Morgan, 2005). Several studies have been conducted to describe the transport of soil particles by flow, which depends on the resistance of the soil, the diameter of raindrops, the flow depth and flow velocity. In general, the energy required for the detachment of the particles is greater than that required to transport. The small and light particles are generally the particles which are transported first; when flow velocity increases also the coarse particles get into the flow. To sum up, the detachment and transport of soil particles by overland flow depend on several variables such as: flow velocity, flow depth, flow discharge, flow shear stress, particle size, sediment concentration in the flow, raindrop impact, unit stream power and slope angle.

According to Merritt et al (2003) there are four main types of erosion processes that can be defined "erosion mechanisms": sheet, rill, gully and channel erosion (Figure 2.7). These types of soil erosion are related to overland flow.
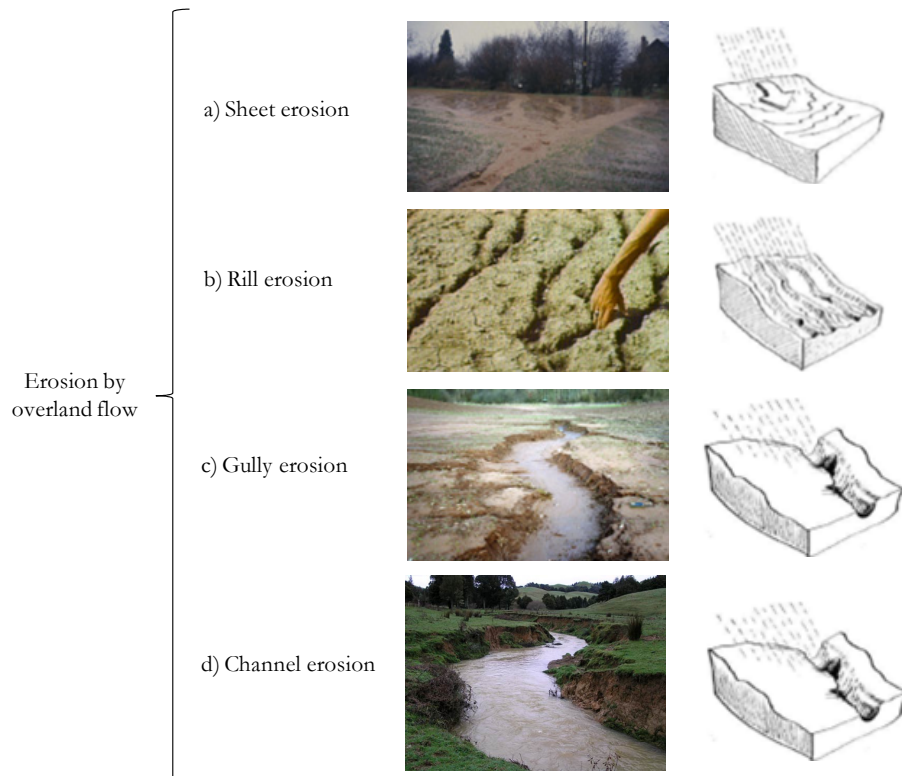
Figure 2.7 Erosion by overland flow: a) sheet erosion; b) rill erosion; c) gully erosion and d) channel erosion.

Sheet erosion (Figure 2.7a) refers to the uniform detachment and removal of soil, or sediment particles from the soil surface by overland flow or raindrop impact evenly distributed across a slope (Hairsine and Rose, 1992a).

Rill erosion (Figure 2.7b) occurs when water moving over the soil surface flows along preferential pathways forming an easily recognizable channel (Rose, 1993). Rill generation depends on the cohesive strength of the soil and the shear forces exerted on the soil. Flow in rills acts as a transporting agent for the removal of sediment downslope from rill and interill sources, although if the shear stress in the rill is high enough the rill flow may also detach significant amounts of soil (Nearing et al., 1994).

Gully erosion (Figure 2.7c), in contrast to rill erosion, describes channels of concentrated flow that are too deep to be obliterated by

cultivation (Rose, 1993; Loch and Silburn, 1996). Gully flows differ from sheet and rill flows in that raindrop impact is not an important factor in terms of flow resistance or in sediment particle detachment (Bennett, 1974). Gully development is considered to be controlled by thresholds, as with rills, although these thresholds have been related to slope and catchment area rather than flow erosivity (Loch and Silburn, 1996).

Channel erosion (Figure 2.7d) involves the direct removal of sediment from stream banks (lateral erosion) or the stream bed. Sediment also enters the stream due to slumping of the stream bank resulting from bank erosion undercutting the stream bank. During high flow periods, a large proportion of the sediment that is transported through the stream network can originate from the stream channel (Merritt et al., 2003).

These types of soil erosion do not necessarily occur in isolation from one another. They are influenced by the landscape factors as well as rainfall characteristics. Loch and Silburn (1996) stated that the development of rill and gully erosion requires the concentration of flow and discharges that exceed critical thresholds, and as such will occur as the length of the slope increases. Hence, the dominant erosion process would be expected to follow a downslope sequence of splash–sheet–rill–gully (Loch and Silburn, 1996) as shown in Figure 2.8.

These erosion mechanisms occur in different part of hillslope (spatially variable) and in different times depending on the rainfall characteristics (temporally variable). A qualitative scheme of rainfall intensity versus rainfall duration is proposed with the distinction of different types of erosion mechanisms (Figure 2.9). It is worth noting that a real rainfall event has seldom a constant intensity while it is composed of distinct storms with different return period (T).
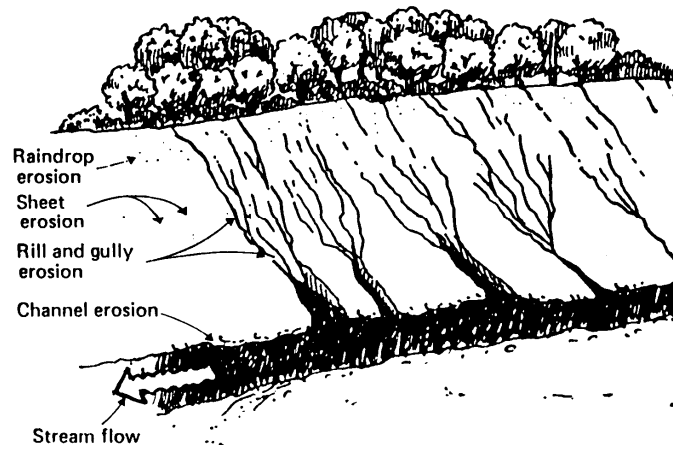
Figure 2.8 Soil erosion mechanisms on a hillslope.
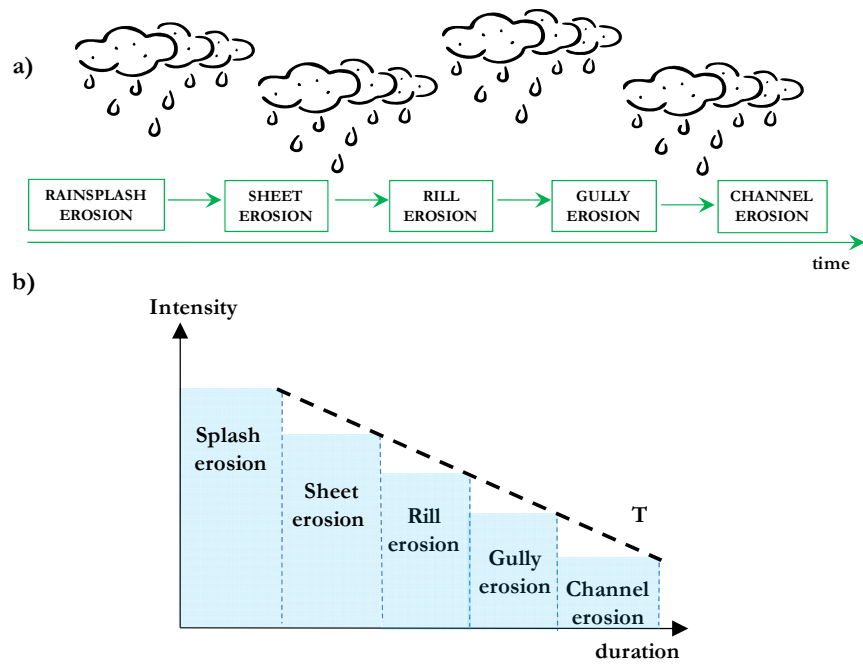
Figure 2.9 A qualitative scheme intensity-duration for different erosion mechanisms: a) temporal scheme and b) rainfall intensity versus duration for different erosion mechanisms.

2.1.3   Spatial and temporal occurrence

Generally, "sediment-water flows" that also include hyperconcentrated flows occur in basins characterised by steep slopes and channels that have large amounts of loose debris and where erosion phenomena can occur as the result of intense rainfall events.

The scientific literature provides examples of these phenomena, occurred in several basins in the world (Batalla et al., 1999; Hürlimann et al., 2003; Marchi et al., 2002, 2009; Marchi and Cavalli, 2007; Godt and Coe, 2007; Santi et al., 2008; Marcato et al., 2012). These basins or sub-basins, that were affected by different sediment-water flows occurred in the past, are characterised by a drainage area variable between 0.1 km^2 (e.g. left subbasin of Rio Cucco, Marchi et al., 2009) to hundreds of km^2 (120 km^2 for Huasamayo stream catchment, Argentina, Marcato et al., 2012, Figure 2.10) with the presence of a main channel that have a length variable between few to several kilometers and average slope angle variable between 9° to 25°.
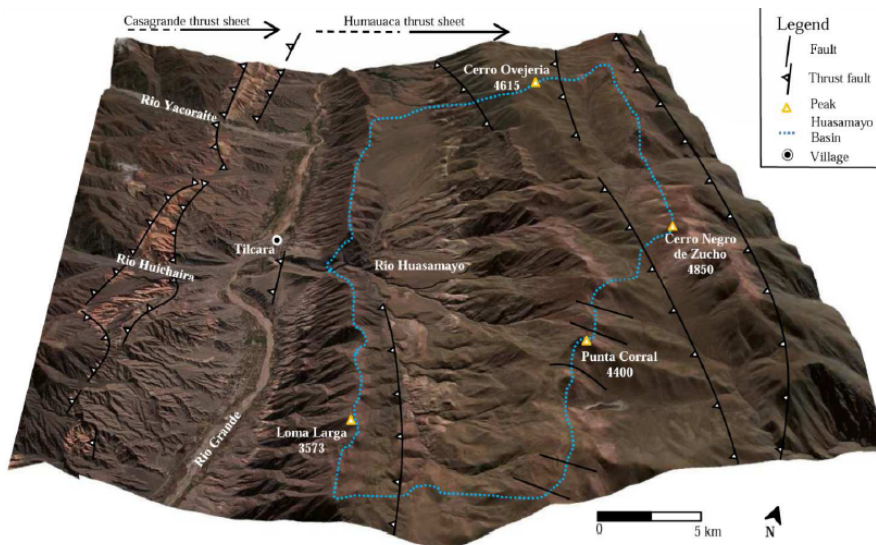
Figure 2.10 Example of areal extension: Huasamayo catchment, Argentina (Marcato et al., 2012).

According to Montgomery and Fofoula-Georgiou (1993), local slope and the contributing drainage area are important factors for the overland flow erosion. According to the authors, channels on slopes in excess of

20-30% are debris flow-dominated (Figure 2.11). In this way, in the same basin, it is possible to individuate sections of channel where debris flows are dominant processes and sections of channel where bedload transport are dominant processes. Depending on the predominance of the two processes, different flow-like phenomena can occur.
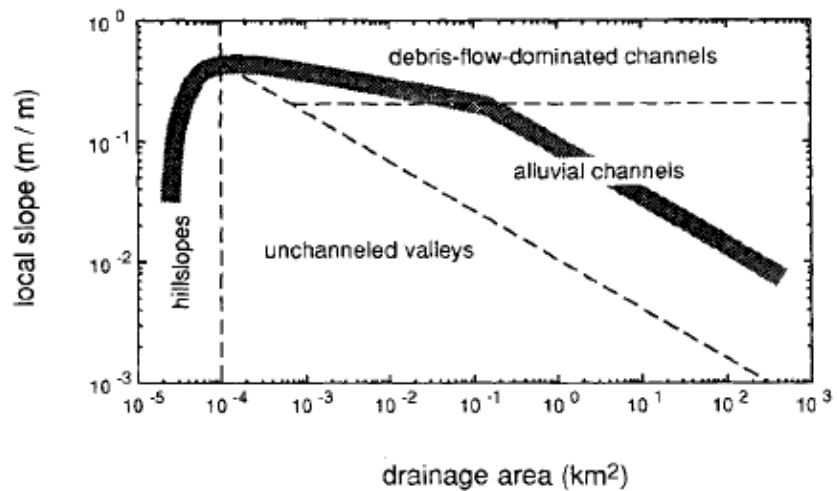
Figure 2.11 Schematic illustration of relations between drainage area and local slope depicting hillslope/valley transition and channel inititation criteria (Montgomery and Fofoula-Georgiou, 1993).

At the outlet of the basins, the alluvial fans testify the erosion processes that have characterised the upstream area during the years and the occurrence of different past flow-like phenomena. Generally, the alluvial deposits are composed of different grain sizes and different materials that are related both to flows occurred in different events and to different stages occurred in the same event. For example, for the 2003 event occurred in the Rio Cucco basin (eastern Italian Alps) (Figure 2.12), Marchi et al. (2009) noted that the sediment deposition on the alluvial fan of the Rio Cucco was dominated by debris flow, but also there are evidences of less-concentrated flows that contributed to transfer of solid material from the drainage basin to the alluvial fan (Figure 2.13).
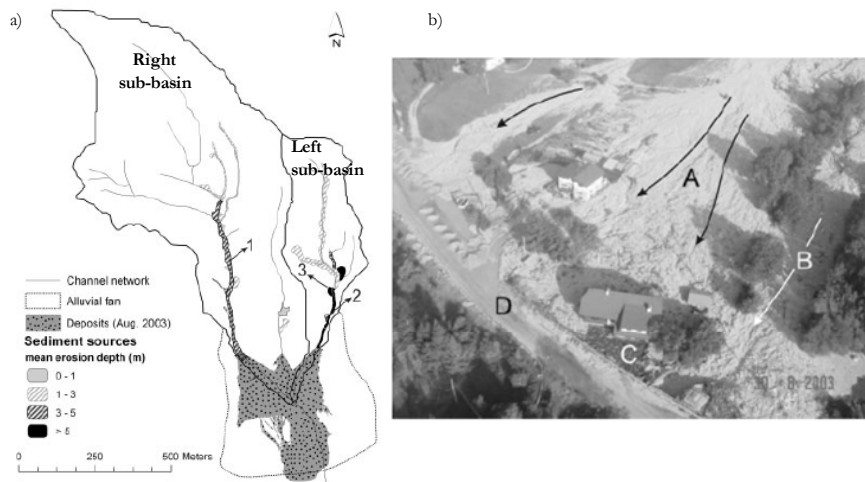
Figure 2.12 Rio Cucco basin - sediment sources for the 2003 event: a) erosion depth; b) deposits on the lower part of the alluvial fan (Marchi et al., 2009).
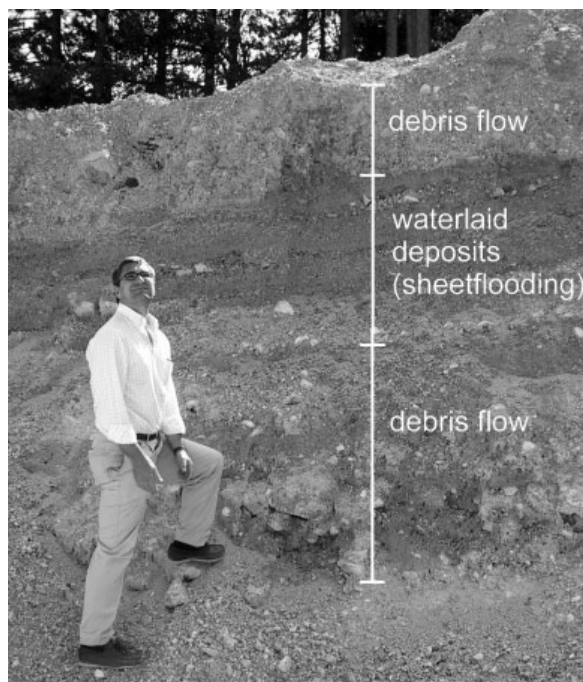
Figure 2.13 Deposits in the central part of the alluvial fans (Rio Cucco, Marchi et al., 2009).

For the same event and based on field surveys, the authors show that the maximum values of erosion depths in the channel systems are often related to their slope, which influences both sediment storage and runoff erosivity. In particular, the authors show that the highest vertical erosion was observed in channels that couple a slope sufficiently high to determine high-flow erosivity (slope=0.3-0.4) with the presence of very thick erodible bed material (Figure 2.14).
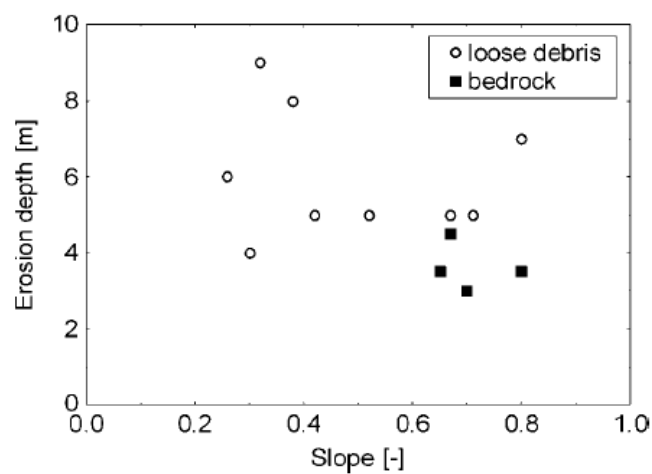
Figure 2.14 Relation between channel slope and depth of vertical erosion. Loose debris and bedrock refer to the bed material observed after the 2003 event (Marchi et al., 2009).

Based on two eyewitnesses that testified time and flow type during the event and on the results of field observations, the authors established a budget between simulated water runoff volumes and solid volumes eroded from the watershed, highlighting that: i) the different behavior of the sub-basins (left sub-basin has a high value of sediment concentration, while the right sub-basin has a low value of sediment concentration) that form the same basin; ii) different phases within the same event and iii) different phenomena like debris flows, hyperconcentrated flows and floods occur at different time and space scales (Figure 2.15).
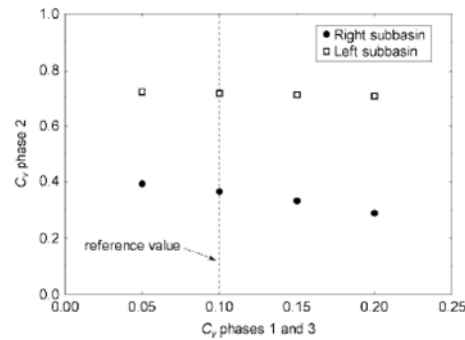
Phase (time interval—Central Europe Time)	Left subbasin			Right subbasin		
	V_w (m³)	C_v (—)	V_s (m³)	V_w (m³)	C_v (—)	V_s (m³)
1 (1530–1700)	4 460	0·10	500	14 320	0·10	1 590
2 (1700–1800)	10 280	0·72	26 010	28 300	0·36	16 230
3 (1800–2000)	4 400	0·10	490	19 650	0·10	2 180
Total	19 140		27 000	62 270		20 000

Note: V_w, water volume; V_s, solid volume; C_v, sediment concentration by volume.

Figure 2.15 Water–sediment balance during the three phases of the 2003 event (Marchi et al., 2009).

Another important distinctive aspect of the hyperconcentrated flows is the strong spatial and temporal variability related to the variations of discharge and sediment concentration over time and space. With reference to these two variables, in the Moscardo torrent, a small channel in the Eastern Italian Alps, monitored for several years, Marchi et al. (2002) analysed the discharges obtained by the ultrasonic sensors and video images recorded during the 1996 event distinguishing different stages and stressing that a single debris-flow wave can be composed of different types of flow (Figure 2.16). In particular, they noted that "the presence of a steep front causes debris-flow hydrographs to have a typical peaked shape, such as that often described in the literature (e.g. Pierson, 1986; Suwa et al., 1993; Iverson, 1997). But the tail of this wave has generally a lower solid concentration and may be a hyperconcentrated flow or even normal streamflow, as far as the type of flow is concerned (Costa, 1984; Pierson, 1986; Genevois et al., 2000). And in some debris flows, like those in the Moscardo Torrent in 1996, the front is preceded by an evident precursory surge, consisting of a hyperconcentrated flow or normal streamflow." Therefore, the hyperconcentrated flows can occur earlier as precursory sign or subsequentely than the occurrence of debris flows.
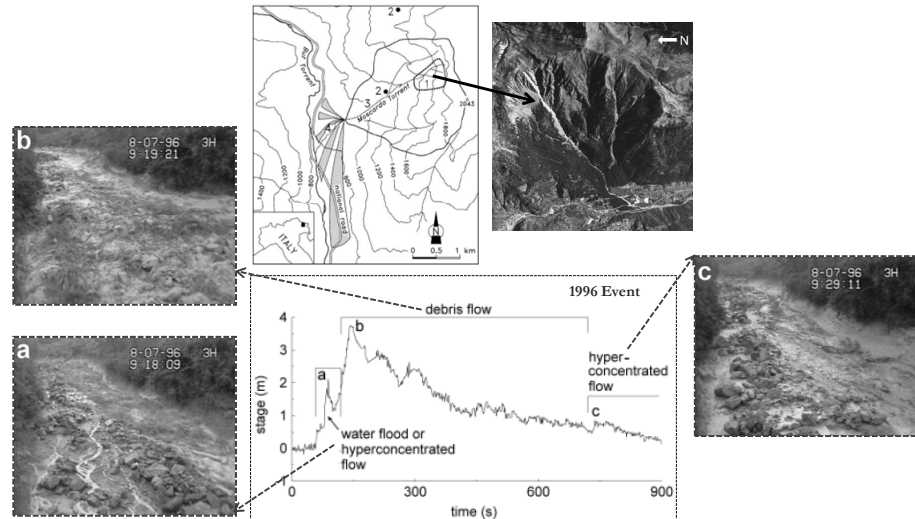
Figure 2.16 A single debris-flow wave (Moscardo Torrent, event of July 8, 1996, upstream ultrasonic gauge) (modified from Marchi et al., 2002).

In order to differentiate between different types of sediment-laden-flows in volcanic channels, Lavigne and Suwa (2004) monitored discharges and sediment concentrations of 21 debris flows, 5 hyperconcentrated flows, and 13 stream flows at the Curah Lengkong channel of Mount Semeru, East Java province, Indonesia. Their study shows that: i) large sediment discharges result from high intensities of rainfall and from the strong erosion of weathered river banks; ii) the discharge of debris flows varies widely over time and following the main surge, discharge usually decreases gradually (Figure 2.17a,b), unless heavy rains fall during the flow occurrence; iii) hyperconcentrated flows and stream flows move more slowly at peak flow than the debris flows and maximum discharge for them is less than the peak discharge of debris flow surges (Figure 2.17c-f), finally iv) there is a high correlation between sediment volume and the maximum discharge of flow for different types of phenomena (Figure 2.18).
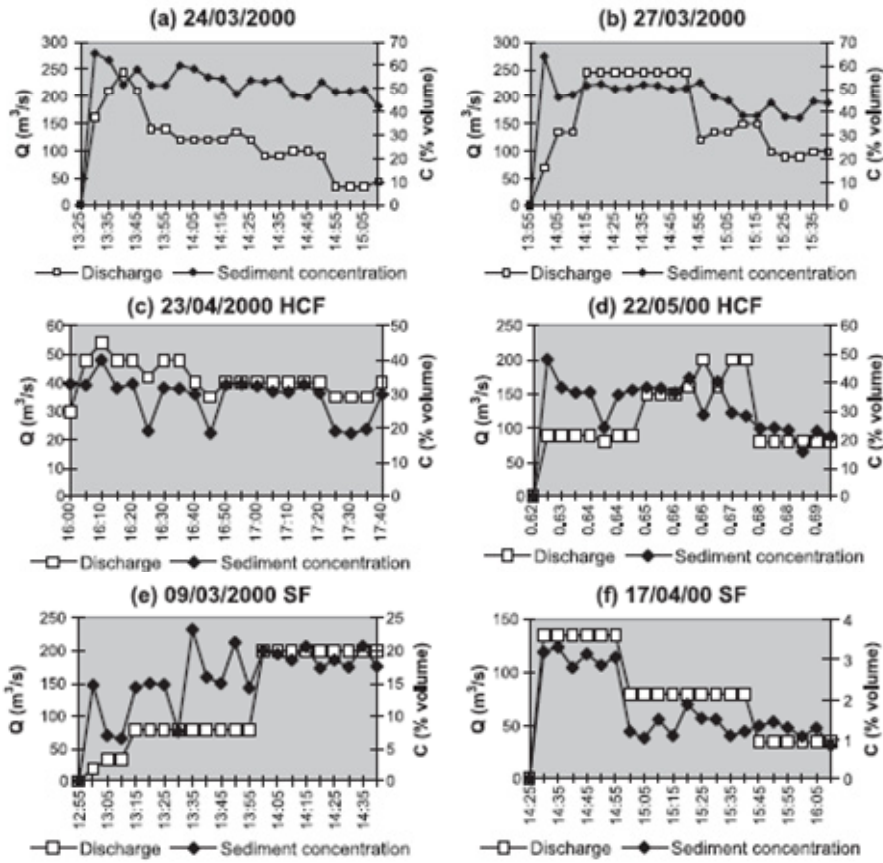
Figure 2.17 Discharge and sediment concentration vs. time for some debris flows (a, b), some hyperconcentrated flows (c, d) and some stream flows (e, f) that occurred in the Curah Lengkong river in 2000 (Lavigne and Suwa, 2004).
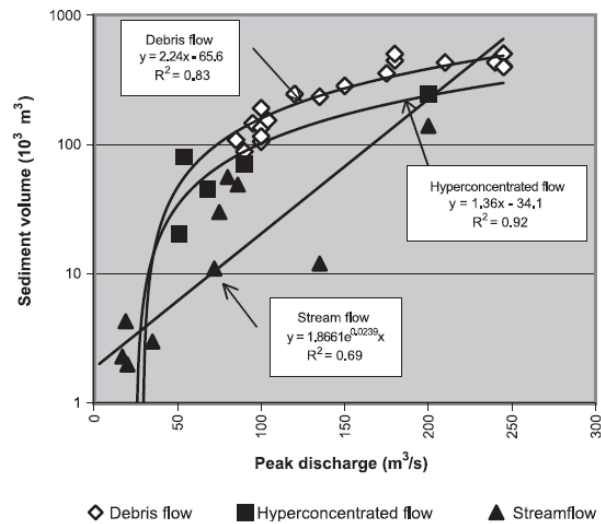
Figure 2.18 Sediment volume vs. peak discharge for debris flows, hyperconcentrated flows, and stream flows in the Curah Lengkong river (Lavigne and Suwa, 2004).

These examples, briefly described, testify the high temporal and spatial variability that usually characterises the "class of sediment-water flows" to which the hyperconcentrated flows belong. In particular, the occurrence of these phenomena strongly depend on: i) rainfall characteristics (intensity and duration) and the relative spatial distribution on the basin; ii) morphometric parameters of the catchment and channel (area, slope angle, length of the channels, among others) that affect the time of occurrence, the discharges and sediment volumes; iii) the hydraulic and mechanical properties of the soils that respectively affect the rainfall infiltration and runoff generation and the slope stability.

2.1.4 Approaches for modeling

General features

During the last decades many different models and relations have been proposed to describe and predict soil erosion by water and associated sediment yield, varying considerably in their objectives, time and spatial scale involved, as well as in their conceptual basis (de Vente and Poesen, 2005).

According to Merritt et al. (2003), these models differ in terms of complexity, processes considered and data required for model calibration. In general, there is no "best" model for all applications and, moreover, several factors can affect the choice of a model. Among these factors, it is worth mentioning:
- data requirements of the model including the spatial and temporal variation of model inputs and outputs;
- the accuracy and validity of the model, reflecting the model capabilities;
- the objectives of the model users, including the ease of use of the model, the scales at which model outputs are required and their form (such as concentration vs load);
- hardware requirements of the model.

For soil erosion analysis, the models can be divided into three main categories (Merritt et al., 2003; Aksoy and Kavvas, 2005; de Vente and Poesen, 2005; Lastoria et al., 2008, Terranova et al., 2009; among others): i) qualitative models; ii) semiquantitative models and iii) quantitative models (encompassing empirical, conceptual, and physically based models) (Figure 2.19).

Qualitative models include models based on the direct observation of the soil erosion in a given area through the use of remote sensing or aerial photo interpretation and through the construction of geomorphologic maps (Terranova et al., 2009; Lastoria et al., 2008).

Semiquantitative models provide results, which are generally expressed in terms of erosion classes computed with reference to different weights given to the factors influencing soil erosion (Lastoria et al., 2008).

Finally, quantitative models provide estimates of soil erosion, through empirical equations obtained from statistical analyses of data collected from field experiments (empirical models), through relationships among the involved variables based on the physical erosion processes (conceptual models) or through mathematical relationships describing all the main processes affecting the soil erosion (physically based models).
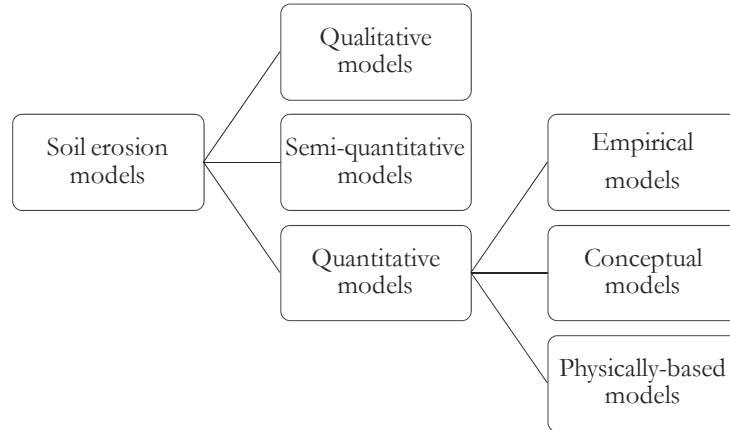
Figure 2.19 Models for soil erosion.

With reference to quantitative models, that are the most used approaches in the scientific literature, they can be divided into three main categories, depending on the physical processes simulated by the model, the model algorithms describing these processes and the data dependence of the model (Merritt et al., 2003):

- Empirical models;
- Conceptual models;
- Physically-based models.

Despite this distinction, most of the models do not fall strictly into one category, as even the physically-based models still retain some empirism in their algorithms (de Vente and Poesen, 2005). Difficulties are due to the combination of natural complexity, spatial heterogeneity, and the lack of available data (Jakeman et al. 1999; Wasson, 2002). Factors used to describe erosion and transport that return in most models are land use, slope, precipitation amount and intensity, runoff and peak runoff rates, runoff shear stress, soil cohesion, and surface roughness. These variables are often difficult to assess, far from constant in space and time, and interact with each other. In this way, the system has a high degree of complexity, that is difficult to express by physical equations (de Vente and Poesen, 2005).

In Table 2.4 some erosion models are reported with the scale of analysis that is used in their approaches. Table 2.5 shows the main input/output data and the processes represented in some models individuated by Merritt et al. (2003).

Table 2.4 Erosion/sediment transport models (modified from Merritt et al., 2003; Aksoy and Kavvas, 2005).

Model	Type	Scale	Reference
USLE	Empirical	Hillslope	Wischmeier and Smith (1978)
MUSLE	Empirical	Hillslope	Kinnel and Risse (1998)
RUSLE	Empirical	Hillslope/Catchment	Renard et al. (1991, 1994)
SEDD	Empirical	Small catchment	Ferro and Porto (2000)
AGNPS	Conceptual	Small catchment	Young et al. (1987)
LASCAM	Conceptual	Catchment	Viney and Sivalapan (1999)
EMSS	Conceptual	Catchment	Vertessey et al. (2001), Watson et al. (2001)
HSPF	Conceptual	Catchment	Johanson et al. (1980)
IQQM	Conceptual	Catchment	Simons et al. (1996)
SWRRB	Conceptual	Catchment	USEPA (1994)
SEDNET	Empirical/conceptual	Catchment	Prosser et al. (2001)
IHECRAS-WQ	Empirical/conceptual	Catchment	Jakeman et al. (1990, 1994a,b), Dietrich et al. (1999)
ANSWERS	Physically based	Small catchment	Beasley et al. (1980)
LISEM	Physically based	Catchment	Takken et al. (1999), De Roo and Jetten (1999)
CREAMS	Physically based	Field 40–400 ha	Knisel (1980)
WEPP	Physically based	Hillslope Catchment	Laflen et al. (1991)
EUROSEM	Physically based	Field Small catchment	Morgan et al. (1998)
KINEROS	Physically based	Catchment	Smith (1981), Woolhiser et al. (1990)
KINEROS2	Physically based	Catchment	Smith et al. (1995a,b)
RUNOFF	Physically based	Catchment	Borah (1989)
WESP	Physically based	Small catchment	Lopes (1987), Lopes and Lane (1988)
CASC2D-SED	Physically based	Catchment	Johnson et al. (2000)
SEM	Physically based	Catchment	Storm et al. (1987)
SHESED	Physically based	Catchment	Wicks (1988)

Model	Type	Scale	Reference
GUEST	Physically based	Plot	Yu et al. (1997), Rose et al. (1997)
PERFECT	Physically based	Field	Littleboy et al. (1992)
TOPOG	Physically based	Hillslope	CSIRO Land and Water, TOPOG Homepage; Gutteridge Haskins and Davey (1991)
MIKE-11	Physically based	Catchment	Hanley et al. (1998)
EROSION2D/3D	Physically based	Catchment	Schimdt et al. (1999)

Table 2.5 Processes represented in some erosion models (Merritt et al., 2003).

Model	Rainfall-runoff	Land surface sediment			Gully	In-stream sediment			Sediment associated water quality	
		G	T	D		G	T	D	Land	In-stream
AGNPS	yes	yes	no	no[a]	yes	yes	yes	yes	yes	yes
ANSWERS	yes	yes	yes	yes	no	no	no	no	no	no
CREAMS	yes	yes	yes	yes	no	no	no	no	yes	no
EMSS	yes	no[b]	no	no	no	yes	yes	yes	no	no
GUEST	yes	yes	yes	yes	no	no	no	no	no	no
HSPF	yes	yes	yes	yes	yes	yes	yes	yes	yes	yes
IHACRES-WQ	yes	no	no	no	no	yes	yes	yes	yes	yes
IQQM	yes	no	no	no	no	no	no	no	no	no
LASCAM	yes	yes	no	no	no	yes	yes	yes	yes	yes
LISEM	yes	yes	no	no	no	yes	yes	yes	no	no
MIKE-11	yes	yes	yes	yes	no	yes	yes	yes	yes	yes
PERFECT	yes	yes	no	no	no	no	no	no	yes	no
SEDNET	yes	yes	no	no[a]	yes	yes	yes	yes	yes	yes
SWRRB	yes	no	no	no	no	yes	yes	yes	yes	yes
TOPOG	yes	yes	yes	yes	no	no	no	no	no	no
USLE	no	yes	no	no	no	no	no	no	no	no
WEPP	yes	yes	yes	yes	no	yes	yes	yes	no	no

G, sediment generation; T, sediment transport; D, deposition.
[a] Requires a sediment delivery ratio (SDR) to compute sediment yield from gross erosion.
[b] Uses prescribed loads for a land use type.

Empirical models

According to Merritt et al. (2003), empirical models are generally the simplest of all model types. They are based primarily on the analysis of observations and seek characterising response from these data (Wheater et al., 1993). Jakeman et al. (1999) state that "the feature of this class of models is their high level of spatial and temporal aggregation and their incorporation of a small number of causal variables". Many empirical models are based on the analysis of catchment data using stochastic techniques and are ideal tools for the analysis of data in catchments

(Wheater et al., 1993). Parameter values in empirical models may be obtained by calibration, but are more often transferred from calibration at experimental sites (Merritt et al., 2003).

Empirical models are often criticized for employing unrealistic assumptions about the physics of the catchment system, ignoring the heterogeneity of catchment inputs and characteristics, such as rainfall and soil types, as well as ignoring the inherent non-linearities in the catchment system (Wheater et al. 1993).

Nonetheless, empirical models are frequently used in preference to more complex models as they can be implemented in conditions with limited data and parameter inputs, and are particularly useful as a first step in identifying sources of sediment (Merritt et al. 2003).

The first and most modern empirical model is the Universal Soil Loss Equation (USLE) (Wischmeier and Smith, 1978) that is used widely within the United States and worldwide. It was developed in the 70s by researchers U.S. Department of Agriculture (USDA) and the model has undergone much research and a number of modifications (e.g. MUSLE, USLE-M., Kinnel and Risse, 1998). The model has also been upgraded to take into account additional information that has become available since the development of the USLE (RUSLE, Renard et al., 1994). Although developed for application to small hillslopes, the USLE and its derivatives have been incorporated into many catchment scale erosion and sediment transport modeling applications.

The basic USLE is an empirical overland flow or sheet-rill erosion regression equation based primarily on observations. It estimates the evarage annual soil loss from hillslopes, computing the soil loss (A) per unit area as product of six terms: the rainfall erosivity factor (R), the soil erodibility factor (K), the slope-length factor (L), the slope-steepness factor (S), the cover and management factor (C) and the support practices factor (P) (Wischmeier and Smith, 1978). Table 2.6 shows the main features of the USLE model.

Table 2.6 Main features of the USLE model (modified from Merritt et al., 2003).

USLE MODEL	
Description and structure model	Soil erosion model, developed in the 1970s by USDA. It is an empirical overland flow or sheet-rill erosion regression equation based primarily on observations. As with most empirical models, the USLE is not event responsive, providing only an annual estimate of soil loss. It ignores the processes of rainfall-runoff, and how these processes affect erosion, as well as the heterogeneities in inputs such as vegetation cover and soil types.
Scale	Hillslope, but it has been incorporated into many catchment scale erosion and sediment trasport model.
Input data	Annual rainfall Estimate of soil erodibility Land cover information Topographical information
Model outputs	Annual estimate of soil erosion. Model outputs are both spatially and temporally lumped.
Erosion/ transport modelling	Equation: $A = R \cdot K \cdot L \cdot S \cdot C \cdot P$ where A is the estimated soil loss per unit area, R is the rainfall erosivity factor, K is the soil erodibility factor, L is the slope-length factor, S is the slope-steepness factor, C is the cover and management factor, and P is the support practices factor (Wischmeier and Smith, 1978).
Limitations	The original model is not event-based and as such cannot identify those events most likely to result in large-scale erosion. Gully erosion and mass movement are ignored and the deposition of sediment is not considered to occur in the modelled area (Zhang et al., 1995).
Revisions and modifications	Modified USLE, revised USLE (Renard and Ferreira, 1993; Renard et al., 1994); USLE-M (Kinnell and Risse, 1998)

Some examples of application of this model are represented by the potential erosion maps for Italy (Van der Knijff et al., 1999) and for the Aterno-Pescara river basin (Lastoria et al., 2008) (Figure 2.20).
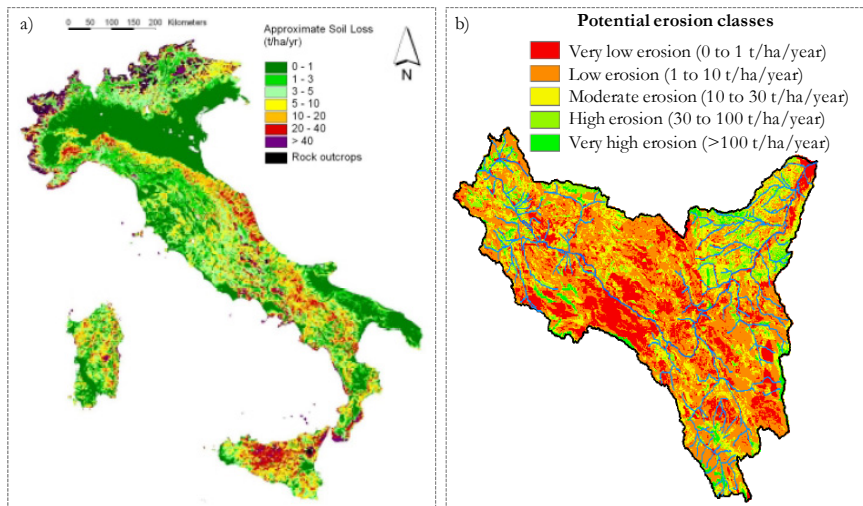
Figure 2.20 Erosion Maps using USLE model: a) for Italy (Van der Knijff et al., 1999); b) for the Aterno-Pescara basin (Lastoria et al., 2008).

Conceptual models

According to Merritt et al. (2003), the conceptual models are typically based on the representation of a catchment as a series of internal storages. They usually incorporate the underlying transfer mechanisms of sediment and runoff generation in their structure, representing flow paths in the catchment as a series of storages, each requiring some characterisation of its dynamic behavior. Conceptual models include a general description of catchment processes, without including the specific details of process interactions, which would require detailed catchment information (Sorooshian, 1991). This allows these models to give an indication of the qualitative and quantitative effects of land use changes, without using large amounts of spatially and temporally distributed input data.

Parameter values for conceptual models have typically been obtained through calibration against observed data, such as stream discharge and concentration measurements (Abbott et al., 1986).

Beck (1987) noted that conceptual models are intermediate between empirical and physically-based models. Whilst they tend to be aggregated they still reflect the hypotheses about the processes governing system behavior. This is the main feature that distinguishes conceptual models from empirical models (Merritt et al., 2003).

An example of conceptual model is represented by the AGriculture NonPoint Source model (AGNPS) (Young et al., 1989). It is an event-based model that simulates runoff, sediment and nutrient transport from agricultural watersheds. The model divides the watershed into square cells uniformly distributed over the watershed. Table 2.7 shows the main features of the AGNPS model.

Table 2.7 Main features of the AGNPS model (modified from Merritt et al., 2003).

AGNPS MODEL	
Description and structure model	Non-point source pollution model developed by the US Department of Agriculture, Agricultural Research Service (USDA-ARS) in cooperation with the Minnesota Pollution Control Agency and the Soil Conservation Service (SCS) in the USA (Young et al., 1989). It contains a mix of empirical and physics-based components and utilises components of existing models in its structure including the RUSLE for predicting soil loss in grid cells. It contains both empirical and quasi-physically based algorithms and is fully distributed with land surface runoff and sediment processes modelled for the individual grid cell, and the outputs routed through to the catchment outlet. The calculations occur in three stages: 1) initial calculations, including estimates of upland erosion, overland runoff volume, pollutants from point source inputs, time until overland flow becomes concentrated and the level of soluble pollutants leaving the catchment via overland runoff, are made for each grid cell in a catchment; 2) the runoff volume leaving the cells containing impoundments and the sediment yields for primary cells are calculated; 3) the calculated sediments and nutrients are then routed through the rest of the cells.
Scale	Rural catchments ranging from a few to over 20000 hectares
Input data	Parameters describing catchment morphology; Land use variables; Precipitation data; For each grid cell, the input parameters include, cell number (from), receiving cell number, SCS curve number, a channel indicator that indicates the existence of a defined channel in a cell, land slope, land slope shape factor, field slope length, channel slope, channel sideslope, Manning's roughness coefficient, soil erodibility factor cover and management

	factor, support practices factor, surface condition constant, aspect, soil texture, fertilisation level, fertilisation availability factor, point source indicator, gully source level, COD factor, impoundment factor, and channel indicator.
Model outputs	Output values for the whole watershed include characteristic storm precipitation and the storm energy-intensity value. Hydrological outputs include runoff volume, peak runoff rate, and the fraction of runoff generated in the cell. Sediment outputs are sediment yield, sediment concentration, sediment particle size and distribution, upland erosion, amount of deposition (%), sediment generated in the cell, enrichment ratios by particle size, and delivery ratios by particle size.
Runoff modelling	Runoff in a catchment is simulated using the SCS curve number method, an empirical rainfall-runoff modelling technique developed in the United States by the Soil Conservation Service (SCS, 1972).
Erosion/transport modelling	Erosion and sediment transport are modelled using forms of the Universal Soil Loss Equation (USLE). Two different versions of the AGNPS model have been developed by the USDA-ARS. The original model implemented the USLE, while more recent versions now implement the RUSLE. A modification of the model, AGNPSm, replaces the SCS curve number and USLE topographic (LS) factor with alternative algorithms and links channel erosion by individual categories of particle size to runoff velocity and replacement of the uniform rainfall input by grid based precipitation input (Grunwald and Norton, 2000). Soil loss is calculated in AGNPS for each cell in the catchment.
Limitations	The grid size selected by the model user is the major factor influencing sediment yield calculations (Panuska et al., 1991)

Several studies have used the event–based AGNPS model and have compared the results to the observed data. Perrone and Madramootoo (1997) modeled a 26 km^2 watershed in Quebec (Suttles et al., 2003). Validation results produced average errors of 21.7% and 13.2% for surface runoff and sediment yield, respectively. Bingner et al. (1989) tested runoff and sediment yield predictions from the event–based AGNPS model on three small Mississippi watersheds, with favorable results (Suttles et al., 2003). Najim et al. (2006) have applied the AGNPS model in order to verify the applicability of the model for the simulation

of runoff, sediment and nutrient yields from a mixed forested watershed in Southeastern Thailand. Their study shows that the AGNPS model can be used in simulating runoff volume, sediment and soluble nitrogen yields from a mixed forested watershed, even though the model is primarily developed for agricultural watersheds (Figure 2.21).
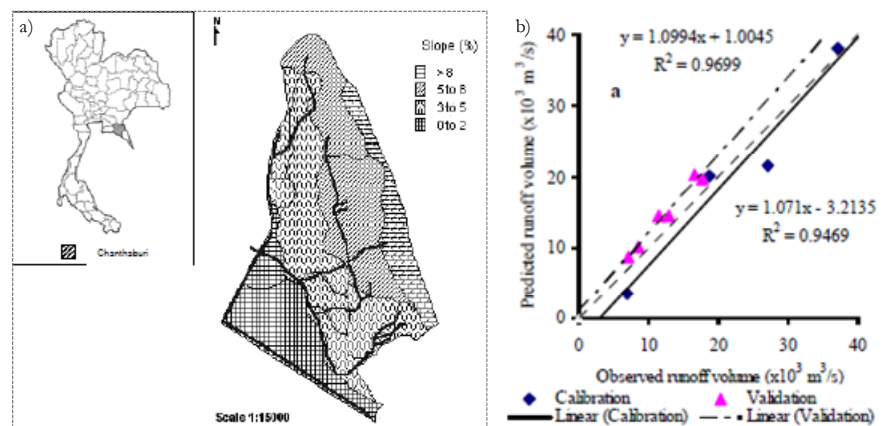
Figure 2.21 Example of AGNPS model application: a) Location of the study area (Southeastern Thailand); b) observed and model predicted outputs. (Najim et al., 2006).

Physically-based models

According to Merritt et al. (2003), the physically-based models are based on the solution of fundamental physical equations describing streamflow and sediment and associated nutrient generation in a catchment. Standard equations used in such models are the equations of conservation of mass and momentum for flow and the equation of conservation of mass for sediment (e.g. Bennett, 1974).

In theory, the parameters used in physically-based models are measurable but in practice, the large number of parameters involved and the heterogeneity of important characteristics, particularly in catchments, means that these parameters must often be calibrated against observed data (Beck et al., 1995; Wheater et al., 1993). This aspest creates additional uncertainty in parameter values (Merritt et al., 2003).

The derivation of mathematical expressions describing individual processes in physically-based models is subject to numerous assumptions that may not be relevant in many real world situations (Dunin, 1975). In general, the equations governing the processes in physically-based

models are derived at the small scale and under very specific physical conditions (Beven, 1989).

According to Aksoy and Kavvas (2005), the process based classification divides this type of models into *lumped* and *distributed*. A lumped model uses single values of input parameters with no spatial variability and results in single outputs, while a distributed model uses spatially distributed parameters and provides spatially distributed outputs by taking explicit account of spatial variability of the process. The model can be *deterministic* or *stochastic* depending upon the way the process is described. In physically-based models, the model is called *one-* or *two dimensional* depending upon the number of dimensions of the mass conservation equation used in the model. Erosion and sediment transport models generally take the non-*stationarity* in the erosion process into account although a number of them are interested only in the *steady state* case. A model is called an *event-based* model if it is used for the simulation of sediment produced by one single rainfall–runoff event. A *continuous model* is used for the simulation of sediment due to many consecutive rainfall–runoff events occurring during a season or longer time period. *Single-size* erosion and sediment transport models can only predict sediment transport for a mean grain size and can give the total sediment mass leaving the catchment. The sediment size distribution is very important in sediment quality since pollutants are usually sorbed to finest particles. This is achieved in *multi-size* models. In a similar manner, models with *rilled structure* perform better in the simulation of the natural topography in the watershed. Table 2.8 shows some physically-based models considering the main features as reported by Aksoy and Kavvas (2005).

Table 2.8 Phisically-based erosion and sediment transport models (Aksoy and Kavvas, 2005).

Model	Lumped	Distributed	Stochastic	Deterministic	1-D	2-D	Steady state	Unsteady state	Event-based	Continuous	Rilled structure	No rilled structure	Single-size	Multi-size
ANSWERS		×		×	×		×		×			×		×
LISEM		×		×	×		×		×		×		×	
CREAMS		×		×	×		×		×		×		×	
WEPP		×		×	×		×			×	×		×	
EUROSEM		×		×		×		×			×		×	
KINEROS		×		×		×		×				×	×	
KINEROS2		×		×		×		×			×			×
RUNOFF		×		×		×		×			×			×
WESP		×		×	×			×			×		×	
CASC2D-SED		×		×		×		×			×			×
SEM		×	×			×				×		×	×	
SHESED		×	×			×				×		×	×	

An important physically-based model is the Watershed Erosion Prediction Project (WEPP) (Nearing et al., 1989), developed in the USA. It predicts soil erosion and sediment delivery from fields, farms, forests, rangelands, construction sites and urban areas (Laflen et al., 1991). The main features of the WEPP model are reported in Table 2.9. This model was applied by Shen et al. (2009) to a catchment in the Three Gorges Reservoir Area (China), with satisfactory results for runoff and sediment yield. On the other hand, Pieri et al. (2007) show that WEPP model under-predict the sediment yield measured in some experimental plots in the Apennines Mountain Range, northern Italy.

Table 2.9 Main features of the WEPP model (modified from Merritt et al., 2003).

WEPP MODEL	
Description and structure model	The Watershed Erosion Prediction Project (WEPP) is a physically-based model developed in the United States. It uses mainly physics-based equations to describe hydrological and sediment generation and transport processes at the hillslope and in-streams scale. The model operates on a continous daily time-step. The model was intended to determine and/or assess the essential mechanisms controlling erosion by water, including anthropogenic impacts. The main processes are erosion and hydrological processes, plant growth and residue processes, water use processes, hydraulic processes and soil processes (Laflen et al., 1991).
Scale	Hillslope, watershed and in-stream scale
Input data	Knowledge of plant growth and residue components; Dates and management practices; Surface runoff volumes, hydraulic roughness and approximations of runoff duration and peak rate; Watershed configuration, channel topography, channel soils, channel management, channel hydraulic characteristics
Model outputs	The hillslope version provides estimates of spatial and temporal distributions of soil loss, sediment yield, sediment size characteristics, runoff volumes and the soil water balance. The profile version also considers sediment deposition and is applicable from the top of a hillslope to a channel. The basic output contains the runoff and erosion summary on a storm-by-storm, monthly, annual and average annual basis.

Runoff modelling	The erosional processes result from the forces and energies developed in hydrologic processes (Laflen et al., 1991). The components of the hydrological processes are climate, infiltration and a winter component that accounts for snow accumulation and melt. The water balance component uses information about climate, plant growth and infiltration to estimate daily potential evapotranspiration and soil and plant evaporation. Rainfall excess is predicted using the Green-Ampt Mein-Larson (GAML) infiltration equation. The peak runoff rate can be simulated using either kinematic wave overland flow routing or simplified regression equations.
Erosion/transport modelling	The erosion processes are sheet and rill erosion and erosion occurring in channels where detachment is due to hydraulic shear. The three stages of erosion (detachment, transport and deposition) are quantified using the rill–interill concept of describing sediment detachment (Laflen et al., 1991; Lane et al., 1995) and the Foster's equation. Sediment detachment and deposition in ephemeral gullies or permanent channels is simulated using a steady-state solution of the sediment continuity equation.
Limitations	The large computational and data requirements of the model may limit its applicability in catchments where there is often few data or available resources. The model does not account for erosion from permanent gullies and still contains a degree of empiricism.

Another important physically-based model, incorporated in GIS system, is the LImburg Soil Erosion Model (LISEM) (De Roo et al., 1996a,b; De Roo and Jetten, 1999). LISEM is a spatially distributed, physically-based hydrological and soil erosion model, developed by the Department of Physical Geography at Utrecht University and the Soil Physics Division at the Winard Staring Centre in Waneningen, the Netherlands, for planning and conservation purposes (Merritt et al., 2003). The main feautures of the LISEM model are reported in Table 2.10.

Table 2.10 Main features of the LISEM model (modified from Merritt et al., 2003).

LISEM MODEL	
Description and structure model	LISEM simulates the hydrology and sediment transport during and immediately after a single rainfall event in a small catchment. Basic processes incorporated in the model are rainfall, interception, surface storage in micro-depressions, infiltration, vertical movement of water in the soil, overland flow, channel flow, detachment by rainfall and throughfall, transport capacity and detachment by overland flow. Also, the influence of compaction (e.g. by tractor wheelings), small paved roads (smaller than the pixel size) and surface sealing on the hydrological and soil erosion processes is taken into account (Jetten, 2002). A new version, called "openLISEM" simulates runoff, sediment dynamics and shallow floods in rural and urban catchments. It is an event based model, that is designed to simulate the effects of detailed land use changes or conservation measures during heavy rainstorms. It is a model designed to be used in disaster risk management, not for long term estimates (http://blogs.itc.nl/lisem/about/). Model simulation is based on the solution of a number of physically-based equations describing water and sediment yield processes.
Scale	Catchments from 0.01 km² to several km²
Input data	Approximately 25 maps are required for simulation, including maps describing catchment morphology, vegetation (e.g. leaf area index, fraction of the soil with crop cover etc..), soil surface (e.g. random roughness); infiltration data depending on the selected infiltration model and rainfall data from single or multiple rainfall gauges. In this last situation, LISEM generates from the latter, a map showing the spatial distribution of rainfall intensity. Thus LISEM incorporates both the spatial and temporal variability of rainfall.
Model outputs	Outputs of the LISEM model include totals for such variables as runoff, sediment, infiltration and storage depression. Maps showing the spatial distribution of such factors as soil erosion and deposition, and maps of overland flow at desired time intervals during the simulation are also produced by LISEM. The model is also capable of producing hydrographs and sediment graphs for a rainfall event simulation at the outlet of catchment.

Runoff modelling	The model evaluates the runoff taking into account processes describing overland flow, channel flow, rainfall, interception, surface storage in micro-depressions and infiltration.
Erosion/transport modelling	LISEM does not simulate concentrated erosion in rills and gullies; rather it simulates flow detachment in the ponded area only. This can be seen as an intermediate between sheet and rill erosion. Processes describing sediment detachment by rainfall, throughfall and overland flow are included in addition to the transport capacity of the flow.
Limitations	The LISEM model requires detailed spatially and temporally variable data inputs. The performance of the LISEM model is constrained by the resolution and quality of GIS data inputs.

In literature, several applications of LISEM model exist at different basins over the world. In particular, the model was successfully calibrated for a 2 km^2 catchment on the Chinese Loess Plateau by Hessel et al. (2003), who also stressed that distinct calibrations are required for small and large runoff events. In addition, Hessel et al. (2006) tested the applicability of LISEM model in two further small catchments (5.7 km^2 and 2 km^2, Figure 2.22) of East African Highlands Mountains (in Tanzania and Kenya) and outlined that the LISEM model can, after calibration, provide accurate predictions of discharge for individual rainfall events, while an overestimation of soil loss from the catchments is achieved and simulated erosion patterns are more widespread than those observed. According to Hessel et al. (2006), these discrepancies can be mainly related to: i) accuracy of input data; ii) uncertainty of measured field data; iii) complexity of rainfall events, soil types and land use and iv) lack of processes not yet implemented in the model (throughflow or baseflow). Globally, the prediction of spatial erosion on a single rainfall event is accurate while average annual erosion is poorly evaluated.
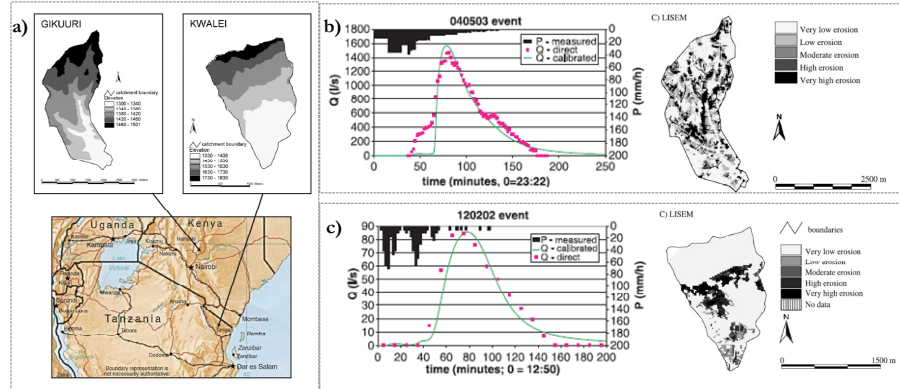
Figure 2.22 Location of African study area (a); discharge and LISEM erosion map for Gikuuri basin (b) and for Kwalei basin (c) (Hessel et al., 2006).

Baartman et al. (2012) applied the LISEM model to Prado catchment in SE Spain (50 km^2, Figure 2.23), in order to: i) test the model's performance for medium-sized catchments, ii) test the ability to simulate four selected typical Mediterranean rainfall events of different magnitude and iii) explore the relative contribution of these different storms to soil erosion using scenarios of future climate variability. It is found that the model is able to simulate storms of different magnitude, but a separate calibration set is needed for each event. In particular, high-magnitude rainfall events potentially contribute much more to total soil loss than lower magnitude events with a higher frequency.
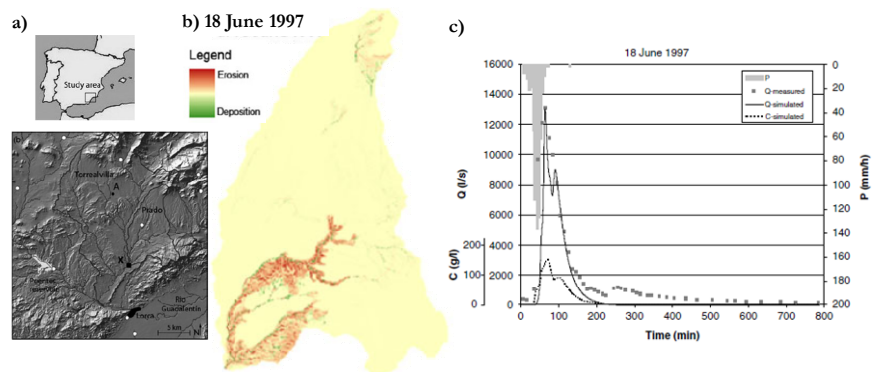
Figure 2.23 Location of Prado Catchment (a); simulated spatial pattern of net total soil loss (b) and precipitation (P, right axis), discharge (Q, second left axis) and sediment concentration (C, first left axis) at the Prado outlet (c) for the 18 June 1997 event (Baartman et al., 2012).

Recently, Rahmati et al. (2013) tested the LISEM model on a catchment (78.5 km^2) located in the North West of Iran. In this case, the accuracy of hydrograph, peak discharge and time to peak obtained through the LISEM model are reasonably accurate as well.

2.2 LANDSLIDES OF FLOW-TYPE

2.2.1 Classification

On a slope, different types of rainfall-induced slope instabilities can occur other than hyperconcentrated flows. Particularly, the landslides of flow-type are among the most dangerous natural hazards because they are frequently characterised by the lack of premonitory signs, long run-out distances and high velocities, causing victims and huge damages to structures and infrastructures. In the literature, several classifications exist for these phenomena.

Sharpe (1938) distinguished the types of movements in slips and flows and his classification was based on the rate of movement (slow to very rapid), type of material (earth or rock) and the role of water/ice (Figure 2.24).
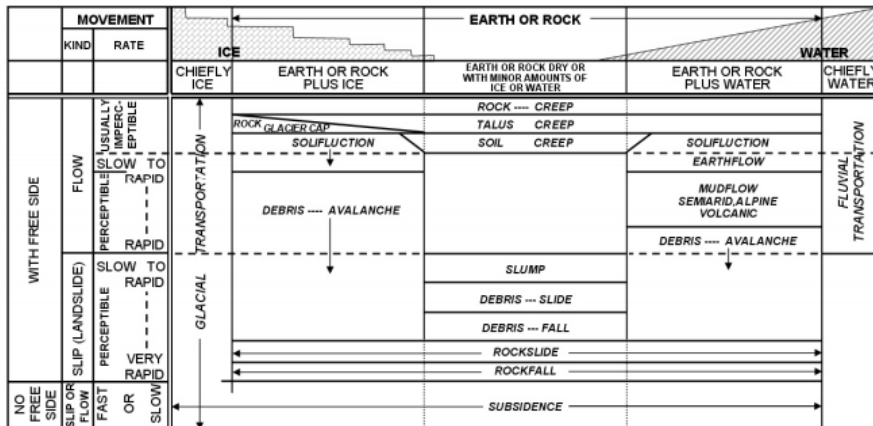
Figure 2.24 Classification of slope movements (Sharpe, 1938).

The classification proposed by Varnes (1978) is based on type of movement and type of material (Figure 2.25). With reference to flows, Varnes distinguished three main types: rock flow, debris flow and earth flows.

TYPE OF MOVEMENT		TYPE OF MATERIAL		
		BEDROCK	ENGINEERING SOILS	
			Predominantly coarse	Predominantly fine
FALLS		Rock fall	Debris fall	Earth fall
TOPPLES		Rock topple	Debris topple	Earth topple
SLIDES	ROTATIONAL	Rock slide	Debris slide	Earth slide
	TRANSLATIONAL			
LATERAL SPREADS		Rock spread	Debris spread	Earth spread
FLOWS		Rock flow	Debris flow	Earth flow
		(deep creep)	(soil creep)	
COMPLEX		Combination of two or more principal types of movement		

Figure 2.25 Slope movement type and processes (Varnes, 1978).

Based on the morphology of slope movements and some considerations on mechanism, material and rate of movement, Hutchinson (1988) identified eight slope movements. With reference to "Debris Movements of Flow-Like form" and based on the morphological features of these slope movements, the author individuated (Figure 2.26): 1) mudslides (non periglacial); 2) periglacial mudslides (gelifluction of clays); 3) flowslides ; 4) debris flows, very to extremely rapid flows of wet debris; 5) sturzstroms, extremely rapid flows of dry debris. According to the author, these phenomena differ markedly in terms of mechanisms: mudslides (1 and 2) predominantly slide rather than flow, flowslides and debris flows (3 and 4) exhibit varying degrees of sliding and flowing, while sturzstroms (5) are essentially flows and in terms of grain-size distribution with high clay contents in mudslides and coarse soils in flowslides and debris flows. In addition, with reference to debris flows, that especially occur in mountainous basins, the author underlines that there is a continuous spectrum of flow phenomena, from sediment-laden rivers (mass transport phenomena) to various types of debris flows (mass movements) (Figure 2.27).

Figure 2.26 Classification of "Debris Movements of Flow-Like Form" (Hutchinson, 1988).
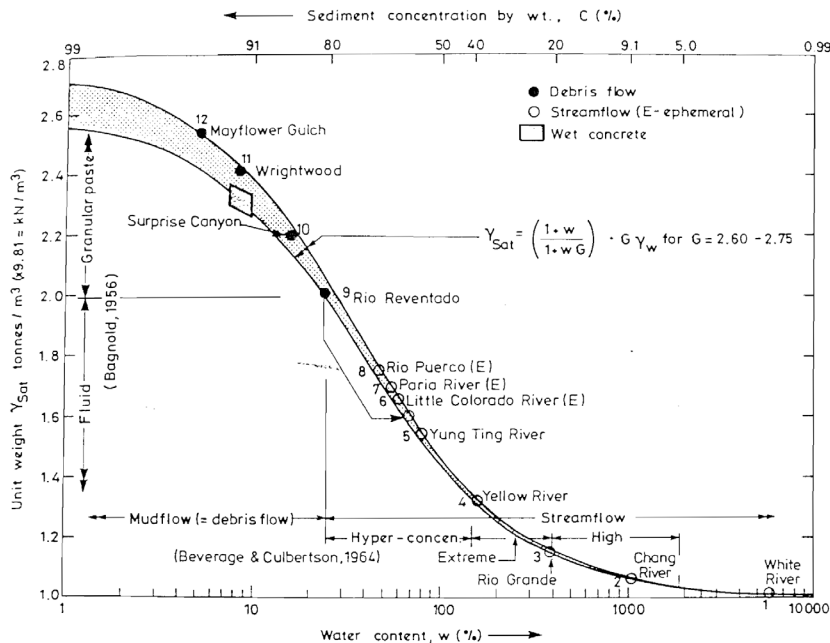
Figure 2.27 Continuous spectrum of sediment concentration, from sediment-laden rivers to debris flows (Hutchinson, 1988).

Cruden and Varnes (1996) analysed the Varnes classification and introduced features related to landslide activity (state, distribution and style) and related to rate of movement, water content and material (Table 2.11).

Table 2.11 Classification of landslide and glossary for forming names of landslides (Cruden and Varnes, 1996).

Type of movement	Type of material		
	Bedrock	Engineering soils	
		Predominant coarse	Predominant fine
Fall	Rock fall	Debris fall	Earth fall
Topple	Rock topple	Debris topple	Earth topple
Slide	Rock slide	Debris slide	Earth slide
Spread	Rock spread	Debris spread	Earth spread
Flow	Rock flow	Debris flow	Earth flow

Activity		
State	Distribution	Style
Active	Advancing	Complex
Reactivated	Retrogressive	Composite
Suspended	Widening	Multiple
Inactive	Enlarging	Successive
Dormant	Confined	Single
Abandoned	Diminishing	
Stabilized	Moving	
Relict		

Description of first movement			
Rate	Water Content	Material	Type
Extremely rapid	Dry	Rock	Fall
Very rapid	Moist	Soil	Topple
Rapid	Wet	Earth	Slide
Moderate	Very wet	Debris	Spread
Slow			Flow
Very slow			
Extremely slow			

Description of second movement			
Rate	Water Content	Material	Type
Extremely rapid	Dry	Rock	Fall
Very rapid	Moist	Soil	Topple
Rapid	Wet	Earth	Slide
Moderate	Very wet	Debris	Spread
Slow			Flow
Very slow			
Extremely slow			

Referring to rate of movement, the authors proposed few changes of the velocity classes proposed by Varnes (1978) and associated to each class a probable destructive significance (Table 2.12). With reference to landslides of flow-type, water content, mobility and evolution of the movement are important factors affecting the transition from slides to flows, stressing that "debris slides may become extremely rapid debris flows or debris avalanches as the displaced material loses cohesion, gains water, or encounters steeper slopes".

Table 2.12 Landslide velocity scale and probable destructive significance of different velocity classes (Cruden and Varnes, 1996).

Landslide velocity class	Description	Velocity	Probable desctructive significance
7	Extremely rapid	>5m/s	Catastrophe of major violence; building destroyed by impact of displaced material, many deaths, escape unlikely.
6	Very rapid	3m/min - 5m/s	Some lives lost; velocity too great to permit all persons to escape.
5	Rapid	1.8m/h - 3m/min	Escape evacuation possible; structures, possessions and equipment destroyed.
4	Moderate	13m/month- 1.8m/h	Some temporary and insensitive structures can be temporarily maintained.
3	Slow	1.6m/year - 13m/month	Remedial reconstruction can be undertaken during movement; insensitive structures can be maintained with frequent maintenance work if total movement is not large during a particular acceleration phase.
2	Very slow	16mm/year - 1.6m/year	Some permanent structures undamaged by movement
1	Extremely slow	<16mm/year	Imperceptible without instruments; costructionpossible with precautions

Leroueil et al. (1996) proposed a "geotechnical characterization" of the slope movements taking into account the mechanical characteristics of rock and soils involved into slope movement and introducing four different stages of the movement: pre-failure stage, failure stage, post-failure stage and reactivated stage (Figure 2.28).
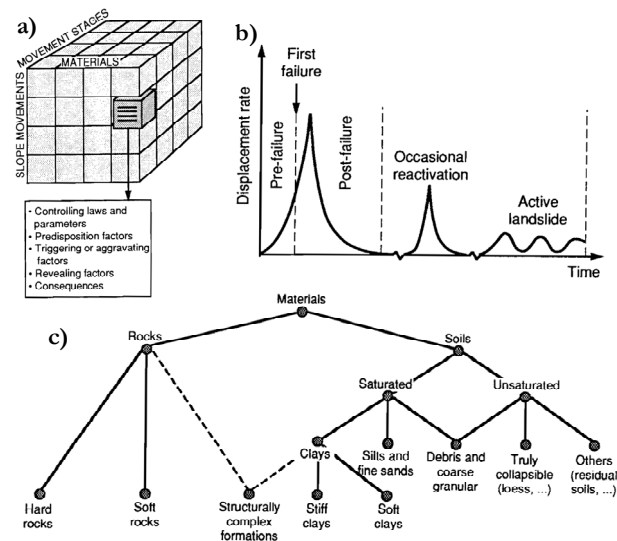
Figure 2.28 Slope movements: a) scheme, b) stages of movement, c) material type (Leroueil et al., 1996).

Hungr et al. (2001) reviewed the landslide classifications, discussing the landslide recognition criteria and focusing on the landslides of flow-type. The authors define these types of phenomena as "flow-like mass movements", indicate the different materials involved in the movement and identify ten groups (Figure 2.29) on the basis of: i) material type, ii) water content, iii) presence of excess pore-pressure or liquefaction at the source of the landslide; iv) presence of a defined recurrent path (channel) and deposition area (fan); v) velocity and vi) peak discharge of the event.

Material	Water Content[1]	Special Condition	Velocity	Name
Silt, Sand, Gravel, Debris (talus)	dry, moist or saturated	- no excess pore-pressure, - limited volume	various	Non-liquefied sand (silt, gravel, debris) flow
Silt, Sand, Debris, Weak rock[2]	saturated at rupture surface content	- liquefiable material[3], - constant water	Ex. Rapid	Sand (silt, debris, rock) flow slide
Sensitive clay	at or above liquid limit	- liquefaction *in situ*,[3] - constant water content[4]	Ex. Rapid	Clay flow slide
Peat	saturated	- excess pore-pressure	Slow to very rapid	Peat flow
Clay or Earth	near plastic limit	- slow movements, - plug flow (sliding)	< Rapid	Earth flow
Debris	saturated	- established channel[5], - increased water content[4]	Ex. Rapid	Debris flow
Mud	at or above liquid limit	-fine-grained debris flow	> Very rapid	Mud flow
Debris	free water present	- flood[6]	Ex. Rapid	Debris flood
Debris	partly or fully saturated	- no established channel[5], - relatively shallow, steep source	Ex. Rapid	Debris avalanche
Fragmented Rock	various, mainly dry	- intact rock at source, - large volume[7]	Ex. Rapid	Rock avalanche

[1] Water content of material in the vicinity of the rupture surface at the time of failure.
[2] Highly porous, weak rock (examples: weak chalk, weathered tuff, pumice).
[3] The presence of full or partial *in situ* liquefaction of the source material of the flow slide may be observed or implied.
[4] Relative to *in situ* source material.
[5] Presence or absence of a defined channel over a large part of the path, and an established deposition landform (fan). Debris flow is a recurrent phenomenon within its path, while debris avalanche is not.
[6] Peak discharge of the same order as that of a major flood or an accidental flood. Significant tractive forces of free flowing water. Presence of floating debris.
[7] Volume greater than 10,000 m^3 approximately. Mass flow, contrasting with fragmental rock fall.
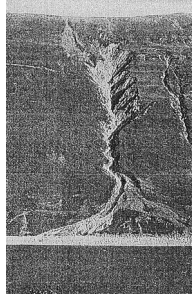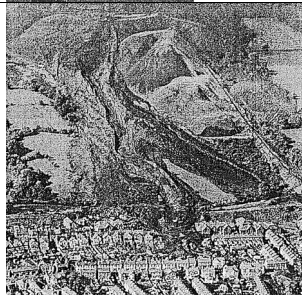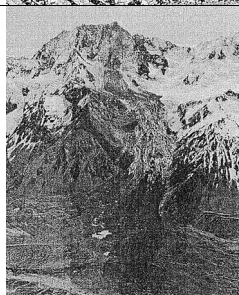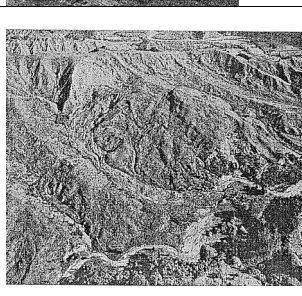
Figure 2.29 Classification of landslides of flow-type (Hungr et al., 2001).

Hutchinson (2004) proposed a review of flow-like mass movements and identified two main groups (Table 2.13): i) phenomena that occur in granular materials and ii) phenomena occuring in fine-grained materials based on morphology, material properties, behavior and mechanisms.

Table 2.13 Classification of flow-like mass movements (Hutchinson, 2004).

Name		Brief description	Examples
Flow-like movements in granular materials	Debris flows	"Very rapid saturated flowsof widely graded rock debris on mountains or, in the case of volcanic debris flows, pyroclastic materials associated with volcanoes"	
	Flowslides	"involve the collapse of saturated high porosity material, generally granular, generating excess pore-water pressures and hence rapid motion in the resulting slide mass"	
	Rock avalanches	"extremely rapid flow-like movements of fragmented rock from large rock slides or rock falls"	
Flow-like movements in fine-grained materials	Mudslides	"have high clay contents and brittleness and are bounded by shear surfaces at about residual strength. They are strongly three-dimensional, shallow translational landslides and are generally slow-moving...."	

Recently, Hungr et al. (2012) proposed an update of state of the art of landslide classification, revising, in particular, several aspects of the well-

known classification of landslides, developed by Varnes (1978), with reference to the definition of landslide-forming materials, in order to provide compatibility with accepted geotechnical and geological terminology of rocks and soils and with reference to modifications resulting from recent developments of the landslide science (Figure 2.30). Referring to landslides of flow-type that involve soils, the authors suggest nine types and provide a description of each one based on material types, velocity, morphology, source area, paths, mechanisms, giving also some examples.

Type of Movement	Rock	Soil
Fall	1* Rock fall	2* *Boulder, debris, silt* fall
Topple	3* Rock block topple 4 Rock flexural topple	5* *Gravel, sand, silt* topple
Slide	6 Rock rotational slide 7* Rock planar slide 8* Wedge slide 9 Rock compound slide 10* Rock irregular slide	11 *Clay, silt* rotational slide 12 *Clay silt* planar slide 13* *Gravel, sand, debris* slide 14 *Clay, silt* compound slide
Spread	15 Rock slope spread	16* *Sand, silt,* liquefaction spread 17* Sensitive clay spread
Flow	18* Rock avalanche	19 *Sand, silt, debris* dry flow 20* *Sand, silt, debris* flow slide 21* Sensitive clay flow slide 22* Debris flow 23* Mud flow 24 Debris flood 25* Debris avalanche 26 Earth flow 27 Peat flow
Slope Deformation	28 Mountain slope deformation 29 Rock slope deformation	30 Soil slope deformation 31 Soil creep 32 Solifluction

The words in italics are placeholders(use only one).
 * Asterisks indicate movement types that usually reach extremely rapid velocities as defined by Cruden and Varnes (1996). The other landslide types are most often (but not always!) extremely slow to very rapid.

Figure 2.30 Summary of the proposed new version of the Varnes Classification system (Hungr et al., 2012).

2.2.2 Triggering mechanisms

The failure and conditions of slope stability is strictly related both to the forces driving to failure and shear strength of soils. In particular, the driving forces are mainly related to the mass forces due to gravity that derive from the application of external loading. On the contrary, soil shear strength essentially depends on variations of effective stresses induced by the action of external factors.

With reference to rainfall-induced flow-type phenomena, a variety of triggering mechanisms are discussed in the scientific literature. They are mainly related to the decrease of soil shear strength caused by the increase of the pore water pressure as a result of several factors like (Cascini et al., 2005; Cuomo, 2006):

- ✓ surface runoff processes (Van Dine, 1985; Takahashi, 1991, van Ash, 1999; van Ash et al., 2009; Berti et al., 1999);
- ✓ increase of the water table (Leroueil, 2004; Dietrich and Montgomery, 1998);
- ✓ groundwater supplies provided by artesian conditions or hidden springs (Mathewson et al., 1990; Onda et al., 2004; Lacerda, 2004);
- ✓ groundwater flow patterns caused by the stratigraphic setting and/or anthropogenic structures and roads (Wolle & Hachich, 1989; Ng & Shi, 1998; Crosta et al., 2003);
- ✓ increase of saturation degree in unsaturated soils (Futai et al., 2004);
- ✓ variations of hydraulic boundary conditions due to the formation of deep rills as a result of erosion processes related to intense rainfall (Deere and Patton, 1972);
- ✓ undrained loading as a result of first time slides triggered by rainfall, that impact on in-place soils (Hutchinson and Bhandari, 1971);
- ✓ soil liquefaction phenomena (Sassa, 1985; Hungr et al., 2001).

Berti et al. (1999) observed a debris flow event occurred in June 1997 in the Dolomites Eastern Alps (Italy) and recorded it through a video camera starting from its initiation area. They noted that the debris flow was originated by an intense rainstorm whose runoff mobilised the loose coarse debris from the upper part of the channel (Figure 2.31).
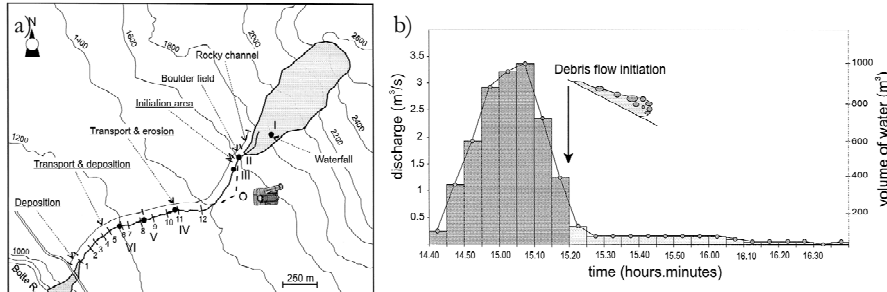
Figure 2.31 a) Schematic map of the 12th June 1997 debris flow event and b) inferred water inflow from the upper rocky basin compared, on a temporal scale, with the actual debris flow initiation. (Berti et al., 1999).

Onda et al. (2004) investigated the role of subsurface water flow paths on slope hydrological processes, landslides and landform developments in steep mountains of Japan. They evaluated the influence of geology on landslide initiation taking into account hydrometric monitoring including the soil water, distribution of bedrock springs, and stream hydrographs in areas where landslide density varies with bedrock type and focusing on the infiltration into bedrock during storm events (Figure 2.32).

Crosta et al. (2003) accomplished a study of the processes involved in slope failures on terraced areas on the basis of the landslides occurred on November 2000 in Valtellina. The authors recognised the influence of the stratigraphical settings of source areas with horizons with vertical contrasting properties and found that the most hazardous landslides were located where the emergence of superficial groundwater or where subsurface water flow convergence occurred (Figure 2.33).
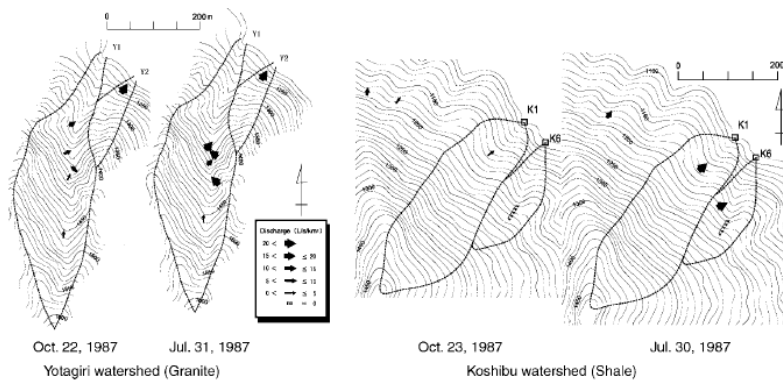
Figure 2.32 Bedrock springs distributions and discharges (Onda et al., 2004).
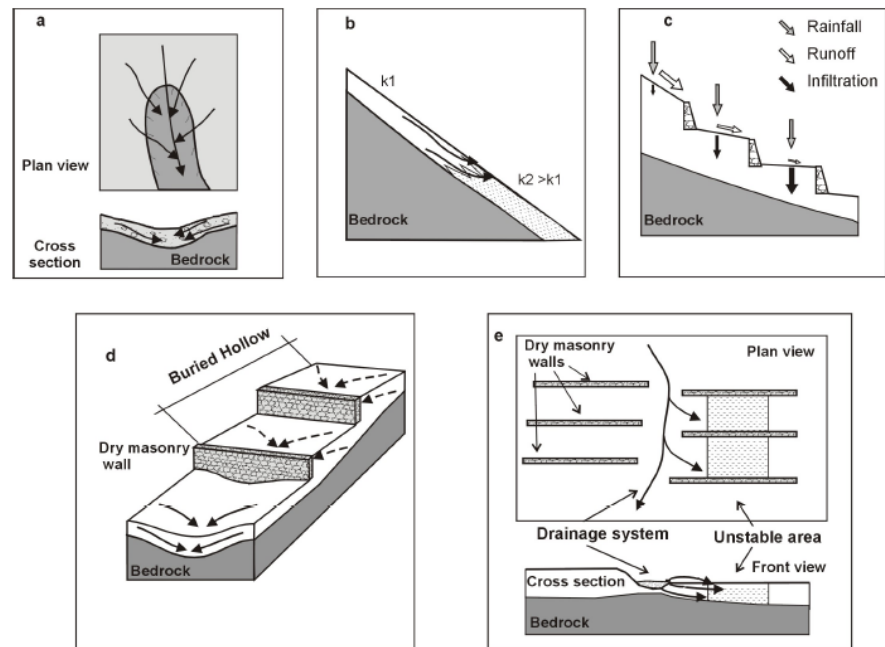
Figure 2.33 Hydrological conditions related to shallow landslides triggering (Crosta et al., 2003).

Starting from the analysis of the landslide source areas of the 1998 event occurred in the Campania region (Southern Italy), Cascini et al. (2008a) identified and mapped six typical triggering mechanisms taking into account geological, geomorphological and hydrogeological features and anthropogenic factors of the study area, respectively named M1, M2, M3, M4, M5, M6 (Figure 2.34). With reference to the most widespread mechanisms, the authors found that: i) the triggering mechanism M1 occurred inside the zero order basins and was related to rainwater infiltrating the ground surface and temporary springs from the bedrock; ii) the triggering mechanism M2 was caused by springs from karst conduits and/or impact of small landslides occurred at the top of bedrock scarps inside the open slopes; iii) the triggering mechanism M3 was related to rainfall infiltration and concentration of runoff water in particular zones close to mountain roads or tracks inside the flanks of valley.
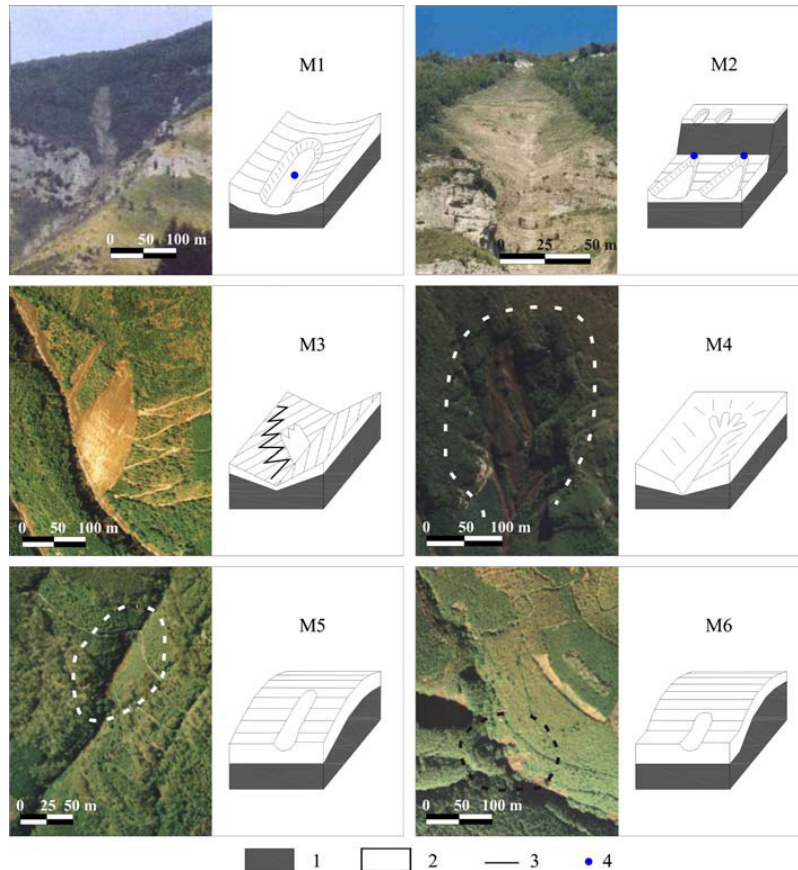
Figure 2.34 Schematic of the typical source areas for the May 1998 flow-like mass movements: 1) bedrock, 2) pyroclastic deposit, 3) tracks, 4) spring from bedrock (Cascini et al., 2008a).

2.2.3 Spatial and temporal occurrence

Both the different criteria used in the landslide classifications proposed in the scientific literature and the several triggering mechanisms observed show that different landslides of flow-type exist, that are characterised by very complex features and generally their spatial and temporal occurrence depends on several factors. They can occur in a variety of environments and can mobilize large quantity of volume which often travel long run-out distances with high velocities.

The spatial occurrence of these type of landslides generally is related to predisponsing factors linked to the susceptibility of an area to trigger the phenomena (e.g. mechanical and hydraulic soil properties, stratigraphy, hydrogeological and geomorphological features, anthropogenic factors, slope angles and aspect, among others). On the other hand, the temporal occurrence is mainly connected to the triggering factors like rainfall events, although some predisposing factors (e.g. soil initial suction) play an important role for their temporal occurrence.

The landslides of flow-type can move quickly downslope at rates of several m/s and they can move instantaneously following a specific trigger such as an intense rainfall even, or they may show a delayed response to critical triggering conditions, for example after a prolonged rainfall event with a gradual rise in pore water pressures (Glade and Crozier, 2005). In this way, they can contemporary affect large areas (Figure 2.35a) or single slope (Figure 2.35b).
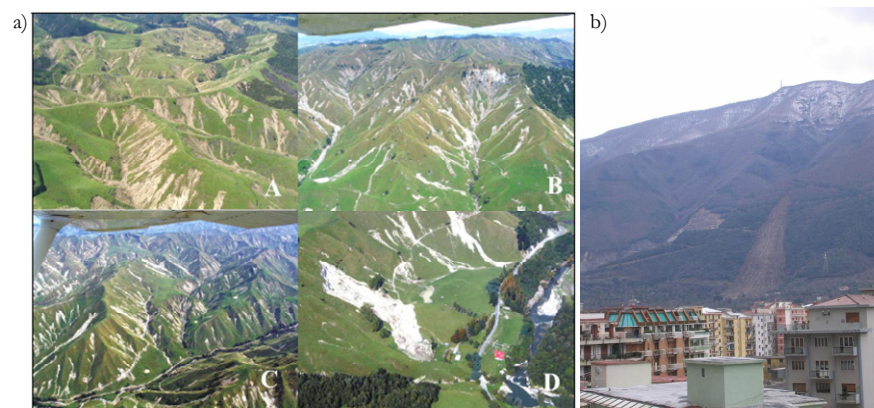
Figure 2.35 Examples of landslides of flow-type on: a) large area (February 2004 event New Zealand, Hancox and Wright, 2005); b) single slope (March 2005 event, Campania region, Italy, Schiano et al., 2009).

With reference to rainfall conditions, several studies have been performed to determine the amount of precipitation needed to trigger slope failures, because landslides triggered by rainfall are mainly caused by an increase of pore water pressure into the ground (Campbell, 1975; Wilson, 1989). Groundwater conditions responsible for slope failures are related to rainfall through infiltration, soil characteristics, antecedent

moisture content and rainfall. Guzzetti et al. (2007) reviewed a series of worldwide empirical rainfall thresholds for landslide initiation (Figure 2.36), including a large range of rainfall intensity and duration.

On the other hand, Cascini et al. (2011) showed that for the 1998 event occurred over an area of 60 km^2 in the Southern Italy, the spatial and temporal occurrence is strongly related to stratigraphy and hydraulic boundary conditions for specific hillslope and over large area (Figure 2.37).
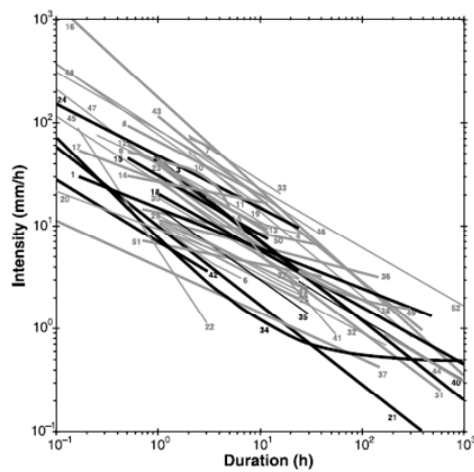
Figure 2.36 Rainfall intensity-duration thresholds (Guzzetti et al., 2007).
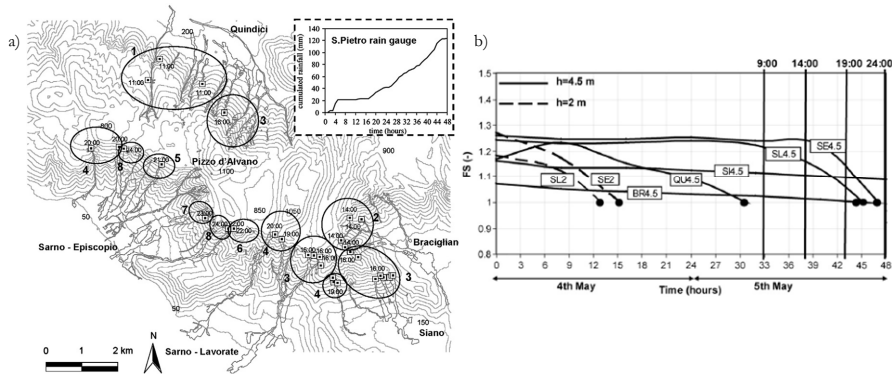
Figure 2.37 Failure time sequence from in-situ evidences (a) and simulated failure time sequence for the landslide source areas M1 (Pizzo d'Alvano massif, Campania region) (Cascini et al., 2011).

2.2.4 Approaches for modeling

Multiple different approaches exist to analyse the triggering stage of landslides of flow-type. Depending on the required results, the input data and the purpose of the analyses, the common approaches can mainly be divided into qualitative and quantitative. The first ones are essentially subjective and produce qualitative evaluations of susceptibility, while the second ones provide numerical estimates in terms of spatial probability of occurrence of the phenomenon (Sica, 2008). Moreover, the susceptibility analysis can be performed through direct approaches, based on field investigations or aerial photographs or satellite images and indirect methods, based on the analyses of indirect correlations between landslides distribution and physical factors characterising the territory. Three common categories of methods can be recognized (Carrara, 1991; Hutchinson, 1995; Aleotti and Chowdhury, 1999; Guzzetti et al., 1999; Fell et al., 2008; Soeters and van Westen, 1996; van Westen, 2004; Sica, 2008): heuristic or empirical models, statistical analyses and deterministic (physically-based or geotechnical) models (Figure 2.38).
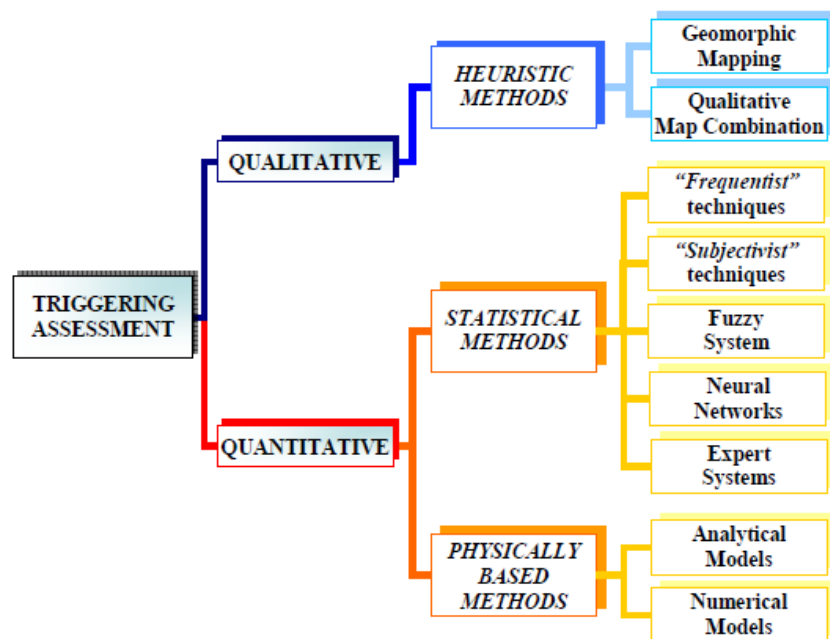
Figure 2.38 Methods and techniques for triggering analysis of landslides (Sica, 2008).

Different applications provided in the literature (Cascini 2008; Fell et al. 2008) suggest the use of each approach, depending on availability, quality and accuracy of data, resolution of zoning, required outcomes and scale of zoning (Table 2.14). With reference to the map scales, Cascini (2008) suggests that: i) at small scale (>1:100000), only heuristic procedures can be used; ii) at medium scale (1:100000 to 1:25000), it is possible to apply heuristic methods and statistical procedures; iii) at large scale (1:25000-1:5000), all methods can be used; and iv) at detailed scales (>1:5000), it is suggested the use of deterministic methods (physically based or geotechnical models).

Table 2.14 Methods required for analyses of existing landslides and characterisation of potential landslides (Cascini, 2008).

Method	Input / Procedure	Topography, landslide inventory, geology, geomorphology	Adding soil classification and depth, terrain units	Adding hydrogeology and geotechnics
Basic	Heuristic or empirical models	X		
Intermediate	Statistical analyses	X	X	
Sophisticated	Deterministic (physically based or geotechnical) models	X	X	X

The *heuristic or empirical models* are qualitative approaches, based on expert judgment and combine the mapping of past landslides and their geomorphological setting. Two main types can be distinguished: i) geomorphic analysis, which is a direct method based on the "a priori" knowledge of all the factors influencing the phenomenon and depends on the ability of expert to understand geomorphologic processes occurring in the area and ii) qualitative map combination, which is an indirect method, based on the experience of the analyst that has to be able to select the relevant factors controlling landslides occurrence, attributing weights and obtaining indexes in order to produce map of susceptibility (Nilsen & Brabb 1977, Sica 2008).

The *statistical methods* provide relationships among the main factors that contribute to landsliding and past and present spatial distribution of slope instabilities (Carrara et al., 1995; Chung and Fabbri, 2003; Corominas et al. 2003; Santacana et al. 2003, Ayalew and Yamagishi 2004; Sica 2008). The simplest statistical methods are based on the determination of the percentage, frequency, incidence of landslides in the classes in which thematic layers showing the geographical distribution of stability/instability factors are ranked (Sica, 2008). More advanced methods employ a variety of techniques, classified according to the adopted "philosophical" classification approach (Michie et al., 1994; Sica, 2008): i) classical (frequentist or Fisherian) statistical techniques, ii) modern (subjectivist or Bayesian) statistical techniques, iii) fuzzy systems, iv) neural network and v) expert systems.

Finally, *physically-based* (process-based or deterministic) *methods* are essentially based on the physical laws controlling the landslide phenomenon. Referring to landslides of flow-type, these methods analyse separately triggering and propagation stages. As for triggering analysis, the most widespread methods can be divided in: analytical methods (e.g. Limit Equilibrium Method) and numerical methods (e.g. Finite Element Method) or some combinations. As for the propagation analysis, the most widespread approaches are numerical models.

With reference to triggering analysis of landslides of flow-type, a widely used approach concerns with the mechanical uncoupling of the analyses of the pore water pressure regime with Limit Equilibrium Methods resulting in the calculation of the factor of safety, through the adoption of a rigid-perfectly plastic behavior of soil. Due to the development of GIS platforms, such models have been applied to the analysis of large areas. Such models, also called "distributed models", are able to take into account the spatial variability of both in-situ conditions and mechanical properties of the involved soils. Due to the complexity of physical laws governing slope stability process, the models proposed in literature are based on simplified conceptual assumptions that make their use suitable only for particular triggering mechanisms (e.g. shallow failure). Among existing distributed physically-based models, the TRIGRS model (Baum et al., 2008) performs a transient seepage analysis referring to the one-dimensional linearised solution of Richards' equation proposed by Iverson (2000) and extended by Baum et al. (2002) to the case of impermeable bedrock located at a finite depth. The TRIGRS-

unsaturated model predicts pore-water pressure regime in unsaturated/saturated conditions, coupling the analytic solution for transient unsaturated infiltration proposed by Srivastava and Yeh (1991) to the original TRIGRS' equation (Baum et al. 2008; Savage et al. 2004). For the unsaturated zone, the model uses the soil water characteristic curves proposed by Gardner (1958). Both TRIGRS models provide the factor of safety at different depths and time intervals at each cell. For the runoff modeling, the models uses a simple method for routing of surface run-off from cells that have excess surface water (i.e. where the rainfall intensity and upslope run-off exceed the saturated hydraulic conductivity of the soil to adjacent down-slope cells where it can either infiltrate or flow farther downslope).

Some applications of TRIGRS models are provided by Salciarini et al. (2006), Godt et al. (2008), Sorbino et al. (2010), Park et al. (2013). For instance, Salciarini et al. (2006) used the TRIGRS model to analyse the susceptibility to shallow landslides in an area in the eastern Umbria Region of central Italy (Figure 2.39), obtaining a reasonable agreement with the landslide inventory map. Moreover, they outlined that the model can give useful results for the characterization of shallow landslide susceptibility when few measured input data are available and reasonable assumptions on input values are made.
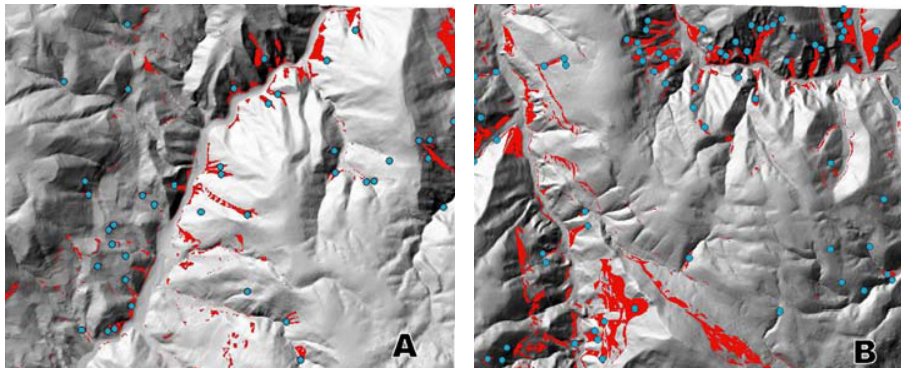
Figure 2.39 TRIGRS results (Salciarini et al., 2006).

On the other hand, Sorbino et al. (2010) performed the analysis of the source areas of huge rainfall-induced shallow landslides occurred in May 1998 inside an area of about 60 km^2 in the Campania region through different physically-based models. In order to compare the results, they

defined the "Success" and "Error" indexes (Figure 2.40), and observed that the TRIGRS-unsaturated model was adequate for the analysis of shallow landslides source areas occurred within the study area, providing the highest ratio between the "Success" and "Error" indexes.
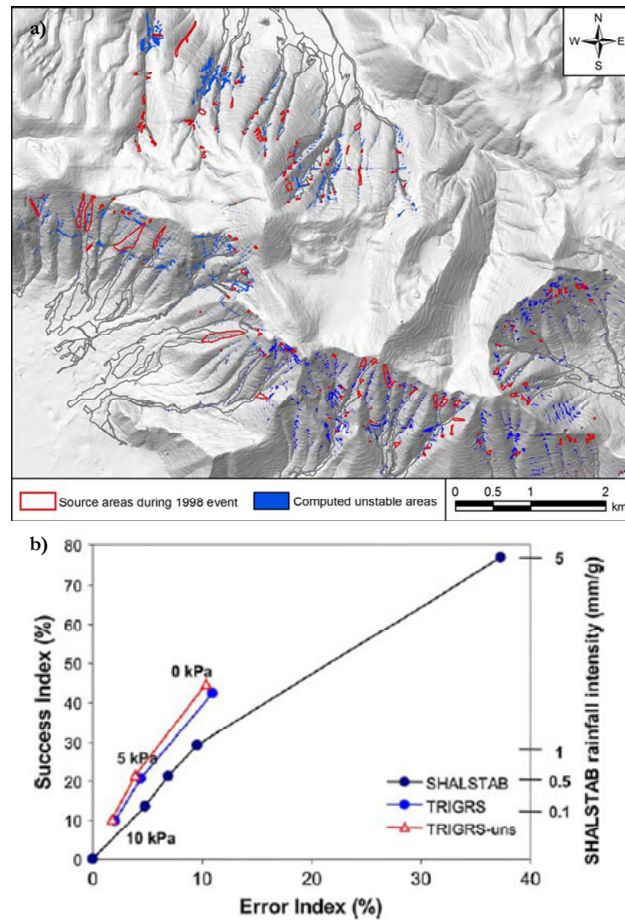
Figure 2.40 Instability scenarios obtained with TRIGRS-unsaturated (a) and "success" and "error" indexes (b) (Sorbino et al., 2010).

2.3 DISCUSSION AND ADOPTED APPROACH

Starting from the analysis of the current literature, it can be stated that heavy rainfall on steep slopes in mountain basins may cause either shallow landslides or soil superficial erosion (Acharya et al., 2009, 2011; Cascini et al., 2013) and different flow-type phenomena may originate in adjacent or overlapping source areas. Consequently, great amount of debris and water can be conveyed at the outlet of steep mountain basins where huge consequences are often registered.

In literature several classifications exist and, for each phenomena some different features (Table 2.15) can be recognised with reference to: i) type of involved materials; ii) sediment concentration; iii) mechanisms of genesis and evolution; iii) velocity and runout. Their peculiar features affect both the spatial and temporal occurrence.

Table 2.15 Main features of flow type phenomena (based on Costa, 1988; Hutchinson 1988, 2004; Coussout and Meunier, 1996; Hungr et al., 2001, 2012).

Features / Flow-type phenomena	Type of material	Sediment concentration	Mechanisms (genesis or evolution)	Velocity and run out
Streamflows (or water floods)	Water (eventually with solid)	1-40%(by wt) 0.4-20%(by vol)	Water discharges; Solid particles moves by suspension and by rolling	0.01-10 m/s
Hyperconcentrated flows (or debris floods)	Water with debris (materials range from sand to cobbles or small boulders)	40-70%(by wt) 20-47% (by vol)	Mass transport phenomenon	Similar to velocities of water during a flood
Debris flows	Debris (materials range from clay to boulders several meters in diameter)	70-90%(by wt) (also 99%) 47-77% (by vol)	Liquefaction during motion or Deposition and remobilization	0.5-20 m/s (also 30 m/s)
Flowslides	Loose granular material: sand, silt, debris and weak rock with metastable and high porosity structure	-	Liquefaction of material in the landslide source area	High velocity (2-10 m/s) and long run-out (> 2km)

However, different limits can be recognised in the classifications, mainly due to: i) different terminology used to identify the phenomenon;

ii) distinction between the phenomena mainly based on the rheological features; iii) difficulty to distinguish a phenomenon from other (especially hyperconcentrated flows, debris flows and water floods); iv) not exhaustive description of triggering and evolution mechanisms; v) analysis of features related to deposition, rheology, fans only when the phenomena are just occurred.

For instance, the distinction between debris flows and debris floods (or hyperconcentrated flows) is generally based on sediment concentration and Hungr (2005) observed that it is difficult to distinguish the phenomena on the base of a quantity that varies both in space and in time. Hungr (2005) proposed, instead, to consider the observed or potential peak discharge of an event. Discharge limited at most to 2 to 3 times that of a major flood is the most important aspect of a debris flood, as it results in relatively limited impacts and relatively low flow depth, and consequently results in limited destructive potential. Debris flows, on the other hand, produce extremely large, peak discharges spontaneously, by means of surge growth processes (e.g. Pierson, 1980, Hungr, 2000). These discharges may be as much as 50 times as large as those of a major flood (VanDine, 1985, Jakob and Jordan, 2001). Consequently, their destructive potential is much greater than that of a flood.

With reference to rainfall that is the main triggering factor of landslides of flow-type, a problem of relevant scientific and societal interest is related to determination of the amount of precipitation needed to trigger slope instabilities. For this reason, Guzzetti et al. (2007) proposed a review of empirical rainfall thresholds (intensity-duration) for the initiation of landslides worldwide (Figure 2.41). However, these empirical thresholds, based on the direct observation of the occurrence of the phenomenon, neglect soil mechanical properties, soil initial conditions and triggering mechanisms. Starting from this consideration, Figure 2.41 proposes a qualitative scheme of rainfall intensity-duration, divided into three zones, which can be related to triggering of different phenomena: 1) heavy and short rainfall can generate erosion processes that can evolve into hyperconcentrated flows; 2) rainfall intensities lower than 100 mm/h and durations higher than about 1 h, can produce shallow landslides; 3) while low and long lasting rainfall can generate deep landslides.
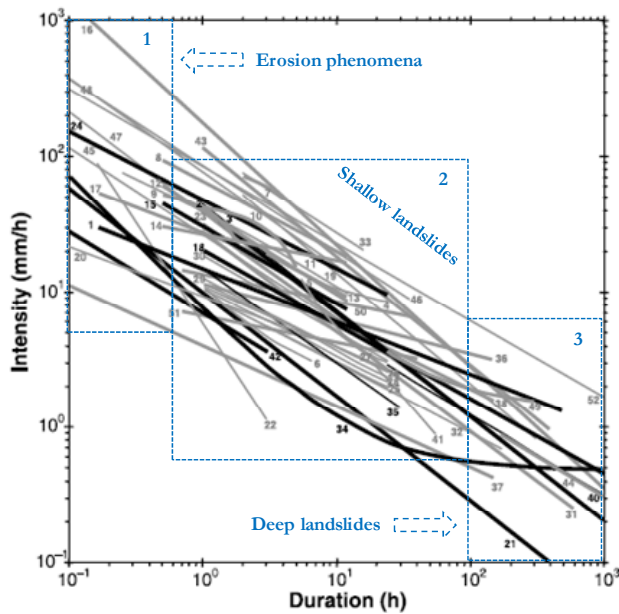
Figure 2.41 Intensity-duration (ID) thresholds for the initiation of landslides (modified from Guzzetti et al., 2007).

With reference to the phenomena and processes occurring during a rainfall event, Figure 2.42 shows the main predisposing and triggering factors, the processes that occur on slope due to rainfall, the genesis and evolution of the phenomena and the distinction mainly based on the sediment concentration. It is worth noting that the combination of different rainfall characteristics (e.g. intensity, duration) and soil properties (e.g. permeability, initial conditions, mechanical parameters) can induce two main processes (infiltration and runoff), whose times and amount of water flowing, generates three main mechanisms of genesis (erosion, liquefaction or failure) that can carry out to the generation and evolution of different flow-type phenomena (hyperconcentrated flows, debris flows or flowslides) characterised by different features mainly in terms of mechanisms of genesis and sediment concentration that can change during the same event.
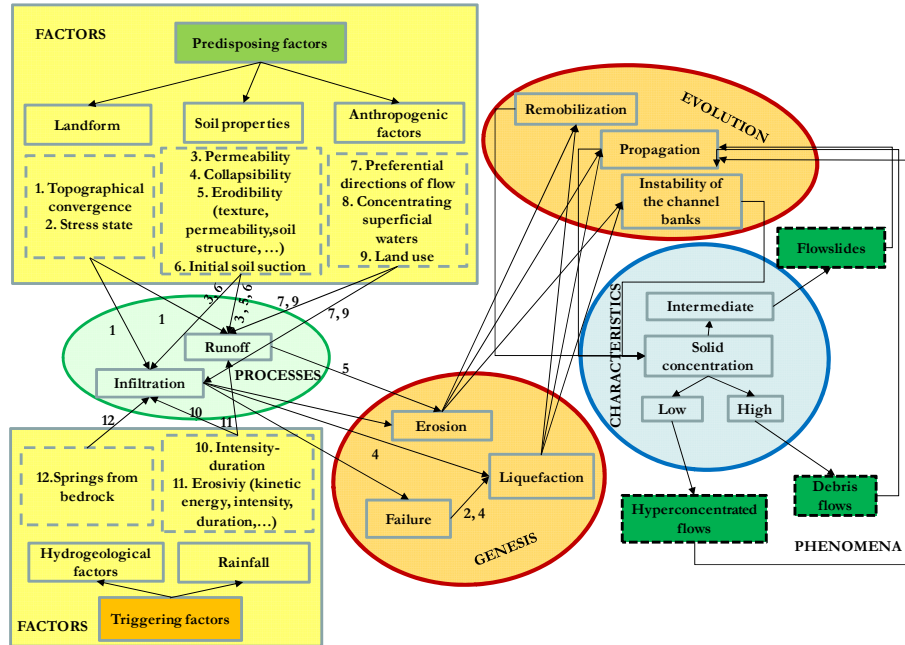
Figure 2.42 Factors and processes for the genesis and evolution of different flow-like mass movements.

Moreover, with reference to the approaches for modeling, in literature different models exist and their application depends on type of phenomena that want to analyse. However, none of these approaches allows the complete simulation of the processes and the genesis of Figure 2.42.

The main purpose of the PhD thesis is to analyse the genesis and mechanisms of hyperconcentrated flows. The latter ones can be defined as mass transport phenomena composed of water and debris (materials variable from sand to cobbles or small boulders) with sediment volumetric concentration variable between 20-47% that can reach velocities similar to water floods at the outlet of the basin affected by this phenomenon. Generally, they occur on steep mountain basins composed by granular unsaturated soils and are induced by heavy and short rainfalls. At the base of these phenomena, three main processes can be recognised: i) rainfall infiltration on ground surface; ii) runoff generation and iii) mobilisation of sediment particles due to erosion processes.

Generally, in literature, the schematisation of the continuum medium for soils is usefully used for the analysis of geotechnical failure mechanisms that produce the triggering of shallow landslides, but this approach is difficult to apply to soil particle mobilisation due to erosion processes. Moreover, the amount of water and sediment that characterises a hyperconcentrated flow at the outlet of mountain basins, is generally obtained through standard approaches that take into account simplified conditions for unsaturated soils that often characterise the steep slopes. For these reasons and also considering the multiple processes as well as their spatial and temporal variability, a multi-scale approach is necessary to investigate many different interrelated aspects (Figure 2.43).

At the slope scale (Figure 2.43a), it is necessary to analyse the mechanisms of rainfall infiltration and runoff generation through a parametric analyses taking into account different unsaturated soil conditions, rainfall intensities and durations and slope angles. A comparison with more traditional methods is also fundamental to understand the differences between different approaches. Moreover, the times to runoff generation have to be also compared with failure times in order to understand the temporal occurrence of both the phenomena.

Considering that these phenomena affect large areas and in order to taking into account the morphometric and topographical characteristics that generally are variable cell by cell on an area represented by Digital Terrain Model (DTM), at large area (Figure 2.43b) it is necessary to perform parametric spatially-distributed analyses in order to capture the spatial occurrence of first-time shallow landsliding and superficial soil erosion phenomena repeatedly occurring in large test area affected by shallow landslides and soil erosion. In particular, the seasonality of some input data (e.g. initial soil unsaturated conditions, soil cover and rainfall conditions) has to be also considered.

Going into details and in order to estimate the amount of water and sediment conveyed at the outlet of the basin as well as the source areas of soil erosion, a parametric analysis is necessary at basin scale (Figure 2.43c) through a physically-based model that takes into account the single processes at the base of soil erosion and the variability of input parameters.

Finally, in order to model the rainsplash erosion mechanism due to raindrops, that generally is analysed by measurements of particles detached in experimental tests, at particle scale (Figure 2.43d) it is

necessary to consider a numerical approach that can reduce the times and costs of the direct observations and that takes into account the mechanics of "raindrop soil detachment".
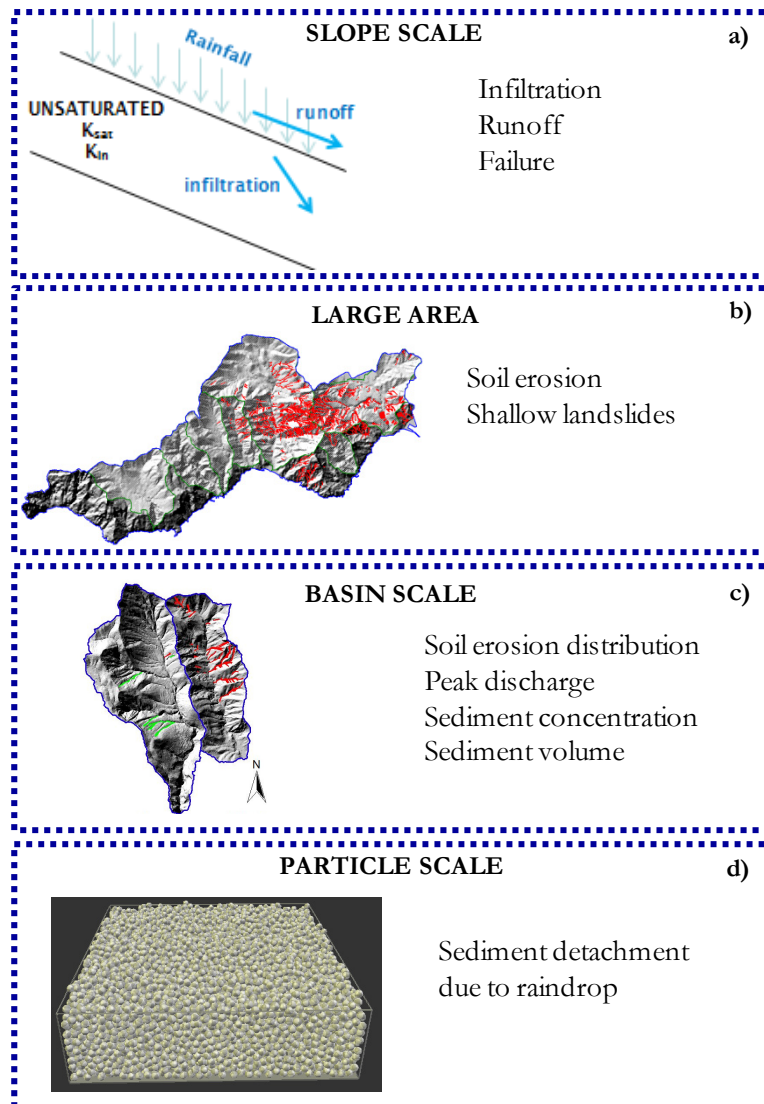
Figure 2.43 Multi-scale approach adopted for the analysis.

3 INFILTRATION AND RUNOFF

Rainfall infiltration process in unsaturated soils is a complex process heavily affecting the slope stability conditions, especially in the case of steep shallow soil deposits (i.e. slope angle larger than 30° and soil thickness up to 5 m). Depending on soil properties, rainfall characteristics and slope morphology, this process is often associated to the runoff generation that, consequently, determines the water discharge and the detachment and transport of soil particles at the outlet of mountain basins. Both processes may generate different flow-type phenomena (Section 2.3) and can produce different runoff discharges which, in turn, determine differences in solid concentration and rheology of propagating flows. For this reason, a proper estimation of the runoff discharge necessarily requires the assessment of the rainfall amount that infiltrates the ground surface.

In the following, starting from an accurate analysis about infiltration and runoff generation – leading to slope instabilities –, an engineering reference framework to evaluate both the amount of rainfall infiltrating the ground surface and runoff flowing at the ground surface as wash out is proposed. A special attention is devoted to the temporal occurrence of both processes whose combination may cause different types of flow-like mass movements.

3.1 LITERATURE REVIEW

3.1.1 In-situ evidences

Direct in-situ observations of landslides and hyperconcentrated flows are rare except for some real-time monitored sites during the events. In particular, important monitoring activities have been carried out in several geographical regions of the world (Zhang et al., 2000; Lavigne et al. 2000; Marchi et al., 2002; Suwa et al., 2009; McCoy et al., 2011) characterised by high frequency of occurrence of landslides of flow-

types. Generally, the investigated stage is the propagation with temporal measurements of the flow depth, velocity, volume and discharge through the use of different measuring instruments located in suitably selected points of the channels (Figure 3.1).

In this way, the measurements of total discharges are the response of the upper part of the basin to the installation point of instrument.
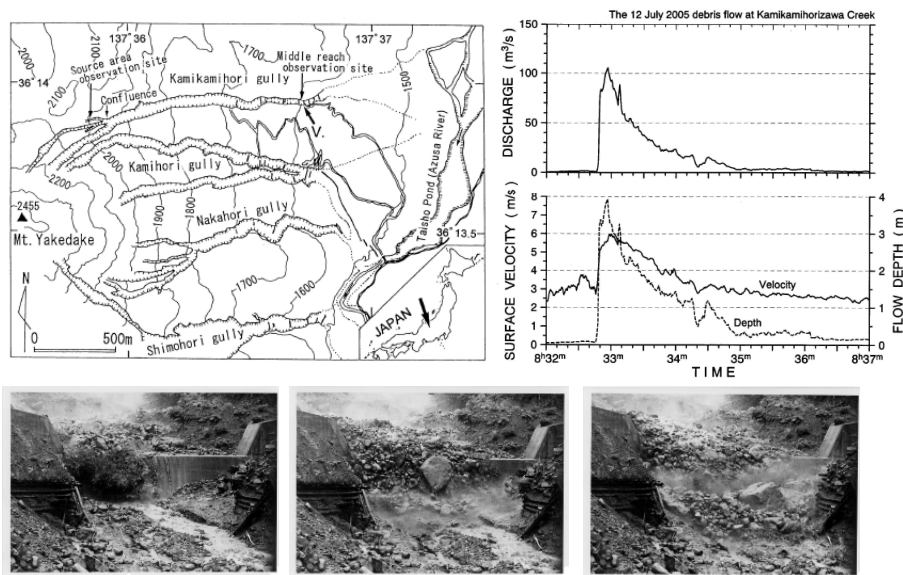
Figure 3.1 Kamikamihorizawa Creek, Mount Yakedake, Nagano, Japan (Suwa et al., 2009).

On the other hand, detailed information is becoming more often available from monitoring of rainfall infiltration and runoff in well-instrumented sites. For instance, based on experimental data from India, Rao et al. (1998) (Figure 3.2) performed a regression analysis which outlines as significant factors in determining the runoff: i) amount of precipitation, over a period of 30 minutes, ii) soil cover, iii) cumulated time since the beginning of the experiment and iv) amount of rain during the previous 2 days. In addition, Zhang et al. (2000) observe in Hubei Province (China) that the infiltration rate depends on the soil initial water content and the presence of stratigraphic discontinuities can influence the infiltration pattern.
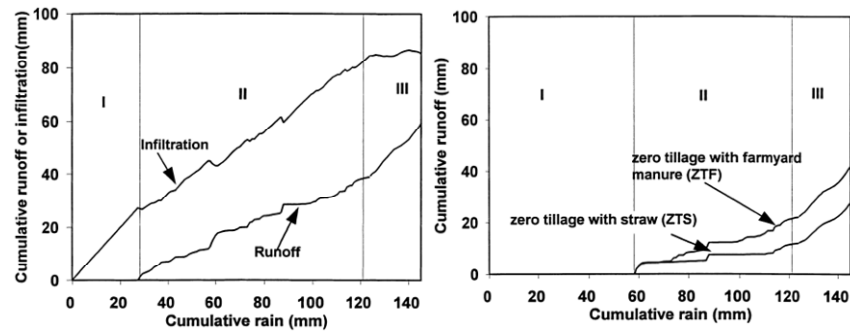
Figure 3.2 Relationship between cumulative rainfall and cumulative runoff or infiltration for different experiments (Rao et al., 1998).

With reference to rainfall, more often the amount of rainfall capable to induce slope instability phenomena is individuated referring to time ranges heuristically selected through an expert judgment. In the literature, many contributions deal with the so-called "critical rainfall" which is usually lower bounded through threshold lines in log-log plots (Frattini et al., 2009). As shown in Chapter 2, examples are provided in Guzzetti et al. (2007) who also show the wide dispersion of the collected data and interpolating lines (Table 3.1 and Figure 2.36). Data dispersion is a weak point of this kind of approach especially for forecasting purposes and it is mainly related to: i) variable in-situ conditions, ii) different temporal resolution of the data, iii) different mechanisms governing the observed soil mass movements.

Table 3.1 Upper and lower envelope curves of Figure 2.36 proposed by Guzzetti et al. (2007).

#	Equation	Range	Envelope curve
37	$I=4.0 \times D^{-0.45}$	$0.1<D<150$	Lower curve
21	$I=10.0 \times D^{-0.77}$	$0.1<D<1000$	
16	$I=176.40 \times D^{-0.90}$	$0.1<D<1000$	Upper curve
52	$I=84.3 \times D^{-0.57}$	$0.1<D<2000$	

This last aspect is investigated with reference to relevant case histories of shallow landslides which are selected from different Countries (i.e. Italy, United Kingdom, Japan, Taiwan, China, United States, Canada, Brazil and Thailand) in the period from 1950 to 2010 (Table 3.2).

Table 3.2 Critical rainfall for 35 selected case histories (Cuomo and Della Sala, 2013a).

ID	Country	Location	Year	Duration (h)	Cumulative rainfall (mm)
1	USA	Seattle	1950	55	81.95
2	UK	Bristol	1952	24	228
3	Italy	Campania Region	1954	16	504
4	USA	Seattle	1956	104	101.92
5	China	Hong Kong	1966	24	525
6	Brazil	Rio de Janeiro	1967	48	586
7	UK	United Kingdom	1968	24	172
8	USA	Appalachians	1977	9	300
9	Canada	Vancouver	1979	24	300
10	Japan	Boso peninsula	1980	72	559
11	USA	California	1982	32	440
12	USA	Seattle	1983	28	36.96
13	USA	Appalachians	1985	24	240
14	USA	Seattle	1986	28	85.4
15	Japan	San-In district	1988	10	500
16	Japan	Boso peninsula	1989	24	350
17	USA	Seattle	1991	53	121.9
18	USA	Seattle	1996	45	109.8
19	USA	Seattle	1997	44	79.64
20	Italy	Campania Region	1998	48	248
21	Italy	Campania Region	1999	38	264
22	Thailand	Thailand	1999	24	290
23	Italy	Tuscany Region	2000	39	210
24	Italy	Tuscany Region	2000	39	210
25	Taiwan	Taiwan	2000	24	370
26	USA	Seattle	2001	37	55.87
27	USA	Seattle	2001	30	92.7
28	Thailand	Thailand	2001	24	100
29	Thailand	Thailand	2003	24	110
30	Japan	Minamata Hishicari	2003	8	337
31	Japan	Minamata Hogawachi	2003	5	265
32	Japan	Minamata Fukagawa	2003	5	265
33	Thailand	Thailand	2006	24	150
34	Japan	Hofu City	2009	20	241
35	Italy	Campania region	2010	19	120.8

These events caused catastrophic consequences in terms of victims and damage and the scientific literature provide a comprehensive data set regarding the duration of the rainfall storms, the cumulative rainfalls and the maximum rainfall intensities. Figure 3.3 shows the average rainfall intensities (1÷53 mm/h) and durations (5÷104 h) for the selected events: the data are somehow correlated by a straight line in a logarithmic plot and lie within the upper and lower envelope curves proposed by Guzzetti et al. (2007).
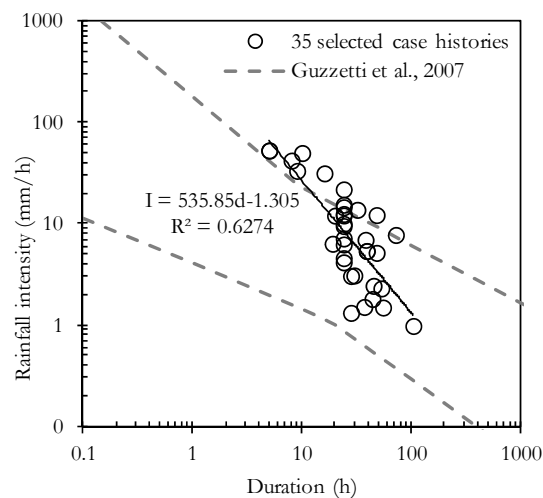
Figure 3.3 Rainfall intensity-duration for 35 selected case histories compared to the threshold for critical rainfall proposed by Guzzetti et al. (2007) (Cuomo and Della Sala, 2013a).

However, such a heuristic approach has important drawbacks as it provides limited chances to understand the governing mechanisms and forecast future events. This is mainly due to the lack of any direct reference to slope geometry and soil mechanical parameters that are completely disregarded. Furthermore, as most of steep slopes lie in unsaturated conditions, a suitable framework should take into account the unsaturated soil conditions as well as the possibility of different mass movements to occur depending on slope features, rainfall and initial conditions. Notwithstanding the potential of in-situ experimental observations, they may suffer of a partial control of local stratigraphic

peculiarities and soil heterogeneities and different approaches deserve attention.

3.1.2   Laboratory evidences

In recent years, infiltration and runoff have been extensively investigated through laboratory experiments (Bryan and Rockwell, 1998; Darboux et al., 2001; Rahardjo et al., 2004; Assouline and Ben-Hur, 2006; Pan and Shangguan, 2006, Acharya et al., 2009, 2011 and others). Slope geometry of the equipments covers a wide range of lengths ranging from 0.4 m to 10 m, widths variable between 0.2 m to 3 m, soil depth ranging from 25 mm to 500 mm and the slope angles variable between 1° to 47°. Different types of soils are investigated ranging from fine to coarse materials and also different surface conditions are considered (for instance, different grass covers or micro-topographic structure). In addition, in the selected experiments, the authors consider different rainfall intensities ranging between 15 and 180 mm/h and different durations ranging between 23 minutes and 8 hours. During the experiments, the authors measure and/or calculate different variables such as soil infiltration rate, runoff initiating time and runoff discharge.

A summary of the selected laboratory tests are reported in Table 3.3.

For instance, Bryan and Rockwell (1998) show that the average time to runoff (time lag between rainfall application and runoff generation) at the terminal weir of the flume decreases when the slope angles increase. Rahardjo et al. (2004) show that the time to runoff decreases with an increase in the rainfall intensity and the infiltration rate decreases with an increase in the duration of rainfall application. The collected data suggest that about 40÷74 % of the total rainfall amount contribute to infiltration, depending on the rainfall intensity, duration, and antecedent moisture conditions in the slope (Figure 3.4). The authors show that there was no runoff during the early stage of the simulated rainfall events. During this period, all the rainfall water contributes to infiltration. As the rainfall continues after some time, the slope starts contributing to runoff and this leads to the initiation of the runoff hydrograph. These results are confirmed by Assouline and Ben-Hur (2006) who show that infiltration rate increases with slope and rainfall intensity. In particular, this effect is more pronounced for higher value of rainfall intensity. Furthermore, as the rainfall intensity increases, the time to runoff is shorter, the infiltration curve decreases more quickly, and the steady infiltration rate

after a long exposure to rainfall becomes higher (Figure 3.5).

Table 3.3 Flume geometry, top soil characteristics, rainfall conditions and measured/calculated variables from selected flume tests.

	GEOMETRY		TOP SOIL					RAINFALL CONDITIONS (***)		Measured or calculated variables (****)
	Flume Size (**)	Slope angle	Texture				Soil depth	I	d	
R (*)	L-W-H (m)	Range (°)	Clay (%)	Silt (%)	Sand (%)	Gravel (%)	(mm)	(mm/h)	(min)	
1	0.4 x 0.2	5 - 20	11	20	69	-	25	42 - 90	60	a, b
	0.4 x 0.2	5 - 20	40	33	27	-	25	42 - 90	60	a, b
2	10 x 0.8 x 0.3	1.5 - 9	18.1	32.5	49.4	-	94-120	42 - 45	65 - 160	a, b, c, d, f, g
3	1.2 x 1 x 0.085	3.4	9.1	26.3 2	47.44	17.14	80	30 - 180	4	a, b, d, e
4	3.6 x 0.4	2 - 10	sand				-	108	-	a, b, d, f
5	2.4 x 2.4	1.1 - 2.9	Glynwood clay loam				70	24	30, 60	-
6	3.7 x 0.61 x 0.23	1.2 - 9.7	18	80	2	-	?	15 - 60	360	a, b, e
7	3.6 x 0.4	2.7 - 10	from very fine to very coarse sand				-	54 - 162	-	a, b, d, e, f
8	4 x 2	2.9 – 11	Fine-silty				208	45, 60	-	a, f
9	0.6 x 0.35 x 0.2	27	Silty Clay underlain Clayey Silt				-	57 - 83	39 - 73	a, c
10	2 x 0.55 x 0.35	15	sandy loam				300	100	70	a, b, c, d, e, f, g
11	0.5 x 0.3	3 - 14	10	2	88	-	100	24, 60	-	a, b, c, e
12	6 x 1 x 0.6	5 - 20	sandy silt loess				500	30, 60	-	c
13	8 x 3	5 - 25	8	68	24	-	300	50 - 150	-	a, d, f
14	1 x 0.6 x 0.2	-	16	66	18	-	-	20 - 40	24, 48	a, c, g
15	2.44 x 0.3 x 0.8	35 - 47	silty loess				100	20, 40	480	a, b
	1.5 x 0.3 x 0.8	5 - 10								

(*) References (R): 1: Zhang et al. (1998); 2: Brayn & Rockwell (1998); 3: Jayawardena & Bhuiyan (1999); 4: Abrahams et al. (2000); 5: Darboux et al. (2001); 6: Romkens et al. (2001); 7: Abrahams et al. (2001); 8: Gomez et al. (2003); 9: Rahardjo et al. (2004); 10: Pan & Shangguan (2006); 11: Assouline & Ben-Hur (2006); 12: Lei et al. (2006); 13: Yao et al. (2008); 14: Shuster et al. (2008); 15: Acharya et al. (2011).
(**) Flume size: L=length; W=width; H=height;
(***) Rainfall conditions: I=rainfall intensity; d=rainfall duration.
(****) a: Runoff discharge; b: Sediment yield rate or detachment rate; c: Soil infiltration rate; d: Flow depth; e: Sediment concentration; f: Flow velocity; g: Runoff initiating time.
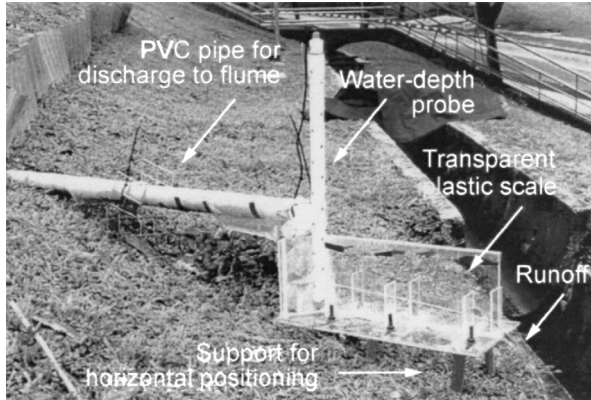
Date (d/m/y)	Rainfall			Runoff			Infiltration	
	Duration (min:s)	Intensity (mm/h)	Total (mm)	Start (min)	Maximum rate (mm/h)	Total* (mm)	Minimum rate (mm/h)	Total* (mm)
(1)	(2)	(3)	(4)	(5)	(6)	(7)	(8)	(9)
09/02/98	39:20	57	37.5	10.0	27	09.7 (25.9%)	30	27.8 (74.1%)
11/02/98	26:00	57	24.8	6.5	31	08.5 (34.3%)	26	16.3 (65.7%)
18/02/98	28:20	83	39.5	4.0	54	16.0 (40.5%)	29	23.5 (59.5%)
20/02/98	43:20	72	52.1	3.8	52	28.7 (55.1%)	20	23.4 (44.9%)
25/02/98	73:20	47	57.2	5.8	42	34.2 (59.8%)	5	23.0 (40.2%)

* Number in parenthesis indicates percentage of total rainfall.

Figure 3.4 Flume tests installation and summary of runoff measurements from simulated rainfalls (Rahardjo et al., 2004).
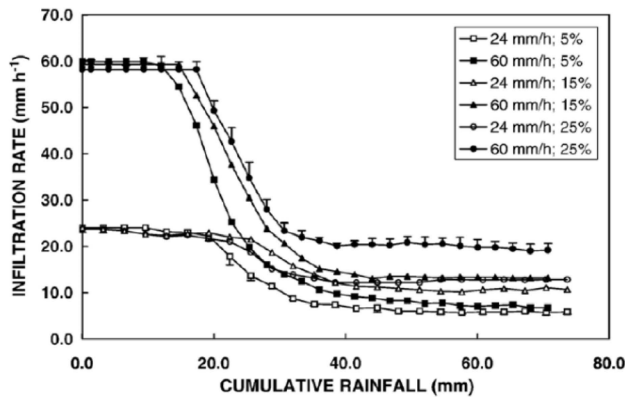
Figure 3.5 Infiltration rate versus cumulative rainfall for two rainfall intensities and three slope gradients (Assouline and Ben-Hur, 2006).

Then, Pan and Shangguan (2006) show that the grass cover reduces significantly the runoff and Darboux et al. (2001) show even that a small modification of micro-topographic structure has a major effect on runoff initiation. Finally, Acharya et al. (2009, 2011) conducted 12 experiments

in a laboratory flume under a rainfall simulator to quantify erosion and shallow landslides in fine-grained silty loess soils (Figure 3.6). They measured sediment and runoff from flume outlet and they observed, for the experiments without failure occurrence, that the runoff discharge increase with slope angle and rainfall intensity, and the steady runoff rates are reached in short time from the beginning of the rainfall.
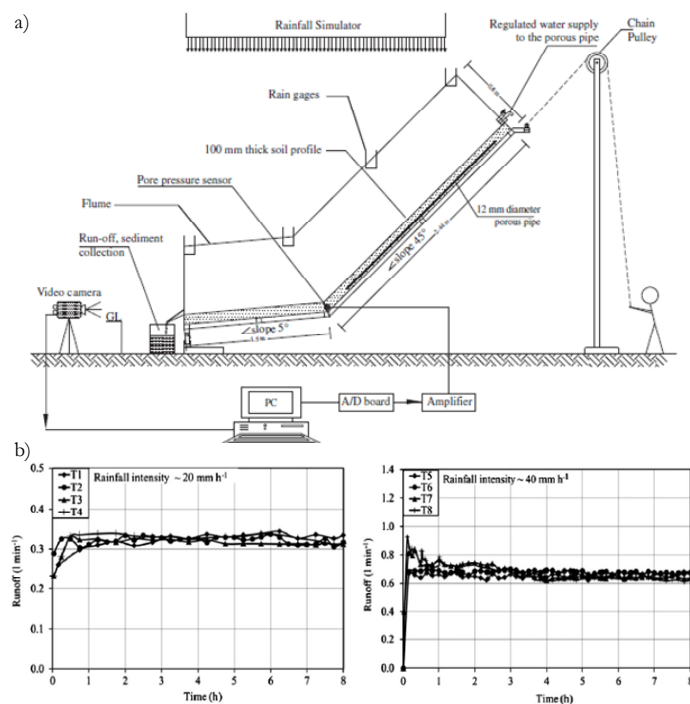
Figure 3.6 a) Schematic diagram illustrating a typical experimental setup and b) runoff measurements for non-failure experiments (Acharya et al., 2011).

3.1.3 Approaches for modeling of runoff

The fundamental equation that governs the flow of water through unsaturated soil is the differential Richard's equation:

$$\frac{\partial}{\partial x}\left(k_x\frac{\partial h}{\partial x}\right)+\frac{\partial}{\partial y}\left(k_y\frac{\partial h}{\partial y}\right)=m_w\gamma_w\frac{\partial h}{\partial t} \tag{3.1}$$

where m_w is the coefficient of volumetric water changes with respect to the change in negative pore pressure and it is equal to the slope of the soil–water characteristic curve, h is the total head, k_x and k_y are the soil conductivity coefficients in x and y directions, γ_w is the unit weight of water, t is the time.

Being this equation difficult to solve analytically, different approximate methods can be considered. In literature, different methods that evaluate the amount of water that infiltrates the ground surface are available. They can be divided in two main groups: i) empirical methods based on empirical relationships and ii) simplified physical methods, derived from appropriate schematisation of the real dynamics of phenomena. These methods, generally, are used in many erosion and sediment transport models in order to estimate the amount of rainfall that flows on the ground surface and that can produce the detachment and transport of sediment.

The empirical methods substantially determine the cumulated infiltration through the application of the balance equation:

$$P_{net} = Q = P - P_{loss} \tag{3.2}$$

where P_{net}, P_{loss} and P represent, respectively, the volume of net rainfall, lost rainfall and total rainfall of the event and Q is the surface runoff.

A well-known empirical method is the Curve Number method (USDA-SCS, 1972) that is based on a simple mass balance equation between the cumulated rainfall, computed from the beginning of the rainfall storm, the runoff and the initial water "losses" before the runoff generation. In particular, this method computes the runoff height Q (mm) as a function of both the rainfall height P (mm) and a storage term S which is a function of a dimensionless index, called "Curve Number" (CN); the latter depends on the soil type (hydrologic soil group), the land-use and the antecedent soil moisture conditions at the time of the rainfall. A modified version of the CN method also includes the effect of slope angle and it was firstly applied to East African soil conditions (Sprenger, 1978). In details, the rainfall-runoff relationship used in this method reads:

$$Q = \frac{\left[P - 0.2 \cdot \left(\dfrac{25400 - 254 \cdot CN}{CN} \right) \right]^2}{P + 0.8 \cdot \left(\dfrac{25400 - 254 \cdot CN}{CN} \right)}$$

(3.3)

where Q is the cumulated runoff depth (mm), P is the cumulated rainfall depth (mm) and CN is the curve number index that, according to Sprenger (1978) depends on: i) hydrological soil group (A, B, C, D), ii) antecedent moisture condition (AMCI, AMCII, AMCIII), iii) land use or cover and iv) slope angle.

The simplified physical methods include methods that propose a description of the infiltration process based on simplified assumptions (e.g. Horton model, 1933) or propose an exact analytical representation of a approximate physical description of the infiltration process (e.g. Green-Ampt, 1911).

As far as the simplified physical methods, it is worth mentioning the Green-Ampt method (Green and Ampt, 1911) that is a 1D vertical infiltration model based on the Darcy's law (1856). The method assumes the presence of a continuous thin sheet of water at the ground surface which causes a downward moving wetting front into an homogeneous soil with a uniform initial water content (throughout the soil profile). Mein and Larson (1973) proposed a modified version of the Green-Ampt method which includes a simple two-stage model for infiltration under a constant rainfall intensity into an homogeneous soil with a uniform initial water content: i) the first stage includes water infiltration before runoff starts; ii) the second stage coincides with the process schematised by Green-Ampt (1911). In details, the equations used to predict the amount of infiltration up to surface saturation F_p is given by Eq. (3.4) while the time to the beginning of runoff (Eq. (3.5)) reads:

$$F_p = \frac{\left| \Psi_f \right| \cdot k_{sat} \cdot (\theta_{sat} - \theta_i)}{P - k_{sat}} \qquad \text{for t=}t_p \text{ and P>}k_{sat}$$

(3.4)

$$t_p = \frac{F_p}{P}$$

(3.5)

where P is the rainfall rate (cm/h), t_p is the time when water begins to

pond on the surface (h), θ_{sat} is the saturated moisture content (dimensionless), θ_i is the initial moisture content (dimensionless), k_{sat} is the saturated hydraulic conductivity (cm/h), ψ_f is the matric pressure at the wetting front (cm).

In the first stage ($t \leq t_p$) the infiltration rate f(t) is equal to rainfall f(t)=P. For the second stage ($t \geq t_p$), the infiltration rate f(t) is described by Eq. (3.6) and the time is described by Eq. (3.7):

$$f(t) = k_{sat} + k_{sat} \frac{|\psi_f| \cdot (\theta_{sat} - \theta_i)}{F} \quad \text{for } t > t_p \tag{3.6}$$

$$t = t_p + \frac{1}{k_{sat}} \left[F - F_p + |\Psi_f| \cdot (\theta_{sat} - \theta_i) \cdot \ln\left(\frac{|\Psi_f| \cdot (\theta_{sat} - \theta_i) + F_p}{|\Psi_f| \cdot (\theta_{sat} - \theta_i) + F} \right) \right] \tag{3.7}$$

where F is the cumulative amount of infiltrated water (cm) and the runoff rate is obtained as difference between rainfall intensity and infiltration rate.

Recently, Grimaldi et al. (2012) proposed a Green-Ampt Curve-Number mixed procedure as an empirical tool for rainfall–runoff modelling in small and ungauged basins. They combined the Green-Ampt method modified by Mein and Larson (1973) with the Curve Number method and applied the new procedure to 100 rainfall–runoff events observed in four small basins, obtaining more realistic results than the Curve Number method.

However, these methods have important limitations. For instance, the CN method doesn't explicitly consider the unsaturated-saturated soil hydraulic properties while considering the effect of slope angle; on the other hand, the modified Green-Ampt method (Mein and Larson, 1973) allows considering measurable soil properties as the soil saturated hydraulic conductivity and the initial moisture content but it refers to a vertical 1D infiltration pattern that is not the general case for water infiltration in a slope. Therefore, different simplifications prevent both methods to properly simulate the infiltration and runoff processes.

3.2 MECHANISMS

A reference scheme for the principal mechanisms of runoff generation is here proposed and later analysed via numerical modeling. Indeed, when a rainfall storm occurs, two main processes affect the unsaturated shallow soil deposits: water infiltration from the ground surface and runoff generation on the ground surface. As also underlined by experimental evidences, the temporal occurrence of one or both these processes depends on: i) slope angle, ii) rainfall intensity and duration; iii) soil hydraulic properties; iv) soil initial conditions. However, different combination of the above parameters may lead to distinct scenarios and it is of interest to outline a framework for engineering purposes.

In general, three different mechanisms can be recognised (Figure 3.7), here named R1, R2 and R3, which discriminate among different scenarios for water infiltration and runoff.

The mechanism R1 takes place when the rainfall intensity (I) is higher than the soil saturated hydraulic conductivity (k_{sat}). Thus, the water cannot infiltrate the ground surface at a larger amount of k_{sat} if initial soil suction is nil and runoff is generated from the beginning of the rainfall storm.

The mechanism R2 occurs when the rainfall intensity (I) is higher than initial hydraulic conductivity (k_{in}) but lower than saturated hydraulic conductivity (k_{sat}); i.e. $k_{in}<I<k_{sat}$. At a first stage rainwater infiltrates the ground surface but then, as soil water content increases, runoff may be generated, provided that rainfall is still continuing.

The mechanism R3 arises when the rainfall intensity (I) is lower than the initial hydraulic conductivity (k_{in}); in this case runoff cannot occur and only water infiltration takes place.

Within this framework it is important evaluating the time sequence of infiltration and runoff compared to: i) cumulated rainfall of the tested area, ii) mechanical soil properties. Furthermore, the infiltration and runoff rates are of primary interest to evaluate the slope stability conditions and to assess the potential occurrence of different types of flow-like mass movements.
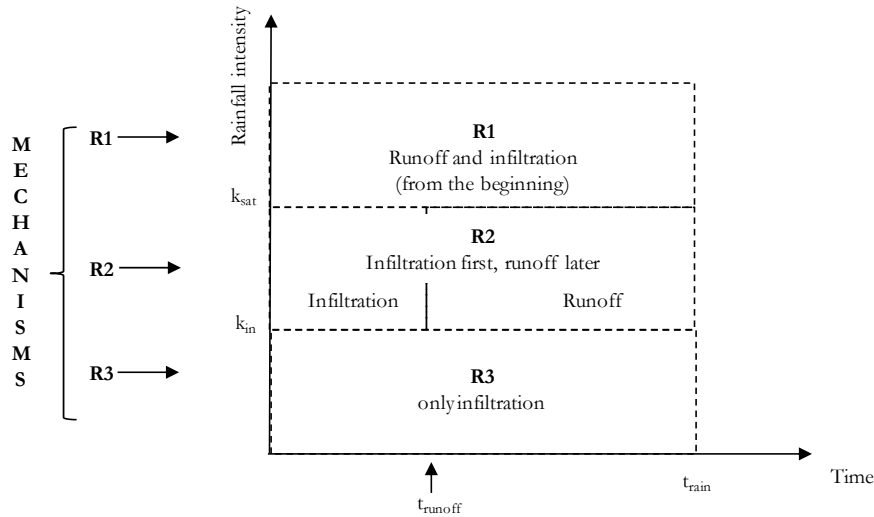
Figure 3.7 A reference scheme for the mechanisms of rainfall infiltration and runoff (Cuomo and Della Sala, 2013a).

3.3 PARAMETRIC ANALYSIS

3.3.1 Input and methods

A parametric numerical analysis is performed and the occurrence of the ponding condition is evaluated by tracking the value of pore water pressures at points of the ground surface. This allows a detailed analysis of both the mechanisms R1 and R2 while the mechanism R3 is not investigated because it has been extensively analysed in the literature (Gasmo et al., 2000; Tsaparas et al., 2002, 2003; Cascini et al., 2008, 2011b).

The commercial finite element code SEEP/W (Geoslope, 2005) is used to integrate the Richards' equation (eq. (3.1)), thus obtaining the transient pore water pressures due to the hydraulic boundary condition applied at the ground surface.

A homogenous slope is considered 150 m long and 2 m thick in the cases of slope angle equal to 20°, 30° and 40° as reported in Figure 3.8a. In particular, the slope is divided into 1500 rectangular elements, of which 1000 in the first half depth with length of 1.5 m and height of

0.1 m while 500 elements, 1.5 m long and 0.2 m high, are considered in the second half depth.

As for the soil hydraulic properties, the upper, middle and lower soil-water characteristic curve of Figure 3.8c,d are considered, which refer to the above mentioned case histories. Particularly, the relationship proposed by Van Genuchten (1980) is used to describe the variation of the volumetric water content $\theta(s)$ with suction (eq. 3.8) and the relationship proposed by Mualem (1976) is referred to express the variation of hydraulic conductivity $k(s)$ with suction (eq. 3.9), as follows:

$$\theta(s) = \theta_r + \frac{\theta_{sat} - \theta_r}{\left[1 + (\alpha s)^n\right]^m}$$

(3.8)

$$k(s) = k_{sat} \times \frac{\left\{1 - (\alpha s)^{n-1} \times \left[1 + (\alpha s)^n\right]^{-m}\right\}^2}{\left[1 + (\alpha s)^n\right]^{m/2}}$$

(3.9)

where θ_{sat} and θ_r are the saturated and residual volumetric water content respectively, k_{sat} is the saturated hydraulic conductivity, α is an empirical parameter (kPa^{-1}) whose reciprocal value can be assumed as the air entry value (a.e.v.), n is a fitting constant reflecting the slope of the volumetric water content curve, and m is a parameter linked to n through the following equation: $m=1-1/n$.

The parameters of the Eqs (3.8) and (3.9) are computed by best fitting the experimental curves reported for the case studies of Table 3.2 and reported in details in Table 3.4. Saturated soil conductivity (k_{sat}) is equal to $10^{-6} \div 10^{-4}$ m/s, volumetric water content equal to $0.37 \div 0.66$, the parameter α equal to $0.1 \div 0.7$ kPa^{-1}, and n equal to $1.3 \div 2.3$. In Figure 3.8c,d the volumetric water content and the conductivity curves are plotted and they span over a wide range, for which the upper, middle and lower limits are also indicated. It is worth noting that: i) the soil water characteristic curves of Figure 3.8c,d are average curves for wetting processes experienced by the soils in the above mentioned case histories (Table 3.2) and ii) in the performed analysis of infiltration processes (wetting process) any hysteretic behavior of the hydraulic properties would be not relevant.
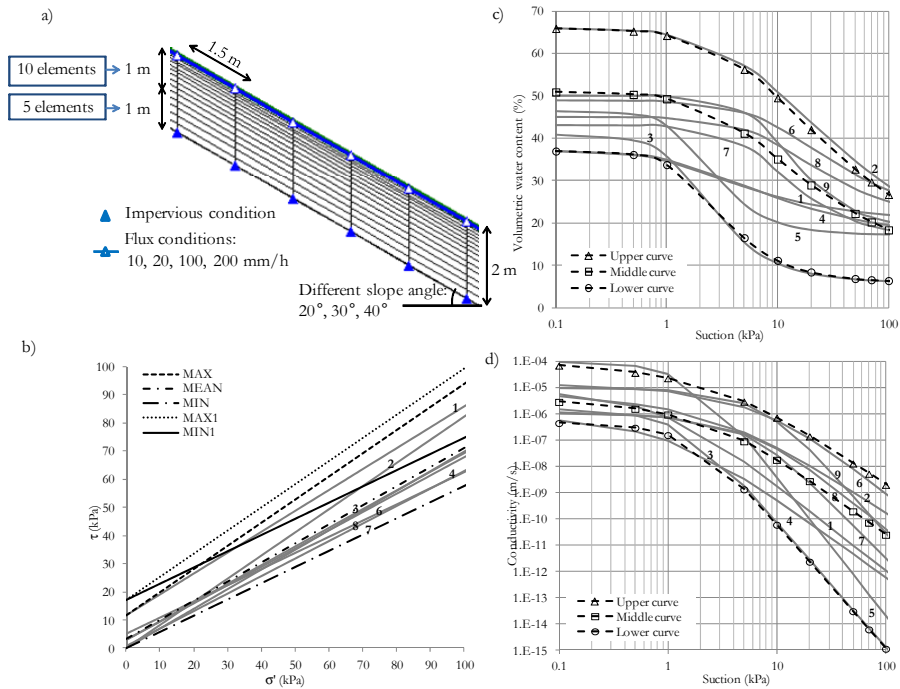
Figure 3.8 Slope geometry and hydraulic boundary conditions (a), soil shear strength (b), hydraulic soil properties (c, d) for the test areas of Figure 3.3 and Table 3.2 (Cuomo and Della Sala, 2013a).

For the hydraulic boundary conditions, different assumptions are made: i) at the bedrock contact, an impervious condition is assumed, ii) at the ground surface, a flux condition is assumed equal to four different rainfall intensities 10, 20, 100 and 200mm/h for durations of 48 h and 72 h (Table 3.5) with cumulated rainfall not exceeding 1000 mm for mechanism R2; for R1 a ponding condition (nearly zero pore water pressures for steep slopes) is assumed on the ground surface. As initial condition, three uniform distributions of suction respectively to 5kPa, 10 kPa and 20 kPa are alternatively assumed all over the slope section. Time step of the analyses is assumed equal to 120 seconds.

Table 3.4 Soil properties for the test areas of Figure 3.3 (Cuomo and Della Sala, 2013a).

ID	Country	Soil-water characteristic curves (Van Genuchten parameters)							
		n	m	a (kN/m²)	θ_{sat}	θ_r	$\theta_{sat} - \theta_r$	k_{sat} (m/s)	α (kN/m²)⁻¹
1	Thailand	1.50	0.333	1.40	0.37	0.20	0.17	1.00E-05	0.71
2	Italy	1.28	0.219	5.26	0.66	4.30E-07	0.66	1.00E-05	0.19
3	USA	2.12	0.528	1.64	0.41	0.06	0.35	1.60E-06	0.61
4	China	1.40	0.286	1.80	0.37	0.15	0.22	1.20E-06	0.57
5	Japan	2.32	0.569	1.83	0.47	0.17	0.30	1.00E-04	0.55
6	New Zealand	1.50	0.333	10	0.49	0.18	0.31	1.49E-05	0.1
7	Italy	1.90	0.474	7	0.43	0.16	0.27	1.10E-06	0.14
8	Italy	1.60	0.375	9	0.45	0.19	0.26	1.30E-06	0.11
9	Italy	2.10	0.524	9	0.5	0.18	0.32	9.26E-06	0.11
Upper	-	1.30	0.231	5	0.66	4.30E-07	0.66	1.50E-04	0.20
Middle	-	1.40	0.286	4	0.51	6.00E-02	0.45	5.00E-06	0.25
Lower	-	2.10	0.524	2	0.37	6.00E-02	0.31	5.00E-07	0.50

ID	Shear strength			
	γ_{sat} (kN/m³)	c' (kPa)	φ' (°)	φ^b (°)
1	-	11.70	36.60	22.00
2	13.10	0.00	39.50	20.00
3	-	3.00	33.60	-
4	-	3.00	33.00	-
5	-	-	-	-
6	17.60	5.00	30.00	-
7	19.40	0.50	32.00	30.95
8	18.70	0.00	35.00	33.95
9	-	-	-	-
min	13.10	0	30.00	20
min	17.07	11.7	30.00	26.73
mea	17.07	3.31	34.24	26.73
max	17.07	0	39.50	26.73
max	19.40	11.70	39.50	33.95

n: fitting constant; m=1-1/n; a: air entry value; θ_{sat}: saturated volumetric water content; θ_r: residual volumetric water content; k_{sat}: saturated hydraulic conductivity; α=1/a; γ_{sat}: saturated soil unit weight; c': effective cohesion; φ': friction angle; φ^b: rate of increase in shear strength due to suction.

For slope stability analyses, standard limit equilibrium methods (e.g. Morgenstern and Price, 1965; Janbu, 1954; among others) are used through the commercial code SLOPE/W (Geoslope, 2005). A rigid-perfectly plastic constitutive model is used for the considered soils, referring to the extended Mohr-Coulomb failure criterion proposed by Fredlund et al. (1978):

$$\tau = c' + (\sigma_n - u_a) \cdot tg\,\varphi' + (u_a - u_w) \cdot tg\,\varphi^b \qquad (3.10)$$

where τ is the shear strength, c' is the effective cohesion, φ' is the friction angle; $(\sigma_n\text{-}u_a)$ is the net total stress at failure on the plane of failure, $(u_a\text{-}u_w)$ is the matric suction and, φ^b is the angle of shearing resistance with respect to matric suction.

Soil mechanical properties are taken from literature with reference to the case histories previously mentioned in the Section 3.1.1; particularly, saturated soil unit weight equal to 13-19 kN/m^3, cohesion equal to 0 - 11.7 kPa and friction angle between 30° and 39.5° (Figure 3.8b and Table 3.4). The complete list of analysed cases is reported in Table 3.5.

Table 3.5 List of cases considered in the parametric analysis (Cuomo and Della Sala, 2013a).

Geometry	Slope angle (°)	20, 30, 40								
	Thickness (m)	2								
Soil water characteristic curve (curves of Figure 3.8)		Lower			Middle			Upper		
Initial condition	Initial suction (kPa)	5	10	20	5	10	20	5	10	20
	k_{in} (mm/h)	4.98·e^{-3}	2.23·e^{-4}	8.66·e^{-6}	0.34	0.07	0.01	10.89	2.68	0.52
Boundary condition at ground surface	Rainfall duration (h)	48, 72			48, 72			48, 72		
	Rainfall intensity (mm/h)	10, 20, 100, 200			10, 20, 100, 200			10, 20, 100, 200		
Expected mechanisms		R1			R1		R2	R2		
		I>k$_{sat}$			I>k$_{sat}$	k$_{in}$<I<k$_{sat}$		k$_{in}$<I<k$_{sat}$		

3.3.2   Numerical results

<u>Time to runoff</u>

Numerical modeling of pore water pressures is aimed to assess the potential occurrence of ponding at the ground surface. Globally, the obtained results show that a major role is played by the interplay of initial conditions and rainfall intensity (Figure 3.9a,b) with a moderate effect of the slope angle (in the investigated range of 20° to 40°) for the highest rainfall intensities (Figure 3.9a).

Particularly, for rainfall intensities larger than the soil saturated hydraulic conductivity (k_{sat}), the pore water pressures at the ground surface immediately vanish (mechanism R1) independently from initial conditions, slope angle and rainfall intensity.

In the case of a rainfall intensity lower than the soil saturated hydraulic conductivity (k_{sat}) but larger than the initial hydraulic conductivity (k_{in}) (mechanism R2), pore water pressures increase in the time and eventually reach a zero value at different times (times to runoff) (Figure 3.9a,b) which are lower than 6 hours for rainfall intensity equal to $100 \div 200$ mm/h and reach $10 \div 56$ hours for rainfall intensity equal to $10 \div 20$ mm/h. Particularly, the following points are evidenced: i) the temporal trend of the pore water pressures on the ground surface strongly depends on the soil water characteristic curves; for the "middle curve" of Figure 3.8c,d, pore water pressures increase faster than for "upper curve" (dashed lines in Figure 3.9a); ii) the higher the rainfall intensity and slope angle, the lower the time to runoff (Figure 3.9a); iii) the time to runoff increases with initial soil suction (Figure 3.9b).
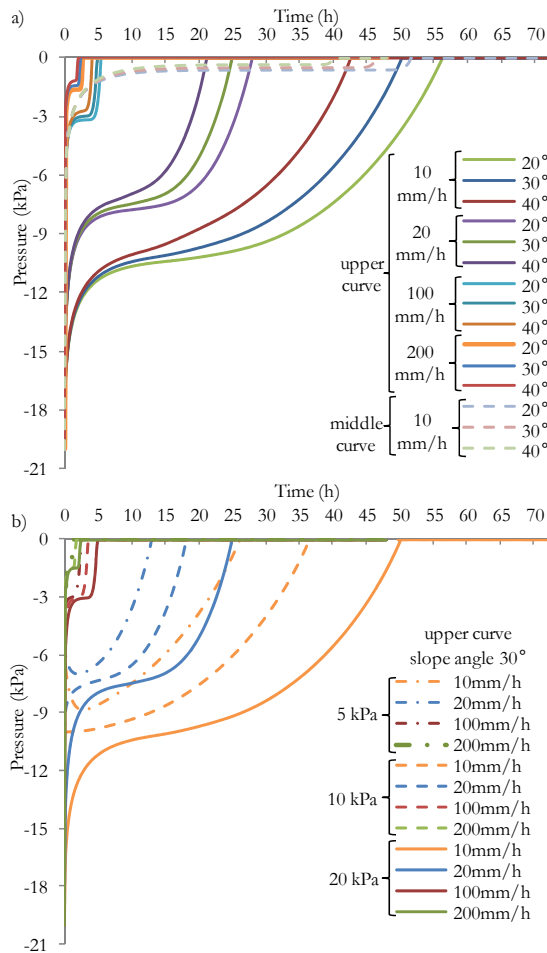
Figure 3.9 Pore water pressure computed assuming (a) an initial soil suction equal to 20 kPa or (b) a slope angle equal to 30° and upper soil water characteristic curve (modified from Cuomo and Della Sala, 2013a).

The slope stability conditions are heavily modified during rainfall infiltration and slope failure may also occur. Particularly, Figure 3.10a refers to the cases when during the rainstorm slope failure occurs before runoff has started. In most of these cases, the slip surface is located at the bedrock contact and the infiltration vectors are parallel to the ground surface. On the other hand, Figure 3.10b shows the cases in which times to runoff is lower than rainstorm duration (namely mechanism R2) and the runoff occurs before slope failure. From this instant later on,

hydraulic boundary conditions at ground surface may also get worse than ponding condition (zero pore water pressures) and a water film with an increasing height may be formed at the ground surface; this, in turn, may lead to the mobilization of single solid grains (or clusters of grains).

Based on the achieved results, it is worth noting that the lower the initial suction, the closer the points are to the envelope curves taken from literature for slope failures (Figure 3.10a); furthermore, in Figure 3.10b, the points corresponding to higher rainfall intensity are outside the literature envelope curves for failure possibly outlining a different triggering mechanism.
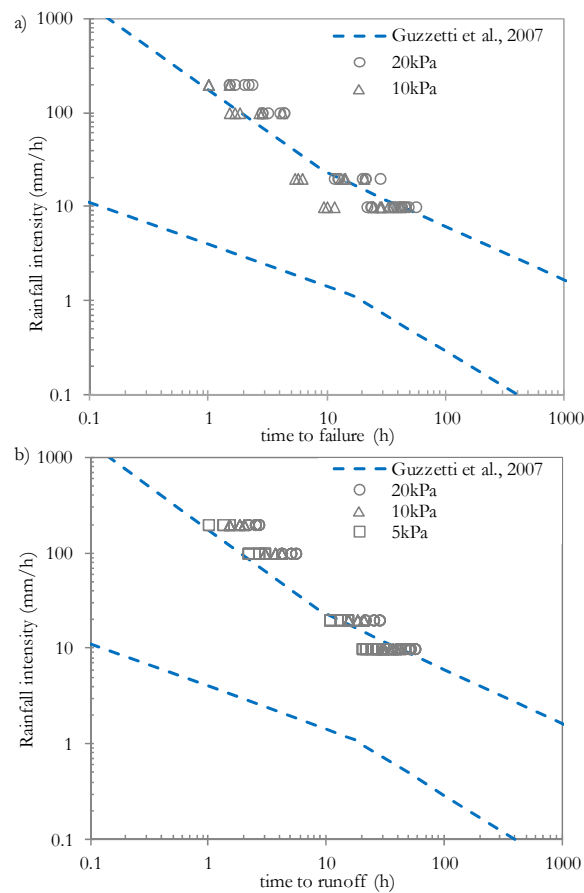
Figure 3.10 a) Failure time for different initial suction when $t_{failure}$ < t_{runoff} and time to runoff for different initial suction in the case of t_{runoff} < $t_{failure}$ (b) (modified from Cuomo and Della Sala, 2013a).

Taking into account the results of either seepage or slope stability analyses, correlations between cumulative rainfall and times to runoff are investigated for the mechanism R2. In particular, Figure 3.11 shows that for initial suction equal to 20 kPa and rainfall intensity not exceeding the soil saturated conductivity (k_{sat}), runoff occurs with a minimum cumulative rainfall of about 400 mm in 2÷ 56 hours independently from slope angle and from soil water characteristic curve (upper or middle curves). However, lower cumulative rainfalls are sufficient for runoff if lower initial soil suctions are considered. For instance, for soil initial suction equal to 5÷10 kPa, runoff occurs due to cumulative rainfall of 200÷400 mm (Figure 3.11). In these cases, slope failure may also occur due to water infiltration and the chance to have runoff at ground surface depends much on the soil strength parameters. Finally, Figure 3.12 shows that for a given rainfall intensity and slope angle, a linear correlation exists between cumulative rainfall at the time to runoff and the initial suction.
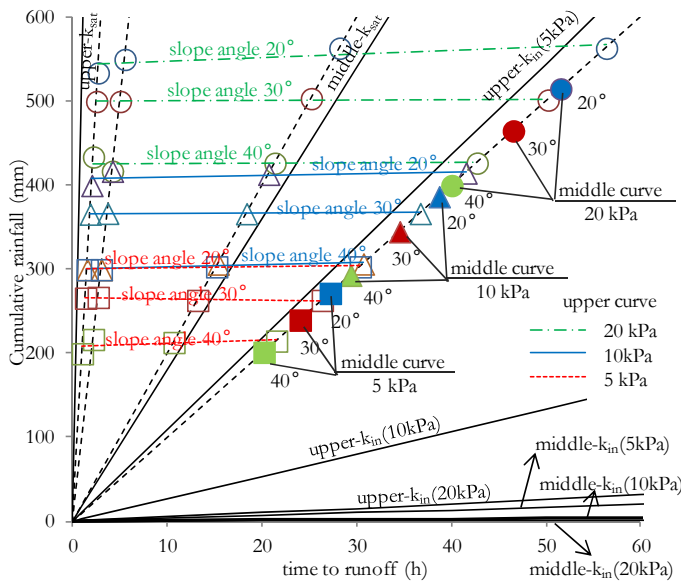
Figure 3.11 Cumulative rainfall at time to runoff for mechanism R2 (Cuomo and Della Sala, 2013a).
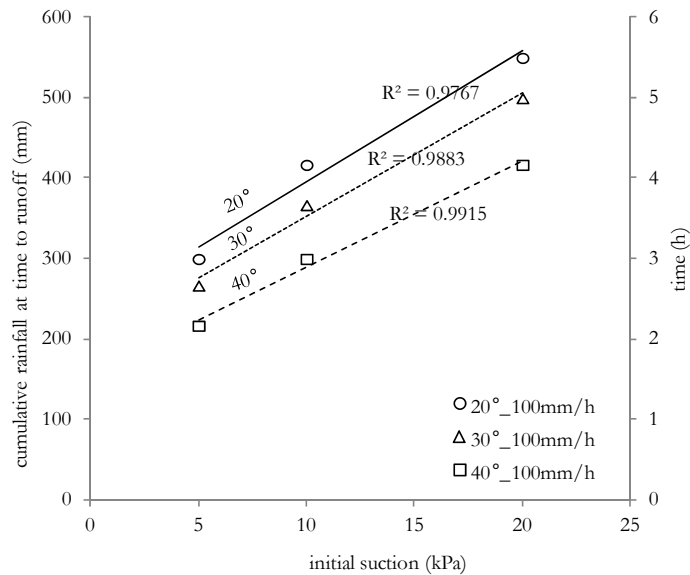
Figure 3.12 Cumulative rainfall versus time to runoff (Cuomo and Della Sala, 2013a).

Infiltration and runoff estimation

For all the cases of Table 3.5, the infiltration rate is computed at points close to the ground surface (z=0.04÷0.05 m) and thus the runoff rate is obtained as difference from rainfall intensity.

In particular, for the mechanism R1, the obtained results are provided in Figure 3.13 which shows that the infiltration rate decreases quickly during the first three hours independently from initial suction and slope angle. Then, the infiltration rate keeps constant (lower than saturated hydraulic conductivity) over a time range strictly dependent on initial suction and slope angle. Finally, the curve decreases again up to a negligible value.
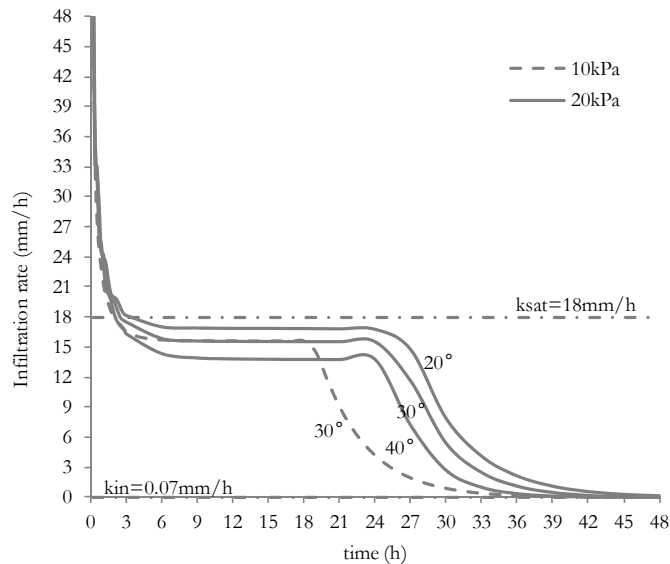
Figure 3.13 Mechanism R1: infiltration rate computed for different initial suctions (Cuomo and Della Sala, 2013a).

For the mechanism R2 and initial suction equal to 20 kPa, it is possible to observe that the runoff rate is strongly influenced by slope angle and soil water characteristic curve, at low rainfall intensities (10÷20 mm/h) (Figure 3.14a). Indeed, after the time to runoff, the runoff rate increases more quickly when the upper characteristic curve is used and more slowly when the middle characteristic curve is considered (Figure 3.14a). For higher values of rainfall intensities, the runoff starts earlier than in previous case and great runoff discharges can take place for long-lasting rainfalls (Figure 3.14a). Furthermore, slope angle is outlined as an important factor for the runoff generation because it strongly affects the time to runoff; for instance, for a steep slope (40°) runoff starts quite earlier than gentler slopes (20°).

For the same mechanism and the same initial suction, the cumulative runoff is evaluated and compared with the cumulative rainfall in Figure 3.14b. This figure shows that the curves change with the slope angle but for the same slope angle the curves slightly change when different rainfall intensities are applied. The obtained results are in agreement with data recorded by Rahardjo et al. (2004) that shows that about 60-26% of the total rainfall contribute to runoff, depending on the rainfall intensity and duration (cumulative rainfall).
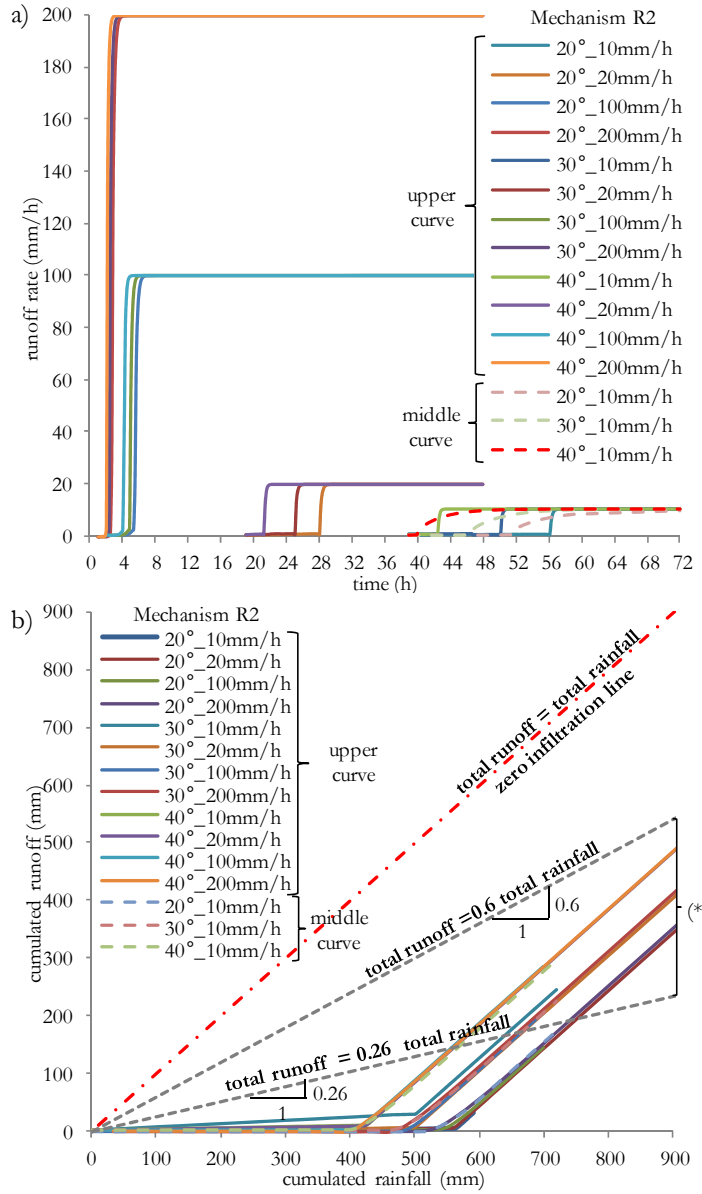
Figure 3.14 Mechanism R2: a) runoff rates, and b) cumulated rainfall versus cumulated runoff. Initial soil suction equal to 20 kPa (Cuomo and Della Sala, 2013a).

<u>Comparison with standard methods</u>

The proposed approach is compared to the Curve Number method (USDA-SCS, 1972) and the modified Green-Ampt method (Mein and Larson, 1973) which are both mostly used for erosion and sediment transport evalutation. In particular, the Curve Number method is used in the empirical RUSLE model (USDA-ARS, 2008) to compute the runoff, later used to estimate a average annual soil loss in a given area; whereas, the Green-Ampt Mein-Larson infiltration equation is used in the hillslope component of the physically-based WEPP method (Ascough et al., 1997) to calculate the runoff for the spatial and temporal estimates of erosion and deposition in watersheds composed of hillslopes and channels and the original Green-Ampt model is used to evaluate the infiltration component in the physically-based LISEM erosion model (De Roo et al., 1999; Jetten, 2002).

In both methods, whose equations are given in details in Section 3.1.3, the cumulated infiltration rate is schematised and computed through nearly linear equations without any knick point corresponding to the occurrence of a triggering mechanism R2. An application of these methods is hereafter proposed for some cases of Table 3.5 with the input data reported in Table 3.6.

Table 3.6 Input data for Curve Number and modified Green-Ampt method (Cuomo and Della Sala, 2013a).

	I (mm/h)	Hydrological Soil Group	CN value (*)
CN method	10, 20, 100, 200	A, B, C, D	54, 75, 86, 92

(*) Antecedent Moisture Condition Class: II; Landuse or cover: woods in poor hydrological condition; Slopes: class V, >20° very steep

	I (mm/h)	k_{sat}	Initial suction (kPa)
G-A method	10, 20, 100, 200	lower, middle (**)	5, 10, 20

(**) Curves taken from Table 3.4

For the highest rainfall intensities (100÷200 mm/h), both standard methods (CN and GA) predict the runoff starting almost at the beginning of the rainstorm (Figure 3.15 and Figure 3.16). On the other hand, the proposed approach predicts a runoff starting after 1÷2 hours if the initial suction is equal to 5kPa (Figure 3.9b).

For lower rainfall intensities (10÷20 mm/h), the Curve Number

method outlines a nil time to runoff (Figure 3.15), while the modified Green-Ampt method shows that runoff starts after 3 hours (Figure 3.16). In the same cases, the proposed approach shows that the runoff occurs after 10 hours when initial suction is equal to 5kPa (Figure 3.9b). Particularly, the modified Green-Ampt method outlines that the lower the rainfall intensity the longer the time to runoff (Figure 3.16) in agreement with the results of the proposed approach (Figure 3.9a).

Finally, a relation between cumulated rainfall and computed cumulated runoff is plotted in Figure 3.17, as provided by the above mentioned methods. It is worth noting that: i) the CN method provides a curve quite close to the zero infiltration line (1:1 steep in the plot), ii) lower runoff estimates come from the modified GA method with low times to runoff independently of initial soil suction, iii) the proposed method outlines a new time pattern for the runoff curve with times to runoff strongly dependent on the initial soil suction.
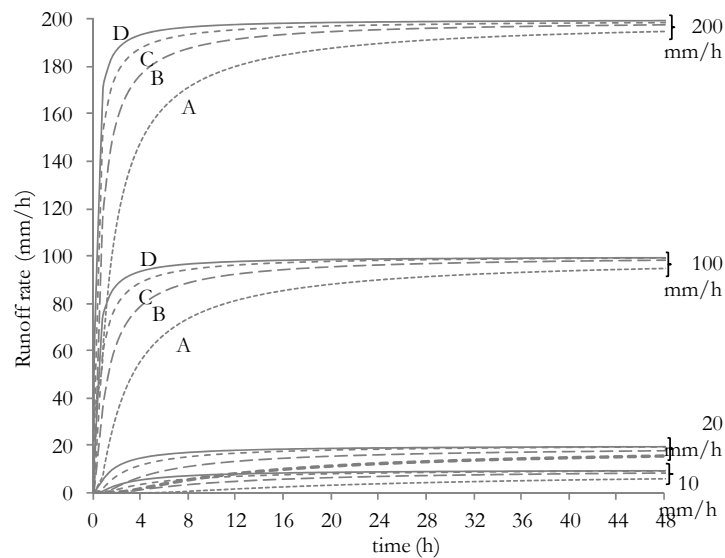
Figure 3.15 Runoff rate versus time as computed through the CN method. Initial soil suction equal to 20 kPa (Cuomo and Della Sala, 2013a).
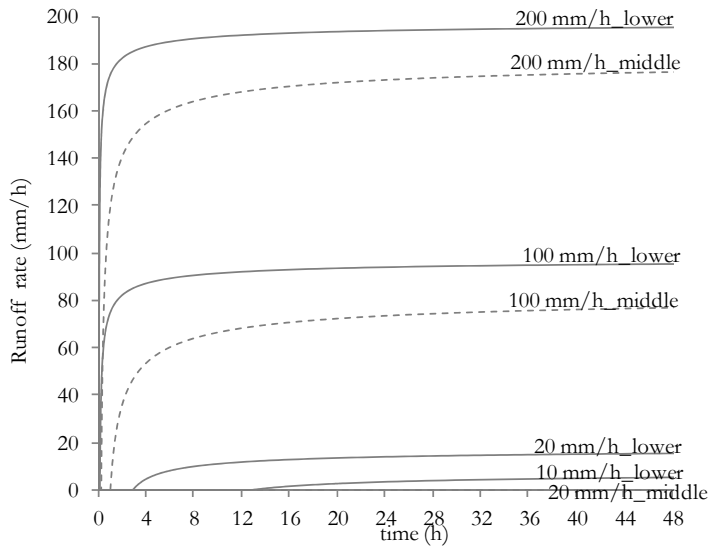
Figure 3.16 Runoff rate versus time as computed through the modified Green-Ampt method. Initial soil suction equal to 20 kPa (Cuomo and Della Sala, 2013a).
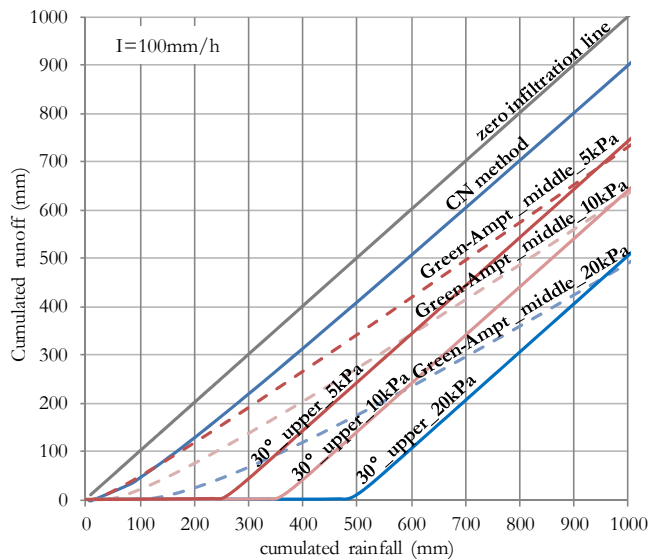
Figure 3.17 Cumulated rainfall versus cumulated runoff computed through Curve Number method, modified Green-Ampt method and the proposed method (Cuomo and Della Sala, 2013a).

3.4 CONCLUDING REMARKS

Rainfall infiltration and runoff may lead to either slope failure or erosion processes in unsaturated shallow deposits. Particularly, depending on the combination of rainfall intensity and duration, different flow-like mass movements may occur, whose distinction is fully necessary for the management and mitigation of the risks posed.

An engineering reference framework is proposed for the evaluation of both the amount of rainfall infiltrating the ground surface in time and the runoff flowing at the ground surface as wash out. This framework is validated through a numerical parametric analysis based on seepage and slope stability analysis. The obtained results show that time to runoff, time to failure and runoff rates are strongly affected by soil water characteristic curves, soil initial conditions, rainfall intensity and slope angle. Furthermore, slope stability analyses show that the temporal occurrence of failure or runoff is related to soil strength parameters.

Finally, it is outlined that simplified standard procedures can provide a poor estimation of the time to runoff and runoff discharge which can be improved through the application of the proposed procedure.

4 THE CASE STUDY

Aimed at evaluating the amount of solid particles mobilised due to runoff, it is fundamental referring to real topography usually represented by Digital Terrain Model (DTM). A case study from Southern Italy is here addressed, whose significance relies on the following reasons: i) it was affected in the past by different flow-like phenomena; ii) it belongs to a large area of the Campania region, composed of hillslopes covered by pyroclastic soil deposits, for which recent studies show that first-time shallow slides may turn into debris flows or debris avalanches while slope instabilities initiated by erosion phenomena generally propagate as hyperconcentrated flows; and iii) it is a well-known and attractive site for tourists all over the world and, for this reason, the risk can increase during some periods of the year.

4.1 GEOLOGICAL SETTING

The study area corresponds to the coastal part of the Campania region (Southern Italy) overlooking the Gulf of Salerno (Figure 4.1). This territory, usually named "Amalfi Coast", covers an extent of approximately 130 km^2 and is included in the UNESCO World Heritage for its physical and natural beauty including terraced orchards, landscape, seaside and wonderful towns such as Amalfi and Positano, which attract thousands of tourists every year. The study area includes the south side of the Lattari Mounts where high steep relieves exist (Figure 4.1), like San Michele mount (1444 m a.s.l.), Cerreto mount (1316 m a.s.l.) and Finestra mount (1145 m a.s.l.) sloping towards the sea coast. On the west side of the study area, minor mounts can be found such as San Costanzo mount (497 m a.s.l.) and also a large flat area, named Agerola plateau, at 600 m a.s.l.

Figure 4.1 Characterisation of the study area: a) hillshade and main basins (data from Autorità di Bacino Destra Sele, 2012), b) Cetara town and c) Maiori town from the sea.

Funnel shaped mountain basins with a high order of drainage networks are widespread (Figure 4.2 and Table 4.1), and are characterised by steep stream channels (Figure 4.2), with a preferential orientation from north to south, which run through engravings of tectonic origin. The largest basin (Regina Maior) covers 33 km^2 and the stream channel runs over a distance of about 10 km from the top of the Chiunzi mount (880 m a.s.l.) to the sea. Table 4.1 shows the morphometric features of the main basins belonging to the study area.

Table 4.1 Morphometric features of main basins in the study area.

Main basins	Urban areas at the outlet	Area (km²)	Perimeter (km)	Length of main stream channel (km)
Furore	Furore	13.2	18.6	8.0
Grevone	Amalfi	7.8	13.6	5.0
Dragone	Atrani	9.3	15.7	6.5
Regina Minor-Sambuco	Minori	5.6	12.1	5.3
Regina Maior	Maiori	33.0	27.1	9.5
V.ne Grande-Cetus	Cetara	3.7	8.1	3.5
Bonea	Vietri s.m.	19.7	22.5	8.0

The Lattari mounts are mainly composed of limestone, formed in the Mesozoic age on the carbonate platform (Autorità di Bacino Destra Sele, 2012). This area has undergone strong compression stages during the Miocene and finally during the Quaternary. The evidences of these vertical displacements can be clearly seen in the vertical scarps, which correspond to the Quaternary fault planes. The powerful rises expose the entire depositional sequence which, although broken up, reaches 4500 meters in thickness: at the base, there are dolomitic stones while in upper portions limestones prevail.
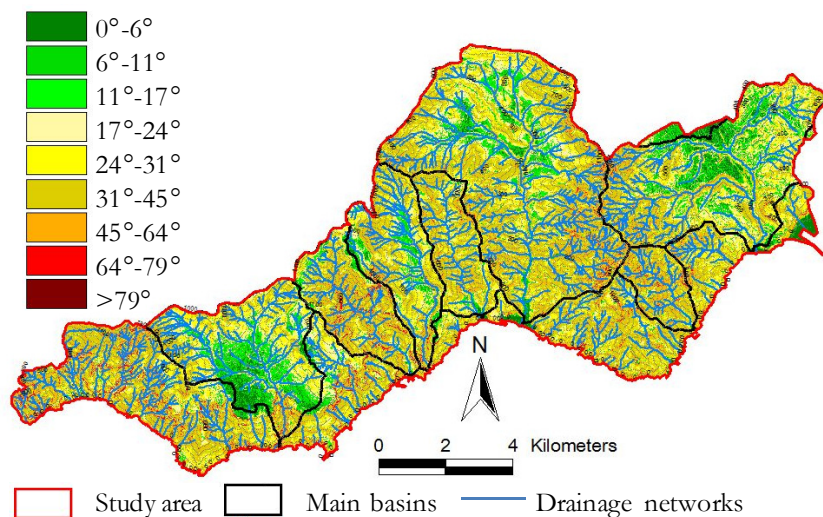
Figure 4.2 Slope angle map of the study area (data from Autorità di Bacino Destra Sele, 2012).

Focusing on the geolithological aspects (Figure 4.3), the study area can be divided into two main sectors: at west, from Positano to Minori and part of Tramonti town, the hillslopes are mainly composed of limestones; only the plateau of Agerola and part of the territory of Scala town are composed of sandy conglomerates and travertine; at east, from Amalfi to Vietri sul Mare, stratified dolomitic stones are prevalent; part of the Cava dei Tirreni town is also composed of sandy conglomerates and travertine (Autorità di Bacino Destra Sele, 2012). The Lattari mounts are highly fractured and karsified structure, that makes these areas very permeable, facilitating the formation of karst processes with the eventual formation of ephemeral water springs from bedrock in the upper portions of slopes (Figure 4.3) (Autorità di Bacino Destra Sele, 2012).
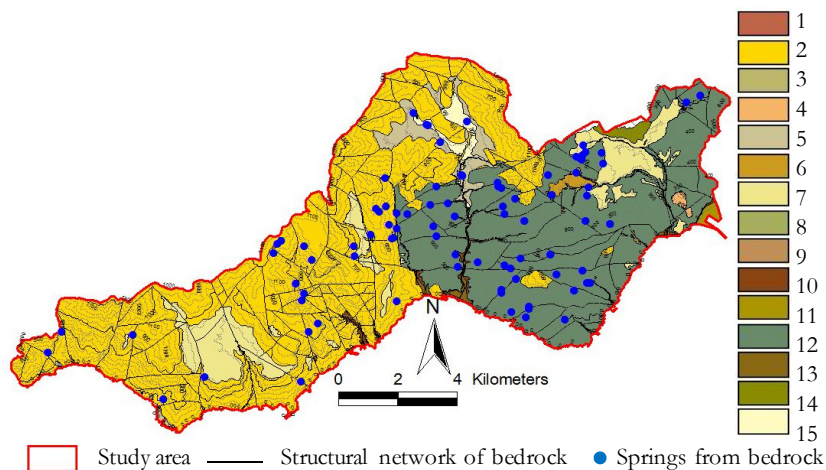
Figure 4.3 Geolithological and hydrogeological map of the study area; 1: pelitic sandstone complex; 2: limestone complex; 3: limestone marl complex A; 4: limestone marl complex B; 5: gravelly conglomerate complex; 6: sandy conglomerate complex; 7: sandy travertine conglomerate complex; 8: loose debris complex; 9: loose marine sand complex; 10: debris complex; 11: articial debris complex; 12: stratified dolomitic stones complex; 13: politic gravelly and sandy complex; 14: pyroclastic sandy and silty complex; 15: tuff stone complex (data from Autorità di Bacino Destra Sele, 2012).

The hillslopes are widely covered by quaternary alluvial soils and pyroclastic soils originating from the explosive phases of the Somma-Vesuvius volcanic activity (it is worth mentioning the eruptions of 79 and 1944; Cascini et al., 2008). The orographic and hydrographic

configuration is strictly related to the geological-structural configuration of the bedrock. Different types of soils cover the hillslopes; in particular (Autorità di Bacino Destra Sele, 2012): i) deposits of debris - pyroclastic soils are prevalent on the hillslopes and consist of ashes/sands or pumice, slag and carbonate clasts linked to processes of colluvial and runoff type; ii) on the ridges, there is the presence of pyroclastic deposits made by falling ash, sand, pumice and slag, sometimes in primary layer with well-developed shallow layers of soil; iii) at toe of the hillslopes, it is possible to recognize deposits of debris - pyroclastic soil, formed of ashes, sands, pumices and slags along with rocky sediments that result from the progressive accumulation of material from the hillslopes; iv) in the channels, there are loose fluvial deposits of different sizes, consisting of angular gravels and pebbles, with the presence of sandy - silty matrix, alternatively; v) in the whole area, scarps of the Mesocenozoic rocks and Quaternary continental deposits are widespread. Moreover, the map of soil thickness (Figure 4.4) shows that: i) on hillslopes, the bedrock is covered by deposits that have a few meters thick (generally less than 2 m); ii) at the toe of hillslopes, the soil thickness can exceed 5 meters.
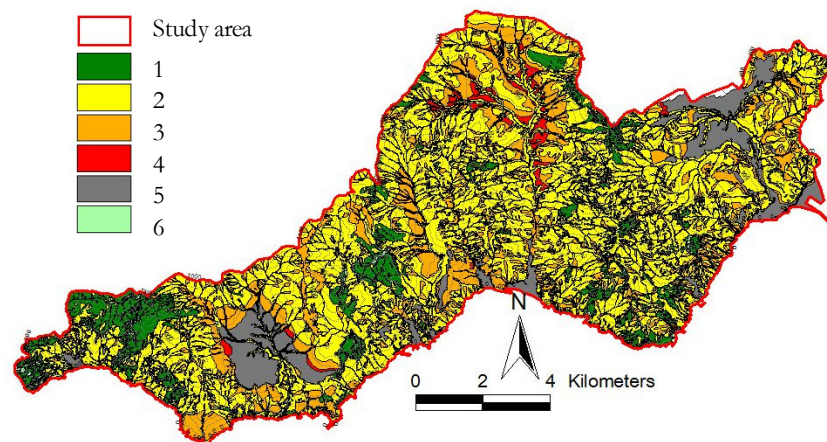
Figure 4.4 Map of deposits thickness of the study area; 1: 0m<h<0.5m, 2: 0.5m<h<2m, 3: 2m<h<5m, 4: 5m<h<20 m, 5: not available; 6: bedrock scarps (data from Autorità di Bacino Destra Sele, 2012).

The geomorphological features (Figure 4.5) of the study area testify the succession of different cycles of erosion-deposition, related to different tectonic and climatic stages occurred during the Quaternary.

These events have left more or less evident signs in the morphology of hillslopes and in the stratigraphy and sedimentology of the deposits. Three main physiographic systems can be distinguished (Autorità di Bacino Destra Sele, 2012): i) carbonate hillslopes characterised by high slope angles and numerous morphological bedrock scarps; ii) main mountain channels characterised by high slopes and rectilinear features that have fixed beds and angles of confluence generally very high; iii) coastal alluvial valley characterised by intense anthropogenic activities.
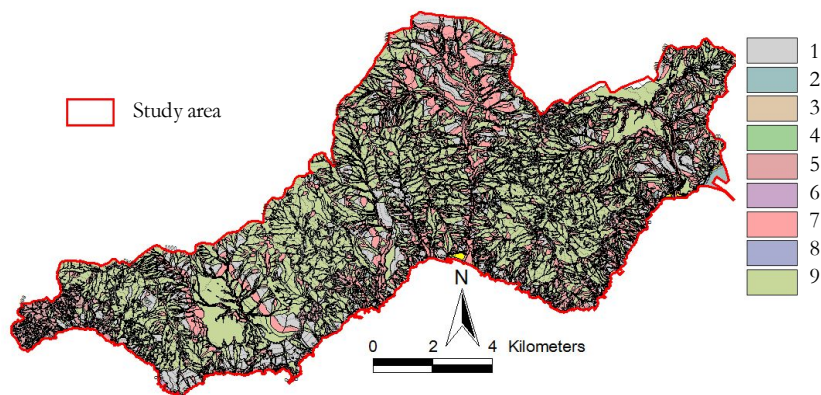
Figure 4.5 Geomorphological map of the study area; 1: litho-structural landforms; 2: anthropogenic landforms, 3: karst landforms, 4: landforms of volcanic genesis, 5: hillslope landforms due to gravity; 6: landforms and elements of marine genesis; 7: river landforms and hillslope landforms due to runoff; 8: hydrography; 9: morphological units and associated landforms of complex genesis (data from Autorità di Bacino Destra Sele, 2012).

In particular, the main landforms (Figure 4.5), widespread in the area, are: i) morphological units and associated landforms of complex genesis (summit with ridges, endoreic plains, river hillslopes and hillslopes of denudation); ii) litho-structural landforms (ridges, litho-structural hillslopes, bedrock scarps); iii) river landforms and hillslope landforms due to runoff (Zero Order Basins, alluvial fans, alluvial talus, river terraces); iv) hillslope landforms due to gravity; v) karst landforms; vi) hydrography (fluvial and torrential channel); vii) landforms of volcanic genesis (volcanic terraces); viii) landforms and elements of marine genesis (scarps of marine erosion, cliffs); ix) anthropogenic landforms. The zero order basins, summit with ridges, river hillslopes and hillslopes of denudation are widely widespread. At the toe of hillslopes, alluvial

fans can be recognised.

With reference to the land use (Figure 4.6), the study area includes: i) anthropogenically modified areas composed by continuous and discontinuous urban fabric and port areas, especially located at the outlet of the main basins and at the toe of the main hillslopes; ii) agricultural areas composed by olive groves, annual crops associated with permanents crops, complex cultivation patterns and land principally occupied with significant areas of natural vegetation, located near the sea and not very steep areas; iii) forests and semi-natural areas principally composed by broad-leaved forest, mixed forests, natural grassland, Mediterranean scrub, transitional woodlands scrubs and sparsely vegetated areas, located in the upper part of the hillslopes.
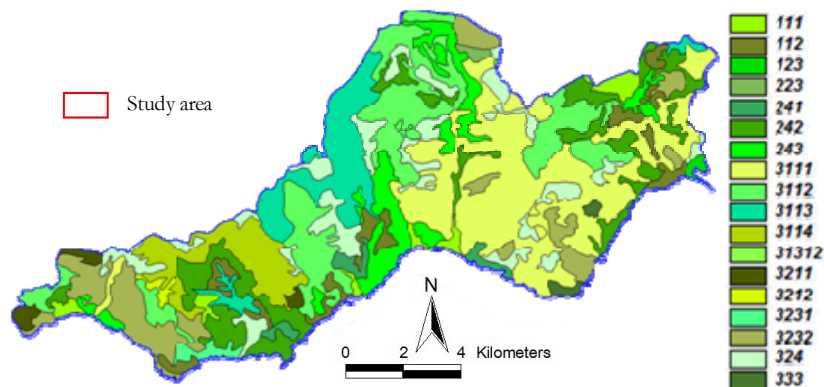
Figure 4.6 Land cover map of the study area; 111: continuously urbanized area, 112: discontinuously urbanized area, 123: harbour areas, 223: olive groves, 241: temporary and permanent crops, 242: complex cultivation patterns, 243: agriculture and natural vegetation, 3111: forests with prevalence of oaks and other evergreen broadleaf, 3112: forests with prevalence of deciduous oaks, 3113: mixed forests with prevalence of other native broadleaf, 3114: forests with prevalence of chestnut, 31312: mixed forests of coniferous and broadleaf with prevalence of deciduous oaks, 3211: continuous grasslands, 3212: discontinuous grasslands, 3231: high mediterranean scrub, 3232: low Mediterranean scrub, 324: areas with forest and shrub vegetation in evolution, 333: sparsely vegetated areas (data from Corine Land Cover IV livello, 2006).

4.2 PAST EVENTS

The complexity of topography, geology, geomorphology, hydrogeology and anthropogenic factors predisposes the area for the occurrence of different rainfall-induced slope instabilities which, in the past, produced several catastrophic events (October 1899, 1910, 1954, among other), especially in the towns located at the outlet of the main stream channels (Figure 4.7a). It is worth noting that most of the events occurred in October and January while the fatalities are mostly recorded in October and November (Cascini et al., 2009) (Figure 4.7b).
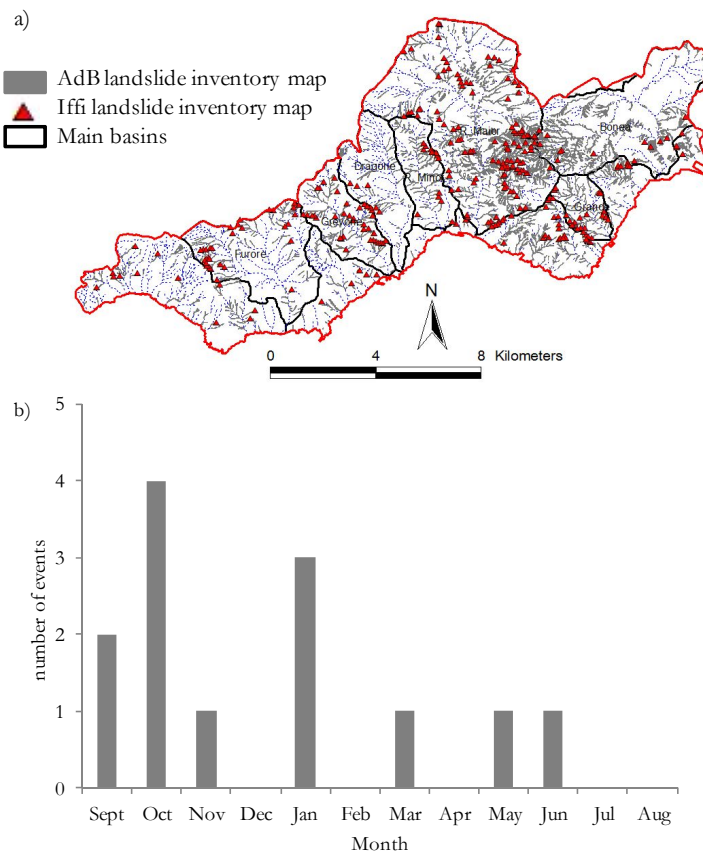
Figure 4.7 Past events: a) Landslide inventory map (data from Autorità di Bacino Destra Sele, 2012); b) monthly distributions of fatal landslides of the flow-type occurred within the study area (data from Cascini et al., 2009).

The major catastrophic events are summarised in Table 4.2. In particular, on 7-8 October 1899, a 12-18 hours rainstorm triggered several shallow landslides and erosion phenomena in the upper zones of the Bonea basin (Vietri sul Mare and Cava de' Tirreni) and caused flow-like mass movements which propagated downstream, causing deaths and heavy damages to structures such as houses, farmlands, roads, railways, cotton industry mills, aqueduct and, bridges (Esposito et al., 2003).

Table 4.2 Major catastrophic events occurred in the study area.

Date	Affected area (km²)	Affected towns in the study area	Damages to people	Damages to buildings and infrastructures
7-8 October 1899	400	Cava dei Tirreni, Vietri sul Mare	100 victims	houses, farmlands, roads, railways, cotton industry mills, aqueduct, bridges
24-25 October 1910	70	Cetara, Maiori, Minori, Vietri sul Mare, Ravello, Tramonti, Furore, Amalfi, Scala	about 200 victims 111 victims at Cetara town	houses, roads, railways, bridges
25-27 March 1924	50	Vietri sul Mare, Maiori, Minori, Furore, Atrani, Amalfi, Praiano, Agerola, Positano	about 100 victims	cultivated fields, houses, roads, bridges
25-26 October 1954	90	Cave dei Tirreni, Vietri sul Mare, Maiori, Minori, Tramonti, Atrani, Amalfi, Praiano, Positano	318 victims 350 injured 10.000 homeless	Buildings, industries, roads, railways, aqueducts
9 September 2010	9	Scala, Atrani	1	Bridges, roads, houses

On 24-25 October 1910, a 36 hours rainfall caused: i) the obstruction of the main stream at the outlet of Cetus basin with debris and trees causing the leakage of water and sediment that flooded the Cetara village and ii) the occurrence of four landslides at the upper part of the basin which inundated the main road with a 5 m thick cover of mud and

debris. As consequence, in the Cetara village, 150 victims were recorded and several buildings, roads and bridges were damaged (Trigila et al., 2007). On 25-27 March 1924, a rainfall of 118.3 mm in 48 hours originated several slope instabilities that caused victims and damages to houses, roads, and bridges (AVI Project, 1994) in a part of the Amalfi town.

On 25-26 October 1954, a cumulative rainfall estimated equal to 504 mm (Tranfaglia and Braca 2004, Cascini et al., 2009; De Luca et al., 2010; Tessitore et al., 2011) affected the east part of the study area (Figure 4.8a) triggering several slope instabilities (Figure 4.8b) that involved several municipalities, causing 325 fatalities and huge damages (Cascini et al., 2008b). During the event, both erosion processes evolving into hyperconcentrated flows (Coussot and Meunier 1996) and first-time shallow slides propagating as debris flows (Hungr et al., 2001) occurred (Cascini et al., 2009). Figure 4.8b shows the source areas of the 1954 event (data from Autorità di Bacino Destra Sele, 2012).
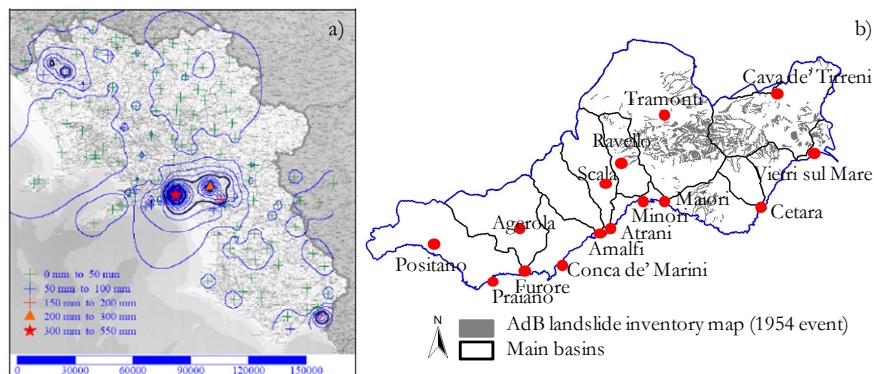
Figure 4.8 a) Rainfall distribution on 26th October 1954 (De Luca et al., 2010); b): landslide inventory map for the 25-26th October 1954 event (data from Autorità di Bacino Destra Sele, 2012).

Finally, on 9 September 2010, an intense rainfall, with maximum hourly intensity equal to 70 mm/h recorded to the raingauge of Ravello (Autorità di Bacino Destra Sele, 2010), affected an area between Agerola and Minori towns. The main basin affected by the event was the Dragone basin where erosion phenomena and shallow landslides were triggered (Autorità di Bacino Destra Sele, 2012) (Figure 4.9a,b). Water

and sediments propagated in the main channel and impacted the Atrani village, causing damages (Figure 4.9c) and a victim.

Figure 4.9 2010 event: a, b) slope instabilities in the upper part of the Dragone basin; c) damage at the outlet of the Dragone basin (photo from Autorità di Bacino Destra Sele, 2010).

As outlined by Cascini et al. (2013), past events can be classified with reference to the extension of the affected area as: i) local (e.g. September 2010), ii) widespread (e.g. October 1910, March 1924, and October 1954) and their occurrence is related to the seasonal effects of rainfall in the unsaturated pyroclastic soils covering the hillslopes. Based on rainfall, suction and historical data, the authors underlined that (Table 4.3): i) in the months of September and October, when the soil suction is variable between 20-30 kPa (period 1, range "high"), mostly erosion phenomena occur, typically turning into hyperconcentrated flows; ii)

from January to May, when the soil suction values are lower than 10 kPa (period 3, range "low"), shallow landslides are triggered, later evolving into debris flows or debris avalanches; iii) in the months of November and December, when the soil suction is variable between 10-20 kPa (period 2, range "medium"), both erosion phenomena and shallow landslides may occur and iv) from June to August, when suction is higher than 30 kPa (period 4, range "very high"), only local erosion phenomena and small-size shallow landslides may be triggered.

Table 4.3 Interpretation of slope instability types based on rainfall, suction and historical data in the Campania region (Cascini et al., 2013).

	Oct	Nov	Dec	Jan	Feb	Mar	Apr	May	Jun	Jul	Aug	Sep
Rainfall *			Rainy							Dry		
Pa - cumulative antecedent (mm)	$Pa < 200$	$200 < Pa < 500$					$Pa > 500$					
Pe - critical 48 hours rainfall event (mm) *	$Pe > 120$	$120 > Pe > 60$					$Pe < 60$					
typical suction range **	high	medium				low				very high		high
some events ***	1910, 1954, 1966 (Lattari mounts)	1999 (Cervinara town)				January 1841 (Gragnano town), March 1924 (Lattari mounts), May 1998 (Pizzo d'Alvano massif),				August 1935 (Gragnano town)		2010 (Atrani town)
Period	1	2				3				4		1

* Data from Rossi and Chirico (1998)
** Data from Cascini and Sorbino (2004)
*** Data from Mete and Del Prete (1999), Cascini et al. (2008b) and Bovolin (2012)

With reference to the erosion phenomena, De Falco (2011) showed that in the Campania region, the most critical seasons are Autumn and Winter when the erosion is intense, while in Spring and Summer, the area is less susceptible to erosion processes, due to either less frequent or less intense rainfall as well as to the presence of vegetation that preserves the ground surface from erosion. Moreover, carbonate hillslopes (Lattari Mounts, Picentini Mounts and Matese Mounts) are outlined as highly susceptible to erosion due to the spatial distribution of rainfall and topographical features of the hillslopes (Figure 4.10).
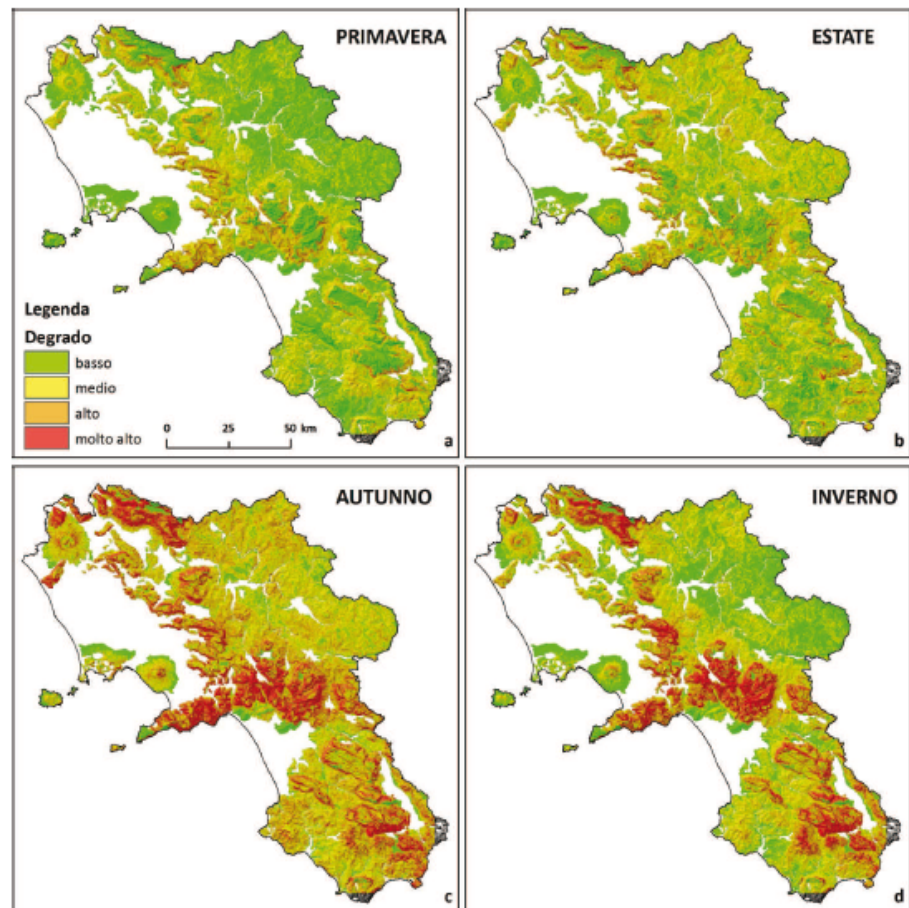
Figure 4.10 Seasonal soil erosion map for the Campania region (De Falco, 2011).

5 SPATIALLY-DISTRIBUTED ANALYSIS OF FLOW-LIKE MASS MOVEMENTS OVER LARGE AREA

In this Chapter, a spatially-distributed analysis of triggering of shallow landslides and erosion phenomena is performed for the case study of Amalfi Coast considering the seasonal variation of input data.

5.1 MODELING OF SHALLOW LANDSLIDES

5.1.1 Methods and input

The analysis of landslide triggering areas is performed through the TRIGRS-unsaturated model (Savage et al., 2004) which implements a transient seepage analysis using the linearised solution of Richards' equation (1931) proposed by Iverson (2000) and extended by Baum et al. (2008) to the case of impermeable bedrock located at a finite depth. As far as the slope stability conditions, the TRIGRS model provides the computed factor of safety (FS) for each cell of the Digital Terrain Model (DTM) at different depths and can take into account the spatial variation of soil thickness and soil properties. Unsaturated soil conditions and soil water characteristic curves are dealt with Gardner's model (Baum et al., 2008), which reads:

$$k(\psi) = k_{sat} \cdot \exp(\alpha \cdot \psi) \tag{5.1}$$

$$\theta = \theta_r + (\theta_{sat} - \theta_r) \cdot \exp(\alpha \cdot \psi) \tag{5.2}$$

where ψ is the pressure head, $k(\psi)$ is the hydraulic conductivity function, k_{sat} is the saturated hydraulic conductivity, θ is the volumetric water content, θ_{sat} and θ_r are the saturated and residual volumetric water content respectively, α is the distinctive parameter of Gardner's curves.

Particularly, $1/\alpha$ represents the (vertical) height of the capillary fringe above the water table. Details of the TRIGRS model are reported in Baum et al. (2008).

The DTM of the study area is obtained from the topographical map at 1:25,000 scale and it consists of 20×20 m cells. This detail of topography appears adequate to compare the possible occurrence of distinct phenomena but not to accurately assess the extent and location of the affected areas. The pyroclastic soil cover map was provided by Autorità di Bacino Destra Sele (2012) at 1:25,000 scale and distinguishes five thickness classes (0-0.5, 0.5-2, 2-5, 5-20, >20m). As for the mean values of soil unit weight (γ=15 kN/m^3), friction angle (φ'=38°), effective cohesion (c'=5kPa) and soil hydraulic conductivity and diffusivity, they are selected among the values used by Sorbino et al. (2010) who successfully back-analysed the triggering of shallow landslides in a study area 10 km far away from the Amalfi Coast (Pizzo d'Alvano massif, May 1998). Boundary conditions are represented by rainfall intensity and duration measured during the event of 25-26 October 1954. Particularly, due to the uncertainties on the measured rainfall pattern (504 mm in about 8 or 16 hours), two boundary conditions are assumed keeping constant the cumulated rainfall amount (504 mm) while considering durations equal to 8 hours (Cascini et al., 2009) or 16 hours (Tessitore et al., 2011, Frosini, 1955, Esposito et al., 2003). As far as the initial conditions, two initial water table depths are considered, which provide mean suction values in the range 20 – 30 kPa at the ground surface, in agreement with the range "high" indicated by Cascini et al. (2013) for the month of occurrence of the event (October).

The analyses are also extended to other cases to evaluate the effects of both the initial conditions (i.e. different soil suctions) and soil hydraulic properties. In the first set of analyses, different initial water table depths are considered, corresponding to suction average values within the ranges "medium" (10-20 kPa), and "very high" (>30kPa) reported by Cascini et al. (2013). In the second set of analyses, slope stability conditions are evaluated with reference to distinct hydraulic properties of pyroclastic deposits derived from Sorbino et al. (2010). The most significant cases and their input data are reported in Table 5.1.

Table 5.1 Input data for the TRIGRS-unsaturated model (modified from Della Sala and Cuomo, 2013).

Case	Initial suction at the ground surface (kPa)	Hydraulic Conductivity k_{sat} (*) (m/s)	Diffusivity D (*) (m²/s)	Parameters of Gardner's curves TRIGRS-unsaturated (*)		
				α (m⁻¹)	Residual water content θ_r	Saturated water content θ_{sat}
1	14.59	1 x 10⁻⁵	5.9 x 10⁻⁵	6.3	0.20	0.66
2	16.43	1 x 10⁻⁵	5.9 x 10⁻⁵	6.3	0.20	0.66
3	20.13	1 x 10⁻⁵	5.9 x 10⁻⁵	6.3	0.20	0.66
4	27.50	1 x 10⁻⁵	5.9 x 10⁻⁵	6.3	0.20	0.66
5	38.58	1 x 10⁻⁵	5.9 x 10⁻⁵	6.3	0.20	0.66
6	16.43	1 x 10⁻⁵	5.9 x 10⁻⁵	6.3	0.20	0.66
7	16.43	6 x 10⁻⁶	4.5 x 10⁻⁵	8	0.25	0.53
8	16.43	8 x 10⁻⁶	5.6 x 10⁻⁵	7	0.20	0.60
(*) Data from Sorbino et al., 2010						

In order to analyse the results, the number (N) of cells that have a factor of safety (FS) lower or equal to 1 are computed for each case, as well as the ratio between the unstable simulated area (A_{unst}) and the total area (A_{tot}) is evaluated (Cuomo and Della Sala, 2013b). Then, the obtained results are compared with the field evidences available for the 1954 event, whose unstable areas are reported in the landslide inventory map provided by Autorità di Bacino Destra Sele (2012) (Figure 4.8b)

5.1.2   Numerical results

With reference to the cases that have the initial soil suction in the range 20-30 kPa (typical values of the period of occurrence of 1954 event) (cases 3 and 4), the achieved results provide a total unstable area lower than the triggering areas recorded during the event for both the selected rainfall conditions (Figure 5.1 and Figure 5.2). Considering that the calibration of the input parameters allows well simulating the stable conditions of the hillslopes before rainfall, it can be argued that the high volume of mobilised material may not be attributed exclusively to the occurrence of shallow landslides.

For initial suction in the range "medium" (cases 1, 2, 7 and 8), and "very high" (case 5), the results (Figure 5.1 and Figure 5.2) furnish an underestimation of the triggering areas of 1954 event, with the exception

of the cases of 16 h rainfall. In these last cases, the unstable area is three times larger than the triggering areas of the 1954 event. These results outline that the rainfall intensity and duration heavily affect the stability conditions of the slopes when the initial suction is low, but these rainfall characteristics have a smaller effect when the initial suction is higher than 20 kPa.

1	October 1954	case 3	case 4	case 1	case 2	case 7	case 8	case 5
2	"High" (20-30)	"High" (20-30)		"Medium" (10-20)				"Very high" (>30)
3	Oct	Sept-Oct		Nov-Dec				Jun-Aug
4	-	20.13	27.50	14.59	16.43	16.43	16.43	38.58
5	4.5	0.21	0.33	1.71	0.45	0.46	0.52	0.37
6	4.5	0.34	0.21	14.23	14.20	14.12	14.13	0.21
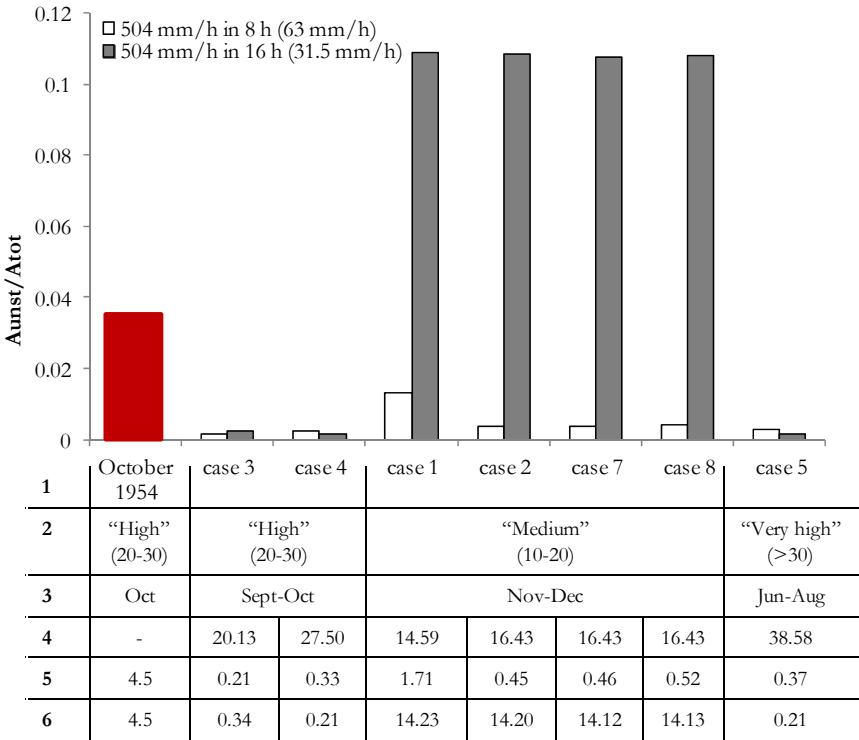
1: Case; 2: Suction (kPa) according to Cascini et al. (2013); 3: months according to Cascini et al. (2013); 4: initial suction at the ground surface (kPa); 5: Aunst (km²) (with FS≤1)-504 mm in 8h; 6: Aunst (km²) (with FS≤1)-504 mm in 16h

Figure 5.1 Ratio between the simulated unstable area and total area for different cases.

In addition, the initial conditions of unsaturated soils play an important role in the slope stability conditions; in particular, for the same rainfall condition: i) when the initial suction is "medium" (Figure 5.1 and Figure 5.2), the unstable areas are greater than in other cases and more variably distributed in the whole study area (cases 1, 2, 7 and 8); ii) when the initial suction is "high" (cases 3 and 4) and "very high" (case 5), the

global simulated unstable area is smaller (Figure 5.1 and Figure 5.2).

With reference to soil hydraulic properties, the analyses (Figure 5.1) show a minor role of these parameters on the stability analyses (cases 2, 7 and 8) within the analysed range.
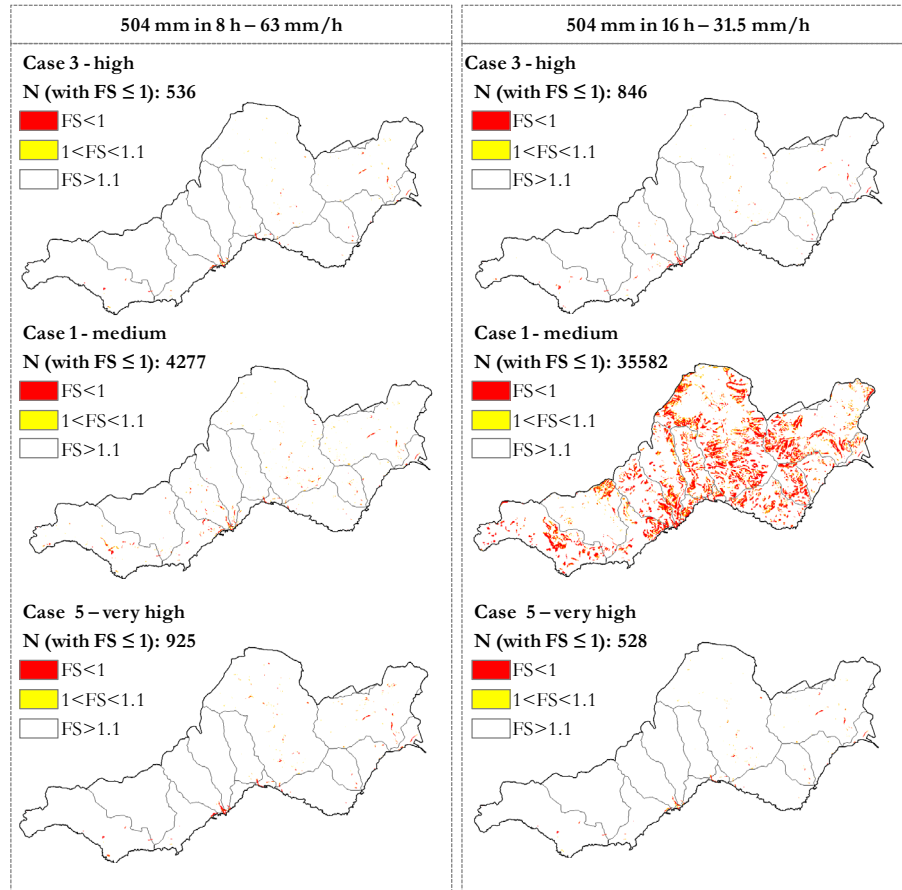
Figure 5.2 Spatially distribution of triggering area obtained by the TRIGRS-unsaturated model for the October 1954 under different hyphoteses.

5.2 MODELING OF SOIL EROSION

5.2.1 Methods and input

In order to assess the source areas of erosion processes, their spatial distribution and the solid volume potentially eroded, the Universal Soil Loss Equation (USLE) model (Wischmeier and Smith, 1978) is applied in a GIS platform. The USLE model, originally based on regression analyses of soil loss rates in USA experiments, is widely used in the world to predict the long-time average soil losses due to runoff-originated soil erosion. The soil loss (A) is estimated using the empirical equation (Eq. 5.3), that takes into account the main factors of erosion processes:

$$A = R \cdot K \cdot L \cdot S \cdot C \cdot P \qquad (5.3)$$

where A is the average annual soil loss (t ha^{-1} y^{-1}), R is the rainfall erosivity factor (MJ mm ha^{-1} h^{-1} y^{-1}), K is the soil erodibility factor (t ha h ha^{-1} MJ^{-1} mm^{-1}), L is the slope-length factor (dimensionless), S is the slope-steepness factor (dimensionless), C is the cover and management factor (dimensionless) and P is the support practice factor (dimensionless). The assessment of the soil loss in the study area is performed for a single rainfall event in order to evaluate the seasonal effects of some input factors on the erosion processes.

Firstly, the analyses are performed with reference to event of 25-26 October 1954, considering the following input data:

✓ The rainfall erosivity factor R is evaluated as the product of the total energy of rainstorm (E) (Eq.5.4, Foster, 2004) and the rainfall intensity (I) (Eq. 5.5) (Wischmeier and Smith, 1978); in particular, two average rainfall intensities respectively equal to 63 mm/h (corresponding to the duration of 8 h) and 31.5 mm/h (corresponding to the duration of 16 h) is used, that represent the same value of cumulated rainfall of the 1954 event (504 mm);

$$E = \sum_{k=1}^{v} 0.29 \cdot P_k \cdot \left[1 - 0.72 \cdot \exp\left(-0.082 \cdot \frac{P_k}{\Delta t} \right) \right] \qquad (5.4)$$

$$R = E \cdot I \tag{5.5}$$

where E is the total rainfall kinetic energy; P_k is the cumulated rainfall; Δt is the interval time in which the rainfall event is divided (in this analysis it is considered only one interval equal to rainfall duration); R is the average erosivity factor; I: average rainfall intensity.

✓ The erodibility factor K, that increases when the soil conductivity decreases, is estimated using the equation (5.6) proposed by Wischmeier and Smith (1978) (Bagarello and Ferro, 2006), considering the soil texture, the soil structure and initial conductivity (linked to the soil suction of the period of occurrence of the event), obtained from the data available in literature (Bilotta et al., 2005; Sorbino et al., 2010) (Table 5.2);

$$K = 2.77 \cdot 10^{-7} \cdot M^{1.14} \cdot (12 - OM) + 4.28 \cdot 10^{-3} \cdot (SS - 2) + 3.29 \cdot 10^{-3} \cdot (PP - 3) \tag{5.6}$$

$$M = f \cdot (100 - cl) \tag{5.7}$$

$$cl = 100 - f - g \tag{5.8}$$

where OM (%) is the organic matter content; SS is the soil structure code (SS=1: very fine granular; SS=2: fine granular; SS=3: med or coarse granular; SS=4: blocky, platy or massive); PP is the permeability class (PP=1: rapid, >127 mm h^{-1}; PP=2: from moderate to rapid, 64-127 mm h^{-1}; PP=3: moderate, 20-64 mm h^{-1}; PP=4: from slow to moderate, 5-20 mm h^{-1}; PP=5: slow, 1-5 mm h^{-1}; PP=6: very slow, <1 mm h^{-1}); f (%) is the silt and very fine sand content, (particles of diameter variable between 0.002 and 0.1 mm); g (%) is the sand content, (particles of diameter variable between 0.1 and 2 mm); and cl (%) is the clay content.

Table 5.2 Input data used to calculate erodibility factor.

f (%)	40
g (%)	60
SS (fine granular structure)	2
OM (%)	0
PP (for soil suction variable between 20-30 kPa, soil conductivity < 1mm/h)	6

✓ The slope-length factor L and the slope-steepness factor S, which affect the amount of cumulative runoff and the runoff velocity, are considered together as the topographic factor (LS) and estimated using the relationship (Eq. 5.9) proposed by Moore and Burch (1986); this latter formulation takes into account the upslope contributing area (A_s) and the slope gradient (α) in order to incorporate the impact of flow convergence:

$$LS = \left(\frac{A_s}{22.13}\right)^{0.6} \cdot \left(\frac{\sin \alpha}{0.0896}\right)^{1.3} \tag{5.9}$$

✓ The factor C, which considers the effect of vegetation cover on the erosion rate and depends on cover type, crop sequence, management practices, growth and development of vegetal cover at the time of the rain (Wischmeier and Smith, 1978), is obtained from the study performed by De Falco (2011) who estimated different C values for each season of the year and for each class of Corine Land Cover map (2006) through the equation proposed by Van der Knijff et al. (1999) referring to Autumn and to two different hypotheses for spatial distribution (homogeneous on the area or variable according to the classes of the Corine Land Cover map, 2006).

✓ Finally, the factor P, which considers the protective effect of support practices, such as terracing, contour tillage, is assumed equal to 1, thus neglecting the positive effect of support practices.

The input data and the analysed cases are given in Table 5.3.

Table 5.3 Input data for the USLE model.

	Case			
	1a	**2a**	**1b**	**2b**
I (mm/h)	63	31.5	63	31.5
Duration (h)	8	16	8	16
Cumulated rainfall (mm)	504		504	
Erosivity R (MJ mm ha^{-1} h^{-1})	9170.24 constant	4353.61 constant	9170.24 constant	4353.61 constant
Initial suction (kPa)	20-30		20-30	
Initial conductivity (mm/h)	<1		<1	
Erodibility K (t h MJ^{-1} mm^{-1})	0.0523 constant		0.0523 constant	
LS factor	variable		variable	
C factor	0.014 constant		variable	
P factor	1 constant		1 constant	

Starting from the soil loss maps, obtained through the USLE model, the maps of eroded thickness are calculated considering the soil unit weight equal to 15 kN/m^3. Then, the number of cells (N) with an eroded thickness higher than or equal to 1 cm, 5 cm and 10 cm are computed. These classes are obtained considering 5, 25 and 50 times a representative diameter (d_{90}) of the grain size distribution of the upper ashy soil (Bilotta et al., 2005). Then, the analyses are performed evaluating the ratio between the eroded area (A_{eros}) obtained by the model and the total area (A_{tot}) and the obtained results are compared with the 1954 event.

For the purpose of evaluating the susceptibility to the erosion phenomena during the year, the analyses are performed considering different seasons: i) Autumn, which includes September, October and November; ii) Winter, which correspond to December, January and February; iii) Spring, which includes March, April and May and iv) Summer, which includes June, July and August. The analyses are carried out considering the seasonal variation of R, K and C factors. In particular, the erosivity factor (R) is obtained from the study performed

by De Falco (2011) who estimated R as the product of the total energy of rainstorm (E) and the maximum 30-minutes rainfall intensity (I_{30}) (Wischmeier and Smith, 1978) for each season in the Campania Region using the rainfall data recorded at the rain gauges. Different values of erodibility factor (K) are obtained by the equation (Eq. 5.6) proposed by Wischmeier and Smith (1978), considering initial soil conductivity that depends on the soil initial suction. The C factor is obtained from the study performed by De Falco (2011) who estimated different C values through the equation proposed by Van der Knijff et al. (1999), considering the Normalized Difference Vegetation Index (NDVI), for each season and for each class of Corine Land Cover map (2006). The input data are given in Table 5.4.

Table 5.4 Seasonal variations for soil erosion: input data for the USLE model.

	Season			
	Autumn	**Winter**	**Spring**	**Summer**
Months	Sept-Nov	Dec-Feb	Mar-May	Jun-Aug
I_{30} (average) (mm/h)	36.89	17.84	17.04	19.02
Erosivity R (average) (MJ mm ha^{-1} h^{-1})	2539.33 Variable	925.50 Variable	737.17 Variable	629.67 Variable
Initial suction (kPa)	20-30	10-20	0-10	>30
Initial conductivity (mm/h)	<1	<1	36-0.18	<1
Erodibility K (t h MJ^{-1} mm^{-1})	0.0523 Constant	0.0523 Constant	0.0458 Constant	0.0523 Constant
LS factor	Variable	Variable	Variable	Variable
C factor (average)	0.014 Variable	0.026 Variable	0.013 Variable	0.015 Variable
P factor	1 Constant	1 Constant	1 Constant	1 Constant

For each season, the results are expressed in terms of: i) number of cells with an eroded thickness higher than or equal to 1 cm, 5 cm and 10 cm (N) and ii) ratio between the eroded area (A_{eros}) obtained by the model and the total area (A_{tot}) Finally, the obtained results are compared between the different seasons.

5.2.2 Numerical results

With reference to the 1954 event, the analyses are performed comparing the eroded area with the unstable area reported in the landslide inventory map (Figure 4.8b), assuming two rainfall intensities (Table 5.3). The results (Figure 5.3, Figure 5.4 and Figure 5.5) show that: i) the spatially distributed C factor causes a decrease of the global eroded area (case 1a compared with case 1b and case 2a compared with case 2b); ii) the area that has an eroded thickness higher than 1 cm overestimates the 1954 event for both rainfall intensities; iii) the area with the eroded thickness higher than 5 cm is comparable with the unstable area recorded during the event; iv) the rainfall characteristics plays an important role on the amount of eroded area; in particular, the higher the rainfall intensity, the larger is the eroded area.

1	October 1954	Case 1a	Case 1b
2	-	20-30	20-30
3	Oct	Sept-Nov	Sept-Nov
4		45.1	22.5
5	4.5	5.9	4.7
6		2.5	1.9

1: Case; 2: Initial suction (kPa); 3: Months; 4: Aeros (with $z_{ero} \geq$ 1cm) (km^2); 5: Aeros (with $z_{ero} \geq$ 5cm) (km^2); 6: Aeros (with $z_{ero} \geq$ 10cm) (km^2)
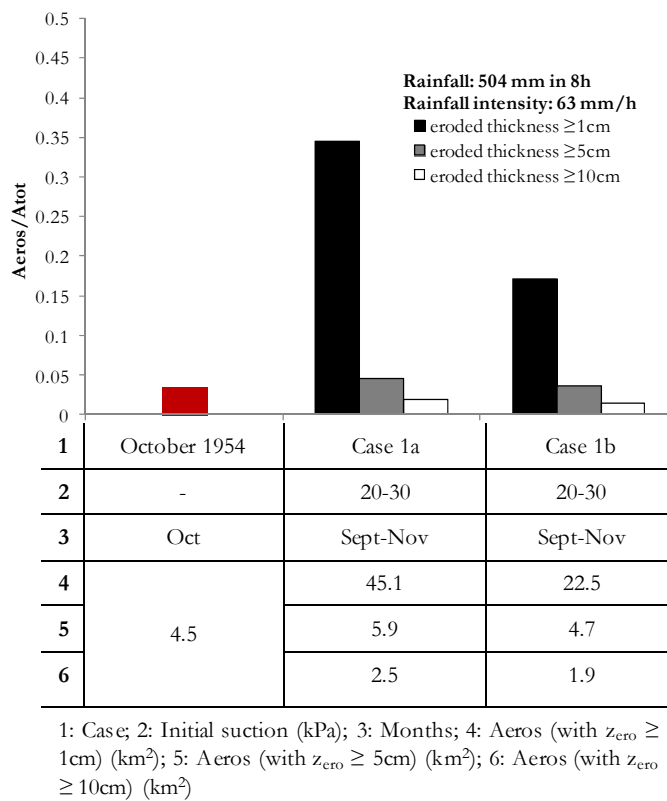
Figure 5.3 Results obtained for the October 1954 event: ratio between the simulated eroded area obtained by the USLE model and total area (rainfall intensity equal to 63 mm/h).
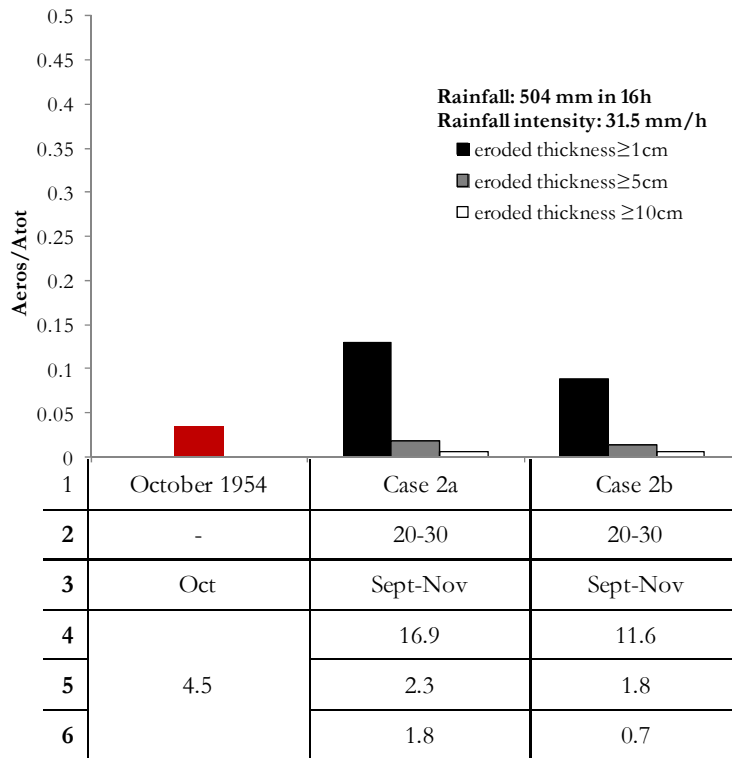
1	October 1954	Case 2a	Case 2b
2	-	20-30	20-30
3	Oct	Sept-Nov	Sept-Nov
4		16.9	11.6
5	4.5	2.3	1.8
6		1.8	0.7

1: Case; 2: Initial suction (kPa); 3: Months; 4: Aeros (with $z_{ero} \geq$ 1cm) (km^2); 5: Aeros (with $z_{ero} \geq$ 5cm) (km^2); 6: Aeros (with $z_{ero} \geq$ 10cm) (km^2)

Figure 5.4 Results obtained for the October 1954 event: ratio between the simulated eroded area obtained by the USLE model and total area (rainfall intensity equal to 31.5 mm/h).
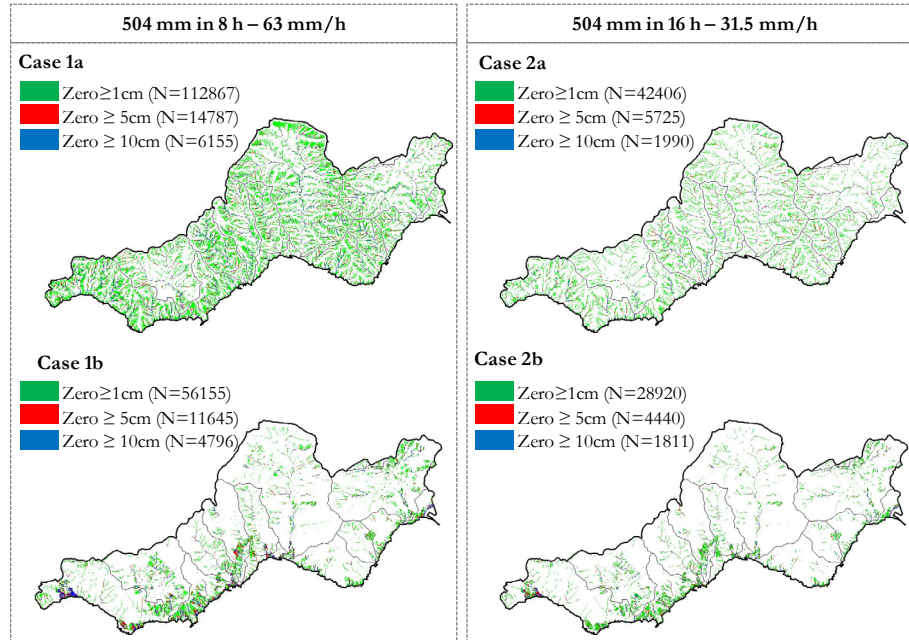
Figure 5.5 Spatially distribution of the simulated eroded area obtained by the USLE model for the 1954 event.

With reference to the seasonal variability of erosion processes, the achieved results (Figure 5.6) show that: i) in Autumn, the rainfall erosivity and the soil erodibility have high values and the eroded area is higher than in other seasons, ii) a lower value of both rainfall erosivity and soil erodibility determines a lower eroded area in Spring and Summer. For initial suction values in the range "high" (Autumn), the achieved results show that the study area is particularly susceptible to erosion. When the initial suction is in the ranges "low" (Spring) and "very high" (Summer), the simulated eroded areas are smaller than in the other period of the year.

1	Autumn	Winter	Spring	Summer
2	Sept-Nov	Dec-Feb	Mar-May	Jun-Aug
3	20-30	10-20	0-10	>30
4	36.89	17.84	17.04	19.02
5	6.48	5.09	1.22	1.33
6	0.90	0.53	0.14	0.15
7	0.36	0.18	0.07	0.07
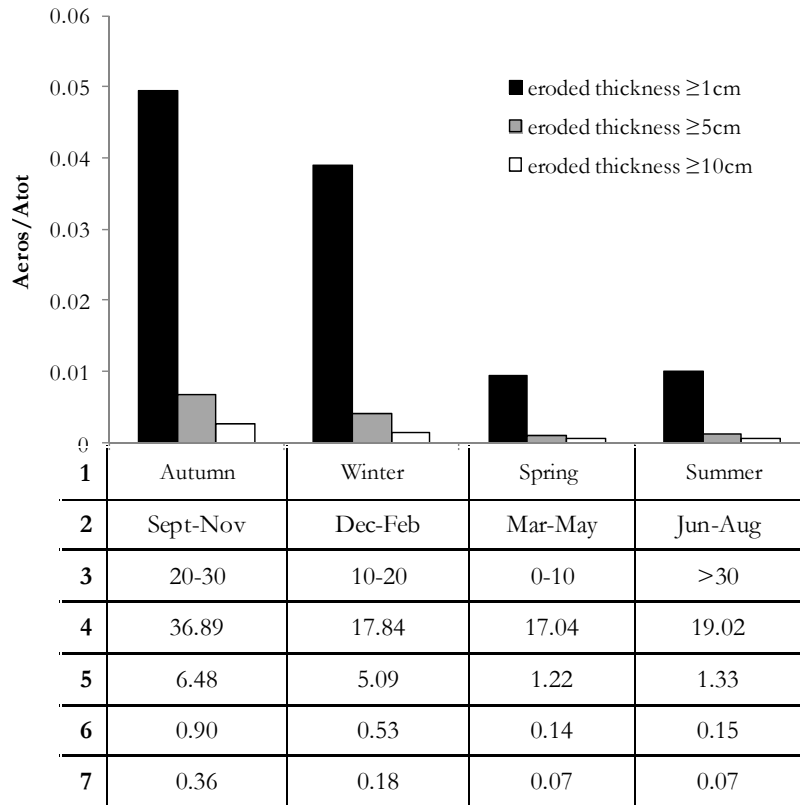
1: Season; 2: Months; 3: Initial suction (kPa); 4: I_{30} (average) (mm/h); 5: Aeros (with $z_{ero} \geq 1cm$) (km^2); 6: Aeros (with $z_{ero} \geq 5cm$) (km^2); 7: Aeros (with $z_{ero} \geq 10cm$) (km^2)

Figure 5.6 Seasonal variations of erosion processes: ratio between the simulated eroded area and total area.

The main and significant results of the performed analyses, summarised in Table 5.5, show that the study area may be affected by shallow landslides and soil erosion in different periods of the year depending on: i) rainfall characteristics, ii) soil suction and iii) soil cover. Referring to ordinary rainfall recorded during the year, the study area is more susceptible to soil erosion processes in Autumn. The amount of eroded material depends on rainfall characteristics, soil erodibility and soil cover. When an extraordinary rainfall event occurs in Autumn as happened on 25-26th October 1954, the eroded area and the potentially-mobilised volume increase, causing a sudden increase of the sediment

discharge at the outlet of the basins. Furthermore, the analyses also show that the occurrence of shallow landslides depend on soil suction that assumes different values during the year (Cuomo and Della Sala, 2013b). In particular, the study area is more susceptible to the triggering of shallow landslides when the soil suction is lower than 20 kPa (especially in Winter).

Table 5.5 Comparison of the main results obtained for shallow landslides and soil erosion processes.

1954 event	Season	Range suction	Initial suction (kPa)	Shallow landslides		Soil erosion (for C costant)		Seasonal soil erosion		
				Rainfall intensity (mm/h)				N z_{ero} ≥1cm	N z_{ero} ≥5cm	N z_{ero} ≥10cm
				63	31.5	63	31.5			
N				N FS≤1		N z_{ero}≥5cm	N z_{ero}≥5cm			
-	Spring	Low	-	-	-	-	-	3072	360	176
-	Winter	Medium	14.59	4277	35582	-	-	12724	1337	443
			16.43	1145	35521	-	-			
11251	Autumn	High	20.13	536	846	14783	5725	16193	2238	899
			27.50	831	538					
-	Summer	Very high	38.58	927	528	-	-	3313	376	175

5.3 DISCUSSION

The inception of flow-like mass movements in steep unsaturated shallow soil deposits during heavy rainstorms is related to two main processes such as slope failure (shallow landslide) and solid particle detachment (soil superficial erosion).

As far as shallow landslides, the achieved results outline that the source areas depend on: i) rainfall intensity and duration and ii) soil initial suction. As it concerns the soil erosion, the performed analyses outline that source areas are related to: i) rainfall characteristics; ii) soil cover use and iii) period of the year. Globally, the achieved results show that the study area may be affected by shallow landslides and soil erosion in different periods of the year depending on: i) rainfall characteristics, ii) soil suction and iii) soil cover. Referring to ordinary rainfall recorded during the year, the study area is more susceptible to soil erosion processes in Autumn. In addition, for a past event, the simulated source areas of shallow landslides are significantly lower than the areas recorded

during the event and the total soil volume mobilised during the event cannot be exclusively related to landslide occurrence. On the other hand, the zones with a simulated erosion thickness greater than 5 cm are comparable with the areas recorded in the field, when the rainfall intensity is very high and soil cover characteristics is assumed spatially variable.

6 PHYSICALLY-BASED MODELING OF SOIL EROSION IN STEEP MOUNTAIN BASINS

This section focuses on soil erosion and a numerical investigation is proposed with reference to two medium-sized steep mountain basins within the study area. Particularly, in order to estimate the amount of water and sediment conveyed at the outlet of the selected basins as well as the source areas of soil erosion, a parametric analysis with a physically-based distributed erosion model is performed. Realistic rainfall scenarios are used to analyse the specific case study, and also to provide general insights on the use of numerical tools for quantitative forecasting of soil erosion along steep slopes and water and sediment discharges at the outlet of a basin.

6.1 SELECTED BASINS AND MAIN PAST EVENTS

Dragone and Sambuco basins (Figure 6.1a,b) are located in the western part of the Lattari Mounts and in the middle part of the Amalfi Coast, with their own outlet respectively corresponding to the urban area of Atrani and Minori municipalities. Both the basins are funnel-shaped with a high-order drainage network, characterised by steep stream channels with a preferential north to south orientation, slope elevations ranging from 0 to 1300 m a.s.l. (Figure 6.1a,b), steep slopes ($\alpha > 30°$) over a large area, 49% for Dragone basin and 70% for Sambuco basin (Figure 6.1c).

Dragone basin extends over a 9.3 km^2 area (perimeter equal to 15.7 km), with a linear main stream channel, 6.5 km long. Uppermost basin is 2 km wide, with a narrow gorge 300 m wide corresponding to the outlet, at Atrani town. Hillslopes are steep with few channels at left-hand side, while gentler slopes with a well developed drainage network are at right-hand side of the basin.

Sambuco basin is 5.6 km^2 large, with a 12.1 km perimeter and a main stream channel 5.3 km long, characterised by a regular shape and lateral hillslopes similarly regular.

Quaternary alluvial soils and air-fall pyroclastic soils are widespread in the study area. On the hillslopes, deposits of debris - pyroclastic soils are present, and consist of ashes/sands or pumice, slag and carbonate clasts, related to colluvial processes of runoff; on the ridges, pyroclastic deposits prevail while at toe of the hillslopes sediments/debris result from the progressive accumulation of material from hillslopes; in the channels, loose fluvial deposits exist, of different sizes, consisting of angular gravels and pebbles, with the presence of sandy-silty matrix; finally, outcrops of the Mesocenozoic rocks and Quaternary continental deposits are widespread in the whole area. Figure 6.1d shows the map of soil deposit thickness, generally lower than 2 m.
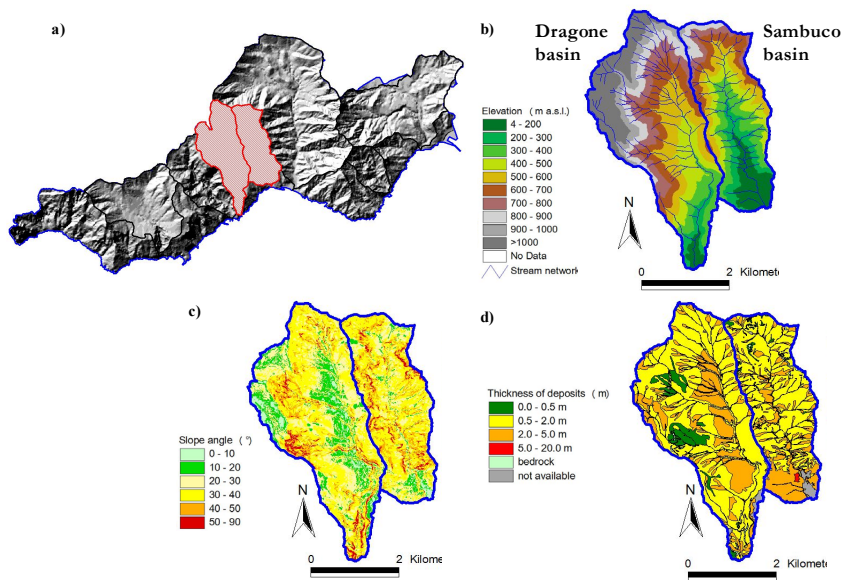
Figure 6.1 Characterisation of Dragone and Sambuco basins: a) location in the study area; b) DTM with cell size 5 m and stream flow network; c) slope angle map, d) map of pyroclastic soil deposit thickness (data from Autorità di Bacino Destra Sele, 2012).

Aimed to have a preliminary characterisation of the selected basins, the latter are subdivided in smaller catchments, e.g. drainage areas equal or higher than 0.25 km^2 or 1.25 km^2, namely sub-basins (Figure 6.2a). Purposely, an automatic procedure available in GIS platforms is used. Then, following the approach proposed by Montgomery and Fofoula-Georgiou (1993), the drainage areas are plotted versus mean slope angles

of sub-basins. Figure 6.2b shows that the sub-basins correspond to "debris-flow dominated channels" (zone 2 in the plot), rather than alluvial channels (zone 4), thus emphasizing the important role that mobilitation of solid particles may have in this study area.
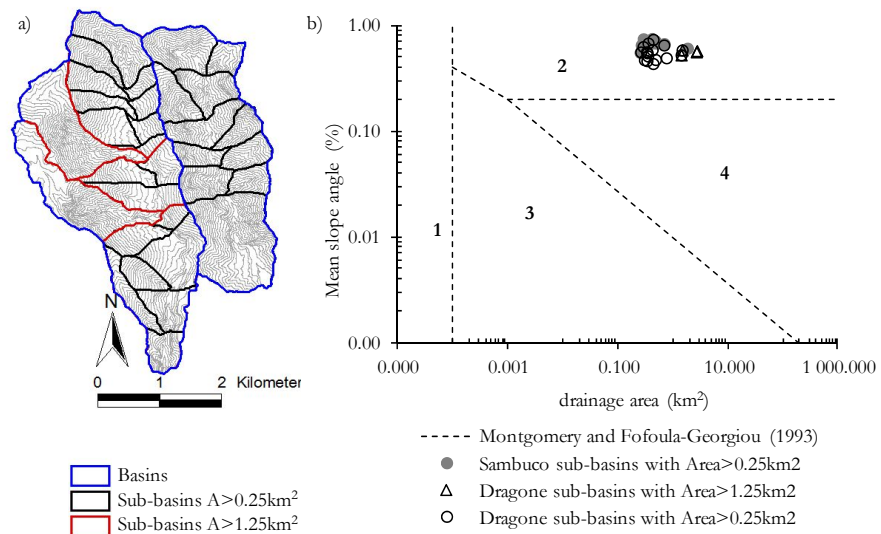
Figure 6.2 a) Sub-basins; b) Drainage area (A) versus mean slope angle (S) for the drainage basins (A>0.25 km², A>1.25 km²) of Dragone and Sambuco basins. Dashed lines (from Montgomery and Fofoula-Georgiou, 1993) subdivide different zones, 1: hillslopes, 2: debris-flows dominated channels, 3: unchanneled valleys, 4: alluvial channels.

Dragone and Sambuco basins were affected by past flow-like mass movements that caused victims and several damages (Esposito et al., 2004; Cascini et al. 2009; Papa et al., 2011).

On 25th October 1954, a heavy rainstorm affected an area of 500 km², from Minori to Salerno towns, with a cumulative rainfall of 504 mm in 8-16 hours and a maximum rainfall intensity equal to 136.8 mm/h (Figure 6.3), recorded at Salerno rain gauge, about 10 km far from the study area (Tranfaglia and Braca 2004, Cascini et al., 2009; De Luca et al., 2010; Tessitore et al., 2011; Esposito et al., 2004). Particularly, De Luca et al. (2010) define this rainstorm as a "hurricane-like event", for his small spatial extension, strong persistence, proximity to the sea coast and occurrence season. Figure 6.3 shows the cumulated rainfall recorded on 25th-26th October 1954 at Salerno rain gauge compared to those

measured in Cava de' Tirreni (8 km far from the study area). During this event, first-time shallow landslides were triggered, later propagating as debris flows (Hungr et al., 2001); particularly, the landslide inventory map of Figure 6.4a indicates a landslide source area equal to 0.18 km^2 in the Sambuco basin. Furthermore, widespread soil erosion processes were observed which evolved into hyperconcentrated flows (Coussot and Meunier 1996). Three inhabitants of Minori died and several buildings and industries were damaged at the outlet of Sambuco basin.

On 9th September 2010, a high rainfall intensity affected an area nearly 100 km^2 large, between Agerola and Minori towns, with a maximum hourly intensity of 92.2 mm, recorded at Pimonte raingauge (8 km far from the study area), and a maximum cumulated rainfall, 115.4 mm in 3 hours, recorded at Ravello raingauge, located inside the study area (CEMPID, 2010). Figure 6.3 provides the cumulated rainfall recorded at Agerola rain gauge (4 km from study area) and Ravello rain gauge (located in the study area) on 9th September 2010. During the event, slope instabilities (Figure 6.4a) and superficial soil erosion (Figure 6.4b) occurred along the slopes and inside the valleys (Autorità di bacino Regionale Destra Sele, 2010). Particularly, the landslide inventory map of Figure 6.4a indicates 0.06 km^2 affected by landslides in the Dragone basin. Thus, flow-like mass movements occurred within a hour and caused a victim and several damages at the outlet of Dragone basin where Atrani town is located. In particular, the peak discharge value of the event was estimated variable between 65-75 m^3/s (Bovolin, 2012) and 98.5 m^3/s (Ciervo et al., 2012) with an observed hydrological response time of about 1h (Ciervo et al., 2012). With reference to solid volume, Bovolin (2012) estimated about 10,000 m^3, Autorità di Bacino Destra Sele (2010) observed a solid volume higher than 20,000 m^3, and Ciervo et al. (2012) estimated a sediment volume lower than 30,000 m^3.
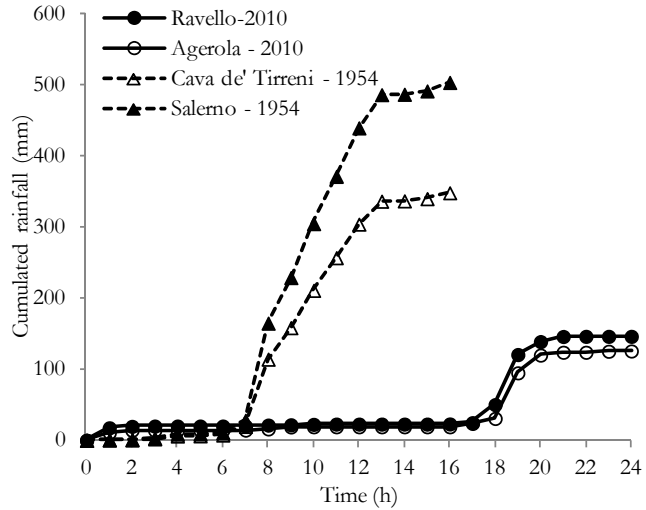
Figure 6.3 Cumulated rainfall measured on 25th-26th October 1954 and 9th September 2010 (data from Esposito et al., 2004 and Autorità di Bacino Destra Sele, 2010).
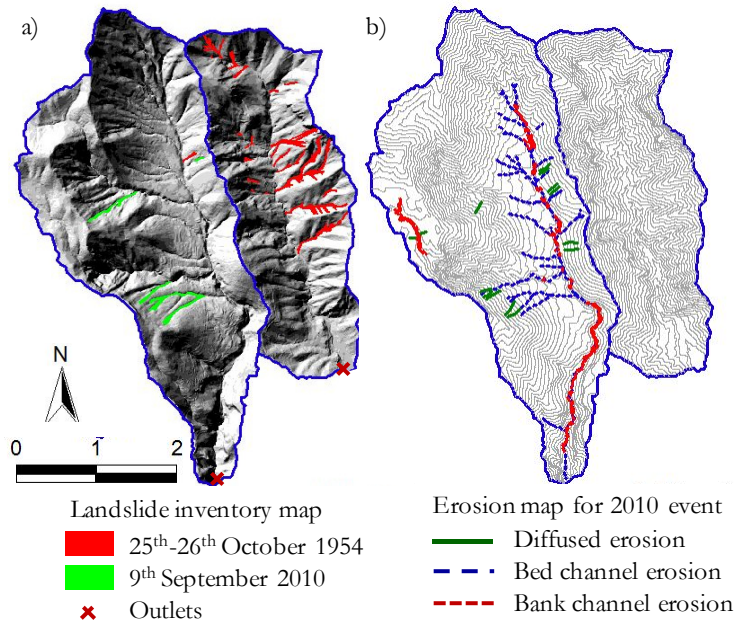
Figure 6.4 a) Landslide inventory map for 1954 and 2010 events occurred in Sambuco and Dragone basin (data from Autorità di Bacino Destra Sele, 2012); b) erosion map for 2010 event (data from Autorità di Bacino Destra Sele, 2010).

6.2 PARAMETRIC ANALYSIS FOR MODELING OF SOIL EROSION

As shown in the previous section, the selected basins were affected in the past by different slope instabilities that mobilised large amount of water and solid material, determining damages and victims. In order to analyse the amount of water and sediment conveyed at the outlet of the selected basins as well as the source areas of soil erosion, a parametric analysis is performed with the physically-based distributed erosion model LISEM. This model, briefly described in the following Section, is selected for the study area because: i) it properly takes into account the key processes regulating superficial soil erosion; ii) is an event-based model; and iii) it is a raster GIS-implemented model that allows accurately simulating the spatial patterns of soil erosion tracking the main transient quantities over the time.

6.2.1 LISEM model

The Limburg Soil Erosion Model (LISEM) is a spatially-distributed model implemented in a GIS platform (De Roo et al., 1994, 1996 a,b; De Roo and Jetten, 1999, Jetten, 2002) which allows taking into account the main processes occurring during a rainstorm in a catchment (Figure 6.5).

Basic processes incorporated in the model are: interception of rainwater by crops and vegetation, splash detachment, water storage in micro-depressions of ground surface, infiltration of the ground surface, overland flow, flow detachment, sediment transport and deposition (i.e. respectively, when the overland flow is capable or not to transport solid particles), channel erosion, runoff over impermeable surfaces.

During the rainfall event, for each cell LISEM calculates: 1) the water that will be stored in the vegetation leaves as interception, 2) the part of water that will be infiltrated on the ground surface, 3) the part of rainfall that will be stored in micro depression on the ground surface; and, finally, 4) the part of water that will be flow as runoff. Subsequently, splash and flow erosion and deposition are calculated using the stream power principle and the water and sediment are routed to the outlet with a kinematic wave procedure.
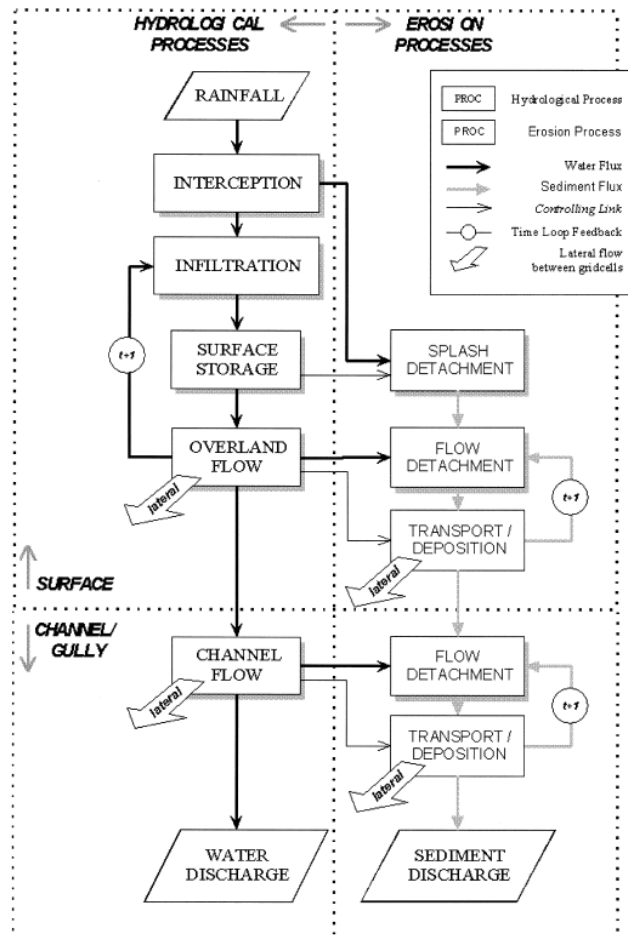
Figure 6.5 Flowchart of the LISEM model (De Roo and Jetten, 1999).

Cumulative water interception by crops and vegetation Cs (mm) is calculated, at a given time and for each cell of a given DTM (Digital Terrain Model), from the maximum canopy storage S_{max} (mm) and the cumulative rainfall since the beginning of the event P_{cum} (mm), as follows (Aston, 1979):

$$C_s = Cp \cdot S_{max} \cdot \left(1 - \exp\left(\frac{-k \cdot P_{cum}}{S_{max}}\right)\right)$$

(6.1)

$$k = 1 - \exp(- co \cdot LAI) \tag{6.2}$$

where Cp is fraction of vegetation cover, k is a parameter related to the canopy openness (co) and determines how fast the canopy fills up and Leaf Area Index (LAI, m^2/m^2) represents the average leaf area of the fraction of the cell that is under vegetation. Depending on vegetation type and starting from LAI value, different empirical equations are implemented in LISEM in order to evaluate Smax.

Surface storage and water release (h_{flow}) are calculated using Eqs. 6.3 and 6.4. The Maximum Depression Storage (MDS) is related by Kamphorst et al. (2000), to Random Roughness (RR, cm) that represents standard deviation of surface heights and terrain slope (S, %). Then, LISEM model assumes that water starts to flow between cells when the total water height (h, cm) exceeds the Starting Depression Storage (SDS), which is heuristically set equal to 10 % of MDS.

$$MDS = 0.243 \cdot RR + 0.010 \cdot RR^2 \cdot 0.012 \cdot RR \cdot S \tag{6.3}$$

$$h_{flow} = \left(h - SDS \right) \cdot (1 - \exp \frac{(- h \cdot (h - SDS))}{(MDS - SDS)}) \quad \text{when } h > SDS \tag{6.4}$$

Water infiltration can be assumed equal to soil saturated conductivity (i.e. runoff equals the amount of rainwater exceeding soil saturated conductivity) or can be calculated through more advanced approaches, among which Green-Ampt model (Eq. 6.5). The latter is based on a simplification of Darcy equation for 1D vertical water flow in a single soil layer, and assumes that the downwards infiltration rate (f, mm/h) can be computed as follows:

$$f = -k_{sat} \cdot \left(\frac{dh \cdot (\theta_{sat} - \theta_i)}{F} + 1 \right) \tag{6.5}$$

where k_{sat} is the saturated hydraulic conductivity (mm/h); dh is the sum of water pressure on the ground surface and soil suction at the wetting front (mm); θ_{sat} is the saturated porosity (-) and θ_i is the initial moisture content below the wetting front (-); F is the cumulative infiltrated rainwater, which fills the available (empty) pore space (θ_{sat} - θ_i) during the

infiltration process up to the infiltration depth (z, mm) reached by the wetting front until the end of the infiltration process.

The runoff is routed downhill towards the catchment outlet with a kinematic wave function. For distributed overland and channel flow routing, an implicit four-point finite-difference solution of the kinematic wave is used together with Manning's equation (Eq. 6.6), referring to the numerical procedure of Chow et al. (1988) and Moore and Foster (1990). The kinematic wave is integrated over the surface flow direction map of Local Drain Directions that consists in a network among each cell and the eight surrounding cells. In particular, the flow velocity v (m/s) is calculated from Eq. 6.7 and the discharge Q (m^3/s) per cell is calculated with equation proposed by Chow et al. (1988) (Eq. 6.7):

$$v = R^{\frac{2}{3}} \cdot \frac{S^{\frac{1}{2}}}{n}$$

(6.6)

$$A = \left(\frac{n \cdot \sqrt[3]{P^2}}{\sqrt{S}} \right)^{\frac{3}{5}} \cdot Q^{\frac{3}{5}}$$

(6.7)

where R is the hydraulic radius (m), calculated with the flow width and average water height; S is the terrain slope (sine); n is the Manning's coefficient; A is the wet cross section (m^2); P is the wet perimeter (m).

Modeling of particle detachment is based on a generalized erosion-deposition formulation described in Morgan et al. (1998) and Smith et al. (1995a), whose details are also discussed in Jetten (2002). It is assumed that the amount of sediment in suspension (e) comes from a continuous balance among splash detachment (D$_s$), flow detachment (D$_f$) and deposition (D$_p$), as follows:

$$e = D_s + D_f - D_p$$

(6.8)

Splash detachment D$_s$ (kg/s) is based on rainfall kinetic energy (Van Dijk, 2002) multiplied by an empirical aggregate stability factor based on splash tests:

$$D_s = \left(\frac{2.82}{A_s} \cdot KE \cdot \exp(-1.48 \cdot d) + 2.96 \right) \cdot P_{net} \cdot \frac{dx^2}{dt}$$

(6.9)

where A_s is the soil aggregate stability (median number of drops to decrease the aggregate by 50%) from the Lowe drop test; KE is the rainfall kinetic energy (J m^{-2} mm^{-1}); d is the depth of the surface water layer (mm); P_{net} is net rainfall (mm); dx^2 is the cell area; and dt is the time step (s).

Flow detachment, sediment transport and deposition are calculated with a stream power based transport capacity equation (Govers, 1990; Morgan et al., 1998); particularly, transport capacity T_C (kg/m^3) is:

$$T_c = \gamma_s \cdot c \cdot (\omega - \omega_c)^d = \gamma_s \cdot c \cdot (v \cdot S - 0.004)^d$$

(6.10)

where γ_s is the bulk density of solid grains (2650 kg/m^3), ω and ω_c are the unit stream power and critical unit stream power (m/s) respectively; S is slope gradient (m/m); v is mean flow velocity (m/s); and c and d are empirically derived coefficients, depending on the texture median (d_{50}) of the upper soil layers.

Referring to Eqs. 6.10 and 6.11, flow detachment (D_f, kg/s) occurs as long as the transport capacity T_C is larger than the concentration of the suspended sediments (C, kg/m), provided that a soil strength threshold, related to soil cohesion, is overcome:

$$D_f = Y \cdot (T_C - C) \cdot Q$$

(6.11)

where T_c is the transport capacity of the flow (kg/m^3), Y is a dimensionless efficiency factor that depends on soil cohesion (Morgan et al., 1998) and Q is the discharge (m^3/s).

Finally, deposition (D_p, kg/s) occurs whenever the transport capacity is less than the total suspended sediment in the flow:

$$D_p = w \cdot dx \cdot v_s \cdot (T_C - C)$$

(6.12)

in which w is the width of flow (m), and v_s is the settling velocity of the particles (m/s).

A more detailed description of the LISEM model can be found in De Roo et al. (1994, 1996 a, b), De Roo and Jetten (1999) and Jetten (2002).

6.2.2   Methods and input

Through the LISEM model (openLISEM, 2013 a, b), the response of the selected basins is investigated for a wide range of realistic scenarios, with the main purpose to analyse the processes of infiltration, runoff and soil erosion under different rainfall conditions and soil properties.

Particularly, starting from a schematisation of the 2010 rainfall event, different rainfall conditions are assumed: i) the rainfall conditions, called E_a, E_b, E_c, include a maximum rainfall intensity fixed to 100 mm/h in 30 minutes (I_{30}), respectively at the beginning, middle and at the end of the rainfall event (3 hours lasting as a whole) with the same cumulated rainfall equal to 112.5 mm (Figure 6.6); ii) the rainfall condition, called E_0, is composed of a maximum rainfall intensity fixed to 100 mm/h in 30 minutes (I_{30}) with a cumulated rainfall of 50 mm (Figure 6.6); iii) the rainfall condition, called E_m corresponding to 126 mm in 3 hours (rainfall intensity equal to 42 mm/h, which is the average value of September 2010 rainfall at Dragone basin) (Figure 6.6).

For the purpose of this analysis, the effects of vegetation is neglected. In particular, the water interception by crops and vegetation is neglected, assuming that the maximum canopy storage (S_{max}) is equal to zero; water storage in micro-depressions of ground surface is small, as the standard deviation of surface heights (RR) is assumed equal to 0.05 cm; splash detachment is a negligible percentage of the total mobilised amount of solid particles (Cuomo et al., 2013).
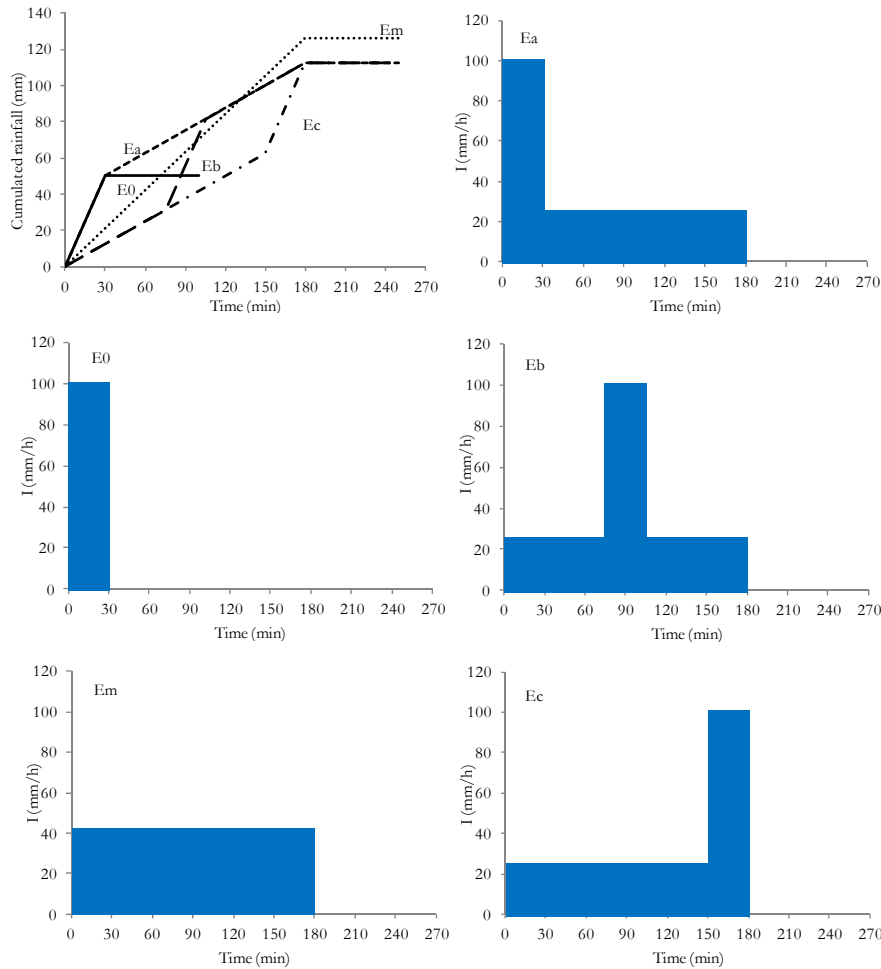
Figure 6.6 Cumulated rainfalls and intensity-duration used for the parametric analysis.

Water infiltration is assumed equal to soil saturated conductivity (i.e. runoff equals the amount of rainwater exceeding soil saturated conductivity) (later named k_{sat} substraction) or computed through the Green-Ampt model in order to taking into account the soil unsaturated conditions. In particular, soil hydraulic properties are taken from Sorbino et al. (2010) and from the values used in the parametric analysis at slope scale of Chapter 3. Table 6.1 summarises the Van Genuchten parameters of three soil water characteristic curves, named "upper", "middle" and

"lower" just used in Chapter 3. Particularly, they are characterised by a soil saturated conductivity (k_{sat}) variable between 1.8 and 540 mm/h, saturated water content (θ_{sat}) variable between 0.37 and 0.66 and initial water content (θ_{in}) equal to 0.08-0.49 for soil suction in the range of 10-20 kPa. Different soil depths are considered, equal to 0.1, 0.2, 0.3 m and 1.0 m.

Table 6.1 Van Genuchten parameters for soil water characteristic curves used in parametric analysis (Chapter 3).

ID	Soil-water characteristic curves (Van Genuchten parameters)							
	n	m	a (kN/m²)	θ_{sat} (-)	θ_r (-)	$\theta_{sat} - \theta_r$ (-)	k_{sat} (m/s)	α (kN/m²)$^{-1}$
Upper	1.3	0.231	5	0.66	4.30E-07	0.66	1.50E-04	0.2
Middle	1.4	0.286	4	0.51	6.00E-02	0.45	5.00E-06	0.25
Lower	2.1	0.524	2	0.37	6.00E-02	0.31	5.00E-07	0.5

n: fitting constant; m=1-1/n; a: air entry value; θ_{sat}: saturated volumetric water content; θ_r: residual volumetric water content; k_{sat}: saturated hydraulic conductivity; $\alpha=1/a$.

Overland flow is simulated with a Manning coefficient equal to 0.08, which is within the range 0.05-0.13 indicated by O'Brien (2009) for sparse vegetation, that is a widespread condition in the study area. Physical and mechanical properties of the soils used in the parametric analysis are taken from Bilotta et al. (2005) and Cascini et al. (2011) for coarser upper ashy silty sands (class B), that is the widespread superficial soil in the study area. In particular, the bulk density of solid grains (G_s) is assumed equal to 2650 kg/m³, median grain diameter (d_{50}) is assumed equal to 0.25 mm, soil cohesion (c') is considered equal to 0.2 kPa, and additional cohesion due to roots is neglected.

For topography and related morphometric features of both the basins, distinct DTMs are used (5x5m, 10x10m and 20x20m), from which local surface drainage direction and maximum slope gradient are computed at each cell of DTM as well as the position of the main catchment outlet is derived (Figure 6.7). For the sake of simplicity and considering the purpose of the analysis, mountain basins are assumed without roads and spatially homogeneous as it concerns: rainfall distribution, hydraulic and mechanical soil parameters, Manning

coefficient and land use.

The time step used in the simulations is 5 seconds, which is well suited referring to DTM cells equal to 5-20 m and water flow velocities in the range of 0.5-5 m/s (Jetten, 2002). All the simulations are characterised by a whole duration equal to sum of the rainfall duration (up to 3 hours) and the hydrological delay time of the basins (not larger than 70 minutes).
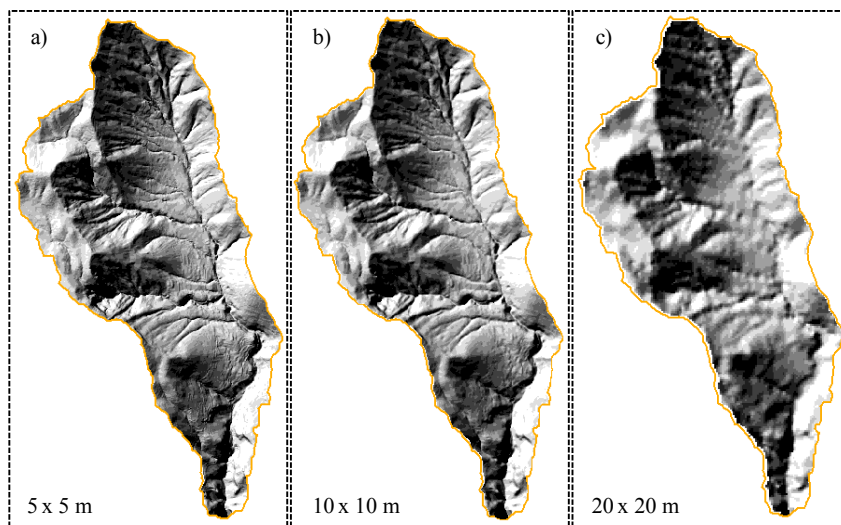
Figure 6.7 DTMs of the Dragone basin used for the parametric analysis.

The list of simulated cases is shown in Table 6.2. The results of each LISEM simulation are elaborated in terms of: i) total discharge (Qtot, m^3/s) and transient volumetric concentration of sediment (Cv, %) at the outlet of each basin, ii) total peak discharge and times of peak discharge, and iii) maximum volumetric sediment concentration. Moreover, for each cell of the DTM, the distribution of soil erosion is mapped for some selected significant cases (Cuomo et al., 2013).

Table 6.2 Input data and list of simulated cases.

ID	Rainfall	Cell (m)	Inf. model	k_{sat} (mm/h)	θ_{sat} (-)	θ_{in} (-)	s (kPa)	z (mm)
Dr02_Eb	Eb	5	S. k_{sat}	28.8	-	-	-	-
Dr04_Em	Em	5	S. k_{sat}	28.8	-	-	-	-
Dr13_Eb	Eb	20	S. k_{sat}	28.8	-	-	-	-
Dr14_Em	Em	20	S. k_{sat}	28.8	-	-	-	-

ID	Rainfall	Cell (m)	Inf. model	k_{sat} (mm/h)	θ_{sat} (-)	θ_{in} (-)	s (kPa)	z (mm)
Sa09_Eb	Eb	5	S. k_{sat}	28.8	-	-	-	-
Sa10_Em	Em	5	S. k_{sat}	28.8	-	-	-	-
Dr21_Eb	Eb	10	S. k_{sat}	28.8	-	-	-	-
Dr22_Em	Em	10	S. k_{sat}	28.8	-	-	-	-
Dr49_Eb	Eb	10	No inf.	-	-	-	-	-
Dr50_Eb	Eb	10	S. k_{sat}	14.4	-	-	-	-
Dr51_Eb	Eb	10	S. k_{sat}	7.2	-	-	-	-
Dr52_Eb	Eb	10	S. k_{sat}	56.7	-	-	-	-
Dr55_Eb (*)	Eb	5	G.A.	18	0.51	0.351	10	100
Dr56_Eb (*)	Eb	5	G.A.	18	0.51	0.290	20	100
Dr57_Eb (*)	Eb	5	G.A.	18	0.51	0.351	10	200
Dr58_Eb (*)	Eb	5	G.A.	18	0.51	0.290	20	200
Dr59_Eb (*)	Eb	5	G.A.	18	0.51	0.351	10	300
Dr60_Eb (*)	Eb	5	G.A.	18	0.51	0.290	20	300
Dr61_E0 (*)	E0	5	G.A.	18	0.51	0.290	20	100
Dr62_Ea (*)	Ea	5	G.A.	18	0.51	0.290	20	100
Dr63_Eb (*)	Eb	5	G.A.	18	0.51	0.290	20	100
Dr64_Ec (*)	Ec	5	G.A.	18	0.51	0.290	20	100
Dr65_Em (*)	Em	5	G.A.	18	0.51	0.290	20	100
Sa66_E0 (*)	E0	5	G.A.	18	0.51	0.290	20	100
Sa67_Ea (*)	Ea	5	G.A.	18	0.51	0.290	20	100
Sa68_Eb (*)	Eb	5	G.A.	18	0.51	0.290	20	100
Sa69_Ec (*)	Ec	5	G.A.	18	0.51	0.290	20	100
Sa70_Em (*)	Em	5	G.A.	18	0.51	0.290	20	100
Dr74_Eb (**)	Eb	5	G.A.	1.8	0.37	0.08	20	200
Dr76_Eb (**)	Eb	5	G.A.	1.8	0.37	0.08	20	300
Dr80_Eb (***)	Eb	5	G.A.	540	0.66	0.42	20	200
Dr82_Eb (***)	Eb	5	G.A.	540	0.66	0.42	20	300
Dr83_Eb (*)	Eb	5	G.A.	1.8	0.51	0.290	20	1000
Dr84_Eb (*)	Eb	5	G.A.	0.18	0.51	0.290	20	1000
Dr85_Eb (*)	Eb	5	G.A.	0.018	0.51	0.290	20	1000
Dr86_Eb (*)	Eb	5	G.A.	18	0.51	0.290	20	1000
Dr87_Eb (*)	Eb	5	G.A.	6	0.51	0.290	20	1000
Dr88_Eb (*)	Eb	5	G.A.	3.6	0.51	0.290	20	1000

k_{sat}: saturated hydraulic conductivity; θ_{sat}: saturated volumetric water content; θ_{in}: initial volumetric water content; s: soil suction; z: soil depth; S. k_{sat}: k_{sat} substraction; G.A.: Green-Ampt model; (*) middle curve; (**) lower curve; (***) upper curve of Table 6.1

6.2.3   Sensitivity analysis

The effect of two rainfall events, with high (E_b) and low (E_m) intensity, is firstly analysed for Dragone and Sambuco basins, referring to the finest available DTM (5x5m) and the simplest infiltration model (k_{sat} substraction).

The achieved results (Figure 6.8) outline that a major similarity for the two basins is the time of peak discharge – particularly, it is equal to 105 minutes for high rainfall intensity (E_b) and 94 minutes for low rainfall intensity (E_m) –. On the other hand, the computed discharges at the outlet of the basins are much different, as they correspond to: i) a 30 minutes lasting peak, 125-220 m^3/s high, for high rainfall intensity (E_b) and ii) a longer lasting peak, 150-200 minutes, equal to 10-30 m^3/s simulated for the low rainfall intensity (E_m).

It is worth noting that transient volumetric sediment concentration Cv strongly depends on topographical characteristics of the mountain basins (i.e. slope angles, flow direction, among other) and rainfall type. The maximum Cv is computed for Dragone basin, equal to 25%, independently of rainfall type; whereas, for Sambuco basin, maximum value of Cv is 20% for high rainfall intensity (E_b) and 16% for low rainfall intensity (E_m).

In addition, it can be noted that the time trend of Cv primarily depends on rainfall intensity, i.e. a long lasting maximum Cv is simulated for E_m while an impulsive response is obtained for high intensity rainfall (E_b).
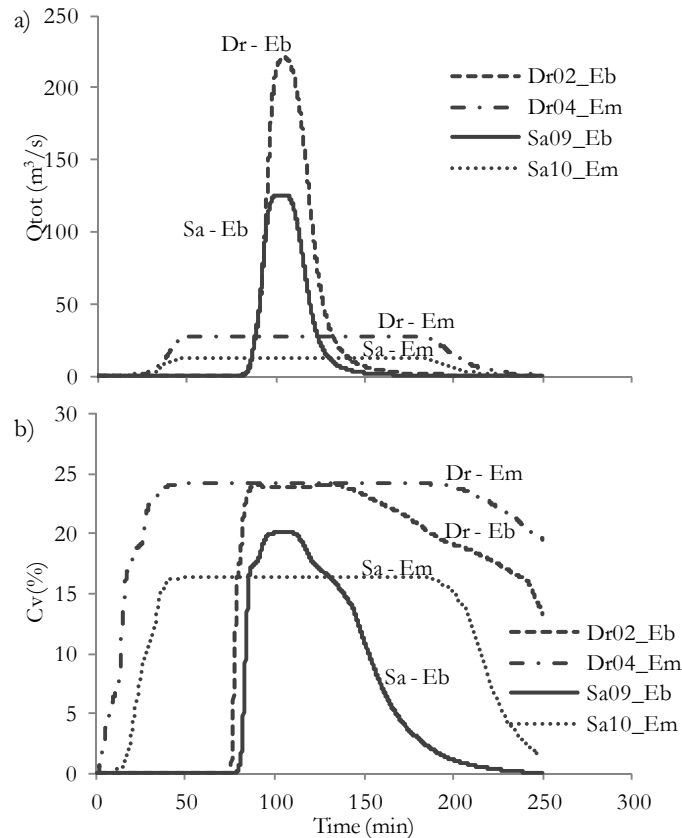
Figure 6.8 Total discharge (a) and transient sediment concentration (b) at the outlet of Dragone and Sambuco basins for different rainfalls (Eb and Em).

The sensitivity of LISEM model to DTM resolution (5, 10 and 20m) is investigated for Dragone basin, which is characterised by the highest simulated values of peak discharge and sediment concentration in Figure 6.8. Comparisons are performed for the previous rainfall events (E_b and E_m), and infiltration model (k_{sat} substraction). The results of Figure 6.9 outline that total peak discharge coincides for finer DTMs (5 and 10m), while is 6-10% lower and 3-20 minutes delayed in time for the coarse DTM (20x20m), for both the rainfall events. This finding agrees those of Hessel (2005), who outlines that peak discharge decreases with grid cell size. On the other hand, Cv is quite more sensitive to DTM resolution; particularly, for high rainfall intensity (E_b), numerical analysis with a 20x20m DTM provides an unrealistic evaluation including two peaks,

147

while finer DTMs allow obtaining similar maximum sediment concentrations with minor differences in their time trends. DTM also affects the spatial evaluation of soil loss; the finest DTMs allow capturing soil erosion phenomena both in steep valleys and flatter areas while the latter are poorly assessed by 20m DTM.

Figure 6.9 Total discharge (a) and transient sediment concentration (b) at the outlet of Dragone basin for different DTMs and rainfall condition (Eb and Em).

In order to improve the previous estimations, different soil conductivity values are considered (57.6, 28.8, 14.4 and 7.2 mm/h) with reference to a single rainfall type (E_b). The analyses are also performed for the heuristic case of fully impervious ground surface. Figure 6.10 shows the results achieved: the lower the soil conductivity, the higher the peak discharge, the faster the maximum sediment concentration is

reached and the longer this maximum concentration value is kept in time. For high soil conductivity (28.8 or 57.6 mm/h), the peak discharge starts to increase when the high rainfall storm begins. In the case that infiltration process is neglected, the higher the peak discharge, the faster the maximum solid concentration is reached and the longer the maximum concentration value is kept.
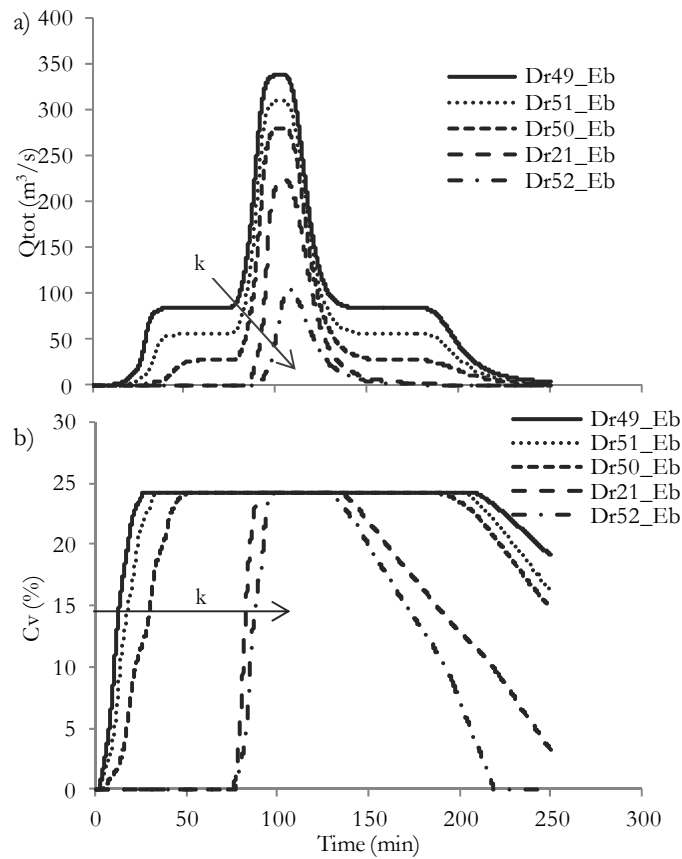
Figure 6.10 Total discharge (a) and transient sediment concentration (b) at the outlet of Dragone basin for different values of soil conductivity.

In order to explicitly take into account the soil unsaturated conditions, a single rainfall event (E_b) is considered, the "middle" soil water characteristic curve (Table 6.1) is accounted for, and the Green-Ampt infiltration model is used with different values considered for: i)

initial water content (θ_{in}=0.35 and 0.29 respectively for soil suction (u_a-u_w) equal to 10 and 20 kPa), and ii) thickness of the unsaturated soil layer (z=0.1, 0.2 and 0.3 m). Soil saturated conductivity (k_{sat}=18 mm/h) and water content at saturation (θ_{sat}= 0.51) are kept constant. Under these hypotheses, different shapes of the discharge plot are simulated (Figure 6.11), consisting of an abrupt increase of peak discharge, that corresponds to high rainfall intensity, with the exception for the case of z=0.3 m and u_a-u_w=20 kPa, in which total discharge starts to increase after the high rainfall intensity period. In addition, the lower the suction and soil thickness, the higher peak discharge, the faster the maximum sediment concentration is reached and the longer this maximum concentration value is kept in time.
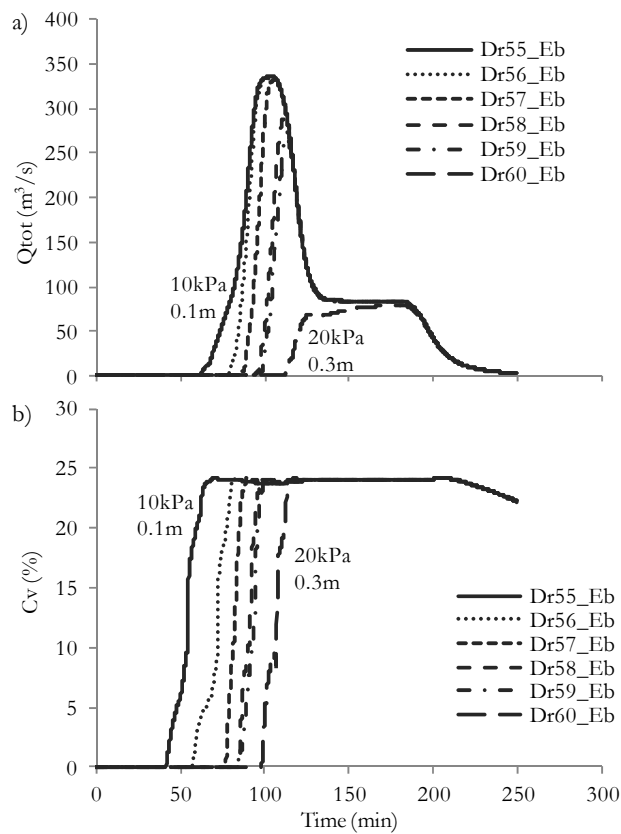
Figure 6.11 Total discharge (a) and transient sediment concentration (b) at the outlet of Dragone basin for different initial soil suction and soil depth.

For the same soil water characteristic curve ("middle curve") and soil suction equal to 20 kPa, the analysis is deepened considering a soil depth equal to 1.0 m and soil conductivity equal to 18 mm/h (k_{sat} of "middle" curve) and 1.8 mm/h, 0.18 and 0.018 mm/h, corresponding to 1/10, 1/100 and 1/1000 of k_{sat}, respectively. The results (Figure 6.12) show that, also for unsaturated conditions, soil conductivity affect the times and total peak discharges; in particular, the higher the soil conductivity, the lower peak discharge and in the case of 18 mm/h no discharge is obtained at the outlet of the basin. Moreover, for the cases of 0.18 mm/h and 0.018 mm/h, it is worth noting that the trend of total discharge is affected by the effect of low rainfall intensity that precedes and follows the highest rainfall intensity. However, in the cases with soil conductivity higher than 18 mm/h, the same maximum volumetric concentration is reached at different times depending on soil conductivity.
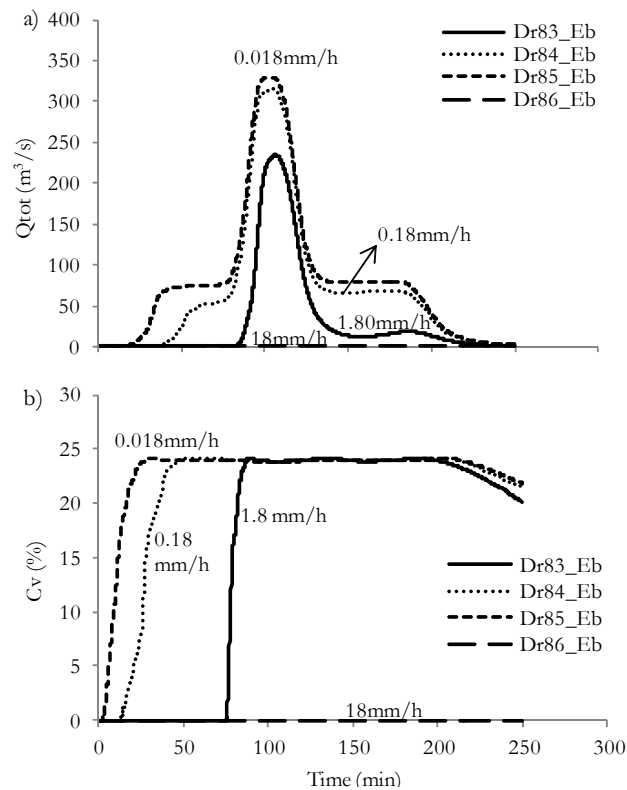
Figure 6.12 Total discharge (a) and transient sediment concentration (b) at the outlet of Dragone basin for middle curve and different soil conductivity.

151

In order to outline the differences which may arise from distinct soil water characteristic curves ("lower", "middle" and "upper" of Table 6.1), a single rainfall event (E_b) is considered, with a soil suction equal to 20 kPa and soil thickness equal to 0.2 m and 0.3 m. Figure 6.13 shows the achieved results when a soil thickness is assumed equal to 0.2 m. In this case, the shape of discharge-time plots and the maximum sediment volumetric concentration are quite similar for "middle" and "upper" curves, corresponding to an abrupt increase of total peak discharge with maximum value for middle curve; for "lower" curve, the discharge-time plot shows a two-peaks trend, the first (and higher) at the end of the high rainfall intensity period and the second corresponding to the end of rainfall event; whereas minor differences are found for the maximum sediment volumetric concentration in all the cases.
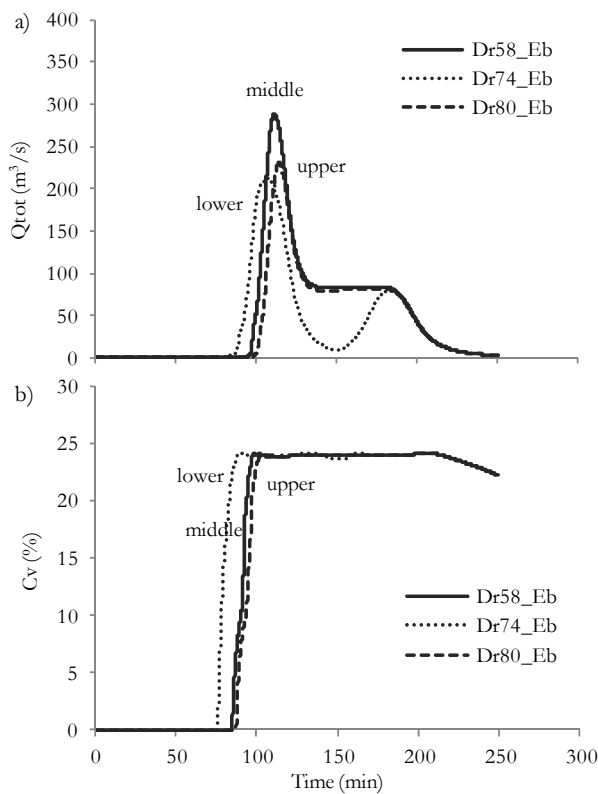
Figure 6.13 Total discharge (a) and transient sediment concentration (b) at the outlet of Dragone basin for different soil water characteristic curves (initial suction equal to 20 kPa and soil depth equal to 0.2 m).

Figure 6.14 shows the achieved results when a soil depth is assumed equal to 0.3 m. In this case, the shape of discharge-time plots, the times of peak discharge and total peak discharges are different for all the soil water characteristic curves. For "lower" curve, a total peak discharge is three times higher and occur earlier than other curves; whereas minor differences are found for the maximum sediment volumetric concentration in all the simulated cases.
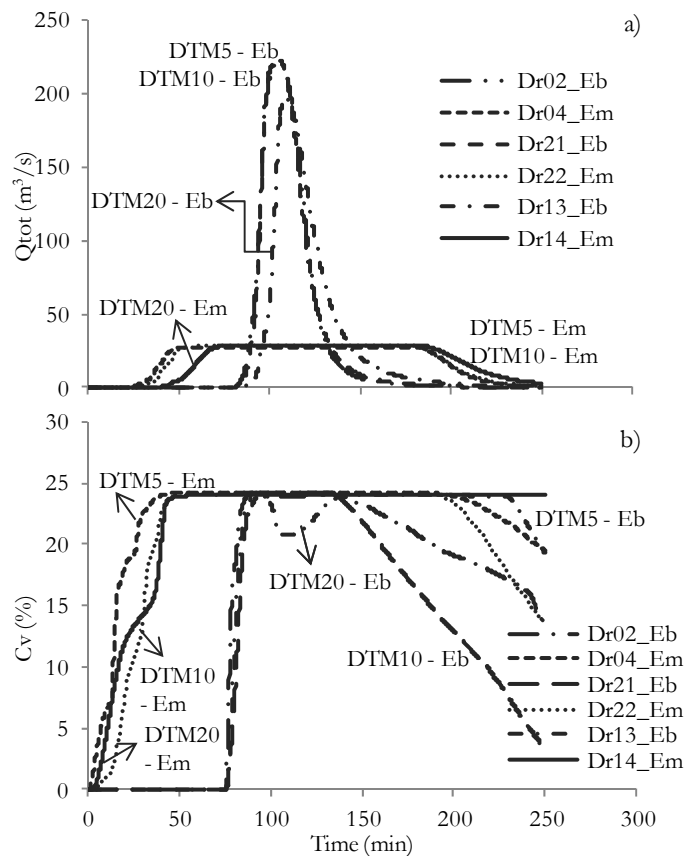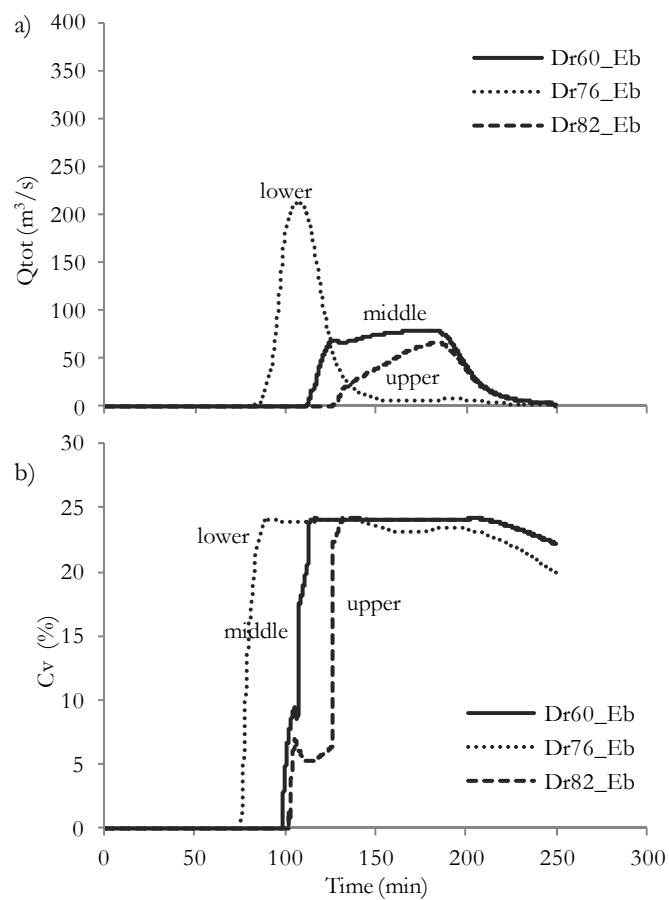

Figure 6.14 Total discharge (a) and transient sediment concentration (b) at the outlet of Dragone basin for different soil water characteristic curves (initial suction equal to 20 kPa and soil depth equal to 0.3 m).

6.2.4   New insights for soil erosion analysis

In this section few selected cases are analysed aimed to provide a wide class of possible slope erosion scenarios with reference to: i) total discharge at the outlet of the basin, ii) sediment concentration, iii) erosion map inside the basins. The first two results are referred to assess the type of phenomena affecting the urban areas located at the outlet of the basin; the last result is used to assess the source zones of flow-like mass movements. Particularly, the role of rainfall characteristics is investigated with reference to rainfalls E_a, E_b, E_c, compared also to rainfalls E_0 and E_m of Figure 6.6. For the sake of simplicity, a single set of soil hydraulic properties is chosen: k_{sat}=18mm/h, θ_{sat}= 0.51, θ_{in}=0.29 (corresponding to 20 kPa), and a 0.1 m thickness of unsaturated soils involved by the infiltration process.

Figure 6.15 and Figure 6.16 provide the total discharges and volumetric sediment concentrations computed for different rainfalls in the Dragone and Sambuco basins, respectively. The obtained results show that: i) a short intense rainfall event (E_0) produces different effects depending on the morphometry of the basin, i.e.: no runoff at the outlet of Dragone basin, while, a total peak discharge of 155 m^3/s for Sambuco basin; ii) temporal sequence of high and low intensities (E_a, E_b, E_c) strongly affects the discharge-time plot, the total peak discharge, time to reach the peak discharge, but the same value of maximum sediment concentration is reached in all the three cases; iii) a moderate rainfall (E_m) produces different discharge-time plots depending on the selected basin, i.e.: for Sambuco basin, the peak discharge and maximum sediment concentration are lower than for other rainfalls while for Dragone basin this rainfall generates a peak discharge higher than for E_a but lower than for other cases, however reaching the same maximum sediment concentration.
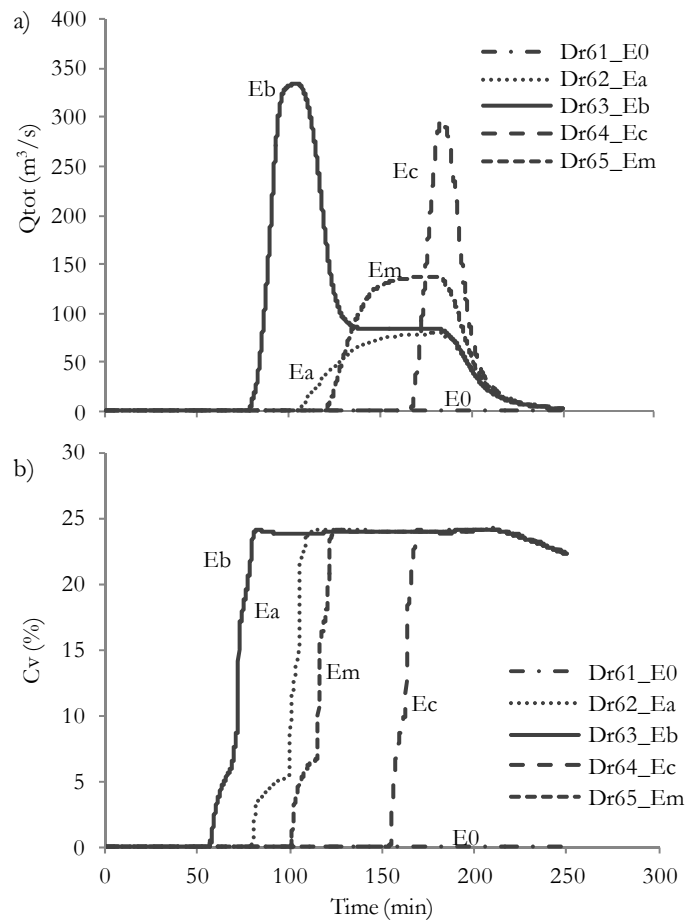
Figure 6.15 Dragone basin: a) total discharge, b) transient sediment concentration for different rainfall conditions.
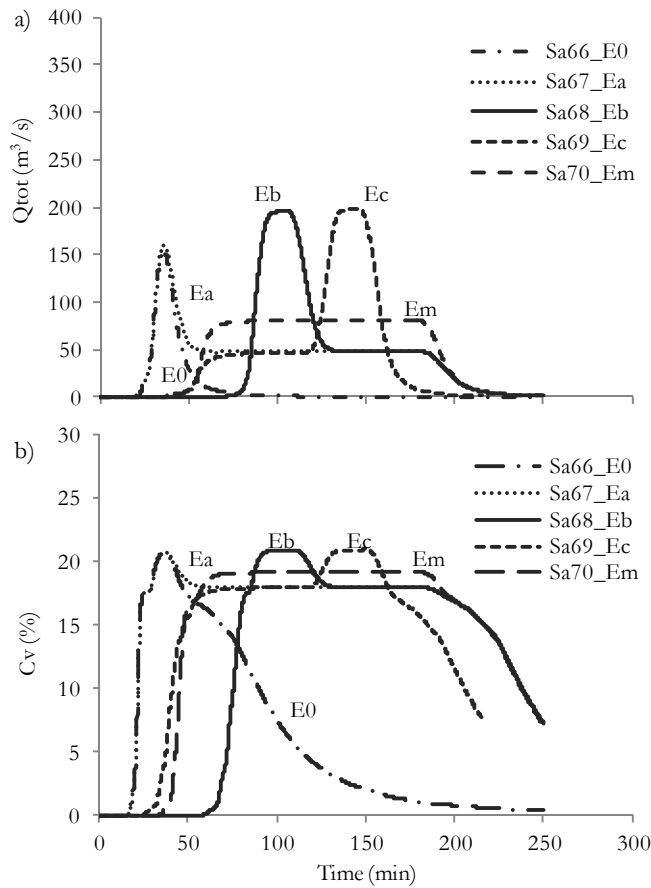
Figure 6.16 Sambuco basin: a) total discharge, b) transient sediment concentration for different rainfall conditions.

A comparison with other some past case studies taken from literature is provided with reference to total sediment volume and total peak discharge. Figure 6.17 and Figure 6.18 show the simulated cases for different rainfall conditions for Dragone and Sambuco basins compared with empirical relationships obtained from in-situ observations of catchments affected by past flow-like phenomena (Mizuyama et al., 1992; Jitousono et al., 1996; Bovis and Jacob, 1999; Rickenmann, 1999; Jacob, 2005; Lavigne and Suwa, 2004). It is outlined a good agreement among the analysed case study and similar phenomena occurred in other environmental contexts, thus confirming the notably susceptibility of the selected basins to the triggering of flow-like phenomena.
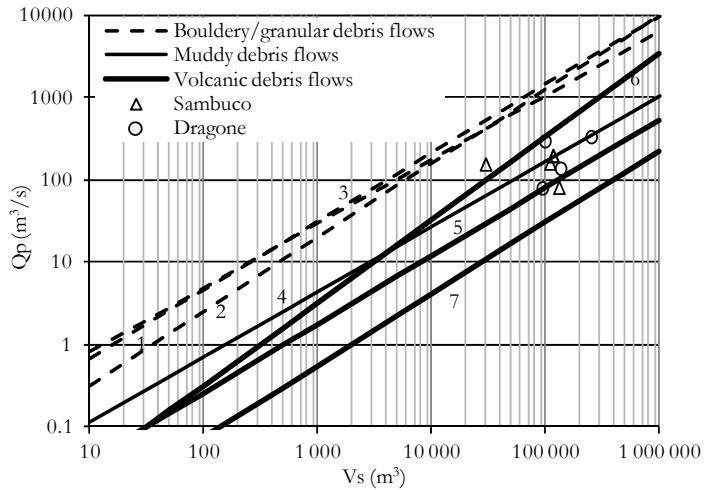
Figure 6.17 Total peak discharge and total sediment volume simulated for Dragone and Sambuco basins, compared to other past case studies taken from literature (1 and 4: Mizuyama et al. 1992; 2 and 6: Bovis and Jakob, 1999; 3: Rickenmann 1999; 5 and 7: Jitousono et al. 1996).
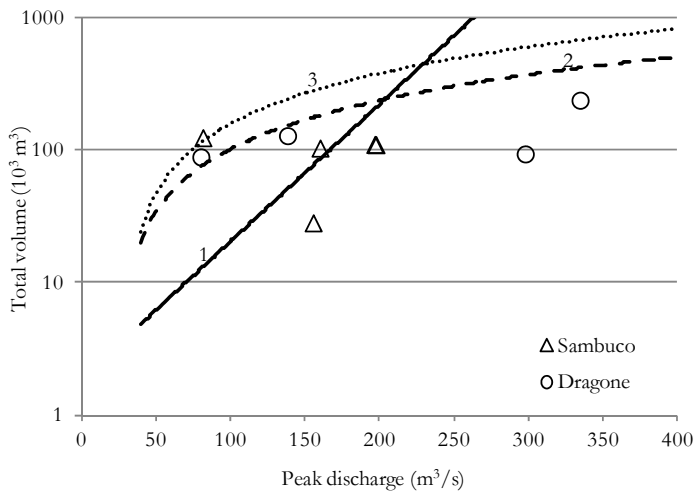
Figure 6.18 Total peak discharge and total sediment volume simulated for Dragone and Sambuco basins, compared to different flow-like phenomena occurred in Curah Lengkong river (Indonesia) (1: streamflow; 2: hyperconcentrated flow and 3: debris flow, correlations taken from Lavigne and Suwa, 2004).

For the two basins, the maximum total eroded volume is obtained for different rainfalls: E_b for Dragone basin and E_m for Sambuco basin. With reference to these two cases, Figure 6.19 provides the spatial distribution of the erosion source areas, with depths higher than 5 cm. In particular, the results show that: i) the erosion source areas particularly affect the main stream channels of the basins; ii) on the Sambuco basin a moderate rainfall (E_m) produces erosion areas more widespread than those due to intense rainfall (E_b).
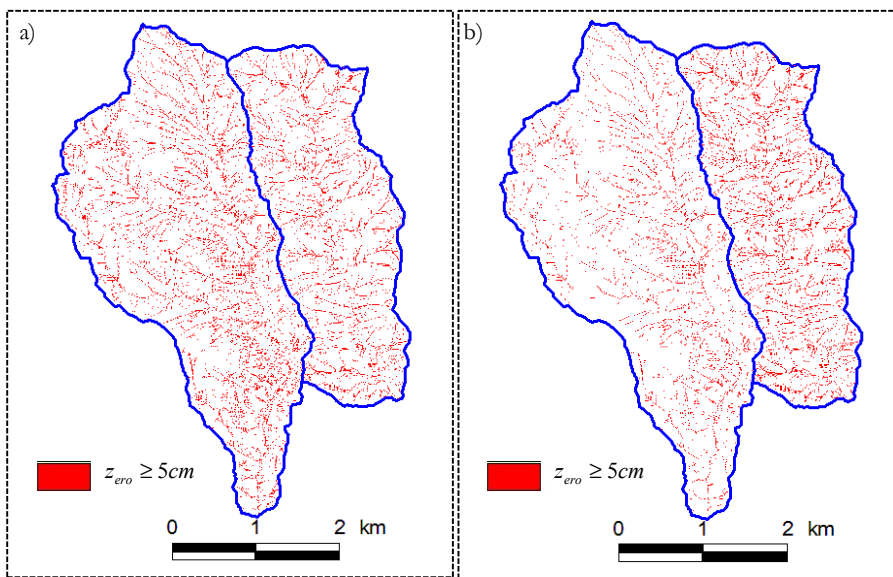
Figure 6.19 Erosion map (erosion depths equal or higher than 5 cm) for Dragone and Sambuco basins: a) E_b rainfall, b) E_m rainfall.

In order to compare the times to total peak discharge between different outlets within the same basin, the Dragone basin and the rainfall event E_b are selected. Four outlets of sub-basins are chosen and the total discharge and volumetric sediment concentration are obtained (Figure 6.20a). The analysis shows that: i) the volumetric sediment concentration is higher than 20% for all the sub-basins, although there are different total peak discharges (Figure 6.20b,c); ii) if the upper outlet (out_4) and lower outlet (out_1) are compared, the time span the two peak discharges is about 10 minutes (Figure 6.20d).
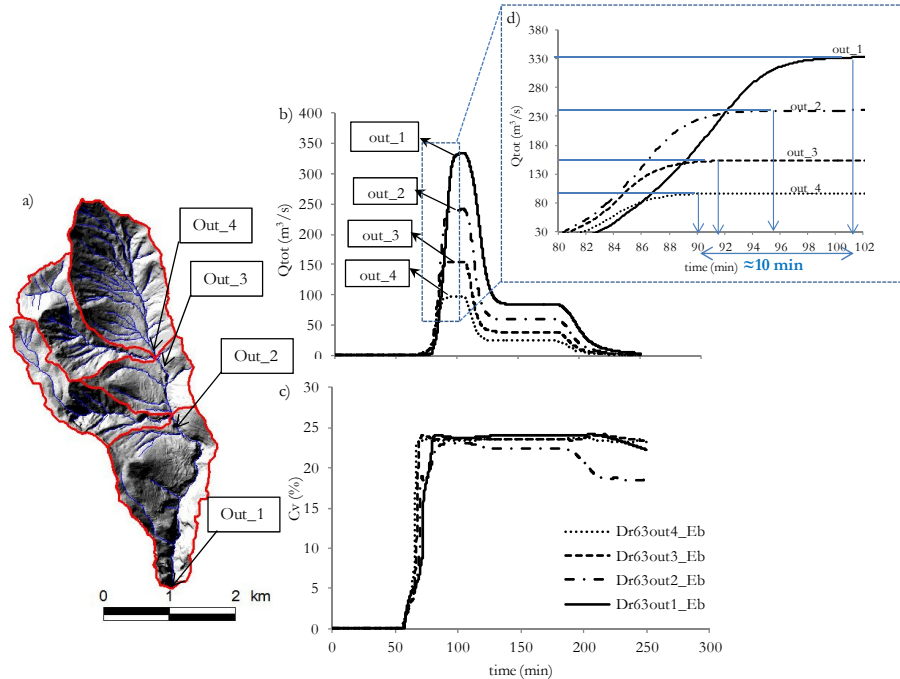
Figure 6.20 a) Selected outlets for the Dragone basin; b) total discharge and c) transient sediment concentration for different outlets; d) details of total peak discharge and time peak discharge.

With reference to Dragone basin, which is characterised by the highest simulated values of total peak discharge and sediment concentration for E_b rainfall condition, the analysis is deepened considering a more realistic soil depth equal to 1 m, the middle soil water characteristic curve, soil suction equal to 20 kPa and different soil conductivity (k) equal to 1.8 mm/h, 3.6 mm/h and 6 mm/h. Figure 6.21 shows that the higher total peak discharge corresponds to the lower soil conductivity, but the same maximum sediment concentration is reached although it has a shorter duration in time.

For these realistic cases, in order to identify the portions of Dragone basin most affected by erosion phenomena, the mean eroded thickness is calculated for most widespread geomorphological landforms (zero order basin, valley concave shaped, very incised torrential valley, valley V-shaped) and for each sub-basin with area higher than 0.25 km². The purpose of this analysis is twofold: i) to identify the areas that require erosion control works in order to reduce the solid discharge at the outlet

of the basin and ii) to indicate the priorities (for action) to makers that have to choose how to allocate economic resources in the risk management.
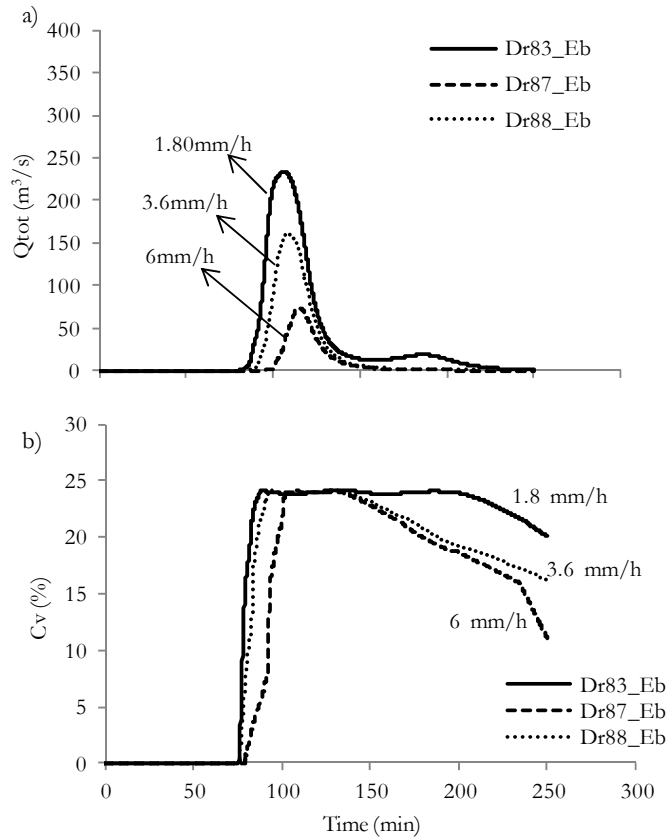
Figure 6.21 Dragone basin: a) total discharge, b) transient sediment concentration for soil depth equal to 1 m and different soil conductivity (indicated as labels to the curves).

With reference to geomorphological units (Figure 6.22), the analysis shows that: i) for each analysed cases the valley V-shaped is affected by high mean eroded thickness; ii) although the zero order basins have a greater extension, they have a lower susceptibility to erosion.

With reference to sub-basins (Figure 6.23), the analysis shows that the mean eroded thickness is lower than 30 cm.
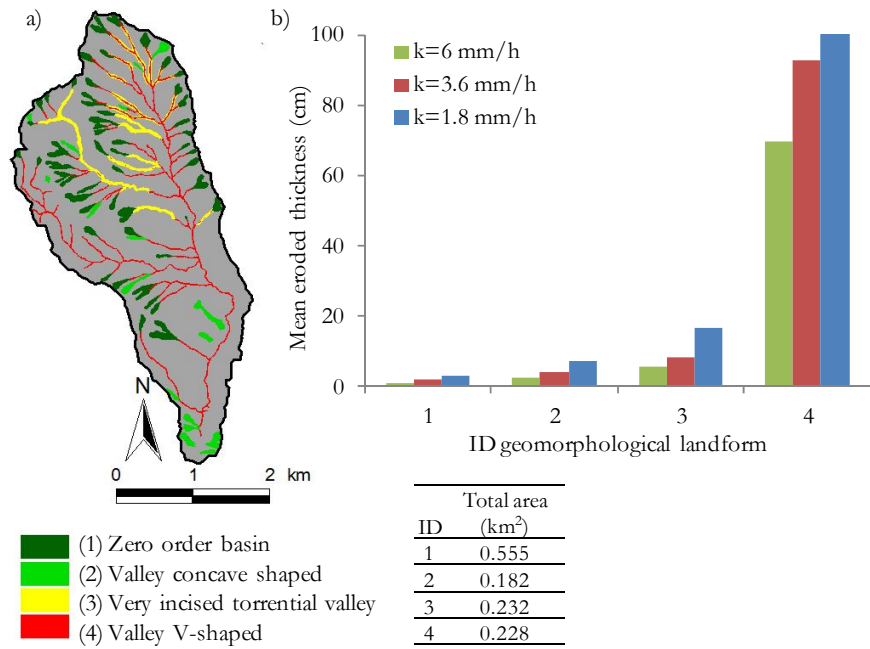
Figure 6.22 a) Spatial distribution of most widespread geomorphological landforms in the Dragone basin; b) mean eroded thickness for the analysed cases.
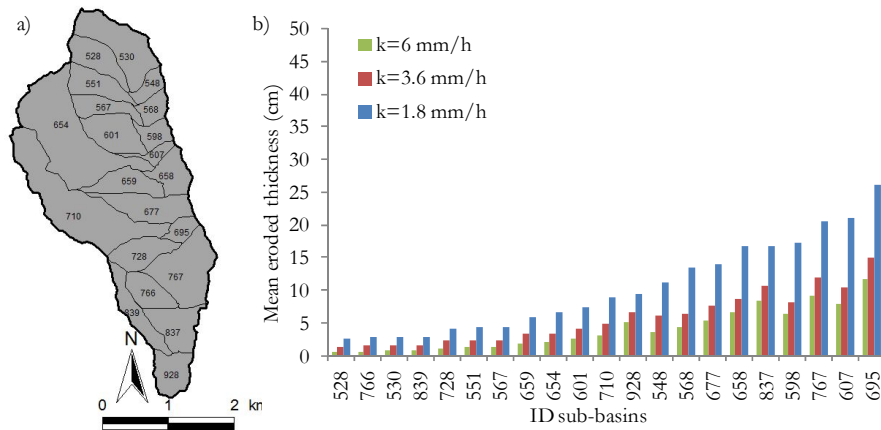
Figure 6.23 a) Sub-basins in the Dragone basin; b) mean eroded thickness for the analysed cases.

Moreover, it is possible to individuate the sub-basins most affected by erosion phenomena (Figure 6.24). The results show that the most affected sub-basins are located in the left-side of main stream channel, for all the simulated cases.
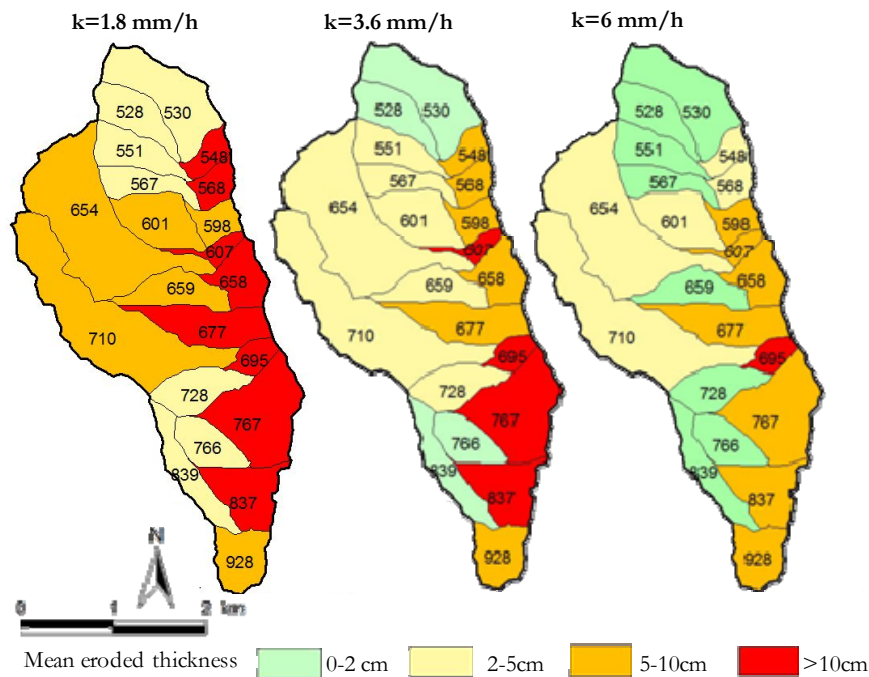
Figure 6.24 Mean eroded thickness for different sub-basins belong to Dragone basin for the selected cases.

6.3 DISCUSSION

A numerical investigation of soil erosion was proposed with reference to two medium-sized steep mountain basins within the study area through a physically-based model for soil erosion. A parametric sensitivity analysis was firstly performed to outline the key factors and processes during heavy rainfall. The achieved results outline that the peak discharge of water and solid particles driven by overland flow depends on rainfall intensity while volumetric solid concentration within the washout is related to the morphometric features of the whole

mountain basin. Volumetric sediment concentration is quite more sensitive to DTM resolution rather than peak total discharge. The lower the soil conductivity, the higher the peak discharge, the faster the maximum solid concentration is reached and the longer this maximum sediment concentration value is kept in time. The higher is the thickness of the unsaturated soil layer, the lower is the value of total peak discharge that is also delayed in time. Furthermore, soil suction is outlined as a key factor for the spatial and temporal evolution of infiltration and runoff in the basin, also affecting the discharge of water and solid particles at the outlet of the basin.

Based on these insights, few selected cases were analysed aimed to provide a wide class of possible slope erosion scenarios. It was shown that, provided the same amount of cumulated rainfall, the sequence of high and low rainfall intensity strongly affects the time-discharge at the outlet of the basin without any significant variation of the maximum volumetric sediment concentration.

In conclusion, distinct realistic rainfall scenarios have been used to analyse the specific case study, and also to provide general insights on the use of numerical tools for quantitative forecasting of soil erosion along steep slopes and total discharge at the outlet of the basin. The results show that accurate qualitative analysis of soil erosion can be made in a variety of initial conditions and for different hydraulic and mechanical properties. Thus, either back-analysis or forecasting of specific real events can be confidently performed.

7 RAINSPLASH EROSION ANALYSIS AT PARTICLE SCALE

In this Section, the mechanism of rainsplash erosion and the amount of the splashed particles is analysed at particle scale, through the Discrete Element Method. The input data and the scheme are suitably defined and a parametric analysis is performed. Finally, the obtained results are compared with experimental evidences reported in the scientific literature.

7.1 EXPERIMENTAL EVIDENCES

The erosion is a process that involves detachment of soil particle from the ground surface followed by subsequent transport of the detached soil material away from the site of detachment (Fujiwara et al., 1986; Kinnel, 2005) (Figure 7.1). The transport of detached particles may occur as the result of raindrops and flow acting singly or together.

Kinnel (2005) identified four detachment and transport systems (Figure 7.2): 1) raindrop detachment with transport by raindrop splash (RD-ST); 2) raindrop detachment with transport by raindrop-induced flow transport (RD-RIFT); 3) raindrop detachment with transport by flow (RD-FT) and 4) flow detachment with transport by flow (FD-FT). The first system, that occurs without the runoff generation, is generally called rainsplash erosion and although it may be considered simple, it involves a series of complex processes composed of three stages (Kinnel, 2005): 1) collision and deformation of a falling raindrop at the ground surface; 2) rupture and collapse of the drop into a thin disk of fluid spraying radially outwards from the point of impact; 3) jetting of daughter ejection droplets in parabolic trajectories away from the original point of impact.
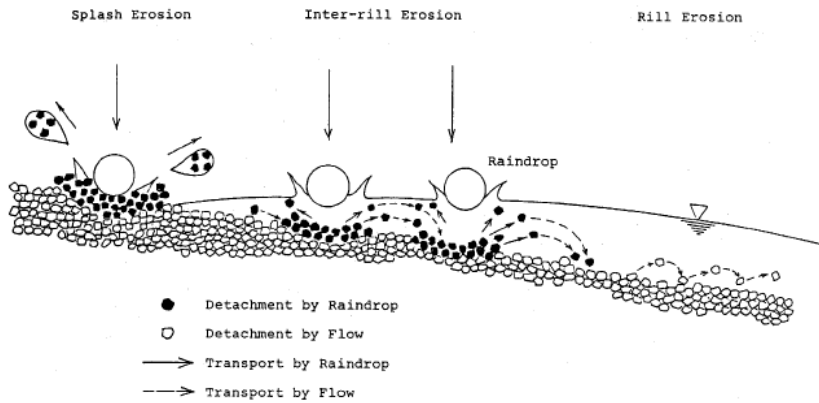
Figure 7.1 Schematic diagram of erosion process (Fujiwara et al., 1986).
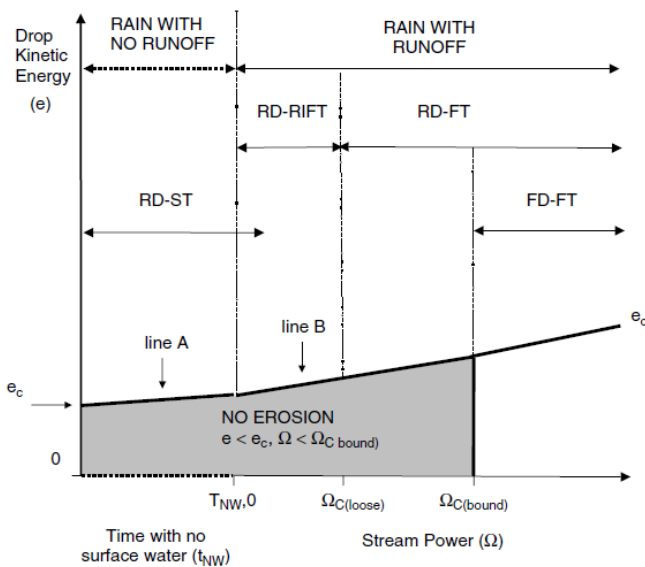
Figure 7.2 Detachment and transport processes associated with variations in raindrop and flow energies (Kinnel, 2005).

In literature, physical understanding of the rainsplash processes causing detachment and transport by falling raindrops has been considerably improved by laboratory experiments (Poesen and Savat, 1981; Nearing and Bradford, 1985; Poesen and Savat, 1981; Ghadiri and Payne, 1986, 1988; Poesen and Torri, 1988; Sharma and Gupta, 1989; Salles et al., 2000; Mouzai and Bouhadef, 2003; Ma et al., 2008) (Figure

7.3) and field experiments (Figure 7.4)(Morgan, 1981; Parlak and Parlak, 2010; Ghahramani et al., 2011; Geißler et al., 2012; Angulo-Martinez et al., 2012). In particular, the raindrop detachment and transport is measured using a variety of techniques, including trays and boards (Van Dijk et al., 2002a) (Figure 7.3 and Figure 7.4) and splash cups (Figure 7.5), and the splashed particles are generally related to rainfall characteristics (mainly kinetic energy, raindrop diameter, rainfall intensity), soil properties (e.g. texture, shear strength) and surface geometry and conditions (e.g. vegetation cover, slope angle, roughness, depth of surface water).
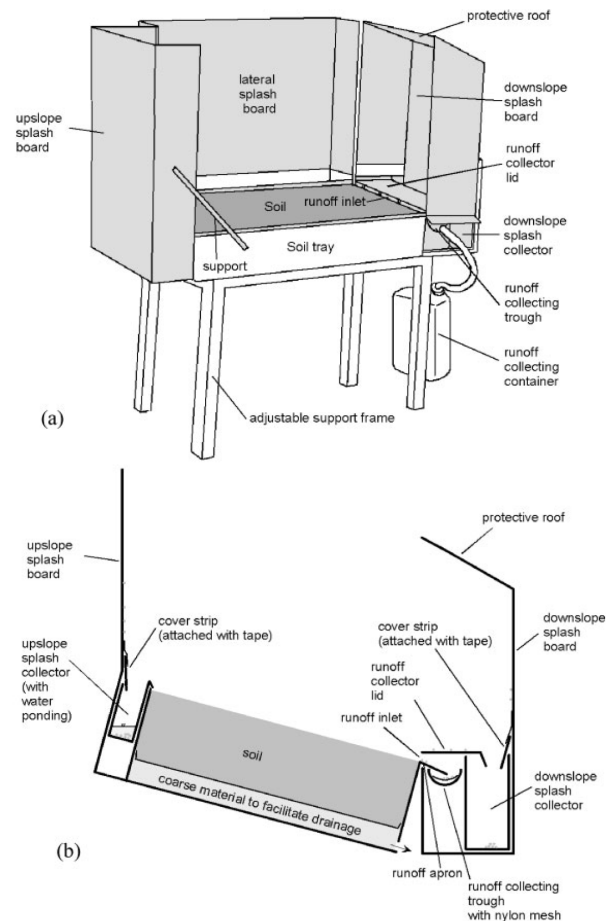
Figure 7.3 Laboratory experiment system for the combined splash and runoff collection system (Van Dijk et al., 2003b).
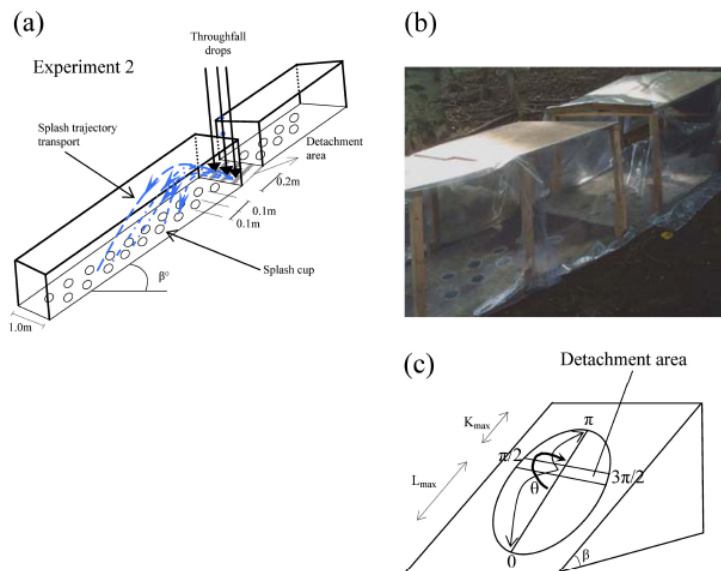
Figure 7.4 Field experiment for measuring mass splashed as a function of distance from a source area (Ghahramani et al. 2011).

The classical method for quantifying splash erosion relies on the use of splash cups, or small traps that collect the soil particles detached and transported by splash (Ellison, 1947; Morgan, 1978; Poesen and Torri, 1988; Salles and Poesen, 1999; Van Dijk et al., 2003a,b; Legout et al., 2005).
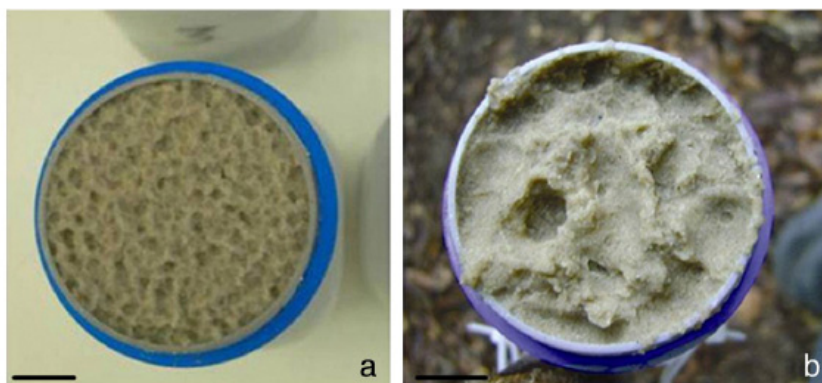
Figure 7.5 Sand detachment from splash cups under open filed (a) and under forest vegetation (b) (Geißler et al., 2012).

Generally, the experimental studies show that the rate of detachment of soil particles (D_r) on bare soil can be expressed by equations of the form (Morgan, 2005):

$$D_r \propto I^a \cdot s^c \tag{7.1}$$

$$D_r \propto KE^b \cdot s^c \cdot e^{-dh} \tag{7.2}$$

where I is the rainfall intensity (mm/h), s is the slope expressed in mm^{-1} or as a sine of the slope angle, KE is the kinetic energy of the rain (J/m^2) and h is the depth of surface water (m). These equations, generally, obtained by experimental measurements, are often implemented in the erosion models and applied to real cases. Examples of these mathematical relationships are reported in details in Table 7.1.

For instance, Wicks and Bathurst (1996) described the hillslope processes analysed in the physically-based SHESED model and the equation for detachment by raindrop impact and leaf drip used by this model is reported in Table 7.1.

With reference to the physically-based LISEM model (Jetten, 2002) described into Section 6.2.1, the splash detachment is related to empirical results of splash tests and is related to the soil aggregate stability (median number of drops to decrease the aggregate by 50%), the rainfall kinetic energy , the depth of the surface water layer, the amount of rainfall (mm) and the impacted area (Eq. 6.9) (Table 7.1).

Jayawardena and Bhuiyan (1999) investigated experimentally the detachment rate due to rainfall impact in interrill areas and they found that it is possible to predict raindrop detachment rate using a simple equation with a rainfall intensity (Table 7.1 and Figure 7.6), also contributing to the development of physically-based erosion models.

Table 7.1 Some experimental equations for rainsplash detachment.

References	Equations and terms
Wicks and Bathurst (1996) SHESED model	$D_r = k_r \cdot F_w \cdot (1 - C_G) \cdot [(1 - C_C) \cdot M_R + M_D]$ $M_R = \alpha \cdot I^{\beta}$ $$M_D = \frac{\left(\dfrac{V \cdot \rho \cdot \pi \cdot D^3}{6}\right)^2 \cdot DRIP\%DRAIN}{\left(\dfrac{\pi \cdot D^3}{6}\right)}$$ Dr: rainsplash detachment (kg m^{-2} s^{-1}); k_r : raindrop soil erodibility coeff. (J^{-1}); Fw: water depth correction factor; CG: proportion of soil covered by ground cover; Cc: proportion of ground covered by canopy cover; MR: momentum squared for rain ((kg m s^{-1})^{2}m^{-2} s^{-1}); MD: momentum squared for leaf drip ((kg m s^{-1})^2 rn^{-2} s^{-1}); I: rainfall intensity (mm/h); α, β: empirical coefficients (dependent on I); V : leaf drip fall velocity (m s^{-1}) P: density of water (kg m^{-3}), D is leaf drip diameter (m); DRIP%: proportion of drainage which falls as leaf drip; DRAIN: canopy drainage (m s^{-1})
Jayawardena and Bhuiyan (1999)	$D_r = 78.461 \cdot I^{0.9914}$ Dr: rainsplash detachment (kg m^{-2} s^{-1}); I: rainfall intensity (m s^{-1})
Jetten (2002) LISEM model	$$D_r = \left(\frac{2.82}{A_s} \cdot KE \cdot \exp(-1.48 \cdot d) + 2.96\right) \cdot P_{net} \cdot \frac{dx^2}{dt}$$ D_r: rainsplash detachment (g s^{-1}); As: soil aggregate stability (kg J^{-1}); KE rainfall kinetic energy (J m^{-2} mm^{-1}); d: depth of the surface water layer (mm); P$_{net}$: net rainfall (mm); dx^2 is the cell area (m^2); dt: time step (s).

Figure 7.6 Rainfall detachment rate versus rainfall intensity (Jayawardena and Bhuiyan, 1999).

As shown by the above equations, the detachment and transport of soil particles by raindrop impact is related to rainfall characteristics. Generally, a rainfall can be represented by a distribution of different drops that attain different terminal velocities (van Dijk et al., 2002b). One of the most widely used parameterisations of raindrop size distribution is the two-parameter exponential distribution function proposed by Marshall and Palmer (1948), that involves the parameter Λ (mm^{-1}) (related to rainfall intensity by a power law equation) and the parameter N_0 (mm^{-1} m^{-3}), that together with Λ determines the total number of drops in a volume of air. Starting from these parameters it is possible to obtain power law relationships between rainfall intensity (mm h^{-1}) and median drop diameter D_{50} (mm), that can be expressed in the general form of Eq. 7.3:

$$D_{50} = \alpha \cdot I^{\beta}$$

(7.3)

where the coefficients α (in h) and β can be obtained by different studies (Laws and Parson, 1943; Atlas, 1953; Brandt, 1988; Kelkar, 1959; Zanchi and Torri, 1980; van Dijk et al., 2002b). For instance, Zanchi and Torri (1980) for the rainfall recorded at Florence (Central Italy) obtained a value of α equal to 0.98 (considering an air temperature equal

to 20°C) and a value of β equal to 0.292 through the flour method and for a rainfall intensity variable between 1-140 mm/h.

A raindrop of fixed diameter D, falling to the ground surface, will attain a certain constant terminal velocity v_D, that, usually is expressed by exponential or power law equations (Atlas and Ulbrich, 1977). However, the pratical application of these equations is limited by the fact that they require the calculation of the Reynolds number, that is a rather complicated function of air and fluid densities, dynamic viscosity and surface tension. For this reason, van Dijk et al. (2002b) proposed a third-order polynomial equation (Eq. 7.4) between terminal velocity and raindrop diameter under standard conditions of air pressure (1 bar) and air temperature (20°C) and for raindrop sizes variable between 0.1-7 mm:

$$v_D = 0.0561 D^3 - 0.912 \cdot D^2 + 5.03 \cdot D - 0.254 \, 1 \qquad (7.4)$$

According to Mouzai and Bouhadef (2003), the rainsplash erosion is related to raindrop force and raindrop pressure applied on the ground surface, that are strictly dependent on density, diameter, fall height, velocity of the raindrop and impact area. In particular, the authors estimates the raindrop impact force (F) and pressure (P) using the Eqs. 7.5 and 7.6 (Riezebos and Epema, 1985):

$$F = \frac{m \cdot v^2}{D} \qquad (7.5)$$

$$P = \frac{F}{A} = \frac{4 \cdot m \cdot v^2}{\pi \cdot D^3} \qquad (7.6)$$

where m, D and v are the mass, the diameter and the terminal velocity of raindrop, respectively.

With reference to the displacement of the detached particles, recent investigations with multiple and high-speed cameras, were performed by Long et al. (2011) in order to investigate particle trajectory and velocity, in three dimensions of space, during the impact, detachment, transport and deposition processes (Figure 7.7). In addition to these ballistic measurements, the authors use photogrammetry to analyse the change in

surface morphology caused by a single droplet impact. Through these measurements, both particle-travel distance and the total amount of detachment are investigated, providing valuable insight into raindrop-erosion processes. Results demonstrate the influence of the interactions of particle size and droplet characteristics on detachment and transport on different slope angles.
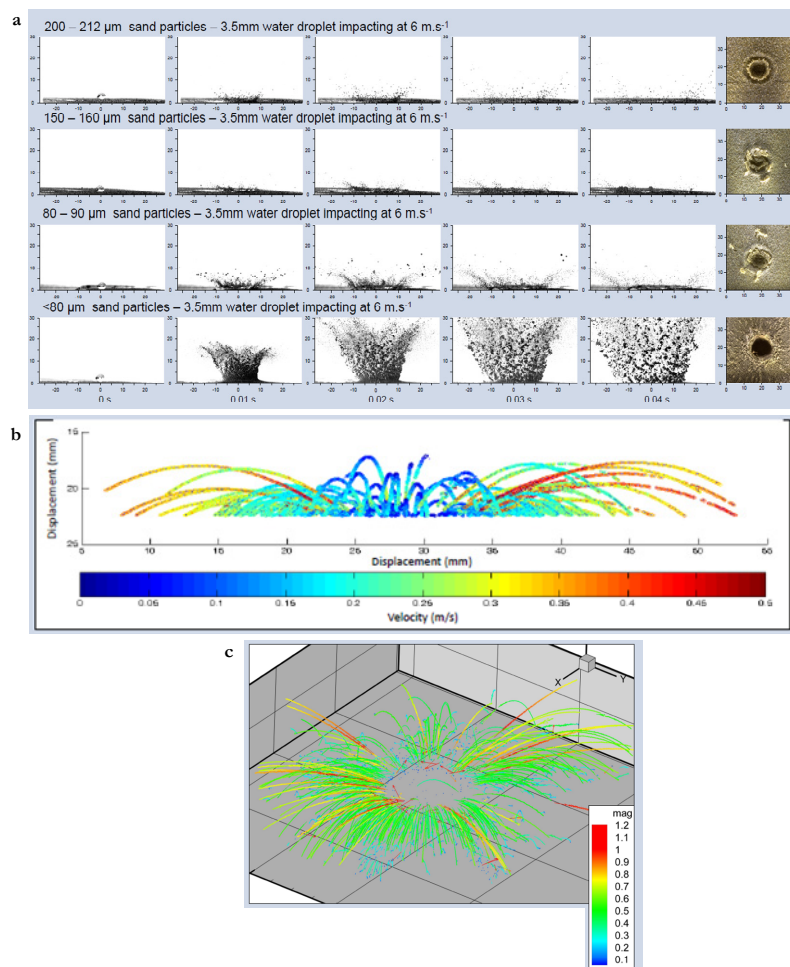
Figure 7.7 Experimental investigation performed by Long et al. (2011).

7.2 PARAMETRIC ANALYSIS

7.2.1 YADE model

General features

The YADE model (Kozicki and Donze, 2008) is based on the Discrete Element Method (DEM) which was introduced by Cundall and Struck (1979). This approach is different from traditional continuum computational method because each element is separated and can move independently from others. In particular, it is based on the use of an explicit numerical scheme in which the interaction of the particles is monitored contact by contact and the motion of the particle modeled particle by particle (Cundall and Struck, 1979). In this way, the DEM approach allows representing the discontinuous nature of granular materials by a set of discrete elements and allows computing the motion of a large number of particles. The approach is fully micromechanical, being the solid phase modeled by defining the mechanical properties of the interaction between the grains that compose it. The soil grain's shape, generally is assumed spherical, except for cases where the specific influence of the grain shape on the soil behavior is investigated. In other cases, polydisperse sphere packings and/or clusters of spheres are often used to reproduce the behavior of granular materials (Catalano et al., 2011).

The Discrete Element Method usually uses the following assumptions (Chen, 2011):
   ✓ all particles are considered rigid and their geometry does not change under the extrusion force between particles;
   ✓ the contacts between particles occur in a small area (contact point);
   ✓ the contact behavior of particles is soft in order to allow some overlap in the contact points between rigid particles;
   ✓ the interaction only occur at the contact between particles and the time step should be small enough to make sure that each particle only has effect on the particles at contact and not on the other particles;
   ✓ the values of velocity and acceleration are constant in each time step and motion of single rigid particle is predicted by Newton's

second law of motion;

✓ time step chosen is so small that, during a single time step, disturbances cannot propagate from any particle further than its immediate neighbors. Then, in each time step, the forces that operate on the other particles are exclusively determined by interaction between the particle and the particle at the contact.

DEM approach solves Newton's equations of motion to resolve particle motion and adds a contact law to resolve inter-particle contact forces. Forces are typically integrated explicitly in time to acquire the time history response of the material using an appropriate quadrature method (Morris et al., 2007). All particles are assumed rigid bodies and the interaction only happens at contacts or interfaces. Behavior at the contacts uses a soft-contact approach and rigid particles are allowed to overlap one another at contact points. According to the force-displacement law, the overlap in every contact will generate an interaction force between particles (Chen, 2011). A set of contact forces acting on the particle and the external stresses (like gravity or forces imposing at the boundary) will cause the motion of particles which is calculated by the Newton's second law. The motion of particles consequently changes the contact condition, resulting in the changes of contact forces between particles, which continually bring about new motion of particles (Chen, 2011).

Based on the modeling of interaction between particles, this method is generally used to simulate the behavior both of frictional granular materials (Cambou and Jean, 2001) and multiphase materials (Gili and Alonso, 2002) by defining microscopical laws. Moreover, the DEM applications are growing in several range of fields, from rock mechanics to computer graphics (Mishra et al., 1992) due to the increase of popularity and the availability of computational times.

Today, DEM is becoming widely accepted as an effective method of addressing engineering problems in granular and discontinuous materials, especially in granular flows, rock mechanics and deformation properties of geomaterials. In addition, the DEM approach can be considered an alternative to the experiments, in order to obtain information about the behavior of granular materials (Catalano, 2012).

<u>Computational cycle</u>

Generally, DEM approach can be divided in the following three stages, that are repeated until the simulation is finished:

1. detection of the contacts between the particles;
2. computation of interaction force, when two particles have slightly interpenetrated.
3. application of Newton's second law of motion in order to determine the resulting acceleration while combining all interaction forces. The equations of motion are integrated over a small time step to relocate a new position for each particle.

The scheme of the computation cycle of a classical DEM is shown in Figure 7.8.

LIST OF INTERACTIONS

NEWTON'S
SECOND LAW OF MOTION

Computation of particles position

INTERACTION LAW

Computation of interaction forces

CONTACT FORCES
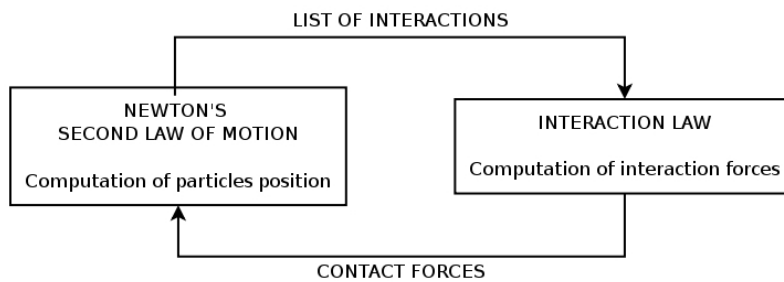
Figure 7.8 Computation cycle of a DEM (Catalano, 2012).

In the case of spherical-shaped particles, in an oriented space of three dimensions i (i=1,2,3), the motion of a particle (that have mass m and moment of inertia J_i) will be characterised by its position (x_i), its translational velocity ($\dot{x}_i$) and rotational velocity ($\dot{\omega}_i$). The translational and rotational accelerations are obtained by applying the Newton's second law of motion, as follows:

$$\ddot{x}_i = \frac{F_i}{m} \tag{7.7}$$

$$\ddot{\omega}_i = \frac{M_i}{J_i} \tag{7.8}$$

where F_i and M_i are the forces and moments applied to each particle.

Interactions law

In YADE, the spherical particles interact according to defined contact laws. Each particle is identified by its radius R, mass m and moment of inertia I. At each time step, the position is computed by integration of the Newton's second law of motion considering the forces and moments applied. The force-displacement law can be described in terms of a contact point (Figure 7.9), defined by the vector $x_i^{[C]}$, lying on contact plane that is defined by its unit normal vector n_i, linking the two centers in particle-particle contacts, and standing on the shortest distance line in ball-wall contacts. The two components of the force acting on the contact plane are related to the corresponding two components of displacement through a normal and a shear stiffness at the contact.
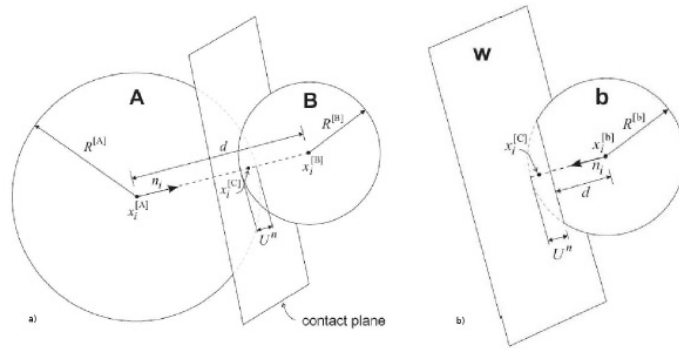
Figure 7.9 Geometry of interactions: a) particle-particle contact; b) wall-particle contact (Catalano, 2008).

With reference to the particle-particle contact, the overlap U_n, defined as the relative contact displacement in the normal direction, and the contact point position $x_i^{[C]}$ are computed as function of the radius R and the position of the centers of the two spheres. The resultant force F_i is composed of its normal component F_i^n and shear component F_i^s:

$$F_i = F_i^n + F_i^s \qquad (7.9)$$

The normal component of the resultant force is obtained as:

$$F_i^n = k_n \cdot U^n \cdot n_i \qquad (7.10)$$

where k_n is the normal stiffness at the contact and it is computed as function of a global stiffness modulus E_{global} and the harmonic mean of interacting spheres radius R_1 and R_2 as follows (Catalano, 2008):

$$k_n = 2 \cdot E_{global} \cdot \frac{R_1 \cdot R_2}{R_1 + R_2} \tag{7.11}$$

The shear stiffness k_s is evaluated as a function of k_n as follows:

$$k_s = \alpha \cdot k_n \tag{7.12}$$

The shear component of the resultant force is computed as a function of the tangent displacement dt, that is initialized to zero and then updated considering each relative shear-displacement increment which results in an increment of the elastic shear force. The motion of the contact is considered in the procedure in order to update the two vectors n_i and $x_i^{[C]}$ at each timestep. The incremental force is then computed as follows:

$$\Delta F_i^s = -k_s \cdot \Delta U_i^s \tag{7.13}$$

where ΔU_i^s is the contact displacement–incremental vector, computed for each timestep as a function of the shear component of the contact velocity. In this way, the contacts between two particles are defined by normal stiffness k_n, shear stiffness k_s and inter-granular friction angle φ_c (Figure 7.10).
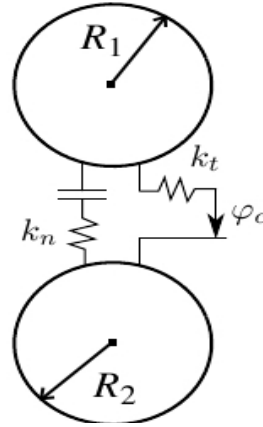
Figure 7.10 Normal and tangential stiffnesses at the contact.

In the case of frictional materials, Coulomb's criterion is assumed at the contact, defining its shear strength. Therefore, for the shear force F_s, an upper limit is defined as function of the normal force F_n and the intergranular friction angle φ_c:

$$\|F_s\| \leq F_n \cdot \tan\varphi_c \tag{7.14}$$

Capillary forces in unsaturated soils

In the case of unsaturated granular materials, an extension of the basic interaction law can be defined in order to take into account the capillary effects (Scholtes et al., 2009), then the cohesive action is ensured by liquid bridges that hold between neighboring particles, resulting macroscopically an apparent cohesion for the material (Catalano, 2012).

In particular, the capillary forces/effects between each pair of particles comes from the presence of interparticular liquid bridges (menisci) (Figure 7.11). The control parameter is the capillary pressure (or suction) u_c, defined as the difference between gas and liquid pressure: $u_c = u_{gas} - u_{liquid}$. Liquid bridges properties (capillary force F_{cap}, volume V and extents over interacting grains) are computed as a result of the defined capillary pressure u_c and of the interacting geometry (spheres radii and interparticular distance) (Figure 7.12) (https://yade-dem.org/wiki/CapillaryTriaxialTest).
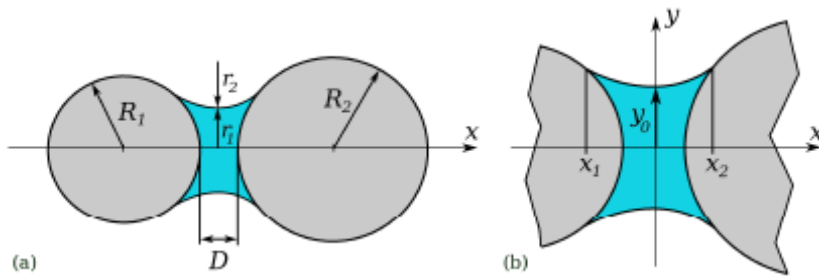
Figure 7.11 Liquid bridge between two particles of inequal sizes: (a) global geometry; (b) details of the bridge (Scholtès et al., 2009).
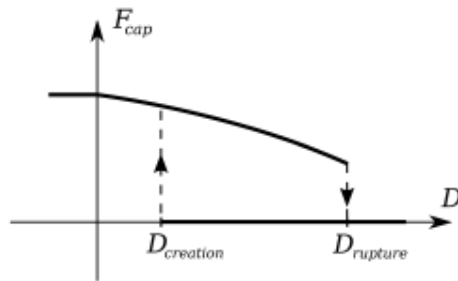
Figure 7.12 Evolution of the capillary force Fcap with the intergranular distance D for a given suction value: a meniscus can form for D>D$_{creation}$ and breaks off for D>D$_{rupture}$ (Scholtès et al., 2009).

7.2.2 Input and methods

The open-source 3D software YADE (Kozicki and Donze, 2008) is used in order to simulate the behavior of a slope under different rainfall conditions and to evaluate the solid particle mobilitation due to raindrop impact. In this section, a parametric analysis of rainsplash erosion is performed in order to evaluate the amount of eroded volume and rainsplash detachment in connection with important geotechnical parameters (e.g soil capillary) with different geometry (e.g. slope angle of the sheme) and under different rainfall conditions (e.g. different rainfall intensities), where each raindrop is represented by its impact force.

In order to take into account the unsaturated condition of the soil, different cases of soil capillary are considered. The capillary effect is taken into account by a YADE's function. Three main steps are necessary to perform the parametric analysis:

1. sample creation through the definition of the geometry (e.g. box, walls, slope angles of the scheme) and the grain size distribution (e.g. shape, number and diameter of soil particles);
2. definition of the soil particle properties (e.g. friction angle, effective cohesion, particle density, Young's modulus, Poisson coefficient and capillary suction at the contact point);
3. definition of the boundary conditions on the ground surface (e.g. raindrop impact force, impact area, number of impacts, impact time duration, time span between two impacts, rainfall duration)

Sample creation

In the DEM simulations, the definition of the sample of particles is an important and complex operation. Generally, in the continuum approaches, the description of the behavior of a granular system is based on the definition of a Representative Elementary Volume (REV) that is the smaller volume portion of the whole system where a constitutive relation can be defined. This relation is representative of the mechanical behavior that can be observed at the macroscopic scale. In the case of DEM, the definition of the REV is more complex, because a lot of exact solutions exist as a result of a lot of possible initial configurations.

Calvetti et al. (1997) and Biarez and Hicher (1994) proposed as volume least ten times greater than the bigger particle size, because they found a good convergence of numerical results with the laboratory experiments measures for this volume (Catalano, 2012). Chareyre (2003) proposed a volume evaluated on the basis of the dispersion of the solution obtained changing the number of particles. Generally, the representativeness is related to the number of particles. If the number of particles increases, the reliability of the considered macroscopic properties increases (Catalano, 2012).

As for a laboratory test, another important aspect is the generation of a good sample for a simulation, because it affects initial density, grain size distribution, porosity, homogeneity and isotropy/anisotropy of the microstructure that, in turn, affect the behavior of the soil and the results of analyses. In particular, for the sample creation, two methods can be used (Catalano, 2012):

- Geometrical methods, based on the algorithms for the positioning of the particles. In this case, the generated particles cloud needs a mechanical stabilization process;

- Dynamical methods, based on DEM simulations that reproduce the deposition of the particles under the effect of gravity or the compaction under the action of external load. In this case, the sample is mechanically stable.

In the analysis, the dynamical method is used applying the effect of gravity, in order to obtain the deposition of the particles on a inclined plane. In particular, in order to obtain the inclination of the plane and reproduce the geometry of a real slope, the gravity is tilted according to different slope angles assumed in the analysis. Figure 7.13 shows the procedure and schematisation adopted for the sample creation.
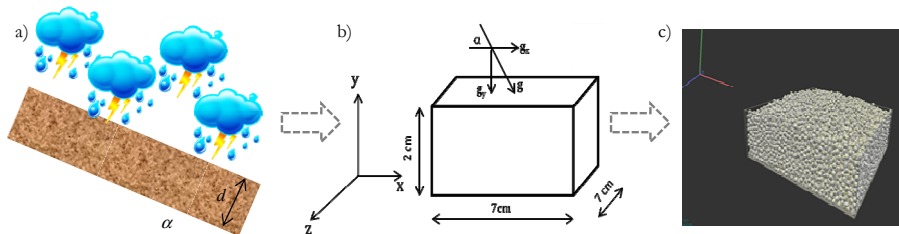
Figure 7.13 Procedure and schematisation adopted for the sample creation.

Figure 7.14 shows the initial and final configuration of the sample generated with the YADE code using the dynamical method.
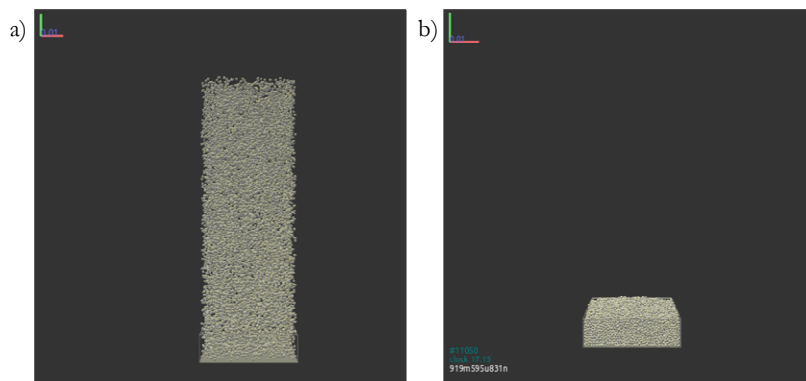
Figure 7.14 Sample creation: a) initial configuration; b) final configuration.

With reference to the box in which the particles are located, boundary walls are assumed rigid and the box has a length equal to 7 cm, a width equal to 7 cm and an height equal to 2.5 cm.

Referring to shape of soil particles, they are assumed as spheres characterised by different diameters belong to the class of "sand" and variable between 1.2 mm and 1.8 mm (Figure 7.15).

Table 7.2 summarises the geometry of the box and the grain size distribution used in the analysis.
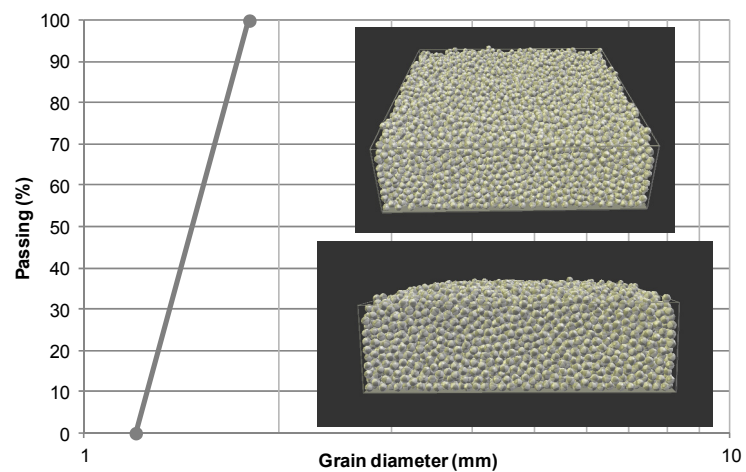
Figure 7.15 Grain size distribution of the sample.

Table 7.2 Geometry and grain size used in the parametric analysis.

Box geometry (cm³)	7 x 7 x 2.5
Slope angle (α) (°)	20, 30, 36, 40
Number of grains (N) (-)	15000
Grain size (mm) Perc. By weinght (%)	1.2 - 1.8 0; 1

Soil properties

In the YADE model, the soil mechanical properties φ', c', respectively friction angle and cohesion, are punctual values related to the contact point between two particles and not to the whole sample. In the parametric analysis, the friction angle and the cohesion at the contact are

assumed equal to 36° and 0 kPa, respectively. The Young's modulus E, soil density ϱ and the Poisson modulus ν are related to the single particle and are assumed equal to 150000 MPa, 1600 N/m³ and 0.5, respectively (Table 7.3).

In order to take into account the soil unsaturated condition, the analysis is performed considering different values of capillary pressure (Table 7.3): i) a case with capillary pressure equal to 0 kPa, that corresponds to totally dry condition (poorly realistic case in nature) or saturated conditions; and ii) two cases that consider the soil unsaturated conditions, with capillary pressure equal to 20 kPa and 30 kPa, respectively. It is worth stressing that, in the analysis the capillary remains constant after the raindrop impact because the model considers the capillary constant in the space and in the time, although it is a very strong hypothesis. This choice simplifies the problem and allows comparing the results between the case with capillary equal to zero and capillary different from zero.

Table 7.3 Soil properties used in the parametric analysis.

Friction angle φ' (°)	36
Effective cohesion c' (Pa)	0
Sphere density ρ (N/m³)	1600
Grain Young's modul E (MPa)	150000
Grain Poisson's modul ν (-)	0.5
Capillary s (kPa)	0, 20, 30

<u>Boundary conditions due to raindrop impact on the ground surface</u>

In order to define the boundary conditions on the ground surface in terms of values of the impact force and its point of application, a procedure composed of four steps is followed:
1. Definition of the value of the raindrop impact force;
2. Definition of the application point of the raindrop impact force;
3. Definition of the particles on which to apply the raindrop impact force.
4. Definition of the times for the impacts.

The first step is related to the assessment of the raindrop impact force starting from the rainfall intensity of an event. The median drop diameter and terminal velocity of raindrop are evaluated using the Eqs. 7.3 and 7.4, respectively. Figure 7.16 shows the trend of these parameters with the rainfall intensities. Finally, using the Eqs 7.5 and 7.6, the raindrop impact forces and pressures are evaluated and their trends with the rainfall intensity are shown in Figure 7.17. In the parametric analysis, different rainfall intensities are assumed considering the hypothesis that a rainfall event of fixed intensity is composed of the drops that have the same diameter and consequently the same impact force. The details of values of rainfall intensity, raindrop diameter and raindrop impact force used in the parametric analysis are shown in Table 7.4.
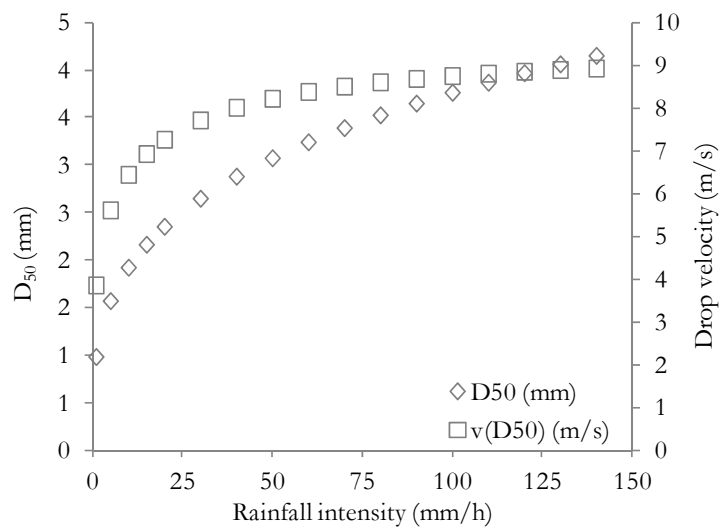
Figure 7.16 Raindrop diameter and velocity versus rainfall intensity.
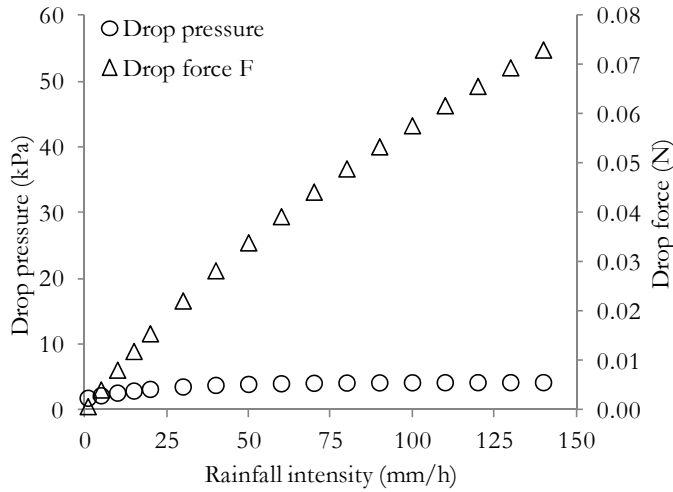
Figure 7.17 Raindrop impact force and pressure versus rainfall intensity.

The second step is related to the identification of the application point of the raindrop impact force. The single raindrop impact on the ground surface is considered randomly located in the space domain. Aimed to define the application point Pij of the single impact force F, an horizontal domain is selected (Figure 7.18).
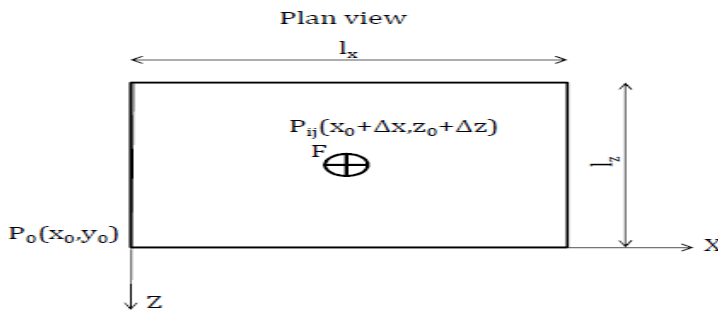
Figure 7.18 Computational scheme for the evaluation of the application point of raindrop impact force.

The generic point Pij is obtained through the coupling of the two random numbers defining a couple random. In this way, the maximum and minimum limit along the two directions of the domain are defined and it is possible to define a numerical range $[0; l_x]$ along the axis x and a

numerical range [0; l_z] along the axis z. For each interval, through a bookkeeping function of python "random.random()" that returns a random number in the defined range, it is possible to obtain, at each step, the numbers necessary for the random couple and finally the point Pij.

The third step is related to the identification of the particles on which to apply the force F. The force F is distributed among the n spheres that belong to the volume of influence (V_{infl}) of the single raindrop. The volume V_{infl} and the number of particles n that belong to this volume, are defined through the following steps: i) definition of the area of influence (A_{infl}); ii) determination of the particle with maximum height (y_{max}) and iii) definition of the thickness of influence (y_{infl}).

The selected area of influence A_{infl} is the area of circle that has the center in the point of impact (Pij) and radius equal to raindrop radius. The scheme used to calculate the area of influence is shown in Figure 7.19.
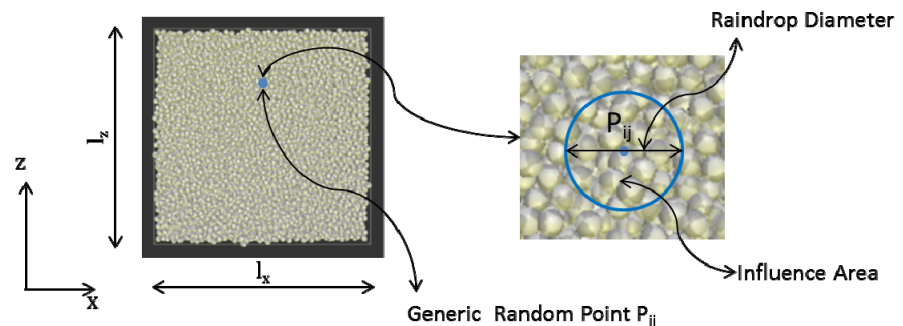
Figure 7.19 Computational scheme for the evaluation of the area of influence.

In order to select the particles with the maximum height, it is necessary to define a random column of particle, obtained from the area of influence and height of the sample (l_y) (Figure 7.20).
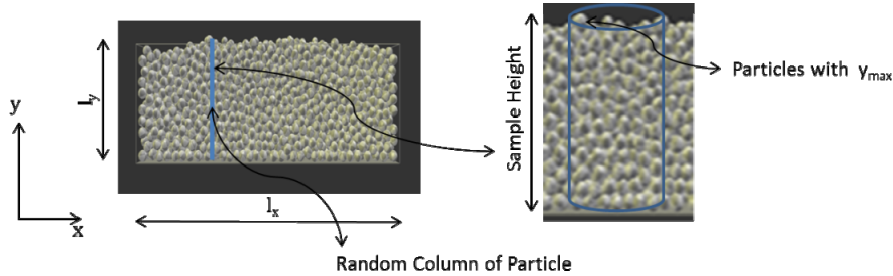
Figure 7.20 Computational scheme for the evaluation of the thickness of influence.

Through the command "ids.append(b.id)" is generated a list, whose elements are numbers (ID) that identify each single particle that belongs to the column. For each ID, it is possible to define some properties of the particle (i.e mechanical properties, size, velocity, position, etc). For each particle, the position along the three axis is calculated and through the command "vett.max()", the maximun value of the y-coordinate is evaluated along the vertical axis, obtaining the value of y_{max}. The thickness of influence is calculated by the following equation:

$$y_{infl} = y_{max} - D_{raindrop} \qquad (7.12)$$

Finally, the volume of influence (Figure 7.21) is defined by the area and the thickness of influence.

Area of influence → circle with center Pij and radius equal to raindrop radius

Volume of influence

Thickness of influence equal to y_{max} – raindrop diameter
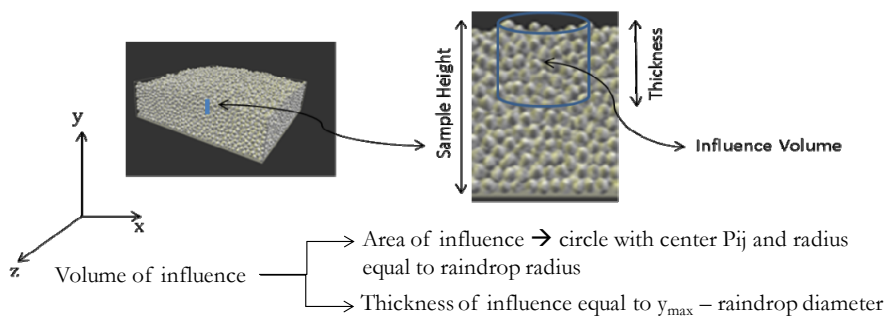
Figure 7.21 Computational scheme for the evaluation of the volume of influence.

In order to simulate the effect of a raindrop, the raindrop impact force F is divided among the particles identified in the volume of influence of the raindrop, obtaining the generic force F(i). The force F(i) is the average force applied on the generic particle (i) and at each impact, it is computed as follows:

$$F(i) = \frac{F}{n} \tag{7.13}$$

where n is the number of particles in the volume of influence and F is the raindrop impact force.

The fourth step is related to the definition of the times for the impacts. The scheme assumed for the times is shown in Figure 7.22.
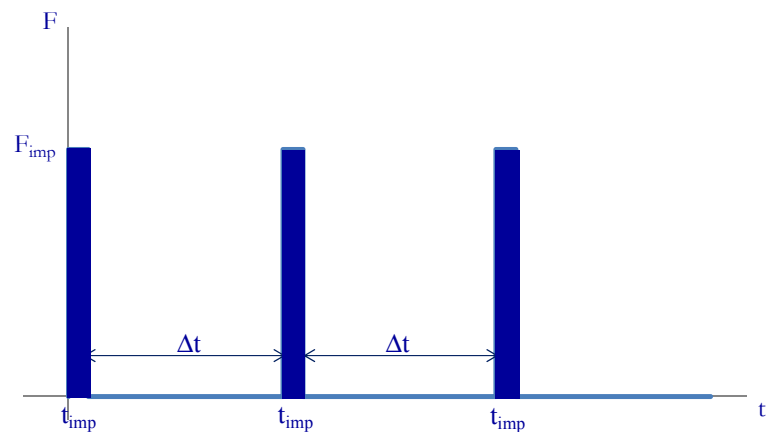
Figure 7.22 Computational scheme for the evaluation of times.

In particular, the impact time duration is computed as follows:

$$t_{imp} = \frac{D}{v} \tag{7.14}$$

where D and v are the diameter and the velocity of raindrop, respectively. In order to reduce the calculation times, the rainfall

duration is assumed equal to 20 s and the time span between two impacts Δt is calculated as follows:

$$\Delta t = t_{imp} \cdot 10 \qquad (7.15)$$

Table 7.4 shows the input data related to boundary conditions on the ground surface used in the analysis.

Table 7.4 Boundary conditions on the ground surface used in the analysis.

Rainfall intensity I (mm/h)	20	50	100	120	150
Raindrop diameter D (mm)	2.35	3.07	3.76	3.97	4.23
Raindrop impact force F (N)	0.016	0.034	0.058	0.066	0.077
Impact time duration t_{imp} (s)	$3.24e^{-4}$	$3.74e^{-4}$	$4.30e^{-4}$	$4.48e^{-4}$	$4.73e^{-4}$
Time span between two impacts Δt (s)	$3.24e^{-3}$	$3.74e^{-3}$	$4.30e^{-3}$	$4.48e^{-3}$	$4.73e^{-3}$
Rainfall duration T (s)	20	20	20	20	20

7.2.3   Numerical results

The DEM simulations are performed by applying the impact forces on the ground surface, according to the criteria shown in the previous section. Figure 7.23 shows the particles on which the impact forces are applied and the temporal evolution of rainsplash erosion.

At the beginning, for a number of iterations equal to zero, the particles are characterised by a value of acceleration and velocity equal to zero (Figure 7.23a); in the middle of simulation, the impacted particles move due to the effect of the impact forces (acceleration and velocity higher than zero) assuming a new position (Figure 7.23b); at the end, it is found that the thickness of particles in the box is lower and, the eroded volume (detached particles) is defined as the sum of the particle volume which crosses the control section. It is accumulated out of the box (Figure 7.23c) and computed for each time step.
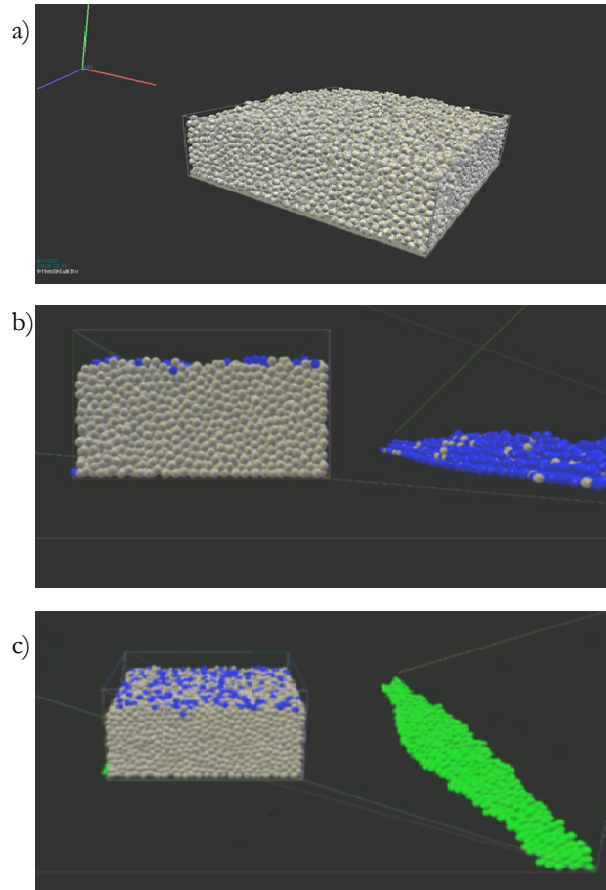
Figure 7.23 Temporal evolution of eroded particles: a) initial configuration; b) intermediate configuration and c) final configuration.

With reference to different soil capillary conditions, for slope angles of the scheme equal to 36° and capillary equal to 0 kPa, there are no differences in the volume accumulated out of the box over the time for different rainfall intensities but for the same rainfall intensity (e.g. 100 mm/h) (Figure 7.24) the volume is higher for case with capillary equal to 0 kPa and moreover it increases slowly in time. This analysis points out that: i) the soil condition plays an important role on the amount of volume accumulated out of the box; ii) the splash detachment and transport is strongly affected by soil condition more than rainfall intensity.
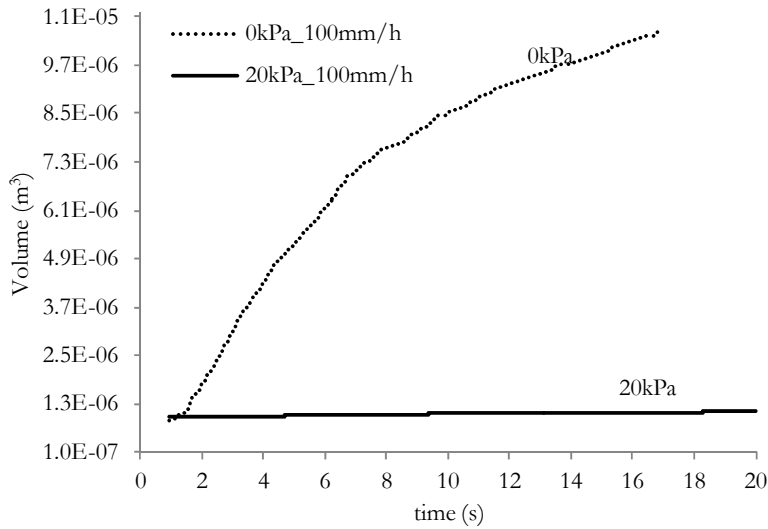
Figure 7.24 Eroded volume over the time for different soil capillary conditions for the rainfall intensity equal to 100 mm/h.

With reference to different rainfall intensity with the soil capillary equal to 20 kPa (Figure 7.25), the volume accumulated out of the box is higher for high rainfall intensities (e.g. 120, 150 mm/h) and it increases more quickly for the heavy rainfall intensity equal to 150 mm/h.
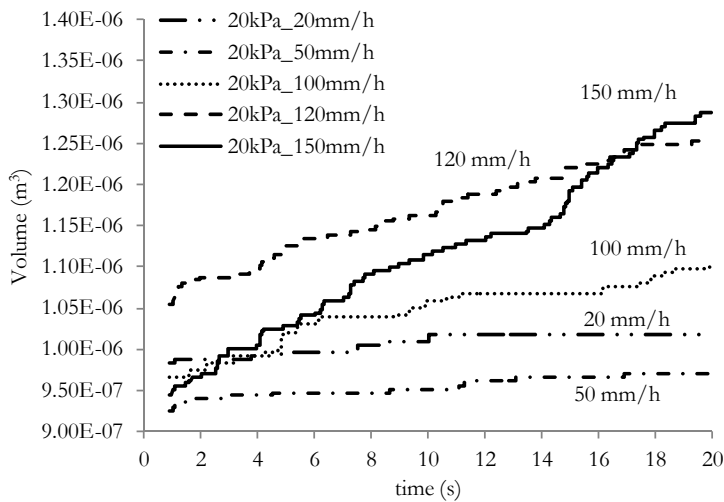
Figure 7.25 Eroded volume over the time for different rainfall intensity and soil capillary equal to 20 kPa.

With reference to different soil unsaturated conditions, it can be noted that for high intensity (e.g. 150 mm/h) (Figure 7.26) the volume is lower for high soil capillary.
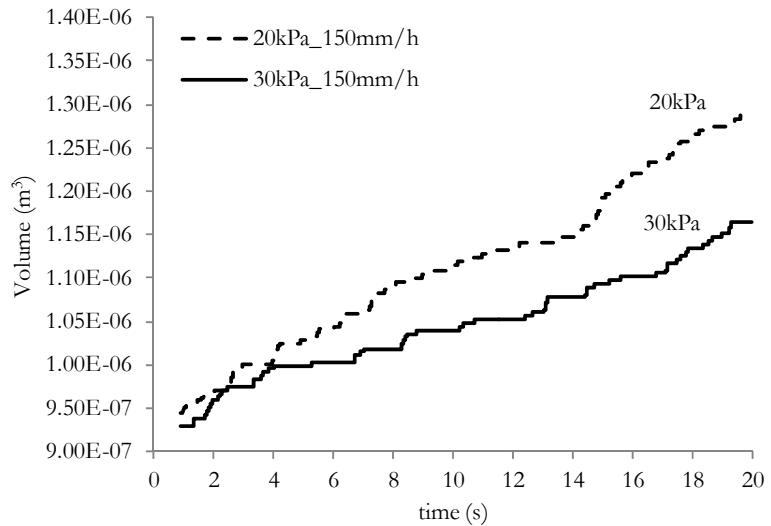
Figure 7.26 Eroded volume over the time for rainfall intensity equal to 150 mm/h and soil capillary equal to 20 kPa and 30 kPa.

If different slope angles are considered, for soil capillary equal to 20 kPa and the same rainfall intensity, the results show that the eroded volume increases with the slope angle (Figure 7.27, Figure 7.28, Figure 7.29).
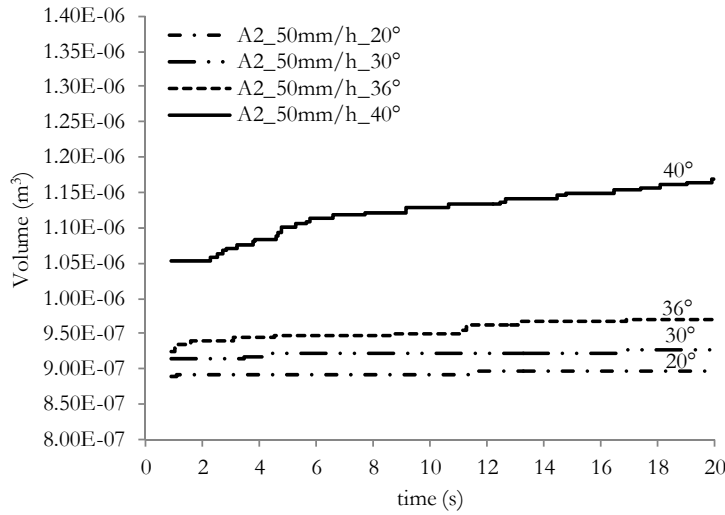
Figure 7.27 Eroded volume over the time for different slope angles of the scheme (rainfall intensity equal to 50 mm/h soil capillary equal to 20 kPa).
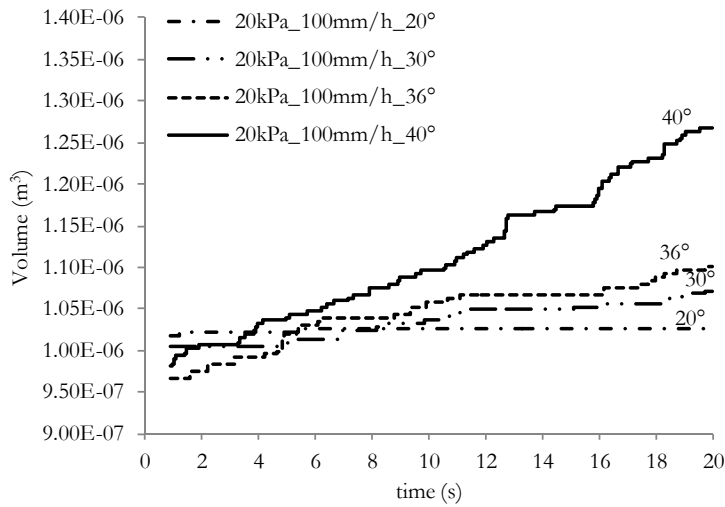
Figure 7.28 Eroded volume over the time for different slope angles of the scheme (rainfall intensity equal to 100 mm/h soil capillary equal to 20 kPa).
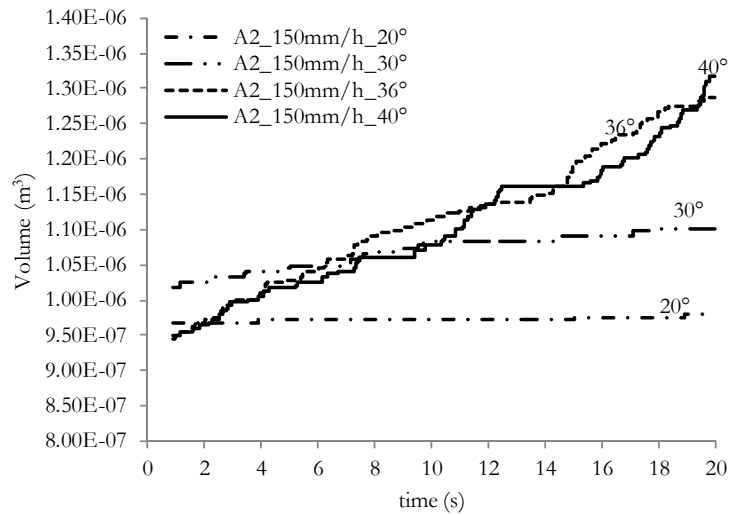
Figure 7.29 Eroded volume over the time for different slope angles of the scheme (rainfall intensity equal to 150 mm/h soil capillary equal to 20 kPa).

Moreover, the analyses are deepened considering the cumulated volume out of the box after 20 seconds. In particular, the number of impacts and the raindrop impact forces applied for each rainfall intensity are reported in details in Figure 7.30.
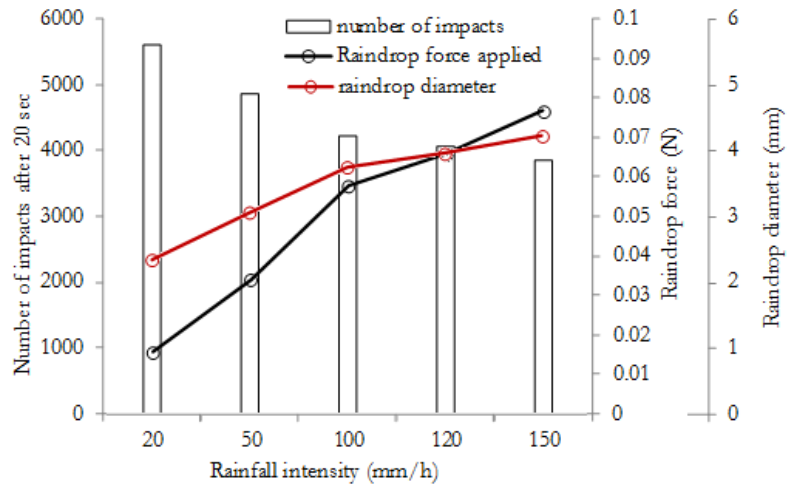
Figure 7.30 Number of impacts after 20 seconds, raindrop impact forces applied and corresponding raindrop diameters for each rainfall intensity.

195

With reference to these analyses, the results (Figure 7.31) show a high correlations between the volume and rainfall intensity, raindrop diameter and raindrop force applied, with a maximum coefficient of determination (R^2) equal to 0.94 and the minimum value of 0.61.

Type of equation	Coefficient of determination R^2	
	20 kPa	30 kPa
	V vs I	V vs I
Exponential	0.8375	0.8945
Linear	0.8387	0.8907
Logarithmic	0.6514	0.9004
Polynomial (2° order)	0.8988	0.9221
Power	0.6515	0.9105

V: cumulated volume after 20 seconds (mm³);
I: rainfall intensity (mm/h).

Type of equation	Coefficient of determination R^2	
	20 kPa	30 kPa
	V vs D	V vs D
Exponential	0.7173	0.9199
Linear	0.7171	0.9117
Logarithmic	0.6514	0.9004
Polynomial (2° order)	0.9414	0.9126
Power	0.6515	0.9105

V: cumulated volume after 20 seconds (mm³);
D: raindrop diameter (mm).

Type of equation	Coefficient of determination R^2	
	20 kPa	30 kPa
	V vs F	V vs F
Exponential	0.7846	0.917
Linear	0.7844	0.911
Logarithmic	0.6172	0.8907
Polynomial (2° order)	0.9242	0.9157
Power	0.6173	0.9017

V: cumulated volume after 20 seconds (mm³);
F: raindrop force (N)

Figure 7.31 Correlations between cumulated volume after 20 seconds and rainfall intensity (a); raindrop diameter (b) and raindrop force (c) (slope angle equal to 36°).

Moreover, the cases with soil capillarity equal to 30 kPa, have higher coefficients of determination than the cases of 20 kPa (Figure 7.31). Finally, the polynomial equations better interpolate the analysed cases and the considered parameters (Figure 7.31).

Starting from the cumulated volume moved out of the box, the eroded thickness is calculated after 20 seconds for each simulated case (different rainfall intensity and different slope angles) under the hypothesis that the overall porosity of the particles cluster, whose initial value is 0.51, remains constant during the simulation. Starting from the eroded thickness after 20 seconds, it is possible to calculate the erosion rate (velocity of rainsplash erosion, mm/s) (Figure 7.32a,b) and estimate the eroded thickness after 30 minutes of rainfall. In particular, it is found that for high rainfall intensity (e.g. 120, 150 mm/h) the erosion rate is higher for low soil capillary and for the same rainfall intensity (Figure 7.32a), it increases with slope angle (Figure 7.32b) showing that the velocity of the rainsplash erosion is strongly dependent on rainfall intensity, soil capillary and slope angle. Figure 7.33 shows the estimated eroded thickness after 30 minutes of rainfall for different rainfall intensity and soil capillary and it results variable between 38 mm and 44 mm with the mean value of 42 mm.

In order to compare the results obtained using this approach with the current literature, the rate of detachment (g/m^2 s) is calculated for each case and a power law correlation is obtained considering the rainfall intensity (mm/h) and slope angle (°), as shown by the equations 7.1 and 7.2 proposed in the literature. The results (Figure 7.34) show good correlations for cases of soil capillary equal to 30 kPa and rainfall intensity equal to 150 mm/h, where the coefficients of determination (R^2) are 0.910 and 0.944, respectively.
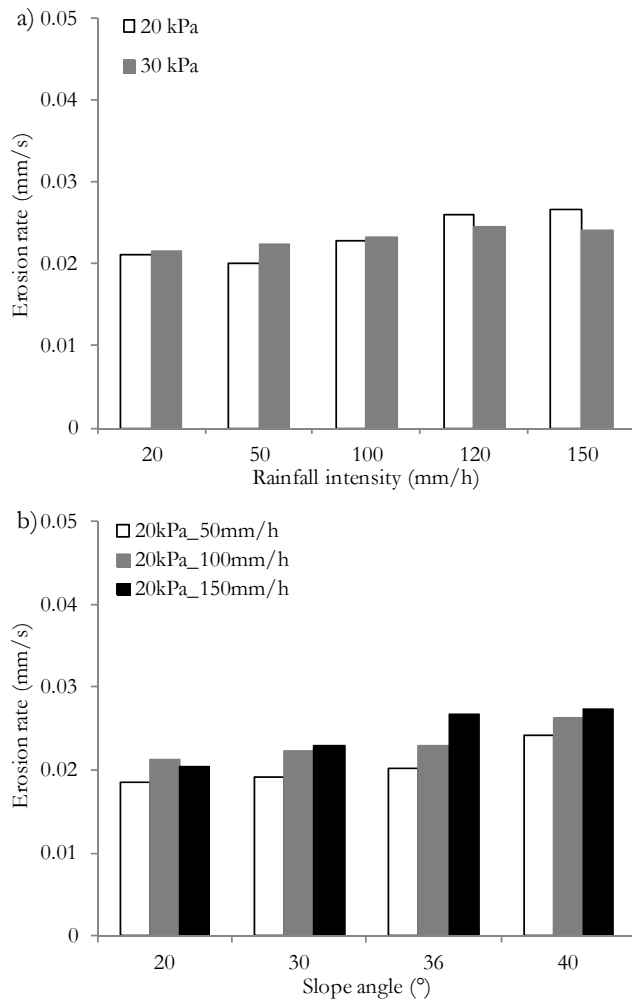
Figure 7.32 a) Erosion rate for different soil capillary and rainfall intensity (slope angle equal to 36°) and b) erosion rate for different slope angles and rainfall intensity (soil capillary equal to 20 kPa).
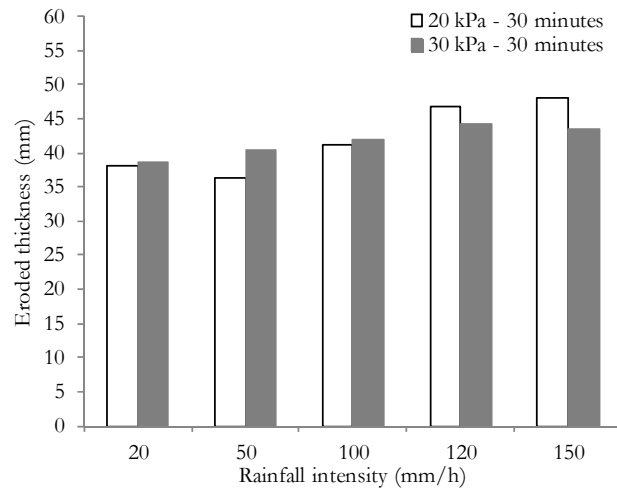
Figure 7.33 Estimated eroded thickness after 30 minutes for different rainfall intensity and soil capillary equal to 20 kPa and 30 kPa (slope angle equal to 36°).

Moreover, the comparison with three literature equations are also performed that are reported into Table 7.1. The results (Figure 7.35), show that the simulated points are within the literature curves especially for high rainfall intensities. This aspect points out that this type of approach can be used to predict the raindrop erosion but a calibration and validation with experimental results are also required.

a)

b)
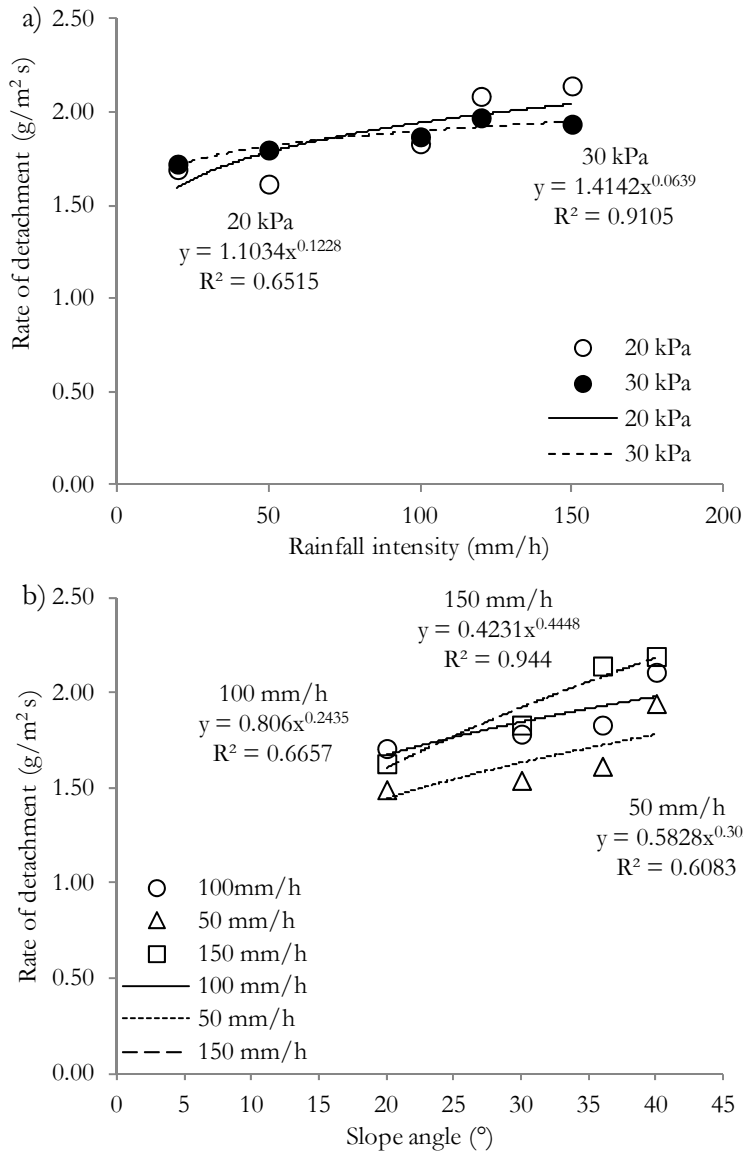
Figure 7.34 Rate of detachment versus rainfall intensity (a) and slope angle (b).
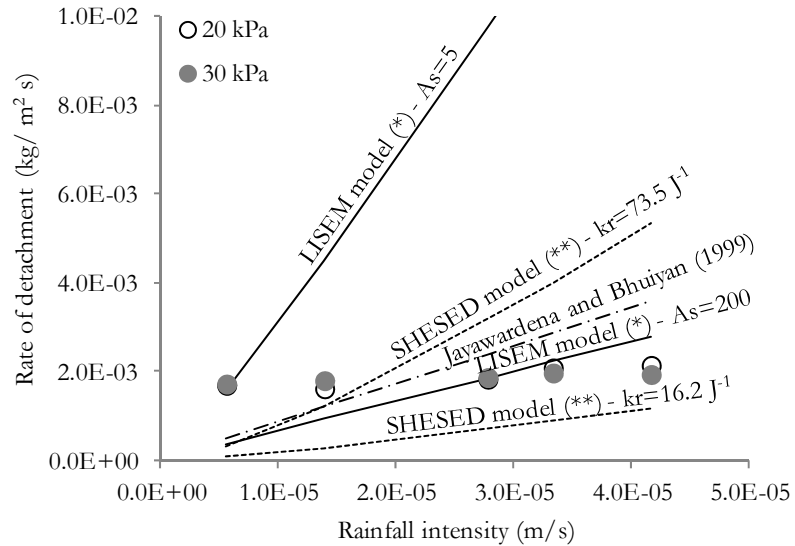
(*) soil aggregate stability As in the range 0.00001-200 (Jetten, 2002)

(**) without water depth and vegetation on ground surface (F_w=1; C_G=0; Cc=o; M_D=0); for I=20mm/h: α=3.75 x 10^{-8} and β=1.5545; for I=50mm/h: α=6.12 x 10^{-8} and β=1.4242; for I=100, 120, 150 mm/h: α=11.75 x 10^{-8} and β=1.52821; kr in the range for different soil texture (values from Wicks and Bathurst, 1996)

Figure 7.35 Rate of detachment versus rainfall intensity for some simulated cases and comparison with literature equations.

7.3 DISCUSSION

A parametric analysis of rainspalsh erosion was performed with the Yade model that is based on Discrete Element Method. The results showed that this approach can be applied to simulate erosion due to raindrop impact but the scheme, the geometry and the input data require considerable efforts in the implementation of code and in the computational times. However, the results are in agreement with the literature formulations.

In details, the analysis showed that the rainsplash erosion strongly depends on rainfall intensity, soil capillary and slope angle. Good correlations exist between the eroded volume and the rainfall

characteristics (e.g. rainfall intensity, raindrop diameter and raindrop impact force). Moreover, it is possible to estimate the eroded thickness for different rainfall durations starting from the results of DEM simulations. Finally, the rate of detachment is related to erosivity parameters (e.g. rainfall intensity) and geometry of the slope (e.g. slope angle) with power law equations in agreement with the literature equations.

8   CONCLUDING REMARKS

Intense rainfall on steep hillslopes may cause either shallow landslides (few meters) or superficial soil erosion (few centimeters) (Acharya et al., 2009, 2011; Cascini et al., 2013) and different flow-type phenomena may originate in adjacent/overlapping source areas. Consequently, great amount of water and debris can be conveyed at the outlet of steep mountain basins where huge consequences are often registered. Cascini et al. (2013) outline that first-time failure may turn into debris flows or debris avalanches (Hungr et al., 2001); conversely, slope instabilities initiated by erosion phenomena generally propagate as hyperconcentrated flows (Coussot and Meunier, 1996). The distinction between different phenomena is fully necessary for the management and mitigation of the risks.

The PhD thesis dealt with the study of hyperconcentrated flows. Starting from an accurate analysis of classifications, triggering mechanisms, spatial and temporal occurrence and approaches for modeling available in the current literature (Chapter 2), it was found that these phenomena are intermediate between water floods and debris flows. They can be defined mass transport phenomena, constituted by water and debris with volumetric sediment concentrations variable from 20 % to 47 % (Costa, 1988), that occur in unsaturated granular soils covering steep slopes. Generally, they are characterised by a great spatial and temporal variability, especially in water discharge and sediment concentration. In this way, suddenly and repeatedly, high peak discharges with high sediment concentration can reach the outlet of the basin and cause victims and damages. This variability, sometimes, makes it difficult to recognize. Moreover, they happen in different environmental contexts, from Alpine basins (Marchi et al., 2002) to steep mountain coastal basins (Cascini et al., 2013) and a better understanding of their genesis is necessary to design suitable measures of risk mitigation and to protect the population that can be affected by these phenomena.

The genesis of hyperconcentrated flows is related to three main processes: i) rainfall infiltration, ii) runoff generation and iii) sediment

particle mobilisation due to erosion processes; with reference to these aspects the PhD thesis wanted to provide an update overview of the genesis processes of an hyperconcentrated flow with specific contributions at different scales of analysis, from large area (> 100 km^2) to single soil particle (diameter < 1cm).

As it concerns **rainfall infiltration and runoff generation** (Chapter 3), the analyses **at slope scale** were performed on a slope section, composed of unsaturated soils whose mechanical and hydraulic properties were chosen among soils affected by past flow-like phenomena (Section 3.1.1). Starting from the rainfall data and soil properties obtained from a long list of international case studies, a FEM numerical parametric analysis (Section 3.3) based on seepage and slope stability analysis was performed in order to validate three mechanisms of runoff generation (Section 3.2). In particular, the mechanism R1 takes place when the rainfall intensity is higher than the soil saturated hydraulic conductivity (k_{sat}); thus, the water cannot infiltrate the ground surface at a larger amount of k_{sat} if initial soil suction is nil and runoff is generated from the beginning of the rainfall storm. The mechanism R2 occurs when the rainfall intensity is higher than initial hydraulic conductivity (k_{in}) but lower than saturated hydraulic conductivity (k_{sat}); at a first stage, rainwater infiltrates the ground surface but then, as soil water content increases, runoff may be generated, provided that rainfall is still continuing. The mechanism R3 arises when the rainfall intensity is lower than the initial hydraulic conductivity k_{in}; in this case runoff cannot occur and only water infiltration takes place. The obtained results (Section 3.3.2) showed that time to runoff, time to failure and runoff rates are strongly affected by soil water characteristic curves, soil initial conditions, rainfall intensity and slope angle. Furthermore, slope stability analyses showed that time to failure can be either shorter or longer than time to runoff depending on soil mechanical parameters. These results point out that the spatial and temporal occurrence and the triggering mechanisms of different phenomena is strongly related to these parameters. Finally, it is outlined that the proposed runoff mechanisms provides more accurate estimates of time to runoff and runoff rates compared to simplified standard procedures (e.g. Curve Number method and Green-Ampt method), implemented in several erosion models, currently available in the literature.

With reference to **solid particle mobilisation due to erosion**, different qualitative mechanisms were recognised in the literature (rainsplash erosion and erosion by overland flow) (Section 2.1.2) and several approaches for modeling are also available (Section 2.1.4). Among these, the quantitative models are the most used approaches because they provide estimates of soil erosion, through empirical equations obtained from statistical analyses of data collected from field experiments (empirical models, e.g. USLE model) or through mathematical relationships describing all the main processes affecting the soil erosion (physically based models, e.g. LISEM model).

In particular, in order to evaluate the triggering of shallow landslides or superficial erosion **at large area** (>100 km^2) the Amalfi Coast study area was selected for his geological setting (Section 4.1), its importance for tourism and having been repeatedly affected by flow-type phenomena (Section 4.2). A spatially distributed multi-hazard analysis was performed through the physically-based TRIGRS-unsaturated model and empirical USLE model, respectively to capture the triggering of shallow landslides and superficial soil erosion taking into account the seasonal variation of some input data. As far as shallow landslides, the achieved results (Section 5.1.2) outlined that the source areas depend on: i) rainfall intensity and duration and ii) soil initial suction. As it concerns the soil erosion (Section 5.2.2), the performed analyses outlined that source areas are related to: i) rainfall characteristics, ii) soil cover use and iii) period of the year. Globally, the achieved results showed that the study area may be affected by shallow landslides and soil erosion in different periods of the year depending on: i) rainfall characteristics, ii) soil suction and iii) soil cover. Referring to ordinary rainfall recorded during the year, the study area results more susceptible to soil erosion processes in Autumn. In addition, for a past event (25th-26th October 1954), the simulated source areas of shallow landslides are lower than those areas recorded during the event and the total soil volume mobilised during the event cannot be exclusively related to landslide occurrence. On the other hand, the zones with a simulated eroded thickness greater than 5 cm are comparable with the areas recorded in field for this event, when the rainfall intensity is very high.

The results obtained over large area and at slope scale highlight that rainfall characteristics, initial soil conditions and soil properties, in turn,

variable during the year, may lead to the triggering of different flow-like phenomena. Moreover, the analyses point out that the unsaturated soils are more susceptible to erosion processes in Autumn, during which catastrophic flow-like phenomena were often registered in the study area (Section 4.2). In this way, it is possible to conclude that in this period, the inception of any flow-like mass movement is mainly related to ground surface erosion.

At basin scale, a numerical investigation (Chapter 6) of soil erosion was proposed with reference to two medium-sized steep mountain basins (Section 6.1) within the study area. In particular, the spatial distribution of erosion source areas, the total discharge and sediment volumetric concentrations at the outlet of the basins for different realistic rainfall scenarios and different input data were investigated using a quantitative physically-based spatially-distributed model (LISEM, Section 6.2.1). The achieved results suggested that the total peak discharge of solid particles driven by overland flow depends on rainfall intensity while volumetric solid concentration within the washout is related to morphometric features of the whole mountain basin. Moreover, the soil conductivity and thickness of the unsaturated soil layer affect times to total peak discharge and times to reach the maximum sediment concentration. In addition, soil suction is outlined as a key factor for the spatial-temporal evolution of infiltration/runoff in the basin (the same results was also obtained at slope scale in the Chapter 3), also affecting the discharge of water and solid particles at the outlet of the basins investigated. Finally, it was shown that, provided the same amount of cumulated rainfall, the sequence of high and low intensity rainfalls (that mainly change for the position of the maximum rainfall intensity in 30 minutes (I_{30}) fixed to 100 mm/h in a 3 hours of rainfall duration) (Section 6.2.4), strongly affects the time-discharge at the outlet of the basin without any significant variation of the maximum volumetric sediment concentration.

However, at the basis of the physically-based models, the infiltration and runoff generation are generally analysed with simplified standard approaches that consider one-dimensional infiltration, overestimating or underestimating the runoff, subsequently used for the evaluation of particles detachment and transport. Moreover, the equations used for rainsplash erosion mechanism are based on the measurements of splashed particles obtained from the laboratory or field tests.

In order to overcome this last limit, a numerical analysis with the innovative Discrete Element Method was preliminary performed (Chapter 7) **at particle scale**. This type of approach allows also overcoming the limitations of other approaches that consider the soil like continuum medium. However, the major difficulties are related to the definition of a representative sample of the soil properties (particle cluster and not single particle properties) and to the evaluation of computational times versus the achievable results. In the parametric analysis, the geometry of the scheme was designed to optimise the computational time versus the achievable results (Section 7.2.2), the raindrop impact forces were evaluated starting from the scientific literature (van Dijk et al., 2002; Mouzai and Bouhadef, 2003) and they depend on the rainfall intensities, raindrop diameters and soil properties which were appropriately selected (Section 7.2.2). The rate of detachment was determined in relation to rainfall intensity, slope angle and soil suction, and a comparison of these results with empirical mathematical equations was performed (Section 7.2.3). These first preliminary results showed that the rainsplash erosion strongly depends on rainfall intensity, soil capillary and slope angle. Good correlations exist between the eroded volume and the rainfall characteristics (e.g. rainfall intensity, raindrop diameter and raindrop impact force). Moreover, it is possible to estimate the eroded thickness for different rainfall durations starting from the results of DEM simulations (Section 7.2.3). Finally, this type of approach can be confidently used to model the rainsplash erosion but other efforts are necessary to improve the modeling.

In conclusion, the quantitative analysis of genesis, mechanisms and features of hyperconcentrated flows is a difficult issue, which however can be confidently tackled at different scales and the achieved results are encouraging for accurate engineering evaluations about this topic.

"Quello che noi facciamo è soltanto una goccia nell'oceano,
ma se non ci fosse quella goccia all'oceano mancherebbe".
(Madre Teresa di Calcutta)

REFERENCES

Abbott M.B., Bathurst J.C., Cunge J.A., O'Connell P.E., Rasmussen J. (1986). *An introduction to the European Hydrological System-Systeme Hydrologique Europeen, SHE. 1. History and philosophy of a physically-based, distributed modelling system.* Journal of Hydrology 87, 45–59.

Abrahams A. D., Gao P., Aebly F. A. (2000). *Relation of sediment transport capacity to stone cover and size in rain-impacted interrill flow.* Earth Surface Processes and Landforms, 25(5), 497-504.

Abrahams A. D., Li G., Krishnan C., Atkinson J. F. (2001). *A sediment transport equation for interrill overland flow on rough surfaces.* Earth Surface Processes and Landforms, 26(13), 1443-1459.

Acharya G., Cochrane T., Davies T., Bowman E. (2009). *The influence of shallow landslides on sediment supply: a flume-based investigation using sandy soil.* Engineering Geology 109, 161–169.

Acharya G., Cochrane T., Davies T., Bowman E. (2011). *Quantifying and modeling postfailure sediment yields from laboratory-scale soil erosion and shallow landslide experiments with silty loess.* Geomorphology 129, 49–58.

Aksoy H., Kavvas M. L. (2005). *A review of hillslope and watershed scale erosion and sediment transport models.* Catena, 64(2), 247-271.

Aleotti P., Chowdhury R. (1999). *Landslide hazard assessment: summary review and new perspectives.* Bulletin of Engineering Geology and the Environment, 58, pp. 21-44.

Angulo-Martinez M., Beguería S., Navas A., Machin J. (2012). *Splash erosion under natural rainfall on three soil types in NE Spain.* Geomorphology,175, 38-44.

Ascough II J.C., Baffaut C., Nearing M.A., Liu B.Y. (1997). *The WEPP watershed model: I. Hydrology and erosion.* Trans. ASAE 40 (4), 921-933.

Assouline S., Ben-Hur M. (2006). *Effects of rainfall intensity and slope gradient on the dynamics of interrill erosion during soil surface sealing.* Catena, 66, 211–220.

Aston A.R. (1979). *Rainfall interception by eight small trees.* J. Hydrol., 42: 383-396.

Atlas D. (1953). *Optical extinction by rainfall.* Journal of Meteorology, 10(6), 486-488.

Atlas D., Ulbrich C. W. (1977). *Path-and area-integrated rainfall measurement by microwave attenuation in the 1-3 cm band.* Journal of Applied Meteorology, 16(12), 1322-1331.

Aulitzky H. (1980). *Preliminary two fold classification of torrents.* Symposium Interpraevent 1980, vol. 4, 285-309.

Autorità di Bacino Regionale Destra Sele (2010). *Rapporto sull'evento del 09/09/2010*, pp. 19.

Autorità di Bacino Destra Sele (2012). http://www.autoritabacinodestrasele.it/

Ayalew L., Yamagishi H., Ugawa N. (2004). *Landslide susceptibility mapping using GIS-based weigthed linear combination, the case in Tsugawa area of Agano River, Niigata Prefecture, Japan.* Landslides, 1:1 73-81.

AVI Project (1994). http://avi.gndci.cnr.it

Baartman J.E., Jetten V.G., Ritsema C.J., Vente J. (2012). *Exploring effects of rainfall intensity and duration on soil erosion at the catchment scale using openLISEM: Prado catchment, SE Spain.* Hydrological Processes, 26(7), 1034-1049.

Bagarello V., Ferro V. (2006). *Erosione e conservazione del suolo.* McGraw-Hill Companies.

Batalla R. J., De Jong C., Ergenzinger P., Sala M. (1999). *Field observations on hyperconcentrated flows in mountain torrents.* Earth Surface Processes and Landforms, 24(3), 247-253.

Baum R.L., Savage W.Z., Godt J.W. (2002). *TRIGRS - a FORTRAN program for transient rainfall infiltration and grid-based regional slope-stability analysis.* U. S. Geological Survey Open-File Report 02-0424.

Baum R.L., Savage W.Z., Godt J.W. (2008). *TRIGRS-A Fortran program for transient rainfall infiltration and grid-based regional slope-stability analysis, version 2.0.* US Geological Survey Open-File Report 2008–1159. Available via: http://pubs.usgs.gov/of/2008/1159/

Beasley D.B., Huggins L.F., Monke E.J. (1980). *ANSWERS-a model for watershed planning.* Trans Am Soc Agric Eng 23, 938–944.

Beck M.B., Jakeman A.J., McAleer M.J. (1995). *Construction and evaluation of models of environmental systems.* In: Beck, M.B., McAleer, M.J. (Eds.), Modelling Change in Environmental Systems. John Wiley and Sons, pp. 3–35.

Beck M.B. (1987). *Water quality modelling: a review of uncertainty.* Water Resources Research 23 (8), 1393–1442.

Bennett J. P. (1974). *Concepts of mathematical modeling of sediment yield.* Water Resources Research. 10:485-492.

Berti M., Genevois R., Simoni A., Tecca P. R. (1999). *Field observations of a debris flow event in the Dolomites.* Geomorphology, 29(3), 265-274.

Beven K. (1989). *Changing ideas in hydrology-the case of physically-based models.* Journal of Hydrology 105, 157–172.

Biarez J., Hicher P. (1994). *Elementary Mechanics of Soil Behaviour: Saturated Remoulded Soil.* AA Balkema.

Bilotta E., Cascini L., Foresta V., Sorbino G. (2005). *Geotechnical characterization of pyroclastic soils involved in huge flowslides.* Geotech Geol Eng 23:365–402.

Bingner R. L., Murphree C. E., Mutchler C. K. (1989). *Comparison of sediment yield models on watersheds in Mississippi.* Trans. ASAE 32(2): 529–534.

Borah D.K. (1989). *Sediment discharge model for small watersheds.* Transactions of the ASAE 32 (3), 874–880.

Bovis M.J., Jakob M. (1999). *The role of debris supply to determine debris flow activity in southwestern B. C.* Earth Surface Processes and Landforms 24, 1039– 1054.

Bovolin V. (2012). *Studio Idraulico dell'evento alluvionale avvenuto ad Atrani (SA) il 9 settembre 2010: PARTE I ricostruzione dell'evento.* Fisciano. Cues ISBN:9788895028965

Bryan R.B., Rockwell D.L. (1998). *Water table control on rill initiation and implications for erosional response.* Geomorphology 23, 151–169.

Calvetti F., Combe G., Lanier J. (1997). *Experimental micromechanical analysis of a 2d granular material: relation between structure evolution and loading path.* Mech. Cohes.-Frict. Mater., 2(2):121–163.

Cambou B., Jean M. (2001). *Micromécanique des matériaux granulaires.* Hermes Science.

Campbell R.H. (1975). *Soil slips, debris flows, and rainstorms in the Santa Monica Mountains and vicinity, southern California.* In: US Geological Survey Professional Paper 851. Washington DC: U.S. Government Printing Office, 51 pp.

Carrara A., Cardinali M., Detti R., Guzzetti F. Pasquid V., Reichenbachd P. (1991). *GIS Techniques and statistical models in evaluating landslide hazard.* Earth Surface Processes and Landform 16:5 427-445.

Carrara A., Cardinali M., Guzzetti F., Reichenbach P. (1995). *GIS technology in mapping landslide hazard.* In: Carrara, A. and Guzzetti, F. (eds.), Geographycal Information Systems in Assessing Natural Hazards. Kluwer Academic Publisher, Dordrecht, The Netherlands, 135-175.

Cascini L., Cuomo S., Sorbino G. (2005). *Flow-like mass movements in pyroclastic soils: remarks on the modelling of triggering mechanisms.* Rivista italiana di geotecnica, 4, 11-31.

Cascini L. (2008). *Applicability of landslide susceptibility and hazard zoning at different scales.* Engineering Geology, 102(3), 164-177.

Cascini L., Cuomo S., Guida D. (2008a). *Typical source areas of May 1998 flow-like mass movements in the Campania region, Southern Italy.* Eng Geol 96(3):107–125.

Cascini L., Ferlisi S., Vitolo E. (2008b). *Individual and societal risk owing to landslides in the Campania region (southern Italy).* Georisk 2(3):125–140.

Cascini L., Cuomo S., Ferlisi S., Sorbino G. (2009). *Detection of mechanisms for destructive landslides in Campania region-southern Italy.* In: Picarelli L., Tommasi P., Urciuoli G., Versace P. (eds) Rainfall-induced landslides: mechanisms, monitoring techniques and nowcasting models for early warning systems. Proceedings of the first Italian Workshop on Landslides, 8–10 June 2009 Naples, Italy, vol 1. Studio Editoriale Doppiavoce, Naples, pp 43–51.

Cascini L., Cuomo S., Della Sala M. (2011). *Spatial and temporal occurrence of rainfall-induced shallow landslides of flow type: A case of Sarno-Quindici, Italy.* Geomorphology 126(1-2): 148-158.

Cascini L., Sorbino G., Cuomo S., Ferlisi S. (2013). *Seasonal effects of rainfall on the shallow pyroclastic deposits of the Campania region (southern Italy).* Landslides, 1-14.

Catalano E. (2008). *Infiltration effects on a partially saturated slope - an application of the discrete element method and its implementation in the open-source software yade.* Master thesis at UJF-Grenoble.

Catalano E., Chareyre B., Cortis A., Barthélémy E. (2011). *A pore-scale hydro-mechanical coupled model for geomaterials.* In Particles 2011 II International Conference on Particle-Based Methods.

Catalano E. (2012). *A pore-scale coupled hydromechanical model for biphasic granular media.* PhD thesis at Université de Grenoble.

CEMPID (Centro Funzionale per la previsione meteorologica e il monitoraggio meteopluvioidrometrico e delle frane – Settore Programmazione Interventi di Protezione Civile sul territorio della Regione Campania) (2010). *Rapporto dell'evento del 9 settembre 2010 nel territorio dei Comuni di Atrani e Scala.* pp.38.

Chareyre B. (2003). *Modélisation du comportement d'ouvrages composites solgéosynthétique par éléments discrets-application aux tranchées d'ancrage en téte de talus.* PhD thesis, PhD thesis at Grenoble University.

Chen J. (2011). *Discrete Element Method (DEM) Analyses for Hot-Mix Asphalt (HMA) Mixture Compaction.*

Chisci G. (1981). *Upland erosion: evaluation and measurement.* In: Proc. of Erosion and Sediment Transport Symposium. p. 331-349.

Chow V.T., Maidment D.R., May L.W. (1988). *Applied Hydrology.* McGraw-Hill, 572p.

Chung C.J., Fabbri A.G. (2003). *Validation of Spatial Prediction Models for Landslide Hazard Mapping.* Natural Hazards, 30:3 451-472.

Ciervo F., Papa M.N., Medina V., Bateman A. (2012). *Ricostruzione e modellazione numerica di un evento di flash flood. Il caso di Atrani 2010.* L'ACQUA. Vol. 3. Pag.21-30 ISSN:1125-1255.

Corine Land Cover IV livello (2006). Available via: http://www.sinanet.isprambiente.it/it/sia-ispra/download-mais/corine-land-cover

Corominas J., Copons R., Vilaplana J.M., Altimir J., Amigò J. (2003). *Integrated landslide susceptibility and hazard assessment in the Principality of Andorra.* Natural Hazards 30, pp. 421 – 435.

Costa J.E. (1984). *Physical geomorphology of debris flows.* In: Costa, J.E., Fleisher, P.J. (Eds.), Developments and Applications of Geomorphology. Springer, Berlin, pp. 268–317.

Costa J.E. (1988). *Rheologic, geomorphic, and sedimentologic differentiation of water floods, hyperconcentrated flows, and debris flows.* Flood geomorphology. In: Baker V.R., Koch el R.C. and Patton P.C. (eds.), Flood Geomorphology, John Wiley and Sons, New York: 113-122.

Coussot Ph., Meunier M. (1996). *Recognition, classification and mechanical description of debris flows.* Earth-Science reviews 40, 209 – 227.

Crosta G., Dal Negro P., Frattini P. (2003). *Soil slips and debris flows on terraced slopes.* Natural Hazards and Earth System Sciences, 3(1-2), 31-42.

Cruden D.M., Varnes D.J. (1996). *Landslide Types and Processes.* In Landslides Investigation and Mitigation. Transportation Research Board, US National Research Council, Turner, A.K. and Schuster, R.L. (editors). Special Report 247, Washington, DC 1996, Chap-ter 3, pp. 36-75.

CSIRO TOPOG Homepage: http://www.clw.csiro.au/topog/intro/intro.html.

Cundall P.A., Strack O.D.L. (1979). *A discrete numerical model for granular assemblies.* Géotechnique 1979; 29(1):47–65.

Cuomo S. (2006). *Geomechanical modelling of triggering mechanisms for flow-like mass movements in pyroclastic soils.* PhD dissertation at the University of Salerno, Italy, pp. 274.

Cuomo S., Della Sala M. (2013a). *Rainfall-induced infiltration, runoff and failure in steep unsaturated shallow soil deposits.* Engineering Geology. Pag.1-10 ISSN:0013-7952. ID:3993054.

Cuomo S., Della Sala M. (2013b). *Spatially distributed analysis of shallow landslides and soil erosion induced by rainfall.* (submitted to Natural Hazards).

Cuomo S., Della Sala M., Capuano C., Rinaldi, F. (2013). *Analisi su area vasta dell'innesco di frane superficiali e fenomeni erosivi indotti da pioggia.* Convegno Nazionale di Geotecnica AGI, Baveno (VB), 4-6 giugno 2014 (submitted to AGI)

Cuomo S., Della Sala M., Novità A. (2013). *Physically-based modeling of soil erosion induced by rainfall on steep slopes.* (submitted to Geomorphology).

Darboux F., Davy P., Gascuel-Odoux C., Huang C. (2001*). Evolution of soil surface roughness and flowpath connectivity in overland flow experiments.* In: Auzet, V., Poesen, J., Valentin, C. (Eds.) , Soil Pattern as a Key Factor of Water and/or Wind Erosion. Catena, 125–139.

Darcy H. (1856). *Les fontaines publiques de la ville de Dijon: distribution d'eaux et fiet ux des eaux.* Victor Dalmont, Paris.

Deere D.U., Patton F.D. (1972). *Slope stability in residual soils.* Proc. 4th Pan-American Conf. Soil Mechanics, Puerto Rico, 1, pp 87 – 170.

De Falco M. (2011). *Approcci innovativi per l'identificazione del degrado per erosione idrica in ambienti agro-forestali mediterranei.* PhD dissertation. University Federico II of Naples, Italy, pp. 294.

De Luca C., Furcolo P., Rossi F., Villani P., Vitolo C. (2010). *Extreme rainfall in the Mediterranean.* Proc. Intern. Workshop on "Advances in statistical hydrology", STAHY 2010, Taormina, Italy, May 23-25, 2010, 11 pp.

Della Sala M., Cuomo S. (2013). *Analisi su area vasta di frane superficiali e fenomeni erosivi indotti da pioggia.* In: Incontro Annuale dei Ricercatori di Geotecnica Università degli Studi di Perugia Pag.1-6 ISBN:9788890642135.

De Roo A.P.J., Wesseling C.G., Cremers N.H.D.T., Offermans R.J.E., Ritsema C.J., Van Oostindie K., (1994). *LISEM: a new physically-based hydrological and soil erosion model in a GIS-environment, theory and implementation.* IAHS Publications-Series of Proceedings and Reports-Intern Assoc Hydrological Sciences, 224, 439-448.

De Roo A.P.J., Wesseling C.G., Ritsema C.J. (1996a). *LISEM: a single event physically-based hydrologic and soil erosion model for drainage basins. I: Theory, input and output.* Hydrol. Proc., 10: 1107-1117.

De Roo A.P.J., Offermans R.J.E., Cremers N.H.D.T. (1996b). *LISEM: a single event physically-based hydrologic and soil erosion model for drainage basins. II: Sensitivity analysis, validation and application.* Hydrol. Proc., 10: 1118-1127.

De Roo A.P.J., Jetten V.G. (1999). *Calibrating and validating the LISEM model for two data sets from the Netherlands and South Africa.* Catena 37 (3-4), 477–493.

de Vente J., Poesen J. (2005). *Predicting soil erosion and sediment yield at the basin scale: scale issues and semi-quantitative models.* Earth-Science Reviews 71 (1–2), 95–125.

Dietrich W.E., Montgomery D.R. (1998). *SHALSTAB: a digital terrain model for mapping shallow landslide potential.* http://istsocrates.berkeley.edu/geomorph/

Dietrich C., Green T.R., Jakeman A.J. (1999). *An analytical model for stream sediment transport: application to Murray and Murrumbidgee reaches, Australia.* Hydrological Processes 13 (5), 763–776.

Dohrenwend R. E. (1977). *Raindrop erosion in the forest.* Michigan Technological University, Ford Forestry Center.

Dunin F. (1975). *The use of physical process models.* In: Chapman, T., Dunin, F. (Eds.), Prediction in Catchment Hydrology-A National Symposium on Hydrology. Australian Academy of Science, Canberra, pp. 277–291.

Ellison W.D. (1947). *Soil erosion studies-Part V. Soil transportation in the splash process.* Agric. Eng. 28:349–351.

Esposito E., Porfido S., Violante C., Alaia F. (2003). *Disaster induced by historical floods in a selected coastal area (Southern Italy).* In: THORNDY- CRAFT, V. R., BENITO, G., BARR IENDOS , M. and LLASAT, M. C. (eds) Proceedings of the PHEFRA (Palaeofloods, Historical Data and Climatic Variabil- ity), International Workshop, Barcelona. CSIC-Centro de Ciencias Medioambientales Serrano, Madrid, Spain, 143–148.

Esposito E., Porfido S., Violante C. (eds) 2004. *Il nubifragio dell'ottobre 1954 a Vietri sul Mare–Costa di Amalfi, Salerno.* Pubblicazione Gruppo Nazionale per la Difesa dalle Catastrofi Idro-geologiche, 2870.

Evans R. (1980). *Mechanics of water erosion and their spatial and temporal controls: an empirical viewpoint.* In Kirkby M. J. and Morgan R. P. C. Eds. Soil erosion. Wiley, Chichester. pp.109-128.

Fell R., Corominas J., Bonnard C., Cascini L., Leroi E., Savage W.Z., on behalf of the JTC-1 Joint Technical Committee on Landslides and Engineered Slopes (2008). *Guidelines for landslide susceptibility, hazard and risk zoning for land use planning.* Eng Geol 102(3–4):85–98. doi:10.1016/j.enggeo.2008.03.022.

Ferro V., Porto P. (2000). *Sediment delivery distributed (SEDD) model.* ASCE, Journal of Hydraulic Engineering 5 (4), 411 –422.

Foster G.R. (1982). *Modeling the erosion process.* In Haan, C. T., Johnson, H. P. and Brakensiek, D. L. Eds. Hydrologic modeling of small watersheds. American Society of Agricultural Engineers Monograph. 5:297-380.

Foster G.R. (2004). *User's reference guide: Revised Universal Soil Loss Equation (RUSLE2).* Report USDA.

Foster G. R., Meyer L. D. (1977). *Soil erosion and sedimentation by water – an overview.* Procs. National Symposium on Soil Erosion and Sedimentation by Water. Am. Soc. Of Agric. Eng., St. Joseph, Michigan. pp.1-13.

Fredlund D.G., Morgenstern N.R., Widger R.A. (1978). *The shear strength of unsaturated soils.* Canadian Geotechnical Journal 15, 313–321.

Frosini P. (1955). *Il nubifragio di Salerno del 25-26 Ottobre 1954.* Giornale Genio Civile, 3-4, 179-188, Rome, Italy.

Fujiwara T., Fukada M., Matsuzaki H. (1986). *The experimental study on the model of soil erosion by the impact of raindrops.* Technology reports of the Yamaguchi University, 3(5), 417-426.

Futai M.M., Lacerda W.A., Almeida M.S.S. (2004). *Evolution of gully processes in unsaturated soils.* Landslides: Evaluation and Stabilization, Lacerda, Ehrlich, Fontoura & Sayao (eds), 2, pp. 1019 – 1025.

Gardner W.R. (1958). *Some steady-state solutions of the unsaturated moisture flow equation with application to evaporation from a water table.* Soil Science, v. 85, p. 228–232.

Gasmo J.M., Rahardjo H., Leong E.C. (2000). *Infiltration effects on stability of a residual soil slope.* Computers and Geotechnics, 26(2), 145-165.

Geißler C., Kühn P., Böhnke M., Bruelheide H., Shi X., Scholten T. (2012). *Splash erosion potential under tree canopies in subtropical SE China.* Catena, 91, 85-93.

Genevois R., Tecca P.R., Berti M., Simoni A. (2000). *Debris flow in the Dolomites: experimental data from a monitoring system.* In: Wieczorek, G., Naeser, N. (Eds.), Proceedings, Second International Conference on Debris-flow

Hazard Mitigation: Mechanics, Prediction, and Assessment. A.A. Balkema, Rotterdam, pp. 283–291.

Geoslope (2005). *User's Guide.* GeoStudio 2004, Version 6.13. Geo-Slope Int. Ltd., Calgary, Canada.

Ghadiri H., Payne D. (1986). *The risk of leaving the soil surface unprotected against falling rain.* Soil and Tillage Research, 8, 119-130.

Ghadiri H., Payne D. (1988). *The formation and characteristics of splash following raindrop impact on soil.* Journal of soil science, 39(4), 563-575.

Gili J. A., Alonso E. E. (2002). *Microstructural deformation mechanisms of unsaturated granular soils.* International Journal for Numerical and Analytical Methods in Geomechanics, 26(5):433–468.

Glade T., Crozier M. J. (2005). *A review of scale dependency in landslide hazard and risk analysis.* Landslide hazard and risk, 75-138.

Ghahramani A., Yoshiharu I., Mudd S. M. (2012). *Field experiments constraining the probability distribution of particle travel distances during natural rainstorms on different slope gradients.* Earth Surface Processes and Landforms, 37(5), 473-485.

Godt J. W., Coe J. A. (2007). *Alpine debris flows triggered by a 28 July 1999 thunderstorm in the central Front Range, Colorado.* Geomorphology, 84(1), 80-97.

Godt J. W., Baum R. L., Savage W. Z., Salciarini D., Schulz W. H., Harp E. L. (2008). *Transient deterministic shallow landslide modeling: requirements for susceptibility and hazard assessments in a GIS framework.* Engineering Geology, 102(3), 214-226.

Gómez J. A., Darboux F., Nearing M. A. (2003). *Development and evolution of rill networks under simulated rainfall.* Water resources research, 39(6), 1148.

Govers G. (1987). *Initiation of motion in overland flow.* Sedimentology. 34:1157-1164.

Govers G. (1990). *Empirical relationships on the transporting capacity of overland flow.* In Erosion, transport and deposition processes, Walling DE, Yair A, Berkowicz S (eds). IAHS: Wallingford; 45–63.

Green W.H., Ampt G.A. (1911). *Studies on soil physics, part I, the flow of air and water through soils.* J. Agric. Sci., 4(1): 1-24.

Grimaldi S., Petroselli A., Romano N. (2012). *Green-Ampt Curve-Number mixed procedure as an empirical tool for rainfall–runoff modelling in small and ungauged basins.* Hydrological Processes.

Grunwald S., Norton L.D. (2000). *Calibration and validation of a nonpoint source pollution model.* Agricultural Water Management 45 (1), 17–39.

Gutteridge Haskins and Davey (1991). *Integrated Quantity/Quality Modelling-Stage 3.* Gutteridge Haskins and Davey, for Department of Water Resources, Sydney, pp. 102.

Guy B. T., Dickinson W. T. (1990). *Inception of sediment transport in shallow overland flow. Catena* Supplement. 17:91-109.

Guzzetti F., Carrara A., Cardinali M., Reichenbach P. (1999). *Landslide hazard evaluation: an aid to a sustainable development.* Geomorphology, 31: 181-216.

Guzzetti F., Peruccacci S., Rossi M., Stark, C. P. (2007). *Rainfall thresholds for the initiation of landslides in central and southern Europe.* Meteorol. Atmos. Phys., 98, 239–267.

Hancox G.T., Wright K. (2005). *Landslides caused by the February 2004 rainstorms and floods in southern North Island, New Zealand.* Institute of Geological & Nuclear Sciences science report 2004/10. 33p.

Hanley N., Faichney R., Munro A., Shortle J.S. (1998). *Economic and environmental modelling for pollution control in an estuary.* Journal of Environmental Management 52, 211–225.

Hessel R. (2005). *Effects of grid cell size and time step length on simulation results of the Limburg soil erosion model LISEM.* Hydrolog. Process., 1915, 3037–3049.

Hessel R, Jetten V., Liu B., Zhang Y., Stolte J. (2003). *Calibration of the LISEM model for a small Loess Plateau catchment.* CATENA 54:235–254.

Hessel R., van den Bosch R., Vigiak O. (2006). *Evaluation of the LISEM soil erosion model in two catchments in the East African Highlands.* Earth Surface Processes and Landforms 31: 469–486.

Horton R.E. (1933). *The role of infiltration in the hydrologic cycle.* Trans. Am. Geophys. Union, vol. 14. pp. 446-460.

Hürlimann M., Rickenmann D., Graf C. (2003). *Field and monitoring data of debris-flow events in the Swiss Alps.* Canadian Geotechnical Journal, 40(1), 161-175.

Hungr O. (2000). *Analysis of debris flow surges using the theory of uniformly progressive flow.* Earth Surface Processes and Landforms: Vol. 25, pp. 1-13.

Hungr O., Evans S.G., Bovis M.J., Hutchinson J.N. (2001). *A review of the classification of landslides of the flow type.* Environ. and Eng. Geosci., VII (3), 221 – 238.

Hungr O. (2005). *Classification and terminology.* In Debris-flow hazards and related phenomena (pp. 9-23). Springer Berlin Heidelberg.

Hungr O., Leroueil S., Picarelli L. (2012). *Varnes classification of landslide types, an update.* In XI international symposium on landslides and engineered, Banff, Canada (pp. 47-58).

Hutchinson J.N., Bhandari R.K. (1971). *Undrained loading, a fundamental mechanism of mudflow and other mass movements.* Geotechnique, 21, n. 4, pp. 353 – 358.

Hutchinson J.N. (1988). *General Report morphological and geotechnical parameters of landslides in relation to geology and hydrogeology.* In Bonnard, C. (Editor), Proceedings, Fifth International Symposium on Landslides, A.A. Balkema, Rotterdam, Vol.1, pp. 3-36.

Hutchinson J.N. (1995). *Keynote paper: Landslide hazard assessment.* In: Bell (ed.), Landslides, Balkema, Rotterdam, 1805-1841.

Hutchinson J.N. (2004). *Review of flow-like mass movements in granular and fine-grained materials.* Proc. of the Int. Workshop "Flows 2003 - Occurrence and Mechanisms of Flows in Natural Slopes and Earthfill", 3 – 16.

Iverson R.M. (2000). *Landslide triggering by rain infiltration.* Water Resources Research, vol. 36, no. 7, pag 1897–1910.

Jakeman A., Littlewood I., Whitehead P. (1990). *Computation of the instantaneous unit hydrograph and identifiable component flows with application to two small upland catchments.* Journal of Hydrology 117, 275–300.

Jakeman A.J., Green T.R., Beavis S.G., Zhang L., Dietrich C.R., Crapper P.F. (1999). *Modelling upland and in-stream erosion, sediment and phosphorus transport in a large catchment.* Hydrological Processes 13 (5), 745–752.

Jakeman A., Post D., Beck M. (1994a). *From data and theory to environmental model: the case of rainfall runoff.* Environmetrics 5, 297–314.

Jakeman A., Post D., Schreider S., Yu Y.W. (1994b). *Modelling environmental systems: partitioning the water balance at different catchment scales.* In: Zannetti, P. (Ed.), Computer Techniques in Environmental Studies V. Computational Mechanics Publications, Southampton, pp. 157–170.

Jakeman A.J., Green T.R., Beavis S.G., Zhang L., Dietrich C.R., Crapper P.F., (1999). *Modelling upland and in-stream erosion, sediment and phosphorus transport in a large catchment.* Hydrological Processes 13 (5), 745–752.

Jakob M., Jordan P. (2001). *Design floods in mountain streams – the need for a geomorphic approach.* Canadian Journal of Civil Engineering, 28, (3), 425-439.

Jakob M. (2005). *A size classification for debris flows.* Eng. Geol. 79, 151–161.

Janbu N. (1954). *Application of Composite Slip Surface for Stability Analysis.* European Conference on Stability Analysis, Stockholm, Sweden.

Jayawardena A. W., Bhuiyan R. R. (1999). *Evaluation of an interrill soil erosion model using laboratory catchment data.* Hydrological processes, 13(1), 89-100.

Jetten V. (2002). *LISEM user manual, version 2.x.* Draft version January 2002. Utrecht Centre for Environment and Landscape Dynamics, Utrecht University, The Netherlands, 64pp.

Johanson R.C., Imhoff J.C., Davis H.H. (1980). *Users Manual for the Hydrologic Simulation Program—Fortran (HSPF) version No. 5.0*, EPA-600/9-80-105. US EPA Environmental Research Laboratory, Athens, GA.

Johnson B.E., Julien P.Y., Molnar D.K., Watson C.C. (2000). *The two-dimensional upland erosion model CASC2D-SED.* Journal of the American Water Resources Association 36 (1), 31– 42.

Jitousono T., Shimokawa E., Tsuchiya S. (1996). *Debris flow following the 1994 eruption with pyroclastic flows in Merapi volcano, Indonesia.* Journal of Japan Society Erosion Control Engineering 48 (special issue), 109–116.

Kamphorst E., Jetten V.G., Guerif J., Pitkanen J., Iversen B., Douglas J., Paz Gonzales A. (2000). *Predicting depressional storage from soil surface roughness.* Soil Sci. Soc. Am. J. 64: 1749-1758.

Kavvas M.L., Govindaraju R.S. (1992). *Hydrodynamic averaging of overland flow and soil erosion over rilled hillslopes.* IAHS Publications 209, 101– 111.

Kelkar V. N. (1959). *Size distribution of raindrops.* Indian J. Meteorol. Geophys,10(2), 125-136.

Kinnell P., Risse L. (1998). *USLE-M: Empirical modelling rainfall erosion through runoff and sediment concentration.* Soil Sci Soc Am J 62 (6), 1667–1672.

Kinnell P.I.A. (2005). *Raindrop-impact-induced erosion processes and prediction: a review.* Hydrological processes, 19(14), 2815-2844.

Knisel W.G. (1980). *CREAMS: A Field Scale Model for Chemicals, Runoff and Erosion from Agricultural Management Systems.* USDA.

Kozicki J., Donzé F. V. (2008). *A new open-source software developed for numerical simulations using discrete modeling methods.* Computer Methods in Applied Mechanics and Engineering, 197(49), 4429-4443.

Lacerda W.A. (2004). *The behaviour of colluvial slopes in a tropical environment.* Landslides: Evaluation and Stabilization, Lacerda, Ehrlich, Fontoura & Sayao (eds), 2, pp. 1315-1342.

Laflen J.M., Lane L.J., Foster G.R. (1991). *WEPP: A new generation of erosion prediction technology.* Journal of Soil and Water Conservation 46, 34–38.

Lane L., Nichols M., Paige G. (1995). *Modeling erosion on hillslopes: Concepts, theory and data.* In: International Congress on Modelling and Simulation Proceedings (Agriculture, Catchment Hydrology and Industry), 1. pp. 1– 17.

Lastoria B., Miserocchi F., Lanciani A., Monacelli G. (2008). *An estimated erosion map for the Aterno-Pescara river Basin.* Eur Water (21/22), 29-39.

Lavigne F., Thouret J. C., Voight B., Young K., LaHusen R., Marso, J., Suwa H., Sumaryono A., Sayudi D.S., Dejean M. (2000). *Instrumental lahar monitoring at Merapi Volcano, Central Java, Indonesia.* Journal of volcanology and geothermal research, 100(1), 457-478.

Lavigne F., Suwa H. (2004). *Contrasts between debris flows, hyperconcentrated flows and stream flows at a channel of Mount Semeru, East Java, Indonesia.* Geomorphology, 61(1), 41-58.

Laws J. O., Parsons D. A. (1943). *The relation of raindrop-size to intensity.* Transactions, American Geophysical Union, 24, 452-460.

Legout C., Leguédois S., Le Bissonnais Y., Malam Issa O. (2005). *Splash distance and size distributions for various soils.* Geoderma 124, 279–292.

Lei T., Pan Y., Liu H., Zhan W., Yuan J. (2006). *A run off-on-ponding method and models for the transient infiltration capability process of sloped soil surface under rainfall and erosion impacts.* Journal of Hydrology, 319(1), 216-226.

Leroueil S., Locat J., Vaunat J., Picarelli L., Lee H., Faure R. (1996). *Geotechnical characterization of slope movements.* In Landslides, Editor K Senneset, Balkema Rotterdam, Vol 1, pp 53-74.

Leroueil S. (2004). *Geotechnics of slopes before failure.* Landslides: Evaluation and Stabilization, Lacerda, Ehrlich, Fontoura & Sayao (eds), 1, pp. 863-884.

Littleboy M., Silburn, M.D. Freebairn D.M., Woodruff D.R., Hammer G.L., Leslie J.K. (1992). *Impact of soil erosion on production in cropping systems. I. Development and validation of a simulation model.* Australian Journal of Soil Research 30, 757–774.

Loch R.J., Silburn D.M. (1996). *Constraints to sustainability-soil erosion.* In: Clarke, L., Wylie, P.B. (Eds.), Sustainable Crop Production in the Sub-tropics: an Australian Perspective. QDPI.

Long E. J., Hargrave G., Cooper J. R., Kitchener B., Parsons A. J., Wainwright J. (2011). *Experimental investigation of particle detachment by raindrop impact: three-dimensional measurements of particle trajectory and velocity.* In AGU Fall Meeting Abstracts (Vol. 1, p. 0698).

Lopes V.L. (1987). *A numerical model of watershed erosion and sediment yield.* PhD thesis, The University of Arizona.

Lopes V.L., Lane L.J. (1988). *Modeling sedimentation processes in small watersheds.* IAHS Publications 174, 497–508.

Ma T., Zhou C., Zhu T., Cai Q. (2008). *Modelling raindrop impact and splash erosion processes within a spatial cell: a stochastic approach.* Earth Surface Processes and Landforms, 33(5), 712-723.

Marcato G., Bossi G., Rivelli F., Borgatti L. (2012). *Debris flood hazard documentation and mitigation on the Tilcara alluvial fan (Quebrada de Humahuaca, Jujuy province, North-West Argentina).* Natural Hazards and Earth System Science, 12(6), 1873-1882.

Marchi L., Arattano M., Deganutti A. M. (2002). *Ten years of debris-flow monitoring in the Moscardo Torrent (Italian Alps).* Geomorphology, 46(1), 1-17.

Marchi L., Cavalli M. (2007). *Procedures for the documentation of historical debris flows: application to the Chieppena Torrent (Italian Alps).* Environmental management, 40(3), 493-503.

Marchi L., Cavalli M., Sangati M., Borga M. (2009). *Hydrometeorological controls and erosive response of an extreme alpine debris flow.* Hydrological Processes, 23(19), 2714-2727.

Marshall J. S., Palmer, W. M. K. (1948). *The distribution of raindrops with size.* Journal of meteorology, 5(4), 165-166.

Mathewson C. C., Keaton J. R., Santi P. M. (1990). *Role of bedrock ground water in the initiation of debris flows and sustained post-flow stream discharge.* Bull. Assoc. Eng. Geol, 27, 73-83.

McCoy S.W., Coe J.A., Kean J.W., Tucker G.E., Staley D.M., Wasklewicz T.A. (2011). *Observations of debris flows at Chalk Cliffs, Colorado, U.S.A.: part 1, in situ measurements of flow dynamics, tracer particle movement and video imagery from the summer of 2009.* In Genevois, R., Hamilton, D.L., and Prestininzi, A, eds., Proceedings of the 5th International Conference on Debris Flow

Hazards Mitigation, Mechanics, Prediction and Assessment, Padua, Italy, June 14-17, 2011, Italian Journal of Engineering Geology and Environment and Casa Editrice Universita La Sapienza, Rome, Italy. DOI: 10.4408/IJEGE.2011-03.B-078.

Mein R. G., Larson C. L. (1973). *Modeling Infiltration During Steady Rain,* Water Resources Research, vol. 2, 384-394.

Merritt W.S., Latcher R.A., Jakeman A.J. (2003). *A review of erosion and sediment transport models.* Environmental Modelling and Software 18, 761– 799.

Meyer L. D., Monke E. J. (1965). *Mechanics of soil erosion by rainfall and overland flow.* Trans. ASAE, 8(4), 572-577.

Michie D., Spiegelhalter D.J., Taylor C.C. (EDS.) (1994). *Machine Learning, Neural and Statistical Classification.* Intenerner version (http://www.amsta.leeds.ac.uk/~charles/statlog/).

Mishra B. K., Rajamani, R. K. (1992). *The discrete element method for the simulation of ball mills.* Applied Mathematical Modelling, 16(11), 598-604.

Mizuyama T., Kobashi S., Ou G. (1992). *Prediction of debris flow peak discharge. Interpraevent.* International symposium, Bern, Switzerland, Tagespublikation, vol. 4, pp. 99–108.

Montgomery D.R., Foufoula-Georgiou E. (1993). *Channel network source representation using digital elevation models.* Water Resources Research,29(12), 3925-3934.

Moore I. D., Burch G. J. (1986). *Modeling erosion and deposition: Topographics effects.* Transaction ASAE. 29:1624-1640.

Moore I.D., Foster G.R. (1990). *Hydraulics and overland flow:* in: Process Studies in Hillslope Hydrology (MG Anderson and TP Burt, eds.) John Wiley, 215-254.

Morgan R.P.C. (1978). *Field studies of rainsplash erosion.* Earth Surf. Proc. Land. 3, 295–299.

Morgan R. P. C. (1981). *Field measurement of splash erosion.* International Association of Scientific Hydrology Publication, 133, 373-82.

Morgan R.P.C., Quinton J.N., Smith R.E., Govers G., Poesen J.W.A., Auerswald K., Chisci G., Torri D., Styczen M.E. (1998). *The European soil erosion model (EUROSEM): a process-based approach for predicting sediment transport from fields and small catchments.* Earth Surface Processes and Landforms 23, 527–544.

Morgan R.P.C. (2005). *Soil Erosion and Conservation.* (3rd edn). Blackwell Publishing: Oxford.

Morgenstern N.R., Price V.E. (1965). *The Analysis of the Stability of General Slip Surfaces.* Geotechnique, Vol. 15, No. 1, 79-93.

Morris J., Johnson S. (2007). *Discrete Element Modeling.* American Society of Civil Engineers: Journal of Geotechnical and Geoenvironmental Engineering, vol. 135, no. 11, November 1, 2009, pp. 1547-1561, 135(UCRL-JRNL-237027).

Mouzai L., Bouhadef M. (2003). *Water drop erosivity: Effects on soil splash.* J. Hydraul. Res., 42, 61 – 68.

Mualem Y. (1976). *A new model for predicting the hydraulic conductivity of unsaturated porous media.* Water Resource Research 12(3): 513-522.

Mutchler C. K., Young R. A. (1975). *Soil detachment by raindrops.* In: Present and prospective technology for predicting sediment yields and sources. USDA-ARS Publication ARS-S. 40:113-117.

Najim M.M.M., Babel M.S., Loof R. (2006). *AGNPS Model Assessment for a Mixed Forested Watershed in Thailand.* Science Asia, 32(1), 53-61.

Nearing M. A., Bradford J. M. (1985). *Single waterdrop splash detachment and mechanical properties of soils.* Soil Science Society of America Journal,49(3), 547-552.

Nearing M.A., Foster G.R., Lane L.J., Finkner S.C. (1989). *A process-based soil erosion model for USDA-water erosion prediction project technology.* Transactions of the ASAE 32 (5), 1587– 1593.

Nearing M.A., Lane L.J., Lopes V.L. (1994). *Modelling soil erosion.* In: Lad, R. (Ed.), Soil Erosion: Research Methods, pp. 127–156.

Ng C.W.W., Shi Q. (1998). *A numerical investigation of the stability of unsaturated soil slopes subjected to transient seepage.* Computers and geotechnics, 22(1), 1-28.

Nilsen T.H., Brabb E.E. (1977). *Slope stability studies in the San Francisco Bay region, California.* Geological Society of America, Reviews in Eng. Geology, 3: 235-243.

O'Brien J.S. (2009). *FLO-2D User manual, version 2009.* Nutrioso, Arizona.

Onda Y., Tsujimura M., Tabuchi H. (2004). *The role of subsurface water flow paths on hillslope hydrological processes, landslides and landform development in steep mountains of Japan.* Hydrological processes, 18(4), 637-650.

OpenLISEM (2013a). http://blogs.itc.nl/lisem/

OpenLISEM (2013b). http://sourceforge.net/projects/lisem/

Pan C. Z., Shangguan Z. P. (2006). *Runoff hydraulic characteristics and sediment generation in sloped grassplots under simulated rainfall conditions.* J. Hydrol. 331(1-2): 178-185.

Panuska J.C., Moore I.D., Kramer L.A. (1991). *Terrain analysis: integration into the Agricultural Non-Point Source (AGNPS) pollution model.* Journal of Soil Water Conservation, 59–64.

Park D. W., Nikhil N. V., Lee S. R. (2013). *Landslide and debris flow susceptibility zonation using TRIGRS for the 2011 Seoul landslide event.*

Parlak M., Parlak A. Ö. (2010). Measurement of splash erosion in different cover crops. Turkish Journal of Field Crops, 15(2), 169-173.

Papa M.N., Trentini G., Carbone A., Gallo A. (2011). *An integrated approach for debris flow hazard assessment – a case study on the Amalfi Coast – Campania, Italy,* in: Proc. Int. Conf. DFHM 5th International Conference on Debris-Flow Hazards Mitigation: Mechanics, Prediction and Assessment, 14–17 June

2011, University of Padua, Italy, 983–992, doi:10.4408/IJEGE.2011-03.B-107.

Perrone J., Madramootoo C. A. (1997). *Use of AGNPS for watershed modeling in Quebec.* Trans. ASAE 40(5): 1349–1354.

Pieri L., Bittelli M., Wu J.Q., Du S., Flanagan D. C., Pisa P. R., Ventura F., Salvatorelli F. (2007). *Using the Water Erosion Prediction Project (WEPP) model to simulate field-observed runoff and erosion in the Apennines mountain range, Italy.* Journal of hydrology, 336(1), 84-97.

Pierson T.C. (1980). *Erosion and deposition by debris flows at Mt. Thomas, North Canterbury, New Zealand.* Earth Surface Processes: Vol. 5, pp.227-247.

Pierson T.C. (1986). *Flow behavior of channelized debris flows, Mount St. Helens, Washington.* In: Abrahms, A.D. (Ed.), Hillslope Processes. Allen and Unwin, Boston, pp. 269–296.

Pierson T.C., Costa, J.E. (1987). *A rheologic classification of subaerial sediment-water flows.* Debris flows/avalanches: Geological Society of America Reviews in Engineering Geology, Costa, J.E., and Wieczorek, G.F., eds., vol VII, p.1-12.

Poesen J., Savat J. (1981). *Detachment and transportation of loose sediments by raindrop splash. Part II. Detachability and transportability measurements.* Catena 8: 19–41.

Poesen J., Torri D. (1988). *The effect of cup size on splash detachment and transport measurements. Part II. Field measurements.* Catena Supplement 12: 113–126.

Prosser I.P., Young B., Rustomji P., Hughes A., Moran C. (2001). *A model of river sediment budgets as an element of river health assessment.* In: Proceedings of the International Congress on Modelling and Simulation (MODSIM'2001), December 10–13, pp. 861–866.

Rahardjo H., Lee T.T., Leong E.C., Rezaur R.B. (2004). *A flume for assessing flux boundary characteristics in rainfall-induced slope failure studies.* Geotechnical Testing Journal 27 (2), 145–153.

Rahmati M., Neyshabouri M.R., Fakherifard A., Oskouei M.M., Ahmadi A., Sheikh J.V. (2013). *Rainfall-runoff prediction using LISEM model in Lighvan watershed, North West of Iran.*

Rao K., Steenhuis T., Cogle A., Srinivasan S., Yule D., Smith G. (1998). *Rainfall infiltration and runoff from an alfisol in semiarid tropical India. 1. No-till systems.* Soil and Tillage Research 48, 51–59.

Renard K.G., Foster G.R., Weesies G.A., Porter J.P. (1991). *RUSLE: revised universal soil loss equation.* Journal of Soil and Water Conservation, 30–33 (January–February).

Renard K.G., Ferreira V.A. (1993). *RUSLE model description and database sensitivity.* Journal of Environmental Quality 22, 458–466.

Renard K.G., Foster G.R., Yoder D.C., McCool D.K. (1994). *RUSLE revisited: status, questions, answers, and the future.* Journal of Soil and Water Conservation, 213– 220 (May–June).

Richards L.A. (1931). *Capillary conductions of liquids through porous mediums.* Journal of Applied Physics 1, 318–333.

Rickenmann D. (1999). *Empirical relationships for debris flows.* Natural Hazards 19, 47–77.

Riezebos H. T., Epema G. F. (1985). *Drop shape and erosivity. Part II: splash detachment, transport and erosivity indices.* Earth Surface Processes and Landforms, Vol. 10, pp: 69-74.

Römkens M. J. M., Helming K., Prasad S. N. (2002). *Soil erosion under different rainfall intensities, surface roughness, and soil water regimes.* Catena,46(2), 103-123.

Rose C.W. (1993). *Erosion and sedimentation.* In: Bonell, M., Hufschmidt, M.M., Gladwell, J.S. (Eds.), Hydrology and Water Management in the Humid Tropics: Hydrological Research Issues and Strategies for Water Management. Cambridge University Press, pp. 301–343.

Rose C.W., Coughlan K.J., Ciesiolka L.A.A., Fentie B. (1997). *Program GUEST (Griffith University Erosion System Template), a new soil conservation methodology and application to cropping systems in tropical steeplands.* ACIAR Technical Reports 40, 34–58.

Salciarini D., Godt J. W., Savage W. Z., Conversini P., Baum R. L., Michael J. A. (2006). *Modeling regional initiation of rainfall-induced shallow landslides in the eastern Umbria Region of central Italy.* Landslides, 3(3), 181-194.

Salles C., Poesen J. (1999). *Performance of an optical spectro pluviometer in measuring basic rain erosivity characteristics.* J. Hydrol. 218, 142-156.

Santacana N., Baeza B., Corominas J., De Paz A., Marturià J. (2003). *A GIS-Based Multivariate Statistical Analysis for Shallow Landslide Susceptibility Mapping in La Pobla de Lillet Area (Eastern Pyrenees, Spain).* Natural Hazards, 30, pag. 281–295.

Santi P. M., deWolfe V. G., Higgins J. D., Cannon S. H., Gartner J. E. (2008). *Sources of debris flow material in burned areas.* Geomorphology, 96(3), 310-321.

Sassa K. (1985). *The mechanism of debris flow.* Proc. 11th International Conf. On Soil Mechanics and Foundation Engineering, San Francisco, 3, pp. 1173 – 1176.

Savage W.Z., Godt J.W., Baum R.L. (2004). *Modeling time-dependent areal slope stability.* In: Lacerda WA, 582 Erlich M, Fontoura SAB, Sayao ASF (eds) Landslides-evaluation and stabilization, Proceedings of 9th 583 International symposium on Landslides, vol 1. Balkema, Rotterdam, pp 23–36.

Schiano P., Mercogliano P., Comegna L. (2009). *Simulation chains for the forecast and prevention of landslide induced by intensive rainfall.* InProceedings of the 1st Italian Workshop on Landslides, Rainfall-Induced Landslide: mechanisms, monitoring techniques and nowcasting models for early warning systems (pp. 232-237).

Schmidt J., Werner M. V., Michael A. (1999). *Application of the EROSION 3D model to the CATSOP watershed, The Netherlands.* Catena, 37(3), 449-456.

Scholtès L., Hicher P.Y., Chareyre B., Nicot F., Darve F. (2009). *On the capillary stress tensor in wet granular materials.*International Journal for Numerical and Analytical Methods in Geomechanics (33), pages 1289–1313. DOI 10.1002/nag.767.

SCS (1972). *Section 4, Hydrology, National Engineering Handbook.* Soil Conservation Service, US 444 Department of Agriculture.

Selby M. J. (1993). *Hillslope Materials and Processes.* 451 pp., Oxford Univ. Press, New York.

Salles C., Poesen J., Govers G. (2000). *Statistical and physical analysis of soil detachment by raindrop impact: rain erosivity indices and threshold indices.* Water Resources Research 36: 2721–2729.

Sharpe C.F.S. (1938). *Landslides and related phenomena:* Columbia University Press, N.Y.

Sharma P.P., Gupta S.C. (1989). *Sand detachment by single raindrops of varying kinetic energy and momentum.* Soil Science Society of America Journal 53: 1005–1010.

Shen Z.Y., Gong Y.W., Li Y.H., Hong Q., Xu L., Liu R.M. (2009). *A comparison of WEPP and SWAT for modeling soil erosion of the Zhangjiachong watershed in the three Gorges reservoir area.* Agric. Water Manage.. 96(10), 1435-1442.

Shields A. (1936). *Anwendung der Ähnlichkeitsmechanik und der Turbulenzforschung auf die Geschiebebewegung.* Mitteilungen der Preussischen Anstalt Wasserbau and Schiffbau. N. 26.

Shuster W. D., Pappas E., Zhang Y. (2008). *Laboratory-scale simulation of runoff response from pervious-impervious systems.* Journal of hydrologic engineering, 13(9), 886-893.

Sica C. (2008). *Modelling the triggering of flow-type slope movements over large areas: limitations and potential of distributed physically based models.* PhD dissertation. University of Salerno, Italy, pp. 226.

Simons M., Podger G., Cooke R. (1996). *IQQM-a hydrologic modeling tool for water resource and salinity management.* Environmental Software 11 (1-3).

Slaymaker O. (1988). *The distinctive attributes of debris torrents.* Hydrol. Sci., 33, 567–573.

Smith R.E. (1981). *A kinematic model for surface mine sediment yield.* Transactions of the ASAE, 1508– 1514.

Smith R.E., Goodrich D.C., Quinton J.N. (1995a). *Dynamic, distributed simulation of watershed erosion: the KINEROS2 and EUROSEM models.* Journal of Soil and Water Conservation 50 (5), 517–520.

Smith R.E., Goodrich D.C., Woolhiser D.A., Unkrich C.L. (1995b). *KINEROS-a kinematic runoff and erosion model.* In: Singh, V.P. (Ed.), Computer Models

of Watershed Hydrology. Water Resources Publications, Littleton, CO, pp. 697–732.

Soeters R., Van Westen C. J. (1996). *Slope instability recognition, analysis and zonation.* Landslides, Investigation and Mitigation, edited by A. K. Turner and R. L. Schuster, Transp. Res. Board Spec. Rep. 247, pp. 129–177, Natl. Acad. Press, Washington, D. C., 1996.

Sorbino G., Sica C., Cascini L. (2010). *Susceptibility analysis of shallow landslides source areas using physically based models.* Natural hazards, 53(2), 313-332.

Sorooshian S. (1991). *Parameter estimation, model identification, and model validation: conceptual-type models.* In Recent advances in the modeling of hydrologic systems. Springer Netherlands. pp. 443-467.

Sprenger F.D. (1978). *Determination of direct runoff with the 'Curve Number Method' in the coastal area of Tanzania/East Africa.* Wasser und Boden, I, 13-16.

Srivastava R., Yeh T.C. J. (1991). *Analytical solutions for one-dimensional, transient infiltration toward the water table in homogeneous and layered soils.* Water Resources Research, 27: 753-762.

Storm B., Jorgensen G.H., Styczen M. (1987). *Simulation of water flow and soil erosion processes with a distributed physically-based modeling system.* IAHS Publications 167, 595– 608.

Suttles J. B., Vellidis G., Bosch D. D., Lowrance R., Sheridan J. M., Usery E. L. (2003). *Watershed-scale simulation of sediment and nutrient loads in Georgia coastal plain streams using the annualized AGNPS model.* Transactions of the ASAE, 46(5), 1325-1335.

Suwa H., Okano K., Kanno, T. (2009). *Behavior of debris flows monitored on test slopes of Kamikamihorizawa Creek, Mount Yakedake, Japan.* International Journal of Erosion Control Engineering, 2(2), 33-45.

Takahashi T. (1991). Debris flow. IAHR Monograph, Balkema.

Takken I., Beuselinck L., Nachtergaele J., Govers G., Poesen J., Degraer G. (1999). *Spatial evaluation of a physically-based distributed erosion model (LISEM).* Catena 37 (3-4), 431–447.

Terranova O., Antronico L., Coscarelli R., Iaquinta P. (2009). *Soil erosion risk scenarios in the Mediterranean environment using RUSLE and GIS: an application model for Calabria (southern Italy).* Geomorphology, 112(3), 228-245.

Tessitore S., Di Martire D., Martino R., Calcaterra D. (2011). *Comparison of 2D models for the simulation of the October 1954 debris flow and flood event at Maiori (Campania region, Italy) -* © Proceedings of the 5th International Conference on Debris-Flow Hazards Mitigation, Padova (Italy), 14-17 Giugno, 2011, Italian Journal of Engineering Geology and Environment - Book: Casa Editrice Università La Sapienza, Rome, Italy, p. 513-522. DOI: 10.4408/IJEGE.2011-03.B-057.

Torri D., Borselli L. (1991). *Overland flow and soil erosion: some processes and their interactions.* Catena Supplement. 19:129-137.

Toy T. J., Foster G. R., Renard K. G. (2002). *Soil Erosion: Process, Prediction, Measure and Control.* John Wiley and Sons, Inc. New York. pp.338.

Tranfaglia G., Braca G. (2004). *Analisi idrologica e meteorologica dell'evento alluvionale del 25-26 Ottobre 1954: confronto con le serie storiche e valutazione del periodo di ritorno di eventi analoghi.* In: Il Nubifragio dell'Ottobre 1954 a Vietri sul mare. Costa d'Amalfi, Salerno. Pubblicazione GNDCI n. 2870: 295-348 (in Italian).

Trigila A., Iadanza C., Rischia I. (2007). *Metodologia di lavoro e struttura della banca dati.* In: In: Agenzia per la protezione dell'ambiente e per i servizi tecnici - APAT, Rapporto sulle frane in Italia. Il Progetto IFFI – Metodologia, risultati e rapporti regionali, pp. 3-30.

Tsaparas I., Rahardjo H., Toll D.G., Leong E.C. (2002). *Controlling parameters for rainfall-induced landslides.* Computers and Geotechnics, 29(1), 1-27.

Tsaparas I., Rahardjo H., Toll D.G., Leong E.C. (2003). *Infiltration characteristics of two instrumented residual soil slopes.* Canadian Geotechnical Journal, 40(5), 1012-1032.

USDA-ARS (2008). *Draft Scientific Documentation Revised Universal Soil Loss Equation Version 2.* <http://www.ars.usda.gov/Research/docs.htm?docid=6028>.

USDA-SCS. (1972). *National Engineering Handbook, Hydrology Section 4.* USDA, Washington,DC.

Van Genuchten M.T. (1980). *A close form equation predicting the hydraulic conductivity of unsaturated soil.* Soil Sci Soc Am J;44:892–8.

USEPA (1994). *SWRRBWQ Window's interface users guide.* US Environmental Protection Agency.

van Asch W. J., Van Beek L. P. H., Bogaard T. A. (2009). *The diversity in hydrological triggering systems of landslides.* In Proceedings of The First Italian Workshop on Landslides (pp. 8-10).

Van der Knijff J. M., Jones R. J. A., Montanarella L. (1999). *Soil erosion risk assessment in Italy.* European Soil Bureau, European Commission. EUR 19044 EN. p. 52.

Van Dijk A.I.J.M. (2002). *Water and sediment dynamics in bench-terraced agricultural steeplands in West Java, Indonesia.* PhD Thesis. Vrije Universiteit, Amsterdam, The Netherlands.

Van Dijk A. I. J. M., Meesters A. G. C. A., Bruijnzeel L. A. (2002a). *Exponential distribution theory and the interpretation of splash detachment and transport experiments.* Soil Science Society of America Journal, 66(5), 1466-1474.

van Dijk A.I.J.M., Bruijnzeel L.A., Rosewell C.J. (2002b). *Rainfall intensity–kinetic energy relationships: a critical literature appraisal.* J.Hydrol. 261,1–23. doi:10.1016/S0022-1694(02)00020-3.

Van Dijk A.I.J.M., Bruijnzeel L.A., Wiegman S.E. (2003a). *Measurements of rain splash on bench terraces in a humid tropical steepland environment.* Hydrol. Processes 17, 513–535.

Van Dijk A. I. J. M., Bruijnzeel L. A., Eisma E. H. (2003b). *A methodology to study rain splash and wash processes under natural rainfall.* Hydrological Processes, 17(1), 153-167.

Van Dine D.F. (1985). *Debris flows and debris torrents in the Southern Canadian Cordillera.* Can. Geotech. J. 22, pp. 44 – 63.

Van Westen C.J. (2004). *Geo-Information tools for landslide risk assessment: an overview of recent developments.* Landslides: Evaluation and Stabilization, Lacerda, Ehrlich, Fontoura & Sayao (eds), 2, pp. 39 – 56.

Varnes D.J. (1978). *Slope movement types and processes.* In Schuster, R. L. and Krizek, R. J. (Editors), Landslides, Analysis and Control, Special Report 176: Transportation Re-search Board, National Academy of Sciences, Washington, DC., pp. 11-33.

Vertessey R.A., Watson F.G.R., Rahman J.M., Cuddy S.D., Seaton S.P., Chiew F.H., Scanlon P.J., Marston F.M., Lymbuner L., Jeanelle S., Verbunt M. (2001). *New software to aid water quality management in the catchments and waterways of the south-east Queensland region.* In: Proceedings of the Third Australian Stream Management Conference, August 27–29, pp. 611–616.

Viney N.R., Sivapalan M. (1999). *A conceptual model of sediment transport: application to the Avon River Basin in Western Australia.* Hydrological Processes 13, 727–743.

Wasson R.J. (2002). *What approach to the modelling of catchment scale erosion and sediment transport should be adopted?* In: Summer, W., Walling, D.E. (Eds.), Modelling Erosion, Sediment Transport and Sediment Yield. IHP-VI Technical Documents in Hydrology. UNESCO, Paris, pp. 1 – 11.

Watson F., Rahman J., Seaton S. (2001). *Deploying environmental software using the Tarsier modelling framework.* In: Proceedings of the Third Australian Stream Management Conference, August 27–29, pp. 631–638.

Wheater H.S., Jakeman A.J., Beven K.J. (1993). *Progress and directions in rainfall-runoff modelling.* In: Jakeman, A.J., Beck, M.B., McAleer, M.J. (Eds.), Modelling Change in Environmental Systems. John Wiley and Sons, Chichester, pp. 101–132.

Wicks J.M. (1988). *Physically-based mathematical modelling of catchment sediment yield.* Thesis submitted for the degree of doctor of philosophy, Department of Civil Engineering, University of Newcastle Upon Tyne.

Wicks J.M., Bathurst J.C. (1996). *SHESED: a physically based, distributed erosion and sediment yield component for the SHE hydrological modeling system.* Journal of Hydrology 175, 213– 238.

Wilson R.C. (1989). *Rainstorms, pore pressures, and debris flows: a theoretical framework.* In: Landslides in a semi-arid environment (Morton DM, Sadler PM, eds),

vol. 2. California: Publications of the Inland Geological Society, pp 101–117.

Wischmeier W. H. (1959). *A rainfall erosion index for a universal soil loss equation.* Soil Sci. Soc. Am. Proc. 23(3):246-249.

Wischmeier W. H., Johnson C. B., Cross B. V. (1971). *A soil erodibility nomograph for farmland and construction sites.* Journal of Soil and Water Conservation. 26:189-193.

Wischmeier W. H., Smith D. D. (1958). *Rainfall energy and its relation to soil loss.* Transactions of the American Geophysical Union. 39:285-291.

Wischmeier W.H., Smith D.D. (1978). *Predicting rainfall erosion losses.* Admin. U.S. dept. Agr. Washington, D.C. Agriculture Hand-book. Sci. And Educ. 357. p. 58.

Wolle C.M., Hachich W.C. (1989). *Rain induced landslides in southeastern Brazil.* Proc. 12th Int. Conf. On Soil Mechanics and Foundation Engineering, Rio de Janeiro, 3, pp. 1639-1642.

Woolhiser D.A., Smith R.E., Goodrich D.C. (1990). *KINEROS, a kinematic runoff and erosion model.* Documentation and User Manual, USDA, Agricultural Research Service, ARS-77. 130 pp.

YADE open-source GNU-GPL software (2013). https://yade-dem.org/doc/

Yao C., Lei T., Elliot W. J., McCool D. K., Zhao J., Chen S. (2008). *Critical conditions for rill initiation.* Transactions of the ASAE (American Society of Agricultural Engineers), 51(1), 107.

Young R.A., Onstad C.A., Bosch D.D., Anderson W.P. (1989). *AGNPS: a nonpoint-source pollution model for evaluating agricultural watersheds.* Journal of Soil and Water Conservation, 168–173 (March–April).

Yu B., Rose C.W., Cielsiolka C.A.A., Coughlan K.J., Fentie B. (1997). *Towards a framework for runoff and soil loss prediction using GUEST technology.* Australian Journal of Soil Research 35, 1191–1212.

Zanchi C., Torri D. (1980). *Evaluation of rainfall energy in Central Italy.* In: De Boodt, M., Gabriels, D. (Eds.). Assessment of Erosion. Wiley, Chichester, pp. 133-142.

Zhang L., O'Neill A., Lacy S. (1995). *Spatial analysis of soil erosion in catchments: a review of modelling approaches.* International Congress on Modelling and simulation (MODSIM95). Water Resources and Ecology 3, 58–64.

Zhang X. C., Nearing M. A., Norton L. D., Miller W. P., West L. T. (1998). *Modeling interrill sediment delivery.* Soil Science Society of America Journal, 62(2), 438-444.

Zhang J., Jiao J.J., Yang J. (2000). *In situ infiltration studies at a hillside in Hubei Province, China.* Engineering Geology 57: 31–38.